ΠΑΝΕΠΙΣΤΗΜΙΟ ΠΑΤΡΩΝ
ΣΧΟΛΕΣ ΕΠΙΣΤΗΜΩΝ ΥΓΕΙΑΣ - ΘΕΤΙΚΩΝ ΕΠΙΣΤΗΜΩΝ
ΤΜΗΜΑΤΑ ΙΑΤΡΙΚΗΣ - ΦΥΣΙΚΗΣ

ΔΙΑΤΜΗΜΑΤΙΚΟ ΠΡΟΓΡΑΜΜΑ ΜΕΤΑΠΤΥΧΙΑΚΩΝ
ΣΠΟΥΔΩΝ ΣΤΗΝ ΙΑΤΡΙΚΗ ΦΥΣΙΚΗ

**ΔΙΠΛΩΜΑΤΙΚΗ ΕΡΓΑΣΙΑ**

# " ΕΠΕΞΕΡΓΑΣΙΑ ΑΤΡΑΚΤΩΝ ΗΛΕΚΤΡΟΕΓΚΕΦΑΛΟΓΡΑΦΗΜΑΤΟΣ ΥΠΝΟΥ ΜΕ ΑΝΑΛΥΣΗ ΑΝΕΞΑΡΤΗΤΩΝ ΣΥΝΙΣΤΩΣΩΝ"

ΙΩΑΝΝΗΣ Σ.ΑΛΕΒΙΖΟΣ
Πτυχιούχος Μηχανικός Τεχνολογία Ιατρικών Οργάνων,
Τεχνολογικού Εκπαιδευτικού Ιδρύματος Αθήνας

Πάτρα, Οκτώβριος 2006, Ελλάδα

UNIVERSITY OF PATRAS
SCHOOLS OF HEALTH SCIENCE - SCIENCE
FACULTIES OF MEDICINE - PHYSICS

INTERDEPARTMENTAL POSTGRADUATE PROGRAM IN
MEDICAL PHYSICS

**MASTER THESIS**

# "EEG SLEEP SPINDLE PROCESSING WITH INDEPENDENT COMPONENT ANALYSIS"

JOHN S.ALEVIZOS
B. Sc. Medical Instruments Technology
Technological Educational Institution of Athens

Patra, October 2006, Hellas

## Supervising Committee:

Professor G. Nikiforidis

Professor E. Ventouras

## Examining committee:

Professor G. Nikiforidis

Professor A. Bezergiannos

Associate Professor P. Papathanasopoulos

To my family

Stavros, Dimitra, Takis

and to Tina

# Acknowledgments

First of all, I would like to express my appreciation to my supervisor, Professor G. Nikiforidis, for his support in the implementation of this master thesis, as well as for the opportunity he gave me to attend and deliver with success this postgraduate program.

Also, I would like to express my deep gratitude to my supervisor, Professor E. Ventouras, for his essential and persistent guidance and precious support in the implementation of this Master Thesis. Without him I wouldn't be at this point now.

I would also like to thank the colleagues from the Sleep Research Unit of the Department of Psychiatry of the University of Athens, Professors C. Soldatos, P. Ktonas, and T. Paparrigopoulos and Mrs. H. Tsekou, for processing and providing the sleep data, recorded in the framework of the Biopattern Network of Excellence (FP6-2002-IST-508803) and used in the present Thesis.

I should also thank my colleagues and friends in MIPA and MEDISP labs, and especially N. Kopsaftis and E. Athanasiadis for all their help and patient. They have been beside me all this time and supported me.

Last, but not least, I must express my appreciation to my family for their love and the assistance all these years.

# Table of Contents


**List of Figures**…… 8
**Abbreviations**…… 10
**Abstract (In Greek)** ……. 11
**Abstract (In English)** ……... 12
**Chapter 1: EEG, sleep EEG, polysomnogram**……. 13
1.1)EEG……... 13
1.1.1) Introduction……... 13
1.1.2) Function of the Electroencephalograph (EEG)……. 13
1.1.3) Characteristics of EEG……. 15
1.2) Sleep EEG…….. 17
1.2.1) Introduction…….. 17
1.2.2) Historical retrospection ……..... 17
1.2.3) Polysomnogram and the Rules of Rechtschaffen and Kales.... 17
**Chapter 2: Sleep spindles……...** 20
2.1) Introduction…….. 20
2.2) Definition and generators of spindles…….. 20
2.3) Spindle topography…….. 21
**Chapter 3: Independent Component Analysis (ICA)……..** 23
3.1) ICA description……..... 23
3.1.1) Introduction……... 23
3.1.2) Statistical independence……..... 23
3.1.3) Definitions of linear ICA models……. 24
3.1.4) Identifiability of the ICA model……... 25
3.1.5) Applications of ICA…….. 26
3.2) Algorithms for ICA…….. 27
3.2.1) Preprocessing of the data…….. 27
3.2.2) Mutual Information Algorithm……. 27
**Chapter 4: Low Resolution Brain Electromagnetic Tomography……** 29
4.1) Theory…….. 29
4.1.1) Introduction……... 29
4.1.2) Inversion problem formulation……. 29
**Chapter 5: Aims of the study……** 32
**Chapter 6: Methodology……** 33
6.1) ICA-Based EEG processing…… 33
6.2) Cortical activity investigation…….. 38
6.2.1) Cortical currents computing using LORETA……... 38
6.2.2) Further processing of LORETA results……..... 42
**Chapter 7: Results (a) LORETA performance evaluation with simulation..** 45
7.1) Simulations…….. 45
7.2) Simulation results……..... 46
7.3) Performance evaluation……... 71
**Chapter 8: Results……..** 72
8.1) Introduction…….. 72
8.2) Spindle 1 (1st Third of the Night) ……... 72
8.3) Spindle 2 (2nd Third of the Night) ……... 88
8.4) Spindle 3 (2nd Third of the Night) ……... 93
8.5) Spindle 4 (2nd Third of the Night) ……... 98
8.6) Spindle 5 (2nd Third of the Night) ……... 103

8.7) Spindle 6 (2nd Third of the Night) ……... 108
8.8) Spindle 7 (2nd Third of the Night) ……... 113
8.9) Spindle 8 (3rd Third of the Night) …….. 118
8.10) Spindle 9 (3rd Third of the Night) …… 126
**Discussion……** 133
**Appendix A: Analysis of Matlab "Specgram" function ……** 135
**Appendix B: Reprojection of Independent Components into EEG recording electrodes ……** 137
**Appendix C: Direct problem solution code explanation ……** 139
**References……** 140

# List of Figures


Figure 1.1: Standardized Outputs in the surface of head with System 10-20 14
Figure 1.2: EEG Recording 15
Figure 1.3: Placement of electrodes of polysomnographic measurement 17
Figure 1.4: Wave pattern of different sleep Stages 18
Figure 2.1: EEG segment with two visually scored sleep spindles 20
Figure 4.1: MNI coordinate system. X axis points towards the right part of the head, Y axis points towards the front of the head and Z upwards 30
Figure 4.2: Distribution of the 2394 cortical voxels used by the LORETA technique. 31
Figure 6.1: Original filtered sleep spindle EEG and the ICs that were computed using ICA 35
Figure 6.2: STFT-related plots ("multiplot") 36
Figure 6.3: Example of ICA-reconstructed EEG 37
Figure 6.4: User interface of the "Electrode Coordinates Maker" program 38
Figure 6.5: Output of the "Electrodes Viewer" program 39
Figure 6.6: User interface of the "Transformation Matrix (LORETA Operator)" program 40
Figure 6.7: User interface of the "EEG/ERP → LORETA" program in the semi-automatic mode 41
Figure 6.8.a: Example of the graph (blue line) of the amplitude of the LORETA sources global maximum, computed for each time sample and the graph (green line) of the filtered EEG at the lead which presented the maximum amplitude in the whole time range of the original single spindle 43
Figure 6.8.b: Example of the graph (blue line) of the amplitude of the LORETA sources global maximum, computed for each time sample and the graph (green line) of the mean value of the filtered EEG at all 8 leads 43
Figure 6.9: LORETA viewer image of a Mean Activity Map 44
Figures 7.2.1: Simulation 1, Frontal right source (source point 1673 at the middle frontal gyrus of the frontal lobe) 47
Figures 7.2.2: Simulation 2, Frontal left source (source point 1175 at the middle frontal gyrus) 48
Figures 7.2.3: Simulation 3, Frontal midline left source (source point 1344 at the medial fontal gyrus of the frontal lobe) 49
Figures 7.2.4: Simulation 4, Centro-posterior midline left source (source point 1915 at the cingulate gyrus of the limbic lobe) 50
Figures 7.2.5: Simulation 5, Parietal left source (source point 2077 at the inferior parietal lobule of the parietal lobe) 51
Figures 7.2.6: Simulation 6, Parietal right source (source point 2085 at the inferior parietal lobule of the parietal lobe) 52
Figures 7.2.7: Simulation 7, Parietal midline right source (source point 1875 at the precuneus of the parietal lobe) 53
Figures 7.2.8: Simulation 8, Occipital midline left source (source point 1372 at the cuneus of the occipital lobe) 54
Figures 7.2.9: Simulation 9, Sources of simulation 2 and 8 combined (source points 1175 and 1372) 55
Figures 7.2.10: Simulation 10, Sources of simulation 3 and 4 combined (source points 1344 and 1915) 56
Figures 7.2.11: Simulation 11, Sources of simulation 1 and 7 combined (source points 1673 and 1875) 57
Figures 7.2.12: Simulation 12, Sources of simulation 5 and 6 combined (source points 2077 and 2085) 58
Figures 7.2.13: Simulation 13, Sources of simulation 3,4 and 5 combined (source points 1344,1915 and 2077) 59
Figures 7.2.14: Simulation 14, Sources of simulation 1,2 and 7 combined (source points 1175,1673 and 1875) 63
Figures 7.2.15: Simulation 15, Sources of simulation 5,6 and 8 combined (source points 1372,2077 and 2085) 67
Figure 8.2.1: Original (filtered) EEGs and ICs for spindle 1 73
Figure 8.2.2: 8 multiplots of the spectral analysis of the original EEG channels for spindle 1 74
Figure 8.2.3: 8 multiplots of the spectral analysis of the ICs for spindle 1 78
Figure 8.2.4.a: EEGs reconstructed by IC 4 82

Figure 8.2.4.b: EEGs reconstructed by ICs 2,6 83
Figure 8.2.5: Source activity analysis for part A of spindle 1 85
Figure 8.2.6: Source activity analysis for part B of spindle 1 87
Figure 8.3.1: Original (filtered) EEGs and ICs for spindle 2 89
Figure 8.3.2: Source activity analysis for part A of spindle 2 90
Figure 8.3.3: Source activity analysis for part B of spindle 2 92
Figure 8.4.1: Original (filtered) EEGs and ICs for spindle 3 94
Figure 8.4.2: Source activity analysis for part A of spindle 3 95
Figure 8.4.3: Source activity analysis for part B of spindle 3 97
Figure 8.5.1: Original (filtered) EEGs and ICs for spindle 4 99
Figure 8.5.2: Source activity analysis for part A of spindle 4 100
Figure 8.5.3: Source activity analysis for part B of spindle 4 102
Figure 8.6.1: Original (filtered) EEGs and ICs for spindle 5 104
Figure 8.6.2: Source activity analysis for part A of spindle 5 105
Figure 8.6.3: Source activity analysis for part B of spindle 5 107
Figure 8.7.1: Original (filtered) EEGs and ICs for spindle 6 109
Figure 8.7.2: Source activity analysis for part A of spindle 6 110
Figure 8.7.3: Source activity analysis for part B of spindle 6 112
Figure 8.8.1: Original (filtered) EEGs and ICs for spindle 7 114
Figure 8.8.2: Source activity analysis for part A of spindle 7 115
Figure 8.8.3: Source activity analysis for part B of spindle 7 117
Figure 8.9.1: Original (filtered) EEGs and ICs for spindle 8 120
Figure 8.9.2: Source activity analysis for part A of spindle 8 122
Figure 8.9.3: Source activity analysis for part B of spindle 8 125
Figure 8.10.1: Original (filtered) EEGs and ICs for spindle 9 127
Figure 8.10.2: Source activity analysis for part A of spindle 9 129
Figure 8.10.3: Source activity analysis for part B of spindle 9 132

# Abbreviations

| | |
|---|---|
| AC | Anterior Commisure |
| BSS | Blind Source Separation |
| EEG | Electroencephalogram |
| ENG | Electromyogram |
| EOG | Electrooculogram |
| FIR | Finite Impulse Response |
| IC | Independent Component |
| ICA | Independent Component Analysis |
| MI | Mutual Information |
| MNI | Montreal Neurologic Instittute |
| MRI | Magnetic Resonance Imaging |
| PC | Posterior Commisure |
| PIC | Projection of Independent Component |
| PSD | Power Spectral Distribution |
| REM | Rapid Eye Movement |
| STFT | Short Time Fourier Transform |
| TF | Time Frame |

# Abstract (In Greek)

Οι υπνικές άτρακτοι είναι απότομες αλλαγές της ρυθμικής δραστηριότητας που χαρακτηρίζονται από σταδιακή αύξηση και κατόπιν μείωση του πλάτους. Εμφανίζονται κυρίως στα στάδια 2,3 και 4 του υπνικού εγκεφαλογράμματος. Τοπογραφικές αναλύσεις έχουν δείξει την ύπαρξη δύο ξεχωριστών τύπων υπνικών ατράκτων, «αργές» και «ταχείς», περίπου στα 12 και 14 Hz, αντίστοιχα. Υπάρχουν ενδείξεις ότι υπάρχουν τουλάχιστον δύο, λειτουργικά, ξεχωριστές γεννήτριες υπνικών ατράκτων, που αντιστοιχούν στις κλάσεις συχνοτήτων. Ο λόγος της εργασίας αυτής ήταν η επεξεργασία υπνικών ατράκτων με την τεχνική Ανάλυσης Ανεξάρτητων Συνιστωσών (ICA) με σκοπό την έρευνα της πιθανότητας εξαγωγής, στα από την ICA ανακατασκευαζόμενα ηλεκτροεγκεφαλογραφήματα (ΗΕΓ), «συνιστωσών» ατράκτων που αντιστοιχούν σε ξεχωριστές δομές ΗΕΓ, και η μελέτη των πηγών που δημιουργούν αυτές τις συνιστώσες.

Χρησιμοποιήθηκαν 8κάναλες καταγραφές υπνικών ατράκτων ΗΕΓ από έναν εξεταζόμενο, που καταγράφηκαν στα πλαίσια του Biopattern Network of Excellence, οι οποίες αρχικά επεξεργάστηκαν με ένα φίλτρο FIR με συχνότητες αποκοπής (-3dB) στα 6 και 21 Hz. Κατόπιν εφαρμόστηκε η ανάλυση ICA και εξάχθηκαν οι ανεξάρτητες συνιστώσες (ICs). Έγινε επιλογή των συνιστωσών οι οποίες θα ανακατασκεύαζαν τα ΗΕΓ και τέλος ανακατασκευάσθηκαν αυτά. Στα ανακατασκευασμένα ΗΕΓ έφαρμόστηκε η ανάλυση LORETA.

Πρωτού γίνει όμως αυτό έγινε μία εξομείωση του «ευθύ» και «ανάστροφου» προβλήματος. Αυτό έγινε για να μελετήσουμε κατά πόσον θα μπορούσαμε να εξάγουμε αξιόπιστα αποτελέσματα από την τεχνική LORETA με τόσο μικρό αριθμό καναλιών καταγραφής. Η μελέτη αυτή έδειξε ότι τα αποτελέσματά μας θα μπορούσαν να μας δώσουν αξιόπιστες πληροφορίες όσον αφορά την ευρεία περιοχή παραγωγής των ατράκτων και όχι την ακριβή τους θέση.

Τα τελικά αποτελέσματα έδειξαν ότι υπάρχει διαφοροποίηση, όσον αφορά την περιοχή παραγωγής τους, και σταθερότητα των πηγών που σχετίζονται με συνιστώσες ατράκτων που ανακατασκευάζονται από ξεχωριστές ομάδες ανεξαρτήτων συνιστωσών (ICs).

# Abstract (In English)

Sleep spindles are bursts of rhythmic activity characterized by progressively increasing, then gradually decreasing amplitude, present predominantly in stages 2, 3 and 4 of the sleep electroencephalogram (EEG). Topographic analyses of sleep spindle incidence suggested the existence of two distinct sleep spindle types, “slow” and “fast” spindles at approximately 12 and 14 Hz respectively. There are indications that there exist at least two functionally separated spindle generators, corresponding to each frequency spectrum class. The purpose of the present study was to process sleep spindles with Independent Component Analysis (ICA) in order to investigate the possibility of extracting, in the ICA-reconstructed EEG, spindle “components” corresponding to separate EEG activity patterns, and to investigate the sources underlying these spindle components.

We used 8-channel EEG recordings of sleep spindles of a single subject, recorded in the framework of the Biopattern Network of Excellence, which were processed by a FIR filter with cut-off frequencies (-3 dB) at 6 and 21 Hz. Afterwards, ICA was applied and ICs were extracted. There were a choice of the ICs which would reconstruct the EEG and the EEG were finally reconstructed. Source analysis using Low-Resolution Brain Electromagnetic Tomography (LORETA) was applied on the reconstructed EEGs.

Before that we made a simulation of the “direct” and “inverse” problem. This was made in order to investigate if we would extract reliable results from the LORETA technique with only 8-channel recordings. The investigation stated that the results could give reliable information only for the brain sites at which the spindle generators were located and not for their exact position.

Results indicate separability and stability of sources related to sleep spindle components reconstructed from separate groups of Independent Components (ICs).

# Chapter 1: EEG, sleep EEG, polysomnogram

## 1.1)EEG

### 1.1.1) Introduction

The human brain constitutes without doubt, the most complicated creation of nature. This small mass (1,5kg) includes an exceptionally multifunctional network of cells, which are named neurons. The functions of this network are responsible for the creation of thoughts, memory, control of activities of body and sentiments. The total superiority of brain, as the greatest calculating machine that has been manufactured until today is obvious. The research for the comprehension of its mechanisms of operation constitutes a titanic work and up to today the percentage of our ignorance is overwhelmingly bigger than the quantity of knowledge that was acquired for 150 years [1].

In the case of nervous system, in which the brain belongs, medical research was very early connected with the study of electric phenomena. In 1791 Galvani published the idea that the "nerves" contain a form of electricity. In 1848 Du Bois-Reymond discovered that the activity of neurons was accompanied by measurable changes of electric voltage. In 1877 Catton had shown that there existed a relation between exterior stimuli and electric activity in the brain of rabbits and apes. The first thorough report on the measurement of voltage differences from the exterior surface of human head from Hans Berger in 1929, delimited the beginning of study of functions of brain through the Electroencephalogram (EEG) [2].

The individual operation of one neuron or even a small group of neurons cannot explain even simple brain operations. It is the sum of electrochemical effects from neuron to neuron, added up for all the regions of brain that creates what we name cerebral operation, which we can only partially detect and study. One of the tools for this study is the EEG.

### 1.1.2) Function of the Electroencephalograph (EEG)

The function of electroencephalograph (EEG) is based on the recording of voltage differences, which are present in the exterior dermal surface of human skull, as a result of the operation of brain. The measured electric signals are weak, from roughly 0,1μV to 200μV, provided that we place the output electrodes in the dermal surface of head.

The first stage in the export of EEG signals constitutes the electrodes, the sensors of the system. Electrodes convert the current of ions inside the human body in current of electrons inside cables, which afterwards lead this current to next stages of processing. In the points in which the electrodes will be placed, which in the case of EEG are points of the dermal surface of head, the skin must be cleaned well with alcohol in order to achieve low resistance of contact, under 5kΩ. One of the more usual EEG electrodes are manufactured by silver (Ag) and silver chloride (AgCl).

In order to exist the possibility of comparison of various EEGs that came from the same or different patients in the same or in different laboratories there exist standards, internationally acceptable for the choice of places of each electrode above the head. The more popular standard of placement of electrodes is the International System 10-20. The name of system is due to the choice of the 20% of distance between the two ears as the distance between two electrodes and also in the choice of the 10% of distance between the two ears as the distance from the ear till its nearest electrode. In this way the places of electrodes are adapted depending on the dimensions of the skull.

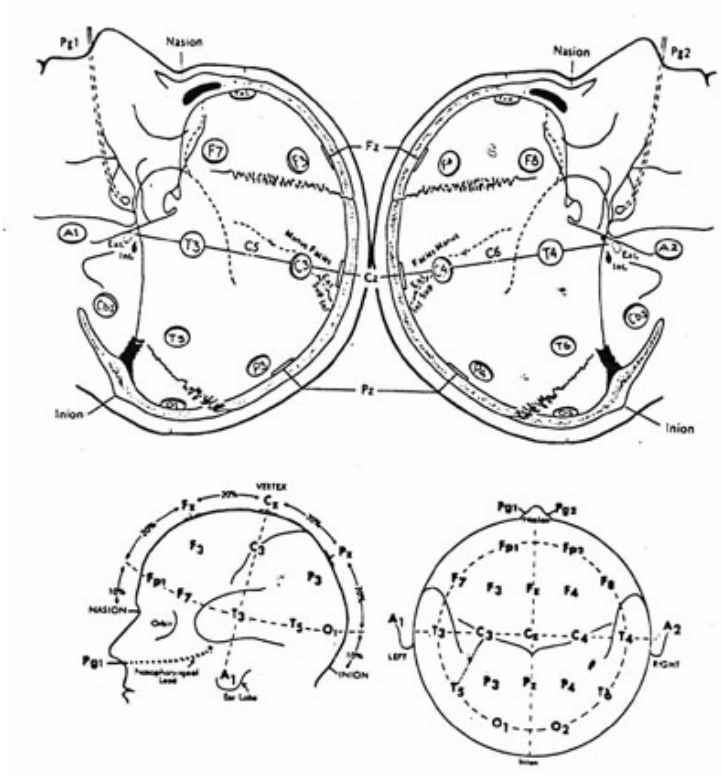



Figure 1.1:Standardized Outputs in the surface of head with System 10-20 [1]

The signal which is amplified in the EEG is the voltage difference between two electrodes**.** In the case of psychophysiology research, usually the measured signal results as voltage difference of an electrode, which may be placed anywhere on the scalp above brain regions (according to the 10-20 system), and a specific electrode common for all the measurements, which constitutes the point of reference, which should not be influenced from cerebral currents. So, in this way we want to have a complete and simultaneous, from all the electrodes, information with regard to each cerebral current of ions which reaches the exterior dermal surface of head [1].

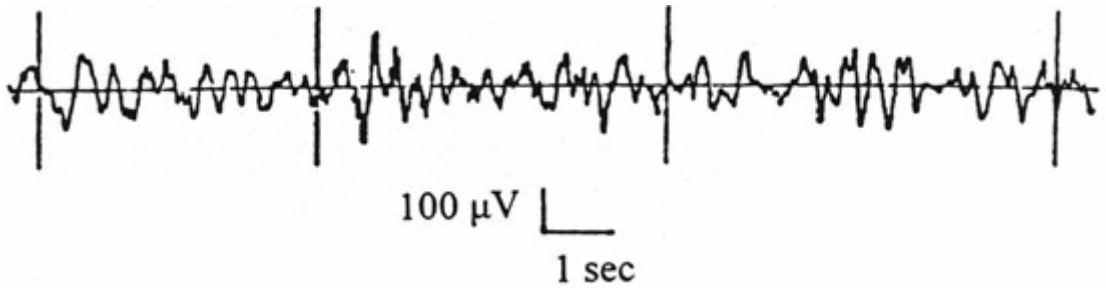



Figure 1.2:EEG Recording

### 1.1.3) Characteristics of EEG

The study of EEG is based on the existence or not of specific waveforms, named rhythms, whose main characteristic are the frequencies by which they are constituted, i.e. their spectrum content. The classification based on the frequency is approximate. A significant volume of research in EEG had been carried out when the use of digital computers were not widespread and the observations were based on the recordings of voltages at recording paper. As the technology allows more precise investigation of the signals, categories are determined explicitly. The main rhythms are alpha, beta, theta and delta, whose frequencies and usual amplitudes are given in Table 1.1.

**Table 1.1**

| Rhythm | Region of Frequencies (Hz) | Amplitude (in μV) |
|---|---|---|
| Delta | 0,5-4 | until 200 |
| Theta | 4-8 | <100 |
| Alpha | 8-13 | <30 |
| Beta | 13-22 | <30 |

The appearance of rhythms has been combined with various levels of vigilance, relaxation, sleep e.t.c. E.g. rhythm alpha is present in roughly 75% of adults. The eyes closure (respectively opening) causes increase (respectively reduction) of alpha rhythm. On the contrary, reduction of alpha activity has been connected with sensory excitation or mental activity. This rhythm took the name alpha because it was the first which was studied from Berger. The beta rhythm, the second which was studied, is the sovereign rhythm present at the phase of complete vigilance of a normal person.

Delta rhythm is connected with the sleep in the normal person and is also the main rhythms in the newborn babies until their second year. Theta rhythm is connected with mechanisms of repression, either at the start oh the relaxation phase, either in combination with beta rhythm in phases of increased attention. It is also present in cases of stress and mental disorders.

The use of EEG in Neurology constitutes a method cheap, painless and simple in its application. From the study of EEG useful conclusions can be extracted on the normal development of Central Nervous System of a person from his/her birth until adulthood. Also EEG can give useful indications in the case of brain diseases (e.g.. Jacobs-Kreutzfeldt, Alzheimer, epilepsy etc). In Psychiatry, the use of EEG has been developed during the last four decades, mainly through the investigation of connections between EEG waveforms, produced under specific test conditions, and various psychiatric disorders, both in vigilance as well as in sleep. In our study we focus on specific sleep waveforms, so we next provide information on sleep EEG

## 1.2) Sleep EEG

### 1.2.1) Introduction

There are many sleep disorders, e.g insomnia, narcolepsy, sleep apnoea; many other disorders manifest sleep disturbances (e.g. depression, schizophrenia, Alzheimer disease, etc.). During sleep, human brain goes through several psychophysiological states that are relatively stable [3].

### 1.2.2) Historical retrospection

The beginning of modern sleep research dates back to the 1930s and is closely connected with the invention of EEG. In 1937, Loomis was the first to observe that sleep is not a homogeneous state during the whole night and described different stages of sleep based on EEG. In 1953, Aserinsky and Kleitman observed a special state of sleep, the rapid eye movement (REM) sleep, during which rapid, binocularly symmetrical eye movements occur, EEG pattern is similar to the one observed during wakefulness, and both respiratory and heart rates are increased in contrast to other sleep stages. Their experiments showed a relationship between REM sleep and dreaming: majority of people awakened from REM sleep reported dreams, whereas people awakened during non-REM sleep did not recall dreams [2]. From overnight recording of EEG and the electrooculogram (EOG), Kleitman with Dement specified the cyclic pattern of REM/ non REM sleep. One cycle of REM/non-REM lasts about 90-100 minutes and during the night, 4-5 cycles occur. Aserinsky and Kleitman also divided non-REM sleep into four stages: 1 through 4, ranging from the lightest sleep in stage 1 to the deepest sleep in stage 4.

### 1.2.3) Polysomnogram and the Rules of Rechtschaffen and Kales

An essential method in sleep research is polysomnography. It is composed of measuring the EEG, the electrooculogram (EOG) and electromyogram (EMG), see Figure1.3.

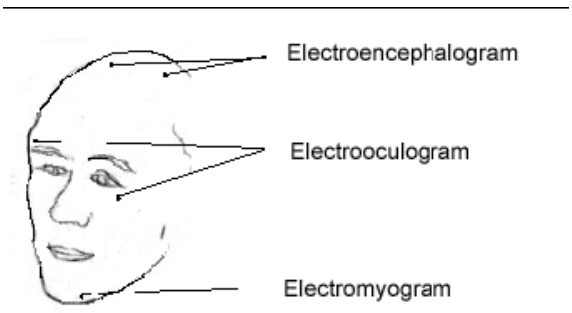



Figure 1.3: Placement of electrodes of polysomnographic measurement [4]

Sleep Stages are scored according to "A Manual of Standardized Terminology, Techniques and Scoring System for Sleep Stages of Human Subject", which was elaborated in 1968 by a committee co-chaired by A.Rechtschaffen and A.Kales [5]. The purpose of these uniform and standard criteria was to increase the comparability and replicability of results from different laboratories. The Manual involves parameters, techniques and wave patterns of polysomnographic recordings. One channel of EEG, two channels of EOG and one channel of EMGs are recorded. The EEG derivations, i.e. electrode pairs, are C4/A1 or C3/A2 according to the 10-20 electrode placement system (see Fig.1.1). The potentials for eyes movements recording are measured at a position 1 cm above and slightly lateral to the outher canthus of one eye and 1 cm below and lateral to the outer canthus of the second eye. The reference electrodes for both eyes are placed on the same ear lobe or mastoid. The EMG is recorded beneath the chin. The placement of electrodes of polysomnographic recording is illustrated on Fig. 1.3. The Stages are scored on an epoch-by-epoch basis, each epoch lasting 20-30. In the following we describe briefly the various sleep stages [4].

**Waking (Stage W)**

There is a low voltage (10 − 30μV) and mixed frequency EEG during wakefulness (see Fig. 1.3). Possible features are alpha activity in EEG and relatively high EMG [4].

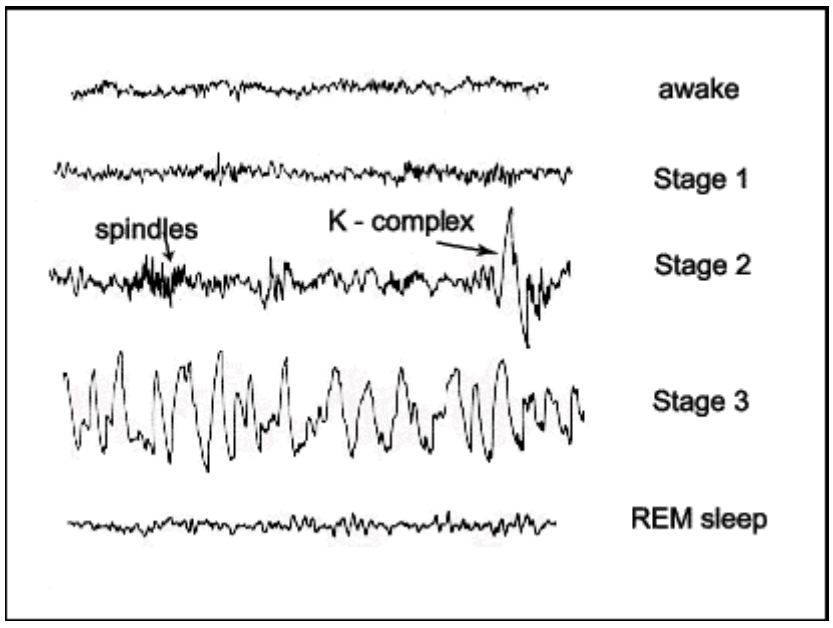



Figure 1.4: Wave pattern of different sleep Stages

**Stage 1**

Stage 1 is characterized by low voltage, mixed frequency EEG with the highest amplitude in 2-7 Hz range (see Fig. 1.4). In Stage 1, after wakefulness slow eye movements can be present. The EMG level is lower than in wakefulness. Stage 1 is also scored when the epoch is characterized with alpha activity combined with mixed frequency EEG and the amount of alpha activity is less than 50% of an epoch [4].

**Stage 2**

Stage 2 is characterized by wave patterns called sleep spindles, which will constitute our research in the present Thesis, and will be analysed in more details in chapter 2, and K complexes and the relative absence of slow waves, i.e. delta rythm (see Fig. 1.3). K complex is a sharp negative wave followed by a slower positive one. Sleep spindles occur in approximately 12-14 Hz frequency range. The duration of these patterns should be 0.5 s at minimum. If the time between two succeeding occurrences of sleep spindles or K complexes is lower than 3 min, this interval is scored as Stage 2, unless there are movement arousals or increased tonic activity. If the time interval is 3 min or more, it is scored as Stage 1 [4].

**Stage 3**

20%-50% of the epoch of EEG record should contain waves with 2 Hz or slower and with the amplitudes above 75 μV if the epoch is scored as Stage 3, see Fig. 1.3. Sleep spindles and K complexes may occur during Stage 3 [4].

**Stage 4**

Stage 4 has the same attributes as Stage 3, but waves with 2 Hz and slower with the amplitudes greater than 75 μV appear more than 50% of the epoch [4].

**Stage REM**

Stage REM shows low voltage and mixed frequency (similarly to Stage 1) of EEG and sawtooth wave pattern is often present (see Fig. 1.3). EMG reaches the lowest level and episodic rapid eye movements occur (REMs) [4].

The rules of Rechtschaffen and Kales have been used for more than 35 years, but they have some disadvantages:
a) They ignore events shorter than 30 seconds. If the interval contains features from more than one Stage, it is scored as the Stage whose features have the longest duration.
b) They are designated for healthy adult people and hence, it is not possible to score atypical patterns in cases of ill people or children.
c) Some wave patterns (sleep spindles or K complexes) are not well defined, especially with respect to automated sleep scoring [4].

# Chapter 2: Sleep spindles

## 2.1) Introduction

As mentioned in chapter 1.2.3 sleep spindles are a distinctive EEG phasic feature of non-REM sleep and are prevalent during stage 2 as compared to slow wave sleep [3,7,8]. While the neurophysiological mechanisms of spindle generation, that involves thalamic and corticothalamic networks, have been recently delineated, their definitive functional meaning still remains to be elucidated [9-12]. Interesting aspects of research concern their intra-cycle temporal dynamics, their time-course across sleep cycles, the reciprocal relationship with delta activity, the effects of sleep deprivation, of circadian factors and of ageing, and their role in information processing [7]. Moreover, specific attention has been paid to the existence topographically distinct "slow" and "fast" spindles (see chapter 2.3), also taking into account the presence of large inter-individual differences.

## 2.2) Definition and generators of spindles

The sleep spindle is one of the hallmarks of human stage 2 sleep and is also one of the few transient EEG events which is unique to sleep. It is commonly known as a group of rhythmic (12-14 Hz) waves characterized by a progressively increasing, then gradually decreasing, amplitude, and it may be present in low voltage background EEG, superimposed to delta activity, or temporally locked to a K complex.[8]

"Sleep spindle" is defined by the standard sleep scoring system as a "term only to describe activity between 12 and 14 Hz" [5,6]. This definition refers to the visual scoring of transient phenomena in polysomnographic recordings, but the routine use of quantitative analysis of EEG activity in assessing spindle frequency power needs some clarification. In fact, spectral analysis (or similar techniques) does not distinguish between background EEG activity and phasic spindle activity. This raises the question of whether changes in power values in a specific frequency range actually correspond to changes in visually-scored sleep spindles. Another way to calculate spindle measures is by using automatic detectors. However, even spindle detection algorithms frequently work by considering EEG activity in different frequency ranges. Furthermore, they show some other problems since they detect a too high spindle amount in stage 1 and in REM sleep, probably reflecting the limitation of automatic devices in recognizing the features of sleep spindles [14,15].




Figure 2.1 : An EEG segment with two visually scored sleep spindles.[27]

Neurophysiological findings have delineated the mechanisms of spindle generation as a combination of intrinsic properties and connectivity patterns of thalamic neurons. Neurophysiological findings point to variations in membrane potentials in the thalamocortical network that oscillate in the frequency range of spindles. These findings found a close relationship between changes at neuronal level in the thalamocortical network and at the macroscopic EEG level, with a reciprocal relationship between sleep spindles and slow waves. Despite this growing interest, the definitive functional meaning of sleep spindles still remains unknown [9-12].

## 2.3) Spindle topography

Although sleep spindles are easily detectable on all EEG scalp derivations, nevertheless specific regional differences do exist. It is observed by visual scoring that, while the majority of spindles is present at the vertex with a frequency of about 14 Hz, slower spindles at 12 Hz are visible over frontal areas. However, for many years the most common knowledge was the greater prevalence of spindles over central or centroparietal areas, even though most studies conventionally used only central electrodes to record sleep spindles not allowing any topographic investigation. Advances in computerized data storage now make a quantitative analysis of multichannel sleep recordings possible. Topographic analyses of sleep spindle incidence and frequency spectral power pointed to the existence of two distinct sleep spindle types: “slow” spindles at ~12 Hz, more pronounced over the frontal sites, and “fast” spindles at ~14 Hz more pronounced over parietal and central sites; these results have been observed by both analyzing spindle power in the 10±16 Hz range and using automatic detectors. Successively, many studies reported the same results with respect to sigma power in various frequency ranges, as well as by using automatic detectors set at 11.5±16.0 Hz or 10±16 Hz [13-20].

These results have been interpreted according to at least two separated spindle generators. Some support for this hypothesis has been provided by recent studies using the low-resolution brain electromagnetic tomography (LORETA). The method highlighted a spindle source in the prefrontal cortex, oscillating with a frequency of <13 Hz, and in the precuneus, oscillating with a frequency of >13 Hz [21].

Nevertheless the matter is still far from being clear [7]. Three issues prevent definitive conclusions. Firstly, most studies showing the two cortically-independent spindles enlarge the bounds of spindle frequency from the traditional 12±14 Hz frequency range including frequency bins traditionally considered to be part of the alpha band. Secondly, there are great inter-individual differences in spindle incidence, and topographical analyses on between-subject averaged data could confound individual (different) cortical topographical distributions with the existence of different topographically-specific spindles. Finally (and more relevantly), spindle frequency could change as a function of the same variables that are liable to differently affect the two types of spindles (age and maturation, homeostatic and circadian factors, menstrual cycle phase, pregnancy and pharmacological agents).

One of the main research aspects investigated by the present Thesis is whether new signal processing techniques may contribute in differentiating “slow” and “fast”

spindle “components”, both on the EEG level, in a single spindle, and on the cortical current level. The signal processing technique used, i.e. Independent Component Analysis (ICA), is developed in the next chapter.

# Chapter 3: Independent Component Analysis (ICA)

## 3.1) ICA description

### 3.1.1) Introduction

Very often we are in need of transforming data we possess into another set of data, which will be easier to process and/or will provide clearly information that cannot be readily extracted from the original data. Denote by $\underline{x}$ an m-dimensional random vector $\underline{x}=(x_1, x_2,\ldots, x_m)^T$ . The problem is to find a function f so that the n-dimensional transform $\underline{s}= (s_1, s_2, ...., s_n)^T$, defined by

$$\underline{s} = f(\underline{x}) \quad (1)$$

has some desirable properties [22]. In most, cases, the representation is sought as a linear transform of the observed variables, i.e.,

$$\underline{s} = Wx \quad (2)$$

where W is a matrix to be determined. Using linear transformations makes the problem computationally and conceptually simpler [22,23]. Several principles have been used and methods have been developed to find a suitable linear transformation. Usually, these methods define a principle that tells which transform is optimal. The optimality may be defined in the sense of optimal dimension reduction or statistical "interestingness" of the resulting components $s_i$, i=1,…,n.

In recent years, a particular method for finding a linear transformation, called independent component analysis (ICA), has been widely used in many scientific areas, including biomedical engineering. As its name implies, the basic aim is to find a transformation in which the components $s_i$ are statistically as independent from each other as possible. ICA can be applied, for example, for blind source separation, in which the observed values of $\underline{x}$ correspond to a realization of an m-dimensional discrete-time signal $\underline{x}(t)$, t=1,2,.... Then the components $s_i(t)$ are called source signals, which are usually original, uncorrupted signals or noise sources. Often such sources are statistically independent from each other, and thus the signals can be recovered from linear "mixtures", i.e. the $x_i$, j=1,…,m by finding a transformation in which the transformed signals are as independent as possible, as in ICA [22,23].

### 3.1.2) Statistical independence

Denote by $s_1, s_2,\ldots, s_n$ some random variables with joint probability density function (pdf) $f(s_1...s_n)$, assuming for simplicity that the variables have zero mean values ,i.e. $E(s_i)$, i=1,…,n. The variables $s_i$ are (mutually) independent, if the joint pdf can be factorized:

$$f(s_{1,\ldots}s_n) = f_1(s_1)\, f_2(s_2)\ldots. f_n(s_n) \quad (3)$$

where $f_i(s_i)$ denotes the marginal pdf of $s_i$ [22]. In the following we should remember that we deal with statistical independence, since we deal with random variables, and

not with other concepts of mathematical independence, for example, linear independence. Independence is distinct from uncorrelatedness, which means that

$$E(s_p,s_q) - E(s_p)E(s_q)= 0, \text{ for } p\neq q \text{ , } p,q,=1,\ldots,n \qquad (4)$$

Independence is a stricter condition than the condition of uncorrelatedness. If the $s_i$ , i=1,…,n are independent, it is

$$E(g_1(s_p)g_2(s_q))- E(g_1(s_p))E(g_2(s_q)) = 0, \text{ for } p\neq q, \; p,q=1,\ldots,n \qquad (5)$$

for any functions $g_1$ and $g_2$ [22]. There is, however, an important special case where independence and uncorrelatedness are equivalent. This is the case when $s_1...s_n$ have a joint Gaussian pdf. Due to this property, independent component analysis is not interesting for Gaussian variables.

### 3.1.3) Definitions of linear ICA models

In the following we give the formulation of the problem to be solved by ICA and consequently of the model that is assumed for the data, in order that they are transformed according to the criterion of maximum independence of the transformed variables (see also eq. 1) We shall only consider the linear case here, though non-linear forms of ICA also exist. In the definitions, the observed m-dimensional random vector is denoted by $\underline{x} = (x_1,...,x_m)^T$.

*Definition 1 (Noisy ICA model): ICA of a random vector x consists of estimating the following model for the data:*

$$\underline{x} = A\underline{s} + \underline{n} \qquad (6)$$

*where the "latent" (or "hidden", "source","original") variables (components)* $s_i$ *in the vectors* $\underline{s}=(s_1,...,s_n)^T$ *are assumed independent. The matrix A is a constant m x n "mixing" matrix, which mixes the original components to produce the observed (linear) "mixture"* $\underline{x}$*.* $\underline{n}$ *is a m-dimensional random noise vector.*[22]

For simplicity the great majority of ICA algorithms and applications have used the following simplified definition, where the noise vector is ommited:

*Definition 2 (Noise-free ICA model): ICA of a random vector x consists of estimating the following model for the data:*

$$\underline{x} = A\underline{s} \qquad (7)$$

*where* A *and* $\underline{s}$ *are as in Definition 1.*[22]

In both cases, the method used for solving the ICA problem produces an A matrix so that the components $s_i$ are as independent as possible, in the sense of maximizing some function $F(s_1,\ldots,s_n)$ that measures independence.

### 3.1.4) Identifiability of the ICA model

The term identifiability means that possessing the mixture $\underline{x}$ we should be able to identify, by solving the ICA problem, only one set of matrix A and vector $\underline{s}$. By imposing the following fundamental restrictions (in addition to the basic assumption of statistical independence), the identifiability of the model can be assured up to a multiplicative constant.

1. All the independent components $s_i$ with the possible exception of one component, must be non-Gaussian.
2. The number of observed linear mixtures m must be at least as large as the number of independent components n. i.e., $m \geq n$.
3. The matrix A must be of full column rank. [22]

Usually, it is also assumed that $\underline{x}$ and $\underline{s}$ are centered, i.e. have zero mean which is in practice no restriction, as this can always be accomplished by subtracting the mean from the random vector $\underline{x}$. If $\underline{x}$ and $\underline{s}$ are interpreted as stochastic processes instead of simply random variables, additional restrictions are necessary. In our Thesis $\underline{x}$ and $\underline{s}$ will be random variables.

A basic indeterminacy in the model, as stated above, is that the independent components and the columns of A can only be estimated up to a multiplicative constant, because any constant multiplying an independent, component in Eq. (7) could be canceled by dividing the corresponding column of the mixing matrix A by the same constant. For mathematical convenience, one usually defines that the independent components $s_i$ have unit variance. This makes the independent components unique, up to a multiplicative sign [24] (which may be different for each component).It should also be noted that the definitions of ICA given above imply no ordering of the independent components. The multiplicative and sign indeterminacy has as result that the independent component cannot be used for directly extracting quantitative measures from their values, but rather their characteristics, such as waveform morphology of temporally evolving components, indicate that they "represent" original independent sources. Quantitative measures have to be extracted from reprojections of vector $\underline{s}_{sub}$ to new mixture, where $\underline{s}_{sub}$ includes a subset of the independent components. The subset is selected according to various criteria, for example those components are grouped together, which present the same morphology and therefore intuitively seem to represent the same source.

The non-Gaussianity restriction is necessary for the identifiability of the ICA model. Indeed, for Gaussian random variables uncorrelatedness implies independence, and thus any decorrelating representation would give independent components. This restriction has an implication for biomedical data, including EEG data, namely that the amplitude variation of the underlying sources and neuroelectric phenomena responsible for the generation of currents and potentials should not possess Gaussian properties [25].

In the models used in the present Thesis it is assumed that assumptions 1-3 above are valid, and we shall use only the noiseless ICA model. We also make the conventional assumption that, the dimension of the observed data equals the number of the

independent components, i.e. n=m. Apart from making matrices square, this assumption provides the minimum number of components to study, which is desirable, since even for our case where we will possess n=8, there is a redundancy in the components' representation of underlying sources, which creates a difficulty in assembling the $\underline{s}_{sub}$ vectors.

### 3.1.5) Applications of ICA

The classical application of the ICA model is in so-called "Blind Source Separation" (BSS) problem. In BSS the observed values of $\underline{x}$ correspond to a realization of an m-dimensional discrete-time signal $\underline{x}(t)$,t=1.2…, as stated in Section 3.1.1. Then the independent components $s_i(t)$, i=1,…..,n, t=1,2,….. are called source signals, which are usually original, uncorrupted signals or noise sources. A classical example of BSS is the "cocktail party problem". Assume that m people are speaking simultaneously in the same room, as in a cocktail party. Then the problem is to separate the voices of the different speakers, using recordings of n microphones in the room. This corresponds to the ICA data model, where $x_j(t)$ is the recording of the j-th microphone, and the $s_i(t)$ are the waveforms of the voices. A more practical application is noise reduction. If one of the sources is the original, uncorrupted source and the others are noise sources, estimation of the uncorrupted source is a denoising operation [22]. Most of the research on ICA has been done with the application of source separation in mind, as will be the case for these Thesis, many authors treat the terms ICA and BSS equivalently, in the sense that both A and $\underline{s}$ are unknown, although BSS could be achieved by applying criteria other than statistical independence [26-28].

Another application of ICA is feature extraction [29-34]. Then the columns of A represent, features, and $s_i$ is the coefficient of the i-th feature in an observed data vector $\underline{x}$. The use of ICA for feature extraction is motivated by the theory of redundancy reduction, i.e. reducing the number of parameters to process in a feature processing analysis, such as a classification problem. It is expected that by selecting only those components that are of interest (for example rejecting obvious noise components) a reduced set of features will result, which will facilitate the classification problem. In this case it should be kept in mind that the indeterminacy stated previously, does not enable the direct use of the $s_i$ variables, but should instead lead to feature reduction in the mixture space, by reprojecting vectors $\underline{s}_{sub}$.

## 3.2) Algorithms for ICA

In this Section, we present the ICA algorithm used in the present Thesis.

### 3.2.1) Preprocessing of the data

The algorithm we used, as many ICA algorithms require a preliminary "sphering" of the data $\underline{x}$, and even those algorithms that do not necessarily need sphering, often converge better with sphered data. Sphering means that the observed variable $\underline{x}$ of Eq. (7) is linearly transformed to a variable $\underline{v}$

$$\underline{v}=Q\underline{x} \qquad (8)$$

such that the covariance matrix of $\underline{v}$ equals unity: $E(\underline{v}\underline{v}^T)=I$. After sphering we have from (7) and (8):

$$\underline{v} = B\underline{s} \qquad (9)$$

where B = QA is an orthogonal matrix, because

$$E(\underline{v}\underline{v}^T)= BE(\underline{s}\underline{s}^T)B^T = BB^T = I \qquad (10)$$

provided that the independent components $s_i$ have unit variance, i.e. $E(\underline{s}\underline{s}^T)=I$ [22]. The problem of finding an arbitrary matrix A in model (7) is thus reduced to the simpler problem of finding an orthogonal matrix B. Once B is found, Eq. (9) is used to solve the independent components from the observed v by

$$\hat{\underline{s}} = B^T \underline{v} \qquad (11)$$

Next we describe the underlying principles of the algorithm used for finding a suitable matrix B for solving the ICA problem.

### 3.2.2) Mutual Information Algorithm

Entropy is the basic concept of information theory. The entropy of a random variable can be interpreted as the inverse of the degree of information that the observation of the variable gives. The more "random", i.e. unpredictable and unstructured the variable is, the larger its entropy. Entropy H is defined for a discrete random variable y as

$$H(Y)= -\sum_r P(y = a_r)\log P(y = a_r) \qquad (12)$$

where the $\underline{a}_r$ are the possible values of y [25]. This definition can be generalized for continuous-valued random variables and vectors, in which case it is called differential entropy. The differential entropy H of a random vector $\underline{y}$ with density $f(\underline{y})$ is defined as:

$$H(\underline{y})= -\int f(\underline{y}) \log f(\underline{y})\, dy \qquad (13)$$

A fundamental result of information theory is that a *Gaussian variable has the largest entropy among all random variables of equal variance*. This means that entropy could be used as a measure of non-Gaussianity. In fact, this shows that the Gaussian distribution is the "most random" or the least structured of all distributions. Entropy is small for distributions that are clearly concentrated on certain values, i.e. when the variable is clearly clustered, or has a pdf that is very "spiky" [25].

Using the concept of differential entropy, we define the mutual information MI between n (scalar) random variables, $y_i$, i= 1…n as follows:

$$MI(y_1,y_2,\ldots..y_n)=\sum_{i=1}^{n} H(y_i) - H(\underline{y}) \qquad (14)$$

From information theory it is known that mutual information is a natural measure of the dependence between random variables [22]. It is always nonnegative, and zero if and only if the variables are statistically independent. Therefore if we could find, based on our observation of the vector of mixtures $\underline{x}$, a vector of random variables $\underline{y}$ that would have pdfs that would in turn minimize MI, we could be assured that $\underline{y}$ will be a solution to the ICA problem, i.e. $\underline{y}$ = s. The algorithm that seek to minimize MI, seek to minimize an objective function $\varphi(\underline{y})$, derived from MI. $\varphi(\underline{y})$ is a real-valued function of the distribution of $\underline{y}$ and serves as objective in the sense that it must be designed in such a way that mixture separation into independent components is achieved when we reach their minimum value.

High order statistics can be used to define objective functions, which are simple approximations to those derived by applying the principle of minimizing MI. High order statistics, means that we use statistical parameters called cumulants, of the desired distribution, higher that second order moments [35]. For zero-mean random variables $y_1, y_2, y_3, y_4$ the 4th order cumulants are:

$$Cum[y_1, y_2, y_3, y_4]= E(y_1y_2y_3y_4) - E(y_1y_2)E(y_3y_4) - E(y_1y_3)E(y_2y_4) - E(y_1y_4)E(y_2y_3) \qquad (15)$$

Whenever the random variables $y_1, y_2, y_3, y_4$ can be split in two groups which are mutually independent, their cumulant is zero. Therefore, independence beyond second-order decor-relation can be easily tested using high-order cumulants [35].

By using, for simplicity, the following notation for the cumulants of the elements of a given vector $\underline{y}$:

$$C_{ij}[\underline{y}]=Cum[y_i,y_j] \text{ and } C_{ijkl}[\underline{y}]=[y_i,y_j,y_k,y_l] \qquad (16)$$

The algorithm used in the software package we used has as objective function the function:

$$\varphi(\underline{y})= \sum_{ijkl \neq ijkk} C_{ijkl}^2[\underline{y}] \quad [35,36] \qquad (17)$$

# Chapter 4: Low Resolution Brain Electromagnetic Tomography

## 4.1) Theory

### 4.1.1) Introduction

In the present chapter we present the LORETA inversion technique (Low Resolution Electromagnetic Tomography) [37,38]. This technique and the software for running it was developed by Roberto Domingo Pascual-Marqui at the KEY Institute for Brain-Mind Research, at the Academic Psychiatric Clinic of Zurich and its aim is the calculation of bipolar sources as well as their territorial distribution in the brain using a model of human brain, which is based on a stereotactic atlas [39,40]. For the calculation of sources, surface voltages are used as inputs. The maximum inputs that can be used are 128 recordings. With initial data the surface voltages, the application calculates distributions of bipolar moment (Am units) at the 3D model of brain, using suitable method of inversion which is presented below. In the advantages of particular application we can include:

A) The calculation of a high number of dipoles in order to cover with high analysis the human brain.

B) The at approach interpretation of source points with the stereotactic atlas, meaning that each point is corresponded to the nearest point of the atlas, in grey matter, white matter or cerebrospinal fluid.

C) The correspondence of elements of volume (voxels) to MRI images.

D) The quick time for the inversion.

E) The automated statistical processing for the differentiation of patients based on their current waveforms.

In the disadvantages of the particular application we can include that we have a three layer model adapted to MRI geometry.

Consequently in the frame of this project we use the advantages of this application for the computation of cortical sources of sleep spindles. So, next we describe the LORETA method.

### 4.1.2) Inversion problem formulation

The equation which connects voltage differences to bipolar moment distribution (called hereafter current density distribution), produced from neural cerebral operation, is the following:

$$\mathbf{\Phi = KJ} \qquad (1)$$

Where **Φ** is a **Nx1** matrix constituted from dermal measurements of electric voltage differences. The coordinates of the measurement points are given from the (cartesian) position vectors $\{s_1,s_2,\ldots,s_N\}$. The **3Mx1** matrix $J=(j^T_1, j^T_2,\ldots, j^T_M)^T$ is constituted by the bipolar moments (units Am) $j_\beta=( j_{x\beta} ,j_{y\beta} ,j_{z\beta})^T$ at the **M** points inside the brain, with **β=1….M**. The coordinates of sources are given from the (cartesian) position vectors $\{v_1,v_2,\ldots v_M\}$. The **Nx3M** matrix **K** is a "transport" matrix.

The interest is focused in the case where **M** points (voxels) of the sources are considered inside the brain, shaping a 3D volume. The total **M** of these points is called the space of solutions and these points are considered to create a smooth "cubic" mesh. At the direct problem, **Φ** is unknown, while $\{s_1,s_2,\ldots,s_N\}$, $\{v_1,v_2,\ldots v_M\}$, **K** and **J** are known. In the inverse problem, only **J** is unknown and usually there exist more unknowns from the number of equations, i.e.**M>N**.

Equation (1) applies to any time instant where **Φ** is known, i.e., for any time of the measured voltages. For known **Φ** and **K**, Loreta computes a unique **J** (though in general there is an infinite number of solutions **J**) based on a criterion which selects **J** as the smoothest possible spatial distribution of currents.

In the LORETA technique a three-layered spherical head geometric model is used with a cubic mesh of source points. In order to apply LORETA to the data of any subject, without the need to recompute matrix K and to keep independence from the geometrical characteristics of the brain of the specific subject, but also in a way that the points of sources correspond approximately to specific points of brain areas, the following methodology was used, in the version of LORETA that was used in the present study:

A digitized model of the human brain, created by the Brain Imaging Center of the Montreal Neurologic Institute was used, called "MNI brain" [37,41]. This model, which was produced based on the "average" of a large number of head MRIs, uses a Cartesian coordinate system shown in Fig. 4.1, called the MNI coordinate system. This system almost matches the Talairach coordinate system, whose point of origin is at a specific brain landmark structure called the anterior commissure (AC). The y axis is the AC-PC line (PC is another landmark, the posterior commissure). The z axis is a vertical line that passes through the interhemispheric fissure and the AC. The x axis is a horizontal line at right angles to the y and z axes that passes through the AC. We can identify any point in the brain relative to these axes, which define the Talairach coordinate system.

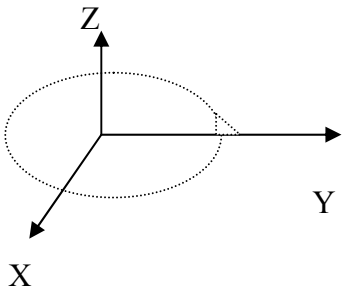



Fig.4.1: MNI coordinate system. X axis points towards the right part of the head, Y axis points towards the front of the head and Z upwards.

For each point in the coordinate space, percentages are given, as probabilities for which brain structure the point belongs. These probabilities were computed based on the structure to which the point belonged in the head MRIs which were included in the "averaging" process. This is the reason that the "MNI brain" is essentially a digital atlas of probabilities.

In the LORETA model, the space of solutions was limited to the grey matter and the hippocampus, as they are defined from the digital atlas of probabilities. A voxel was considered to belong in the grey matter according to the following conditions:

A) The possibility that it belongs to the grey matter is bigger than the possibility that it belongs to the white matter.

B) The possibility that it belongs to the grey matter is bigger than the possibility that it belongs cerebrospinal fluid.

C) The possibility that it belongs to the grey matter is > 33%. [37]

According to the above neuroanatomical restrictions, sources are computed M=2394 voxels with a 7mm resolutions. These voxels are presented in Figure 4.2.

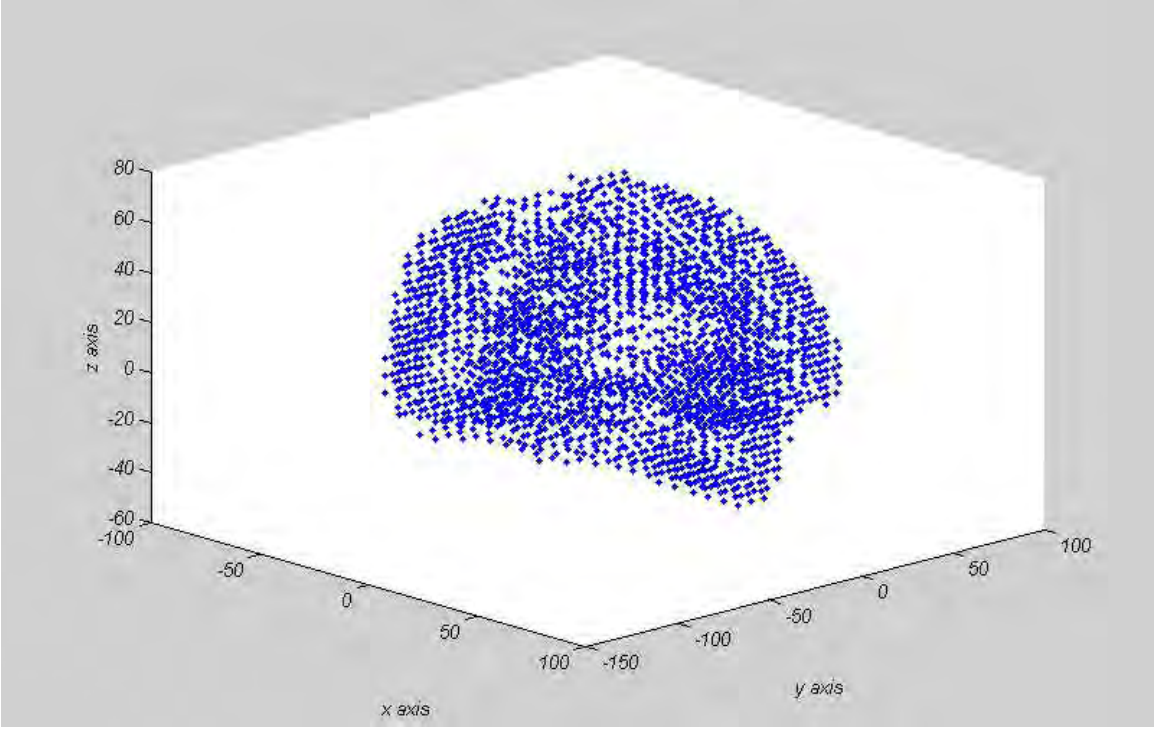



Figure 4.2: Distribution of the 2394 cortical voxels used by the LORETA technique. The MNI coordinate system is used to represent the points.

# Chapter 5: Aims of the study

The aim of the present study was the use of ICA for processing sleep spindles' EEG in order to investigate the possibility of extracting, in the ICA-reconstructed EEG, spindle "components" corresponding to (mostly temporally) separate EEG activity patterns, whether of the same or different frequency content. These components should be reconstructed by judicious selection of ICs, which are produced by applying ICA to the sleep spindle EEG, so that each group of selected ICs, when reprojected to the EEG channels, "recreates" the spindle component which it is "representing". Furthermore, we wanted to investigate the cortical sources underlying these spindle components, using the LORETA technique [40]. In this way we wanted to test one of the principles of ICA, namely that the EEG reconstructed by each separate IC, and by extension groups of ICs, presents spatial stationarity of its sources, and also we tried to make a contribution to the on- going research concerning the existence of distinct sources for the "slow" and the "fast" spindle types.

# Chapter 6: Methodology

## 6.1) ICA-Based EEG processing

A single subject's (healthy male) all-night polysomnographic recording was examined. EEG signal were acquired with sampling frequency fs=512 Hz, at leads F4, C4, P4, O2, F3, C3, P3, O1. From the sleep spindles that were visually detected 9 were used in the present study. Spindles were selected from the three parts of the night, with a duration of at least 1.25 sec and in a way to include both spindles who did show a frequency shift in their duration, according to the experienced scorer who did the spindle detection and the selection, as well as spindles who had a uniform spectral content in their whole duration. Spindles were filtered using a $128^{th}$-order finite impulse response (FIR) bandpass filter, implemented with the fir1 function of the Matlab Signal Processing Toolbox software, with cut-off frequencies (3 dB) at 6 and 21 Hz.

ICA was applied to the original 8-lead filtered EEG recordings, which contained a single (according to the scorer) spindle, using the EEGLAB toolbox, which is compatible with Matlab software. We loaded EEGLAB, imported to it the 8-lead EEG recording, providing specific parameters asked by the program (number of channels, data format, time points per epoch, data sampling rate, channel locations) ran ICA using the "jader" subroutine (which is based on the JADE ICA algorithm) and finally we exported the ICs, providing again specific parameters (output file name, transpose matrix, number of significant digits to output). In Fig.6.1 we present an example of the original filtered 8-lead EEG single spindle recording and the respective ICs that were computed. We should keep in mind that the order of the numbering of the ICs is not related to the ordering of the EEG leads.

The most important step in the analysis consisted of dividing the original single spindle timeframe into parts that reflect different spindle-like activities, called spindle parts or "components", within that spindle. The division was based on the existence in the lead recordings of a distinct waxing-waning cycle and/or on a transition from "low" to "high" frequencies (or vice versa).

Frequencies $\geq$ 14 Hz were considered "high" and, together with the "limit fast" frequency of 13 Hz, were considered as representing fast spindles. Frequencies $\leq$ 12 Hz were considered "low", representing slow spindles. The division of the single spindle timeframe was based on visual examination of both the original filtered EEG recordings and of the frequency content of these recordings, per each lead. Short-Time Fourier Transform (STFT) was applied to the EEG, so that the temporal evolution of the main frequency of the lead signal might be inspected in the timeframe of the spindle. For each lead recording of each single timeframe, a "multiplot" was created, in order to facilitate the frequency content inspection of the signal. An example is given in Fig.6.2 for lead F4 of the original EEG shown in Fig.6.1. In all plots of the multiplot the horizontal axes represent time (in sec). In Plot A we present the original filtered EEG at lead F4, the vertical axis representing the signal's amplitude in μV. In plot D we present the spectrogram of the signal shown in plot A, computed using the specgram function of the Matlab Signal Processing Toolbox.

The STFT was computed for a window of 1 sec resulting in a frequency of 1 Hz. STFT was computed for successive windows, moving the starting point of the window one sample at the time and the successive STFTs were overlapped. The frequencies for which the STFT was computed extended to the Nyquist frequency (fs/2= 256Hz), but we plotted only the frequencies in the range 0 to 20 Hz, as can be seen in the vertical axes of plot D (see also Appendix A for details concerning the application of the related Matlab functions). The color of each point in the plot encodes the magnitude (absolute value), in dB, of the overlapped STFTs for the specific time point, which in turn reflects the power spectral density (PSD) function of the overlapped 1-sec long original EEG windows. We shall not forget that although the final plot gives an impression of high temporal resolution in the analysis of the frequency content, it is the product of overlapping successive 1-sec long spectrogram segments, each segment being composed of 1 Hz-wide horizontal strips, whose value in all the points of the (1-sec)*(1-Hz) strip is the absolute value (in dB) of the discrete-time Fourier Transform of the 1-sec long segment for the particular frequency corresponding to the strip. In order to extract the essential part of the information present in the spectrogram of plot D, we computed, at each sampling time point, the global maximum of the spectrogram in the 9 to 17 Hz range and present it in plot C, whose vertical axes is in Hz, the frequency at which this maximum takes place and in plot B the magnitude in dB of the maximum. In plot B we are not interested in the value of the maximum per se. Instead we wanted to be able to compare the information of the magnitude relation of these maxima.

If the division of the original single spindle timeframe into parts could take place, according to the division criteria stated above, i.e. spindle parts could be discerned, then an inspection of the ICs followed, in order to select those ICs who possessed spindle-like morphology and would best correspond to the previously selected parts of the EEG, both concerning the time duration and their frequency content. Multiplots were also created for the ICs, in order to facilitate the selection of ICs. For facility of the exposition of the methodology, we suppose in the following that the original single spindle timeframe was divided into two successive parts, A and B. Therefore, it is expected that some ICs would be grouped together and be considered as "representatives" for the spindle component present in part A and some other ICs for part B. Even if ICs' activity possessed temporal coincidence and had similar frequency content with an EEG part, they were not included in the representative IC group for that part, if their spindle-like waveform extended significantly (e.g. for more than 0.5 sec) into the other part. Furthermore, ICs where excluded from the group, if their maximum power frequency varied between low and high inside the part. On the other hand, if an IC possessed spindle-like waveform whose frequency content corresponded to the frequency content of the EEG for one of the parts, but the waveform did not extend to the entire time length of the part, that IC was nevertheless included in the representative IC group for that part, because that specific IC was expected to have a significant contribution in the faithful reconstruction of the spindle component that would follow and also we did not wish to divide the original single spindle timeframe into excessively short parts. It should be noted that in the process of (approximate) matching of the EEG waxing-waning cycles to the corresponding cycles of the spindle-like waveforms of the ICs, the boundaries defining the parts of the EEG could be modified based on the information provided by the morphology of the ICs, which could possess a much clearer starting and/or stopping point for the cycle of the activity, than the original filtered EEG. This morphological characteristic

was expected for the ICs and is directly related to the signal separation properties of ICA. In some cases it was actually the observation of the ICs that provided the primary visual information for the division of the EEG into parts. The ICs selection procedure described above could result in cases were only one IC was included in the group of ICs representing a part of the EEG.

After ICs had been selected as representatives of the parts, the 8-lead EEG was reconstructed, for the whole time duration of the original single spindle, once based only on the ICs belonging to the group representing the spindle component in part A (stated in the following as "group A" for shortness), and once based only on the ICs of group B (see Fig.6.3). See also Appendix B for a description of the ICA-based EEG reconstruction techniques' details. Spectral analysis was also applied to the reconstructed EEGs, so that a comparison could be made between the frequency spectrums of the reconstructions, their generating ICs and the original EEGs, in order to confirm the division of the EEG parts and the grouping of the ICs. The above procedure should enable, as stated briefly in the Aims Chapter above, the extraction, in the ICA-reconstructed EEG, of spindle components corresponding to temporally and/or spatially separate spindle EEG activity patterns.

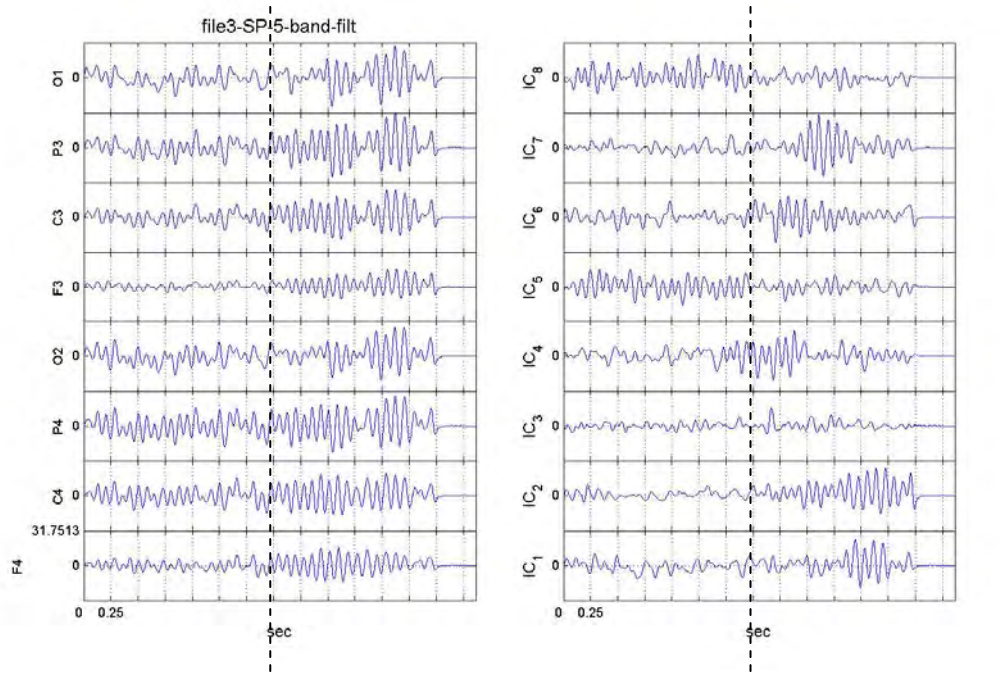



Figure 6.1: Original filtered sleep spindle EEG (left) and the ICs that were computed using ICA (right). In both plots a vertical dashed line indicates the time point of division of the original single spindle timeframe into two parts A (from 0 to 1.75 sec) and B (from 1.75 sec to the end of the single spindle timeframe). The vertical axis values of the filtered EEG recordings range from -31.7513 μV to 31.7513 μV. The ICs exact values do not possess an interest, due to the sign and multiplicative constant indeterminacy of the results of ICA. The absolute maximum value of all the ICs (in this case a positive maximum of IC 7 at approximate 2,35 sec) dictated a common range for the representation of the ICs.

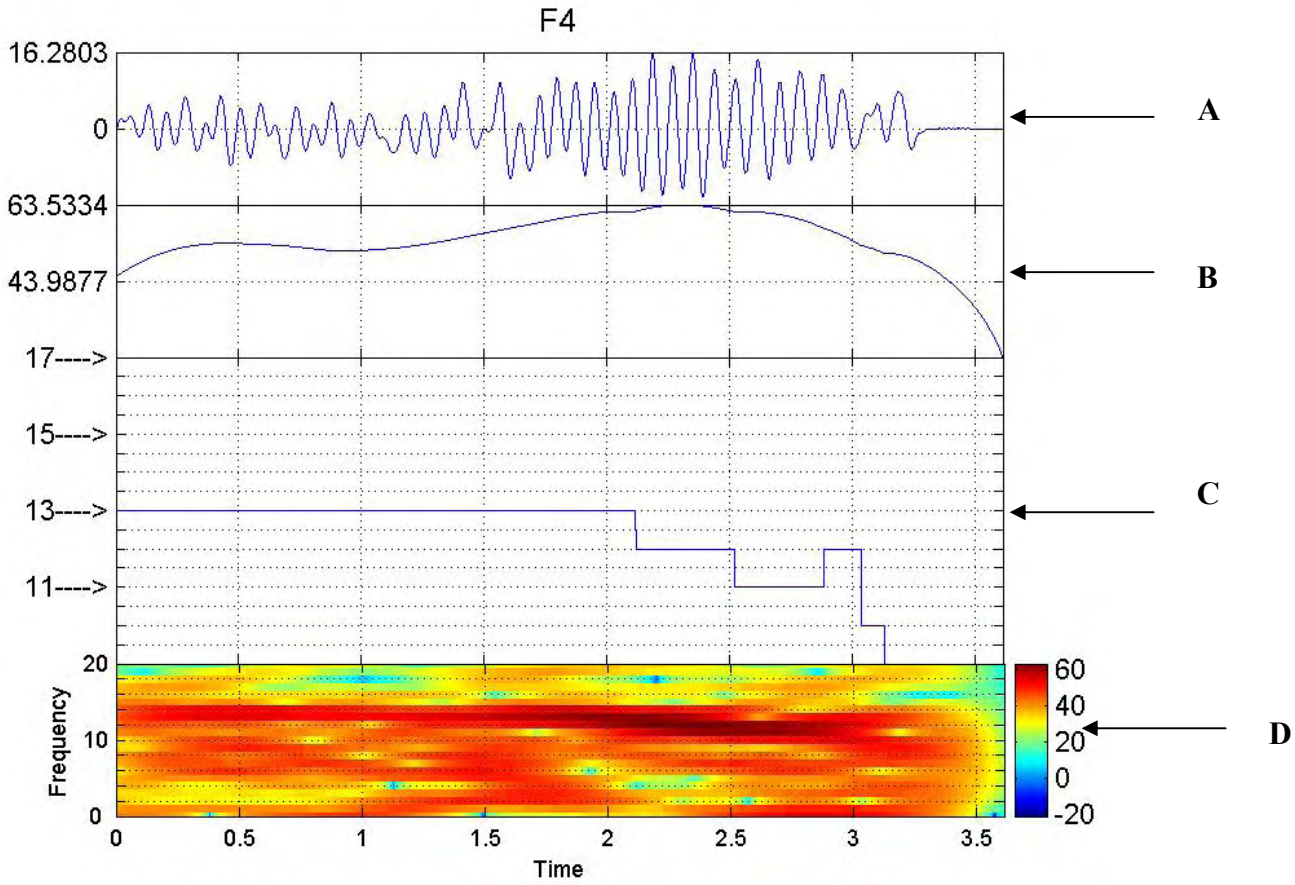



Figure 6.2: STFT-related plots ("multiplot") for lead F4 of the original filtered spindle recording given in Fig 6.1. In plot A is shown the filtered EEG lead (the y axis extends from -16.2803 μV to 16.2803 μV). In plot D is shown the spectrogram of the signal shown in plot A, for the frequency band 0-20 Hz. For each sampling time point the values of the spectrogram along the vertical axis are 20log(abs(Y)), where Y is the overlapped STFTs, for the frequency band 0-20 Hz. The colorbar to the right of plot D shows the color encoding of the spectrogram values. Note that the range of the spectrogram values (and the related color encoding) covers the range of values computed for the 0-20 Hz range of frequencies, and not the whole range of spectrogram values computed for the whole range of frequencies (0 to 256 Hz) for which the spectrogram was computed. In plot B we show, for each sampling time point, the global (in the range 9-17 Hz) maximum of 20log(abs(Y)) and in plot C the frequency (in Hz) at which this maximum occurs.

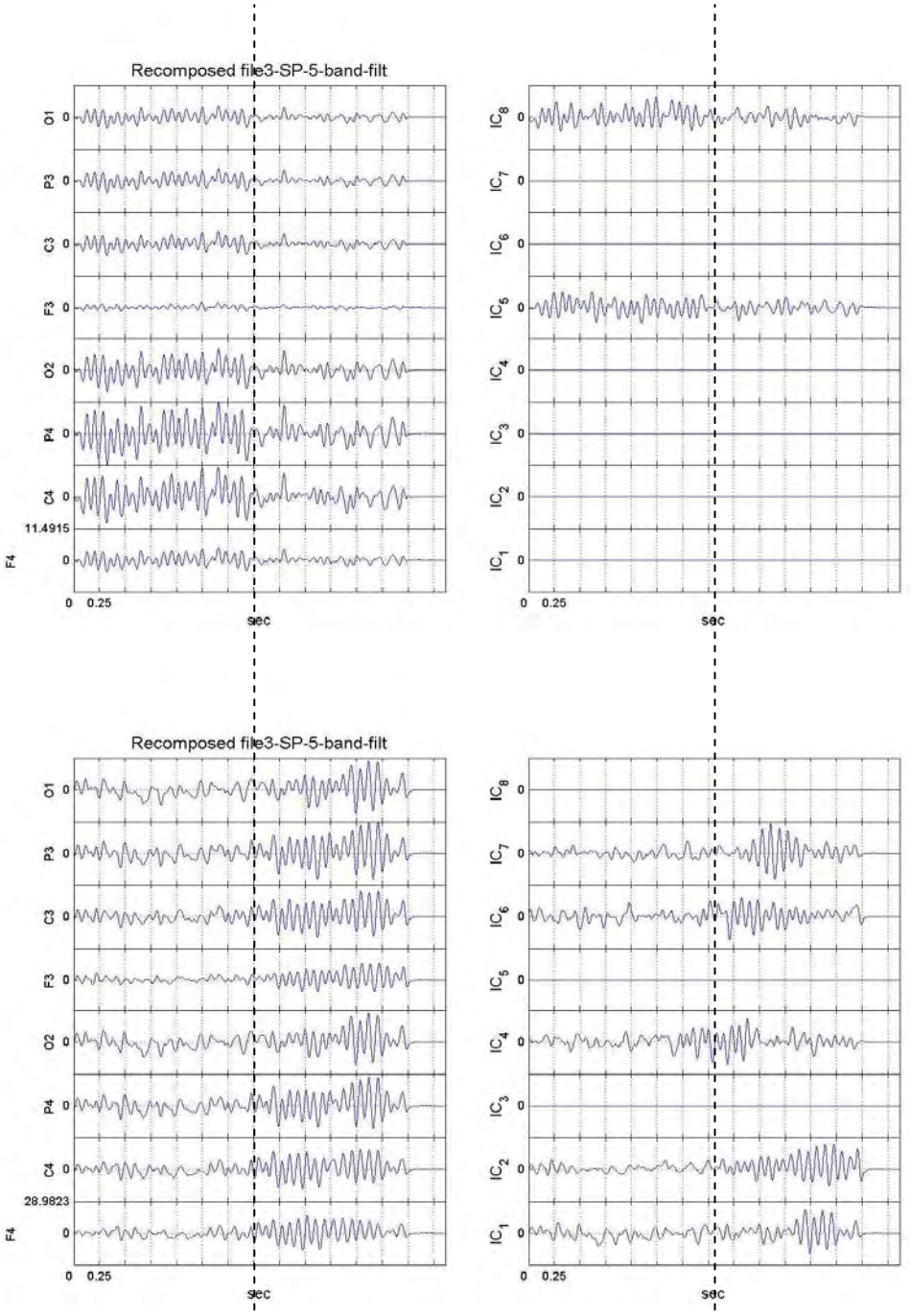



Figure 6.3: Example of ICA-reconstructed EEG. In Fig.6.3.B and 6.3.D are shown the ICs of the group representing part A of the original single spindle timeframe (see Fig 6.1) and part B respectively. In group A belong ICs 5 and 8 and in group B ICs 1, 2, 4, 6, 7. In Fig 6.3.A and 6.3.C are shown the EEG reconstructed by the ICs shown in Fig.6.3.B and 6.3.D respectively. The μV range for the plots of Fig 6.3 A and C are shown in the F4 lead vertical axis. As expected, since no spindle-like activity existed in part B of the timeframe for ICs 5 and 8, the EEG reconstructed by these ICs did not possess spindle-like activity either, in part B on the timeframe. The same held for part A of the timeframe for the EEG reconstructed by ICs of group B. In all plots the vertical dashed line at 1.75 sec indicated the time point of division of the original single spindle timeframe.

## 6.2) Cortical activity investigation

### 6.2.1) Cortical currents computing using LORETA.

Next we used the LORETA method for investigating the sources underlying the spindle components, as these components were represented by the EEG reconstructed by the respective ICs groups. LORETA was used to compute the 3D distributions of bipolar moments, reflecting current density, for each time sample, for both the original EEGs and the reconstructed ones. The source point distribution corresponds spatially to the geometrical centers of the 2394 cortical volume elements (voxels) mesh, as stated in Chapter 4.1.2, shown in Fig. 4.2. The inversion of each 8-lead EEG to intracranial current activity results in the production of 2394 waveforms, each waveform lasting for the whole duration of the initial single-spindle timeframe. In the following we describe in details the steps needed for the production of these waveforms.

The first program to use from the LORETA software package was the "Electrode Coordinates Maker". By selecting the electrodes (leads) which constitute the EEG recordings (i.e in our case F3, C3, F4, C4, O1, O2, P4 and P3) the program saves the electrode coordinates in a Cartesian coordinates system related with the Talairach atlas standard coordinates. In Table 4.1 we present these coordinates which must be saved in a *.xyz file for use by other programs in the following. The file containing the EEG values to be inverted should consist of ASCII formatted columns of the potential values in μV, each column corresponding to a specific lead. The order of the selection of the EEG leads using "Electrode Coordinates Maker" must be exactly the same as the order of the electrode columns at the EEG-containing files. In Fig.6.4 we present the user interface of the "Electrode Coordinate Maker" program.

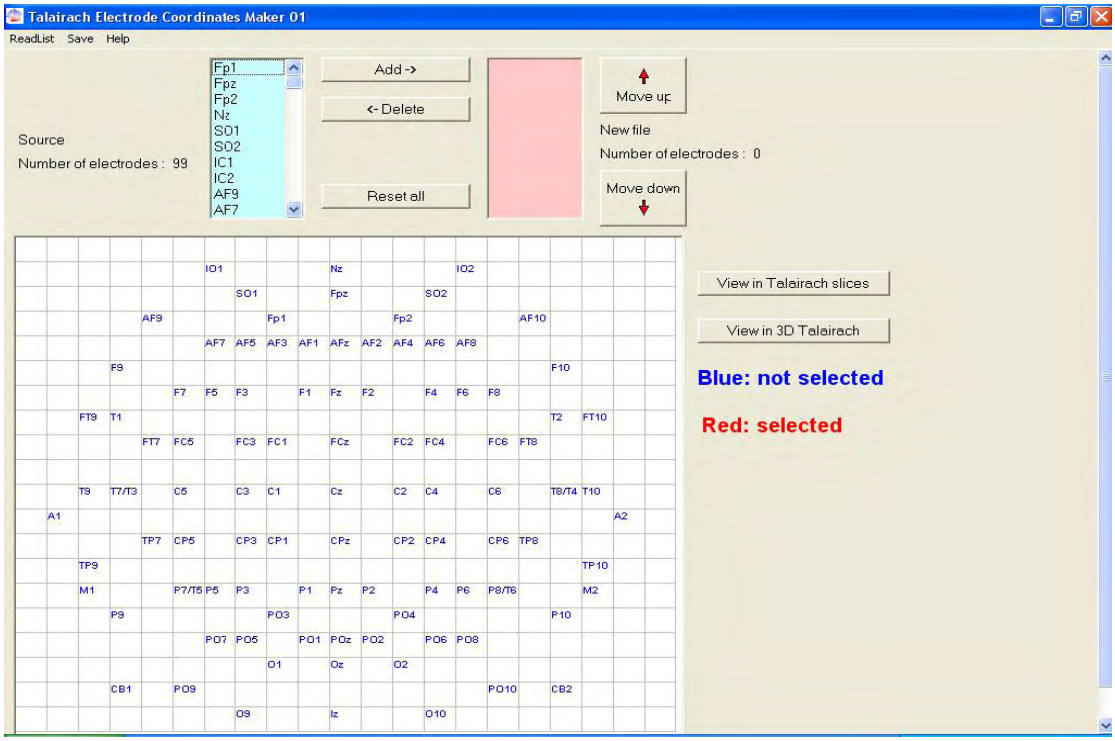



Figure 6.4: User interface of the "Electrode Coordinates Maker" program [40]

After the electrode selection we can use another program of the LORETA software package called “Electrodes Viewer”, in order to check visually the selected electrodes. In Fig.6.5 we show the output of this program which consists of a 3D image, showing the 8 electrodes we chose, superimposed on an image of the cortex.

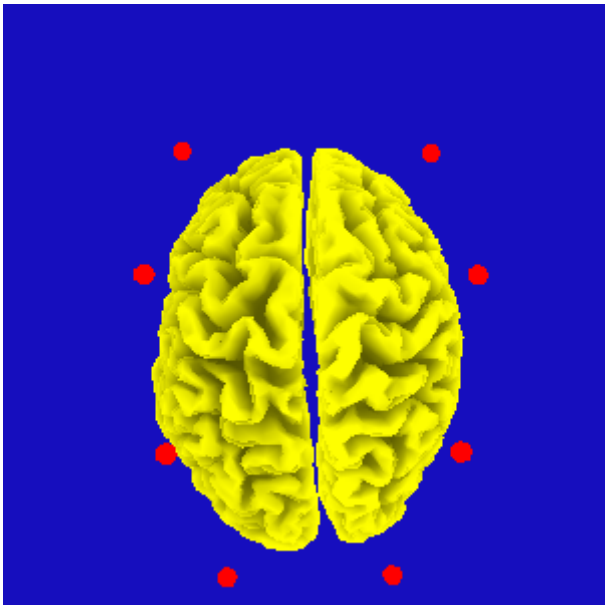


Figure 6.5: Output of the “Electrodes Viewer” program. 3D image of the 8 selected electrodes of our application superimposed on an image of the cortex. [40]

As we have mentioned previously, (Chapter 4.1.2), LORETA needs to calculate a transport matrix (called transformation matrix in the following, according to the LORETA software nomenclature) in order to solve the inversion problem. The program called “LORETA Operator” calculates the transformation matrix using as input the electrode coordinates file created by the “Electrode Coordinates Maker” program. The other set of coordinates needed for the calculation of the transformation matrix, i.e. the coordinates of the 2394 voxel centers, where current software activity will be computed, is fixed and known in advance by the program. The program asks the user to give a name for saving the transformation matrix file.

Additionally, the user must define the smoothing factor. The smoothing factor controls the smoothing of the current source activity between neighboring sources. As the smoothing factor increases a reduction of the absolute value of the peaks of current activity distribution is observed. On the other hand, because the total energy of the distribution remains the same (since it depends on the EEG values to be inverted), the current activity distribution spreads spatially. In our case we used a zero value for the smoothing factor so that we calculate an as much as possible spatially localized source distribution. In Fig.6.6 we present the user interface of this program.




Figure 6.6: User interface of the "Transformation Matrix (LORETA Operator)" program. [40]

The program actually performing the inversion of the EEG voltages is the "EEG/ERP → LORETA" program, taking as inputs the transformation matrix, which was calculated above and the EEG-containing file. The user must also define the first and the last time frame of the EEG file on which to make inversions, which is equivalent to defining at which line of the EEG-containing file the inversions will start (first time frame) and at which line the inversion will stop (last time frame), including this last line. This program cannot calculate the inversion of an EEG file if that file exceeds 512 time frames. Since the EEG in our case was sampled at a 512 samples/sec rate and the spindles selected for the processing lasted longer than 1 sec, our files exceeded the 512 time frames limit, so we had to split them in "epochs", i.e. smaller EEG files containing at most 512 lines, using a program, also provided at the LORETA package, called "Long EEG recordings → Epochs".

The "EEG/ERP → LORETA" program calculates the inversion and puts the output into a file, with the same name as the EEG file, but with a .lorb extension. This is the

LORETA file with the cortical current activity, in binary format, and can be viewed with the "LORETA-KEY Viewer" program. The "EEG/ERP → LORETA" program has 3 functional modes: the manual mode for computing the inversion of 1 EEG-containing file at a time, and the semi-automatic and pseudo-automatic modes. Using the two last modes we can, with one run session of the program, calculate the inversion of many EEG files. In the semi-automatic mode we manually select the EEG files we want to invert and the program, using a transformation matrix selected by the user and time frames defined by the user commonly for all the EEG files to be processed, processes the EEG files. In the pseudo-automatic mode, a batch file can be written by the user, where each EEG file to be processed can use a different transformation matrix, be saved in a .lorb file with a name selected by the user, as can be the first and the last frames at the EEG file to be inverted. Of course, now we might have more than one output file. In Figure 6.7 we present the user interface for the semi-automatic mode, used in our case.

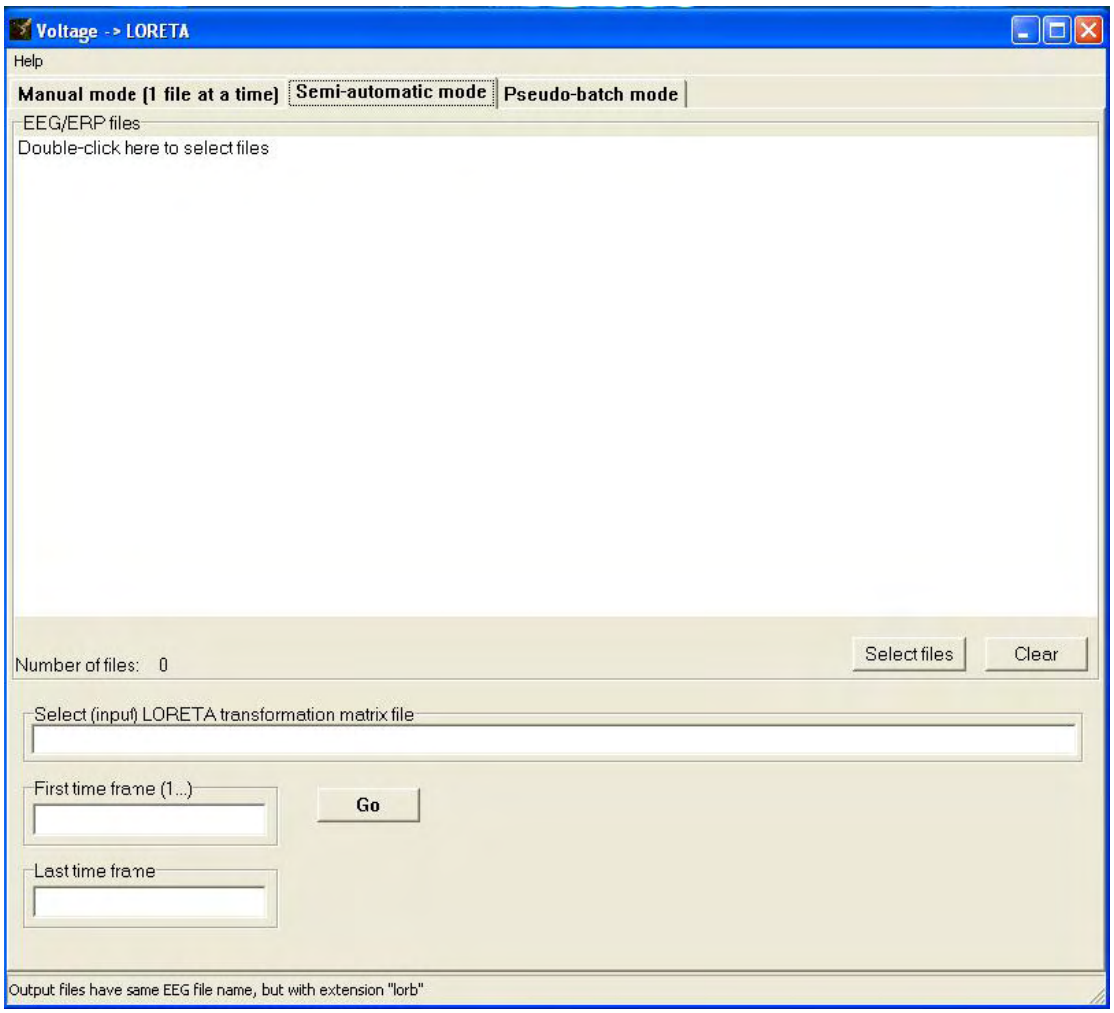



Figure 6.7: User interface of the "EEG/ERP → LORETA" program in the semi-automatic mode of operation. [40]

### 6.2.2) Further processing of LORETA results

As stated earlier we applied LORETA to the original EEG, to the EEG reconstructed by the ICs of group A and to the EEG reconstructed by the ICs of group B, denoted in the following for brevity EEG-O, EEG-A, EEG-B. We should keep in mind that EEG-O, EEG-A and EEG-B contain 8-lead EEG values for the whole time frame of the original single spindle, therefore spanning both part A and part B of this timeframe.

LORETA computes the inversion in 512-lines-long input EEG files, as stated earlier, so we concatenated the "split" LORETA result file, in order to have three LORETA results files, each containing the inversion results as applied to EEG-O, EEG-A and EEG-B.

The study of the sources of both the original EEG and the EEGs reconstructed by the ICs groups was done for each part (A and B) of the original single-spindle timeframe separately. Of course, the results of the study were compared for the two parts. In order to proceed with this study we subsequently divided each of the three previously concatenated LORETA results files into two files each using as separation point the point which was defined by the EEG division rules. The result was to have two LORETA results files for each EEG, i.e. part A and part B, for each of the three EEG files to which LORETA was applied, denoted in the following, for brevity, as L-EEG-O/A, L-EEG-O/B, L-EEG-A/A, L-EEG-A/B, L-EEG-B/A, L-EEG-B/B, where the letter after the "L-EEG-" indicated the EEG file to which LORETA was applied and the letter after the slash indicated the part of the original single-spindle timeframe, to which the LORETA results correspond.

Next we inspected, through the "LORETA-KEY Viewer" (denoted hereafter LORETA viewer for brevity), the source distribution for each of the six L-EEG* files, for each time sample. Our interest was focused on the location of the point were the global maximum of the bipolar moment distribution occurred, on the value of that maximum, as well as to the extent of the distributions in the various cortical areas. The amount of information present in the totality of the distributions, for the six L-EEG* files, for all the time samples contained in each file is overwhelming and does not help in easily extracting information about the overall distribution (i.e. over the entire time length of parts A and B) of the sources that produce the original EEG and the ICA-based reconstructed EEGs, i.e. the spindle components. We had to search for a methodology to apply, so that this information could be extracted in a concise manner from the L-EEG* files.

A preliminary inspection of the temporal evolution of the distributions showed that the activity, and especially their maximum values, computed at each time sample, evolved in a gradual manner, i.e. the amplitude of the global maximum, computed for each time sample, presented a sinusoidal morphology (See Figures 6.8), clearly following the spindle-like morphology of the potential waveforms, on which the computation of the sources was based, having in mind when comparing potential values' waveforms to the maximum source strengths' waveforms, that we computed, through LORETA, the absolute magnitude of the cortical dipole moments. On the other hand, the loci of maximal activity presented frequent "hops" of the maximum's location, although the set of points where these maxima occurred was rather limited. Whether this was reflecting real source distribution shifts, or was due to the limited

number of potential (electrode) points available for the inversion, could not be elucidated by the data available in the present study. These hops were apparent also when we restricted our inspection only to the time samples when the waveform of the maximum dipole moment presented a local maximum (i.e. the circled time samples in Fig.6.8.a and b).

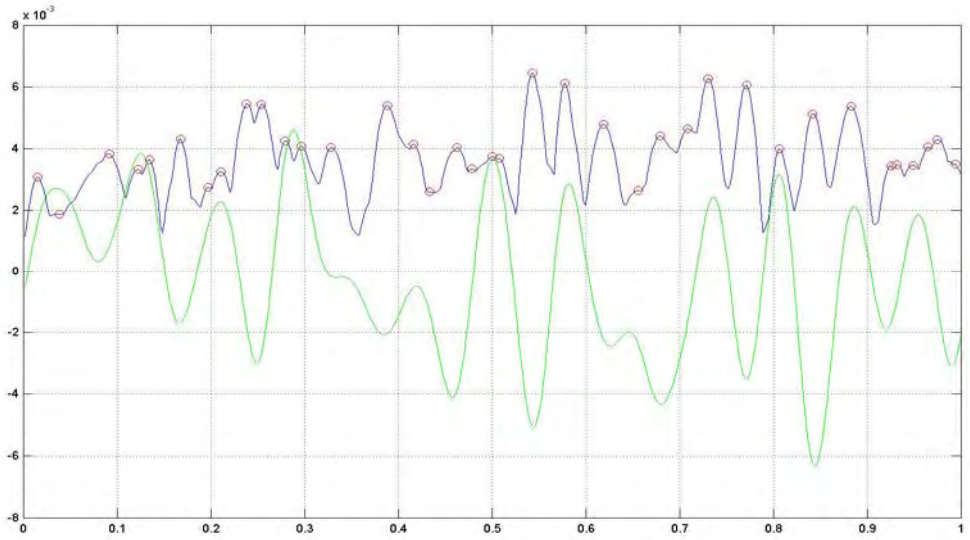



Figure 6.8.a: Example of the graph (blue line) of the amplitude of the LORETA sources global maximum, computed for each time sample and the graph (green line) of the filtered EEG at the lead which presented the maximum amplitude in the whole time range of the original single spindle, i.e. lead F4 presented in Fig. 6.1. In the LORETA values graph we indicate the local maxima with red circles.

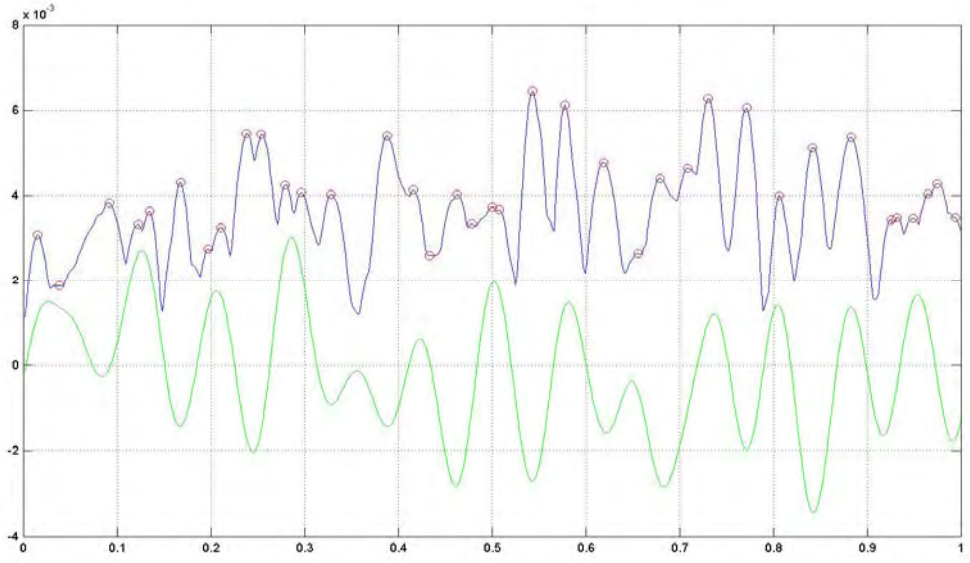


Figure 6.8.b: Example of the graph (blue line) of the amplitude of the LORETA sources global maximum, computed for each time sample and the graph (green line) of the mean value of the filtered EEG at all 8 leads presented in Fig. 6.1. In the LORETA values graph we indicate the local maxima with red circles.

Having in mind these characteristics of the distributions, we decided that a way to extract the information we wanted, avoiding the temporal displacements of the loci of maximal activity, while on the same time keeping an average measure of the magnitude of the activity of each source region, was to compute the (temporal) mean dipole moment amplitude, for the whole duration of the respective part, for each of the 2394 source point locations, for each of the six L-EEG* files. Therefore, six files were produced, denoted as M-L-EEG-O/A, M-L-EEG-O/B, M-L-EEG-A/A, M-L-EEG-A/B, M-L-EEG-B/A, M-L-EEG-B/B. For each part the original spindle timeframe we possessed three 3D mean source activity maps, one for the sources of the original EEG in that part, and one map for the sources of each EEG reconstruction, i.e. each spindle component. We expected that these activity maps would represent faithfully the most active cortical regions, on average, for the respective time frame, to the limit of spatial accuracy imposed by the restriction of the existence of only 8 leads on which to base the inversions, as indicated also by the research presented in Chapter 7.

These 3D mean source activity maps could be viewed with the LORETA viewer. An image of such a view is given in Fig.6.9. As we can see, it has only one time frame (start TF1=1, end TF2=1). The final step in the analysis was the comparison of the mean value images and more specifically of the value of the amplitude and the voxel location of the first four current activity local maxima, as given by the FindMinMaxWin subroutine of the LORETA viewer.

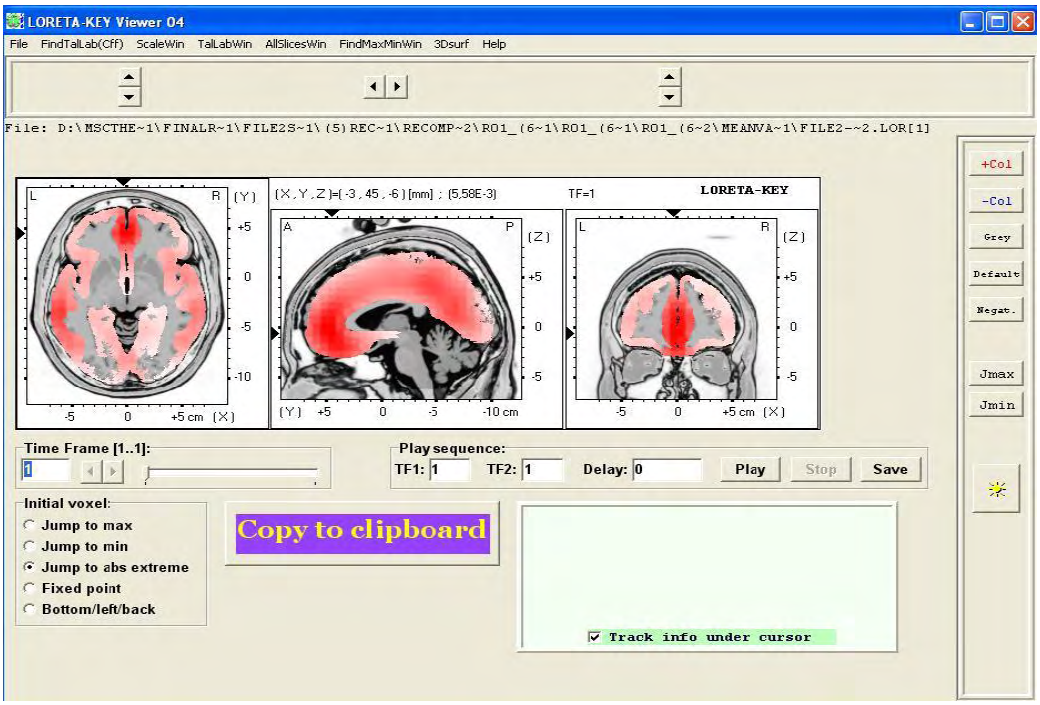



Figure 6.9: LORETA viewer image of a Mean Activity Map. [40]

# Chapter 7: Results (a) LORETA performance evaluation with simulation

## 7.1) Simulations

LORETA has been usually applied to multichannel EEG recordings, where the number of channels usually exceeds 20. In our case we had only 8 leads for covering the whole head surface. We had to check to which extent the localization accuracy of the LORETA technique holds, with such a small number of electrodes, though from previous studies in inverse problem techniques it has been known that when a very small number of head leads are used, the accuracy is reduced but, if the electrodes covers evenly the head surface and do not present artifacts, there is at least information to be gained concerning gross brain region localization of the source activity [42].

In order to carry on the investigation we had to perform a simulation, in which we solved the direct problem, with known brain sources, and then applied the LORETA inversion method. After that, we could compare the results from the inversion and the positions of the known brain sources and see the extent of localization accuracy, which LORETA retains using the 8-channe recording.

The coordinates of the 2394 sources in the MNI coordinate system are given in the file "LORETAtalairach.xyz" of the LORETA package. The coordinates for 99 leads, whose potentials may be used as input data for LORETA are given in file "TCoord99.xyz". LORETA does not compute the inverse problem based on these coordinates, since LORETA uses a spherical head model and the coordinates of both the electrodes and the source points, as given by the MNI atlas, correspond to an average human brain geometry, which, of course, is not spherical. Rather, LORETA uses a model where the leads are projected to a sphere of radius 1 and the source points are also projected into the interior of that sphere. The coordinates of the leads and sources points, in the unit radius sphere are given in files "TCoord99sph.xyz" and "GRIDCO~2.xyz", respectively, of the LORETA package. After the LORETA solution has been computed, the LORETA viewer backprojects the source points of the unit radius sphere to the MNI coordinates of "LORETAtalairach.xyz" and creates the source distribution images that are present to the user.

Based on the above operation mode of LORETA, the methodology we used for our simulations was the following: We selected one or more source points, from "LORETAtalairach.xyz", where the known simulated sources would be positioned. We also selected which electrodes we wanted to include in the simulation. In order to solve the direct problem we used a program written in previous research work, "dir60120.exe", which computes the potential, at a spherical head surface, created by currents sources located inside the inner shell of a three shell (scalp, skull, brain) spherical head (see Appendix C for a description of the function of the program). The sources are assumed static, i.e. the temporal evolution of the strength and position of the sources is not included in the study. This program used the coordinates provided for the selected source points in the "GRIDC0~2.xyz" file. A radial bipolar point source was simulated at each point with the positive current source being upwards and the negative downwards. Using "dir60120.exe", the potentials that are created by the

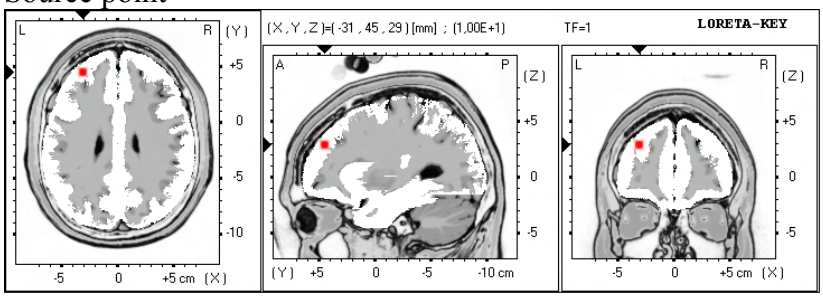
sources are computed at points on the spherical head surface of unit radius, as given by the coordinates of the electrodes, selected for each simulation, in file "TCoord99sph.xyz". These direct problem solution results are then inputted to LORETA, using also the "Electrode Coordinate Maker" program (see Chapter 6.2.1 Cortical currents computing using LORETA.), and the solution of LORETA is then compared to the positions of the original sources. In all the simulations we performed, we checked the localization accuracy for 8–lead recordings (i.e. leads F4, C4, P4, O2, F3, C3, P3, O1), for 16-lead recordings (i.e. leads F4, C4, P4, O2, F3, C3, P3, O1, AF10, T8/T4, PO10, AF9, T7/T3, PO9, FPz, Iz) and 39-lead recordings (i.e. leads F4, C4, P4, O2, F3, C3, P3, O1, AF10, T8/T4, PO10, AF9, T7/T3, PO9, Fpz, Iz, IO2, F8, C6, P8/T6, O10, IO1, F7, C5, P7/T5, O9, AF5, AFz, AF6, PO5, POz, PO6, FT9, A1, P9, FT10, A2, P10, Cz). The reason for this was that we wanted to compare the degradation of localization when using a small (8) compared to a large number of electrodes. The location of the electrodes can be seen in Figure 6.5.

## 7.2) Simulation results

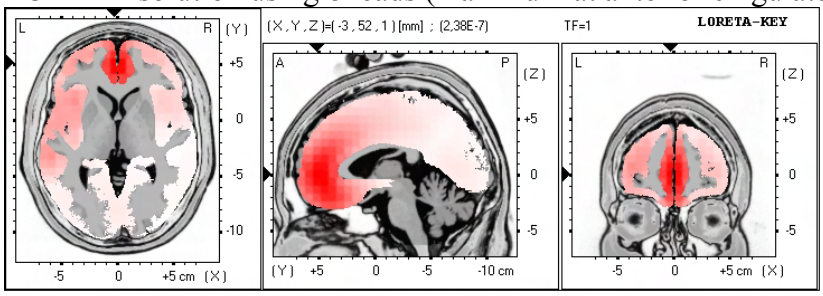
In the following images we present the results of the simulations. In each image produced by the LORETA viewer there are three slices of the head (transverse, saggital, coronal), centered at the point of maximum activity, whose MNI Cartesian coordinates are given

**Figures 7.2.1, Simulation 1: Frontal right source (source point 1673 at the middle frontal gyrus of the frontal lobe):**

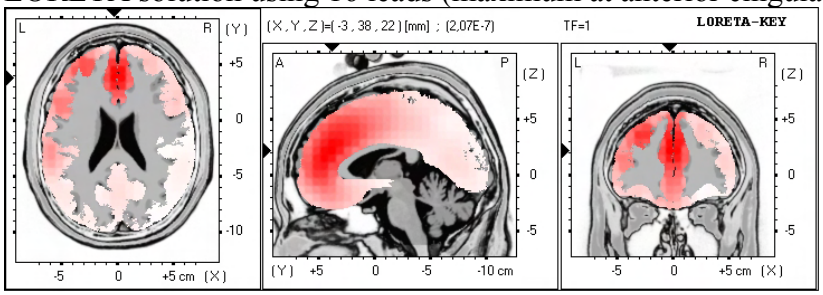
Source point



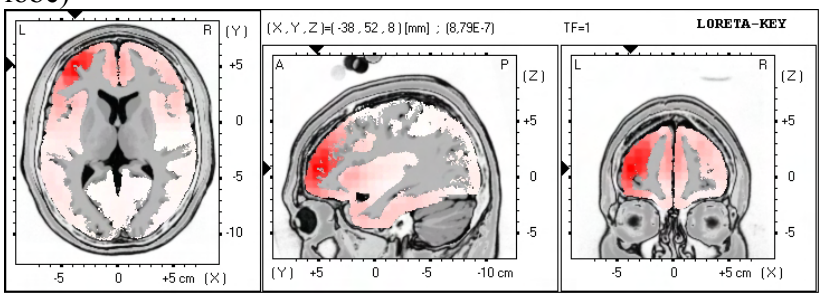

LORETA solution using 8 leads (maximum at anterior cingulate of the limbic lobe)




LORETA solution using 16 leads (maximum at anterior cingulate of the limbic lobe)



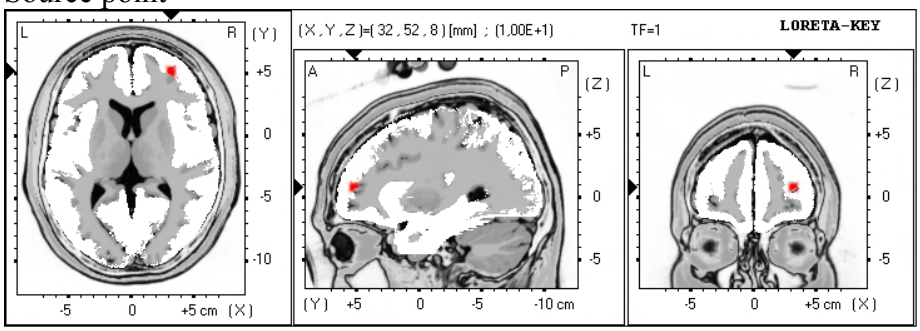

LORETA solution using 39 leads (maximum at middle frontal gyrus of the frontal lobe)



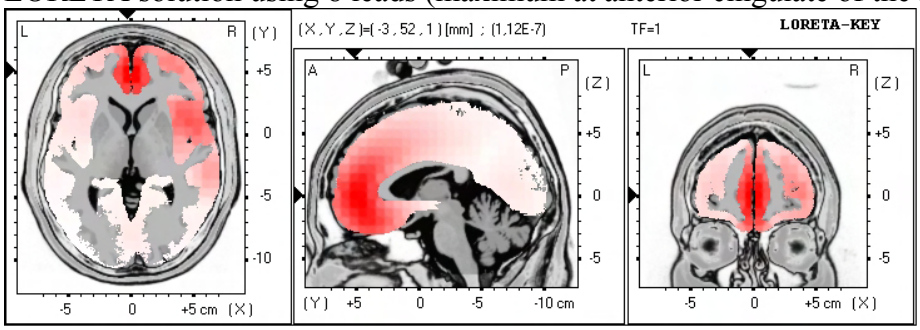

Comment: The 8-lead solution keeps the frontality and the hemisphere location of the source, though the source is again, as in simulation 1, lowered and significantly moved to the midline. The best localization is achieved for the 39-lead solution.

**Figures 7.2.2, Simulation 2: Frontal left source (source point 1175 at the middle frontal gyrus):**

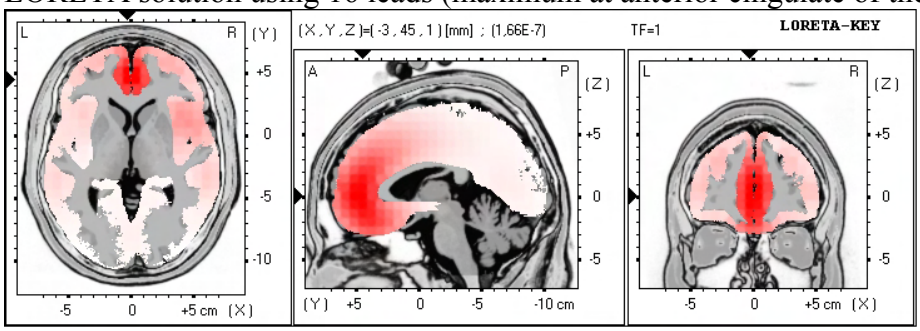
Source point



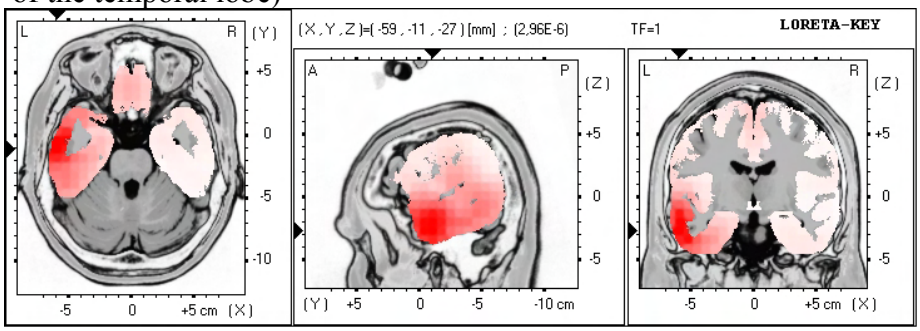

LORETA solution using 8 leads (maximum at anterior cingulate of the limbic lobe)




LORETA solution using 16 leads (maximum at anterior cingulate of the limbic lobe)



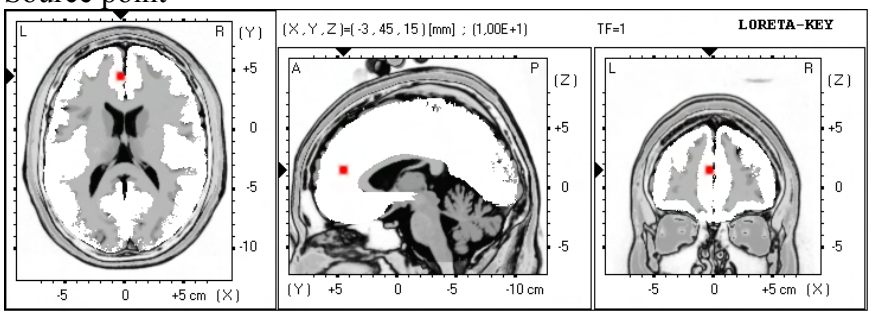

LORETA solution using 39 leads (maximum at fusiform gyrus of the temporal lobe)



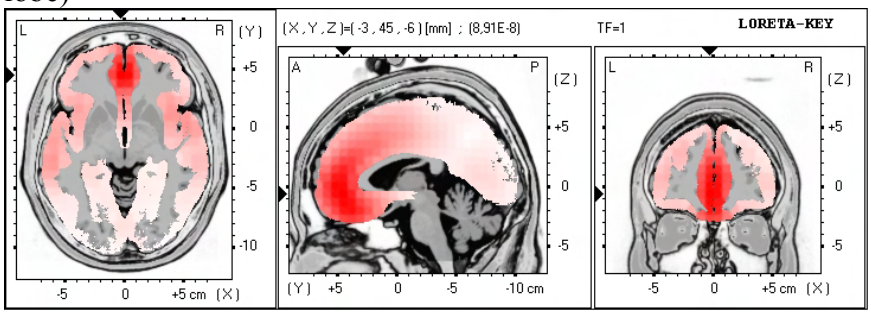

Comment: The 8-lead solution keeps the frontality, but not the hemisphere position of the source, though the source is lowered and significantly moved to the midline. The best localization is achieved for the 8-lead solution.

**Figures 7.2.3, Simulation 3: Frontal midline left source (source point 1344 at the medial fontal gyrus of the frontal lobe):**

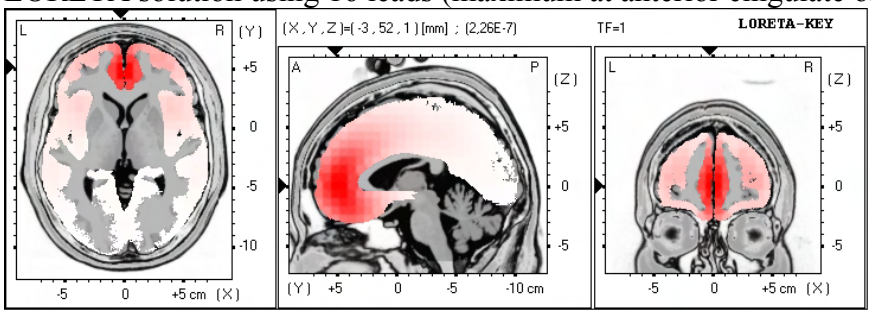
Source point



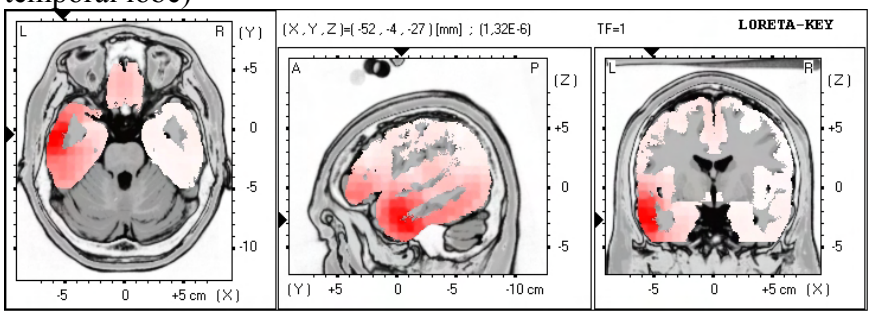

LORETA solution using 8 leads (maximum at medial frontal gyrus of the frontal lobe)




LORETA solution using 16 leads (maximum at anterior cingulate of the limbic lobe)



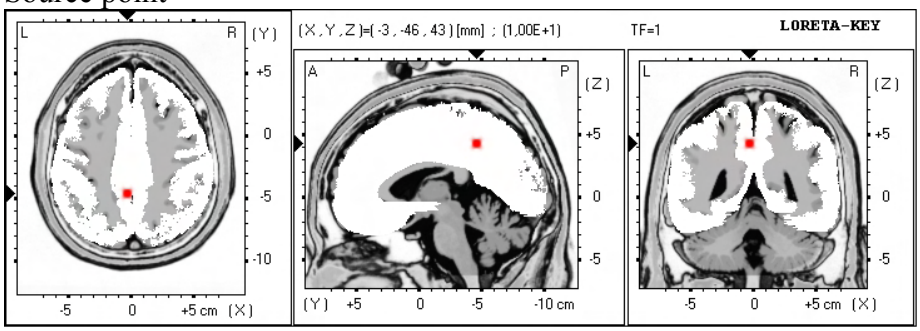

LORETA solution using 39 leads (maximum at middle temporal gyrus of the temporal lobe)



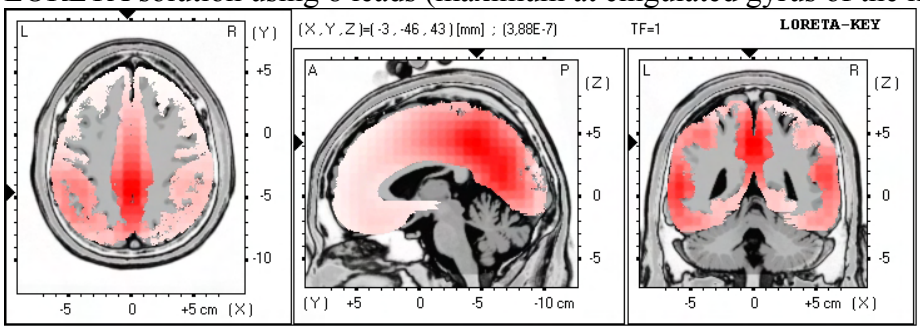

Comment: The 8-leads solution provides an almost correct localization, providing correct X an Y coordinates of the maximum source (i.e. both hemisphere and frontality of the original source is kept) while slightly lowering (Z is reduced) the position of the source. The best localization is achieved for the 8-lead solution.

**Figures 7.2.4, Simulation 4: Centro-posterior midline left source (source point 1915 at the cingulate gyrus of the limbic lobe):**

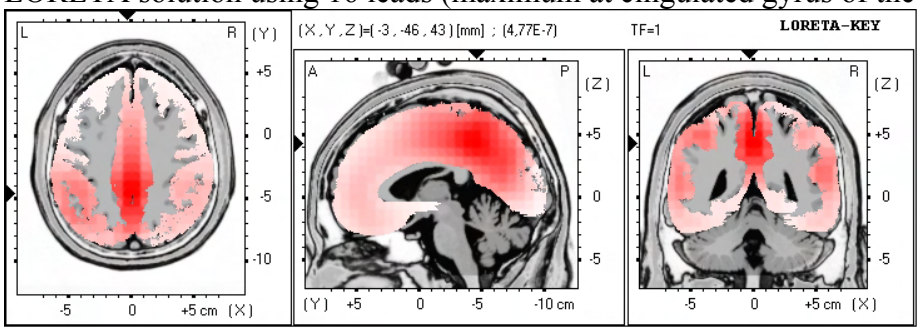
Source point



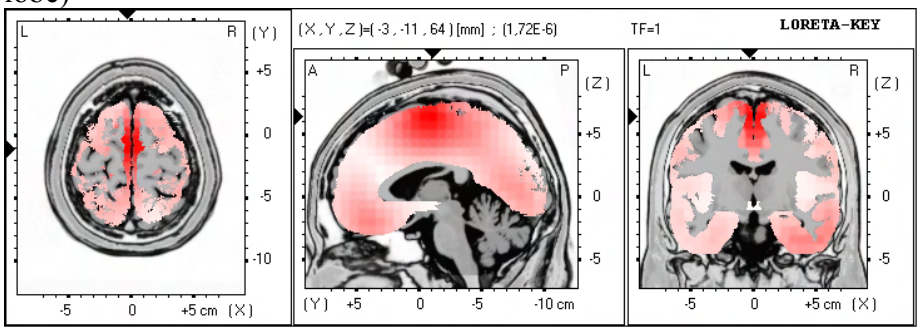

LORETA solution using 8 leads (maximum at cingulated gyrus of the limbic lobe)




LORETA solution using 16 leads (maximum at cingulated gyrus of the limbic lobe)



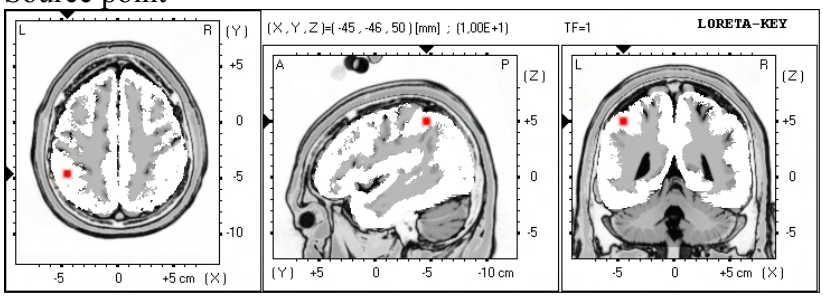

LORETA solution using 39 leads (maximum at medial frontal gyrus of the frontal lobe)



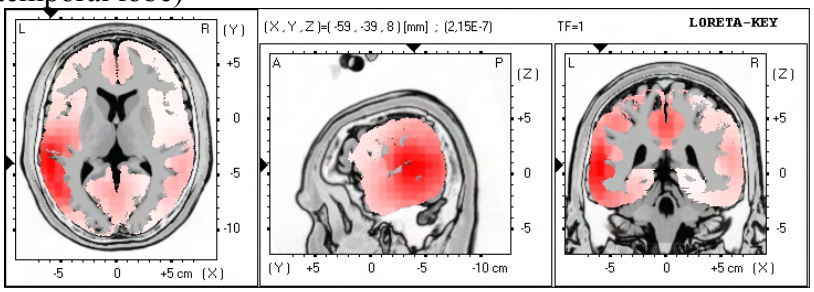

Comment : The 8-leads solution provides an absolutely correct localization of the maximum source activity, while presenting also two spurious secondary left and right hemisphere activity loci. The best localization is achieved for the 8-lead solution.

**Figures 7.2.5, Simulation 5: Parietal left source (source point 2077 at the inferior parietal lobule of the parietal lobe):**

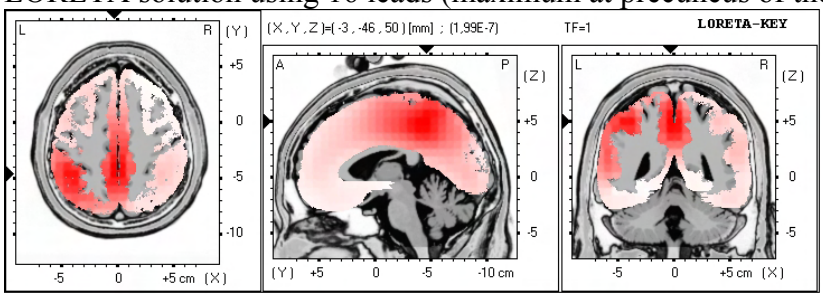
Source point



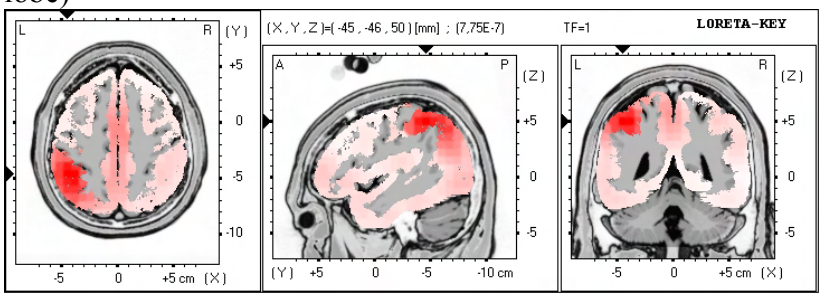

LORETA solution using 8 leads (maximum at superior temporal gyrus of the temporal lobe)




LORETA solution using 16 leads (maximum at precuneus of the parietal lobe)



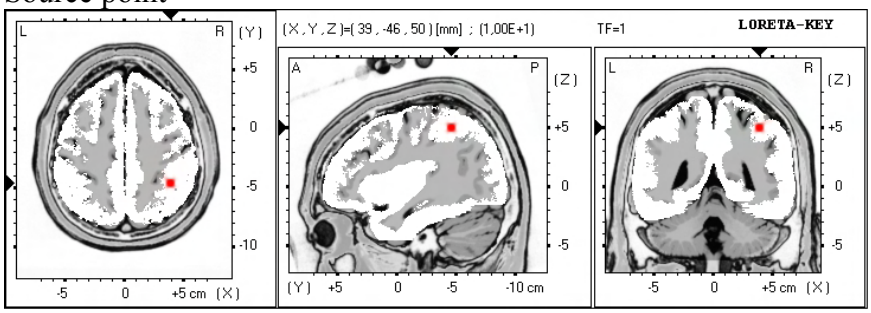

LORETA solution using 39 leads (maximum at inferior pariental lobule of the parietal lobe)



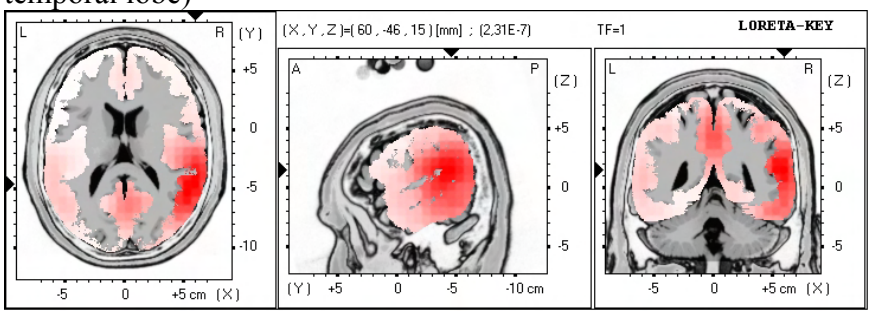

Comment : The 8-leads solution keeps the hemisphere location of the source, as well as the location of the source at the back left quarter of the brain, although due to the reduction of the Z position of the solution, the source is reconstructed in the temporal instead of the parietal lobe, (but not moved to the midline, as was the case for the simulation 3). The best localization is achieved for the 39-lead solution.

**Figures 7.2.6, Simulation 6: Parietal right source (source point 2085 at the inferior parietal lobule of the parietal lobe):**

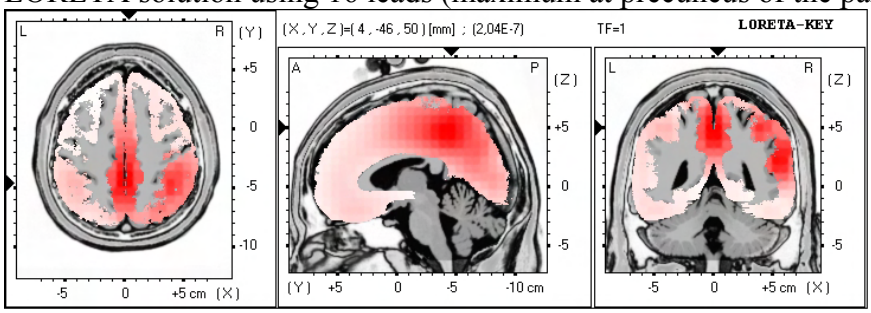
Source point



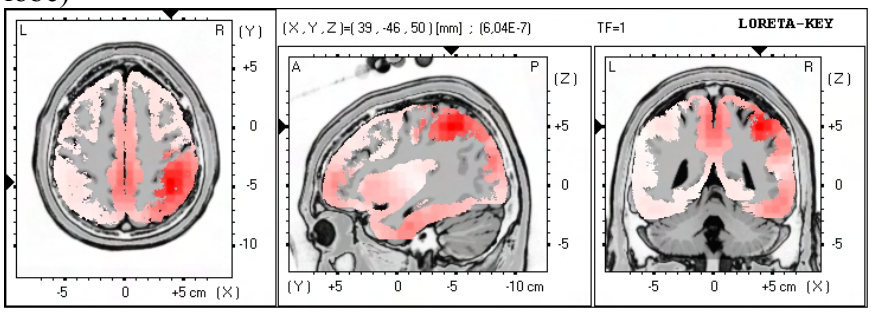

LORETA solution using 8 leads (maximum at superior temporal gyrus of the temporal lobe)




LORETA solution using 16 leads (maximum at precuneus of the parietal lobe)




LORETA solution using 39 leads (maximum at inferior parietal lobule of the parietal lobe)

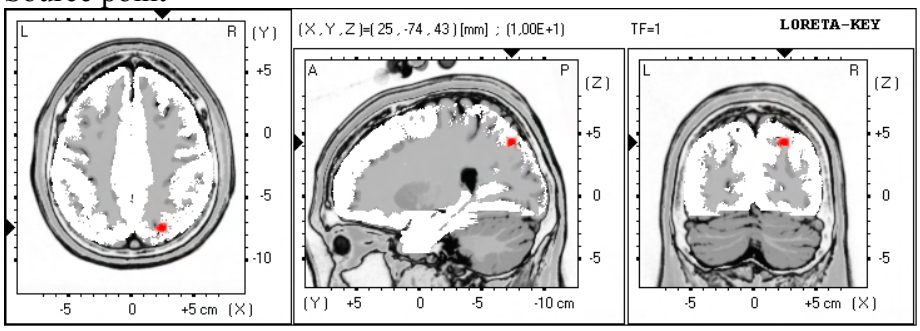



Comment : The 8-leads solution presents characteristics similar to those for simulation 5, i.e. it keeps the hemisphere position of the original source, as well as the location of the source at the back right quarter of the brain, although due to reduction

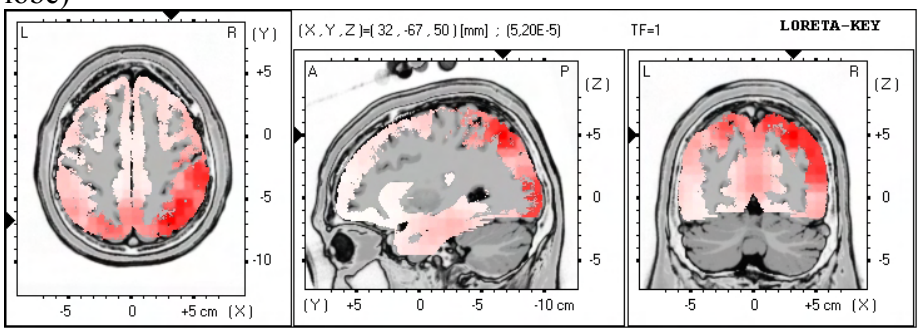
of the Z position of the solution, the source is reconstructed in the temporal instead of the parietal lobe. The best localization is achieved for the 39-lead solution.

**Figures 7.2.7, Simulation 7: Parietal midline right source (source point 1875 at the precuneus of the parietal lobe):**

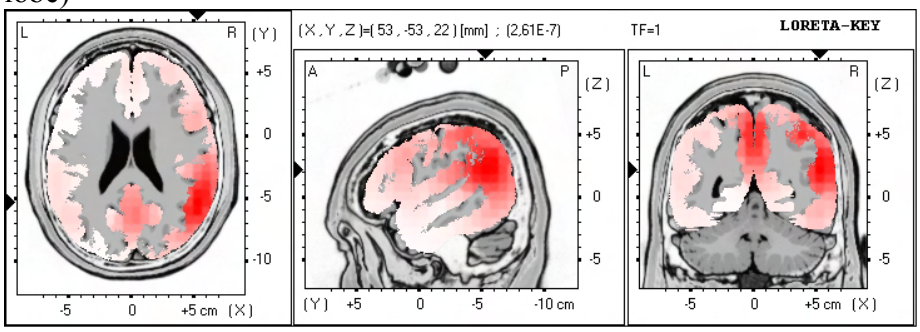
Source point



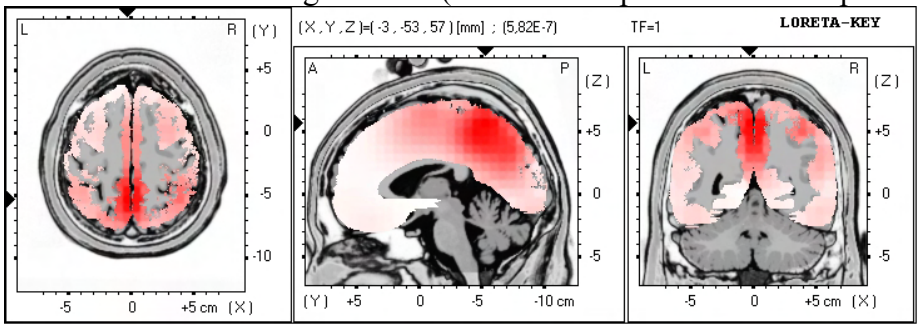

LORETA solution using 8 leads (maximum at superior parietal lobule of the parietal lobe)




LORETA solution using 16 leads (maximum at inferior parietal lobule of the parietal lobe)



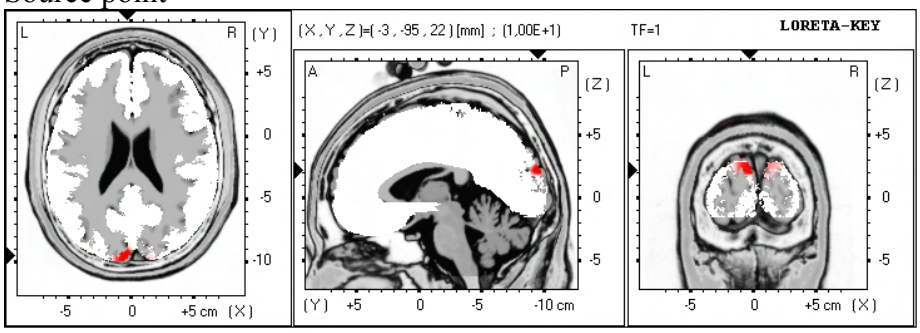

LORETA solution using 39 leads (maximum at precuneus of the parietal lobe)



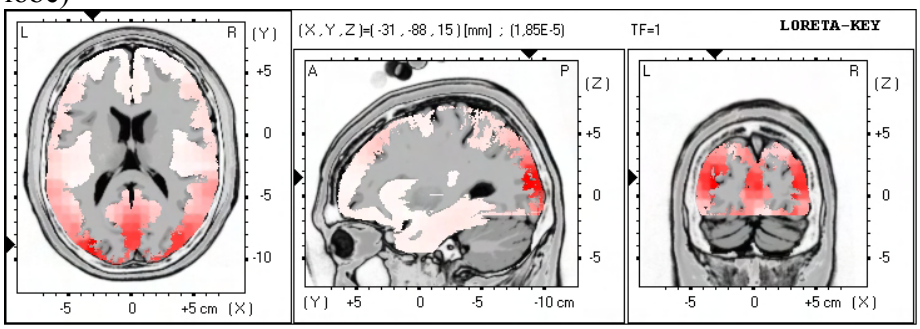
Comment: The 8-leads solution provides a very good match to the original source, keeping hemisphere and lobe position of the original source, with all coordinates of the maximum activity location being closer than 1 cm to the coordinated of the original source. The best localization is achieved for the 8-lead solution.

**Figures 7.2.8, Simulation 8: Occipital midline left source (source point 1372 at the cuneus of the occipital lobe):**

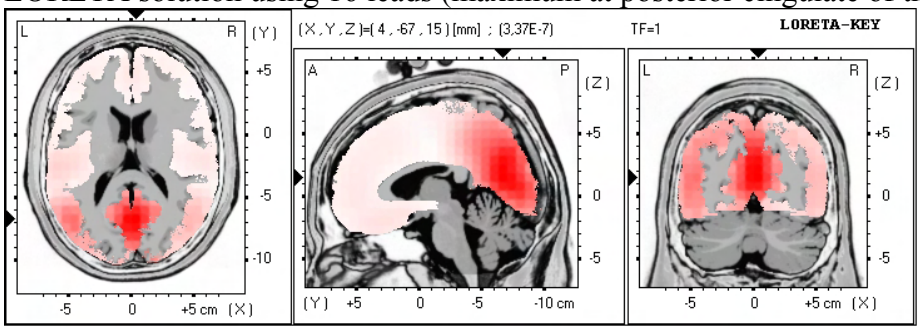
Source point



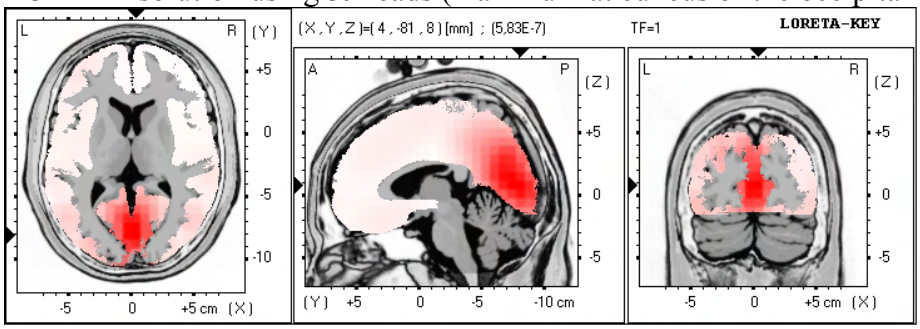

LORETA solution using 8 leads (maximum at middle occipital gyrus of the occipital lobe)




LORETA solution using 16 leads (maximum at posterior cingulate of the limbic lobe)



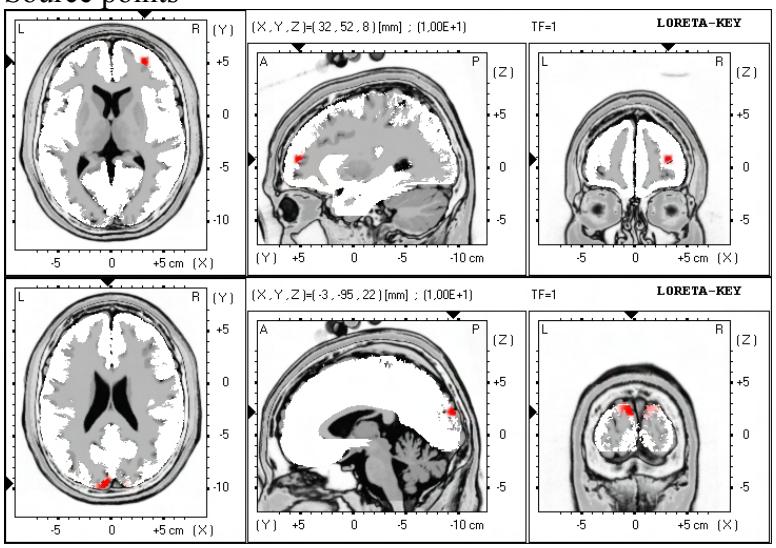

LORETA solution using 39 leads (maximum at cuneus of the occipital lobe)



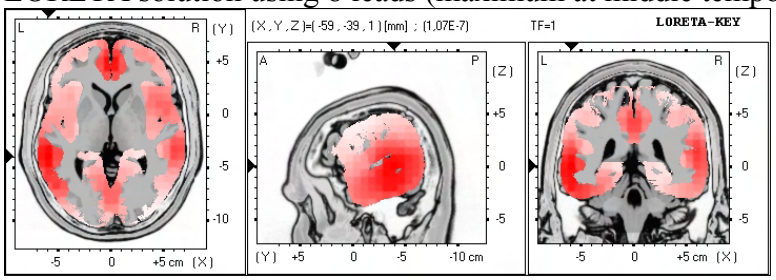
Comment: The 8-lead solution keeps the hemisphere position of the original source, as well as the location of the source at the occipital lobe, although removed from the midline. The best localization is achieved for the 8-lead solution.

**Figures 7.2.9, Simulation 9: Sources of simulation 2 and 8 combined (source points 1175 and 1372)**

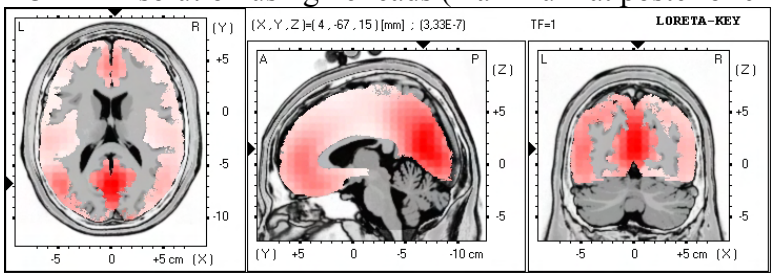
Source points



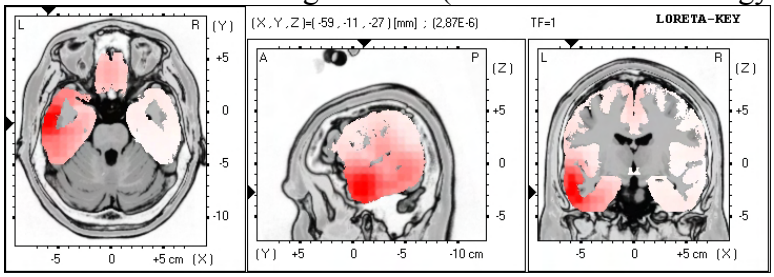

LORETA solution using 8 leads (maximum at middle temporal gyrus)




LORETA solution using 16 leads (maximum at posterior cingulate of the limbic lobe)



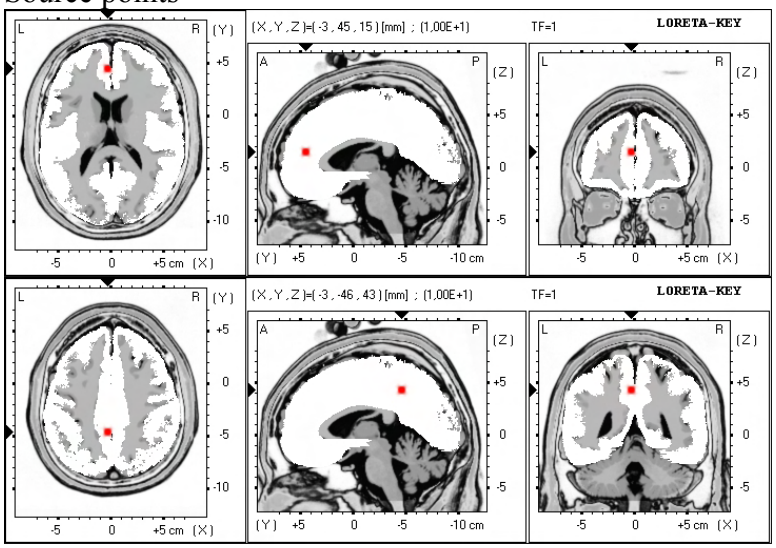

LORETA solution using 39 leads (maximum at fusiform gyrus of the temporal lobe)



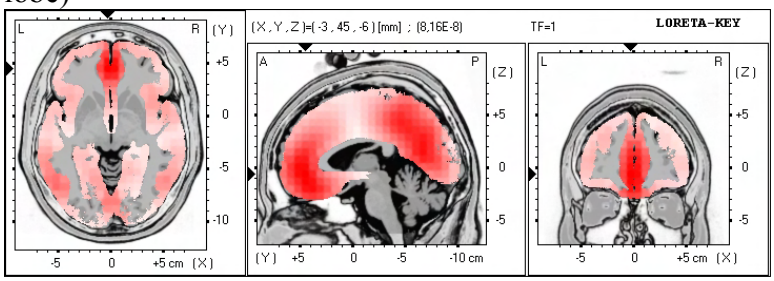
Comment: The 8-lead solution locate some locus of maximal activity in the back right portion of the brain and another locu, of nearly the same intensity, in the frontal region, although the anatomical positions of the local maxima are misallocated. It is interesting to note that both 16-lead and 39-lead solutions also position the back source in different anatomical region but furthermore, the frontal source is greatly reduced.

**Figures 7.2.10, Simulation 10: Sources of simulation 3 and 4 combined (source points 1344 and 1915)**

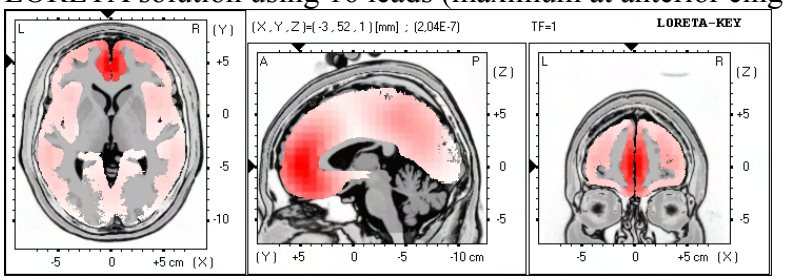
Source points



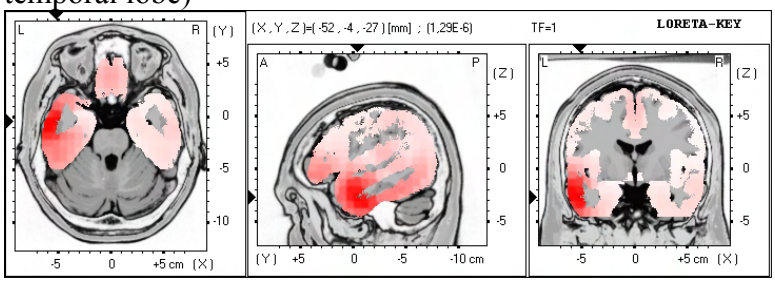

LORETA solution using 8 leads (maximum at medial frontal gyrus of the frontal lobe)




LORETA solution using 16 leads (maximum at anterior cingulate of the limbic lobe)



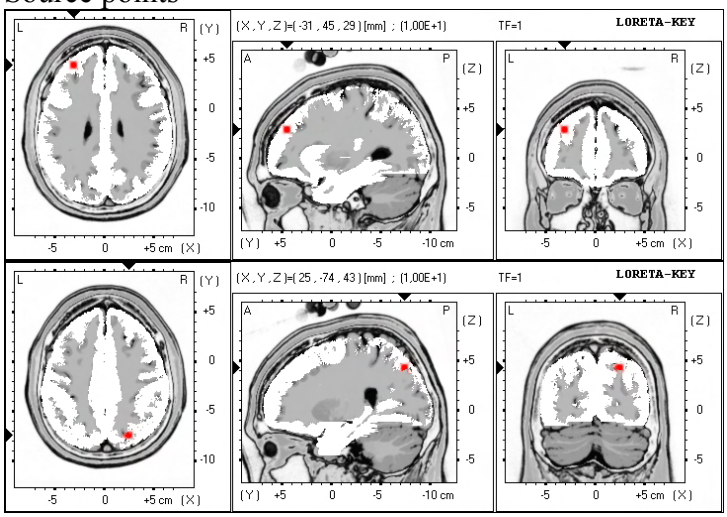

LORETA solution using 39 leads (maximum at middle temporal gyrus of the temporal lobe)



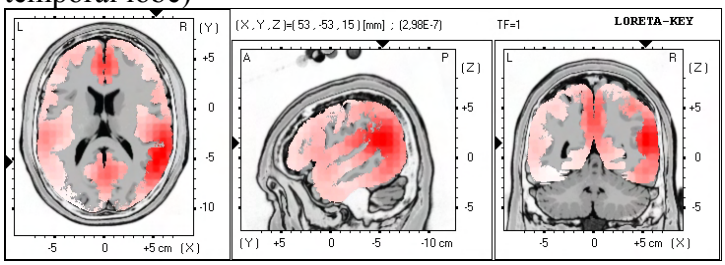
Comment: As was the case for the single source simulations, the 8-lead solution provides an accurate localization of both original sources, keeping hemisphere position and proximity to the midline. The 8-lead solution is better than the 16- or 39-lead solutions.

**Figures 7.2.11, Simulation 11: Sources of simulation 1 and 7 combined (source points 1673 and 1875)**

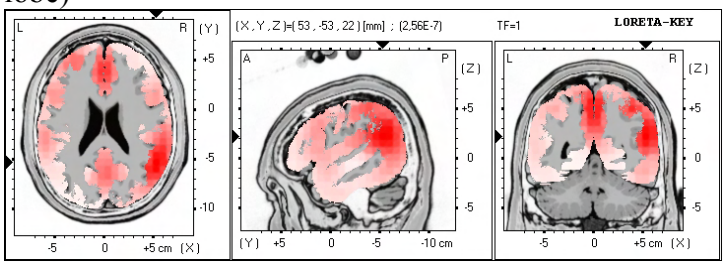
Source points



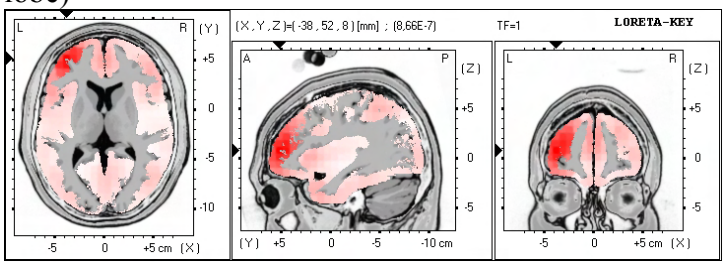

LORETA solution using 8 leads (maximum at superior temporal gyrus of the temporal lobe)




LORETA solution using 16 leads (maximum at inferior parietal lobule of the temporal lobe)



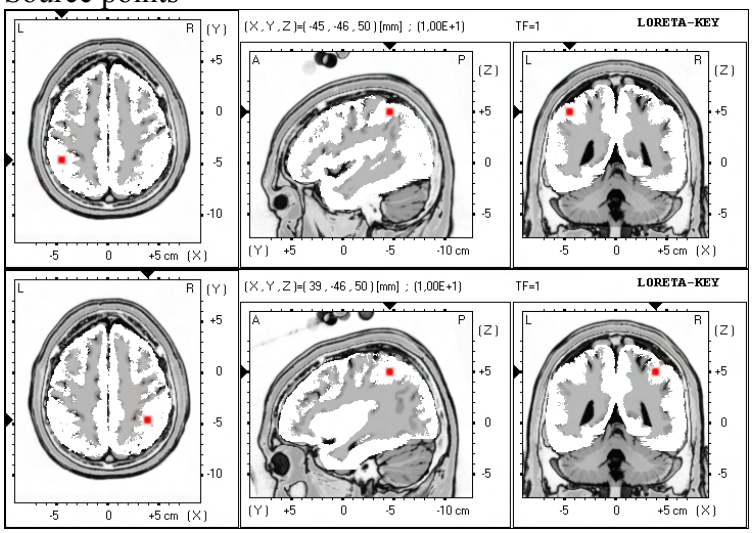

LORETA solution using 39 leads (maximum at middle frontal gyrus of the frontal lobe)



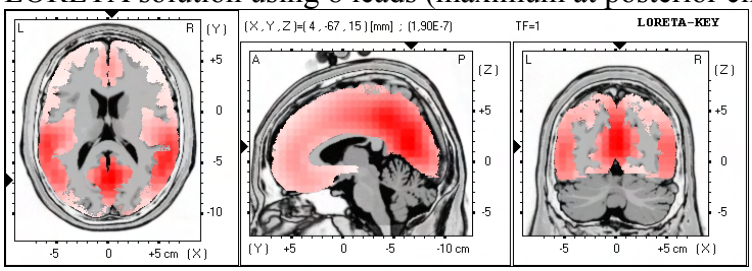
Comment: Again the performance of the 8-lead solution for the combined sources resembles the performance for the single sources, correctly locating a frontal locus of activity (although transferred to the midline) and a back right locus (although transferred from the temporal to the parietal lobe). The 16-lead solution presents the same characteristics as the 8-lead solution, while the 39-lead solution localizes accurately the frontal source "losing" the back source.

**Figures 7.2.12, Simulation 12: Sources of simulation 5 and 6 combined (source points 2077 and 2085)**

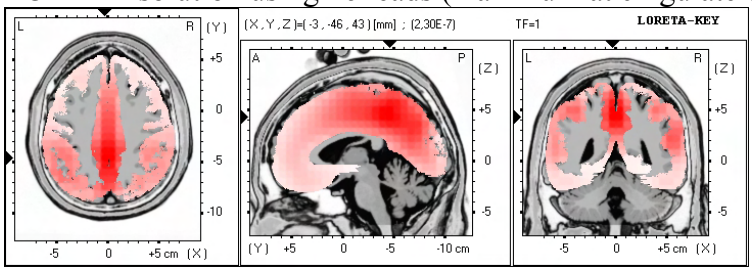
Source points



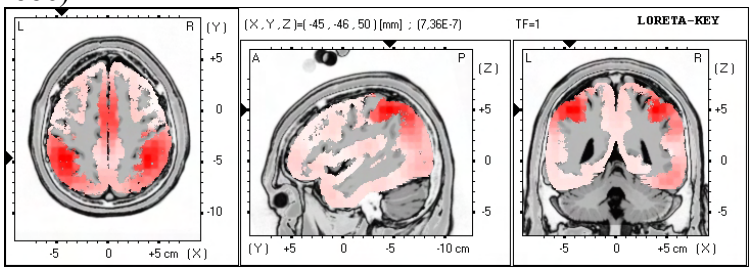

LORETA solution using 8 leads (maximum at posterior cingulate of the limbic lobe)




LORETA solution using 16 leads (maximum at cingulate of the limbic lobe)




LORETA solution using 39 leads (maximum at inferior parietal lobule of the parietal lobe)

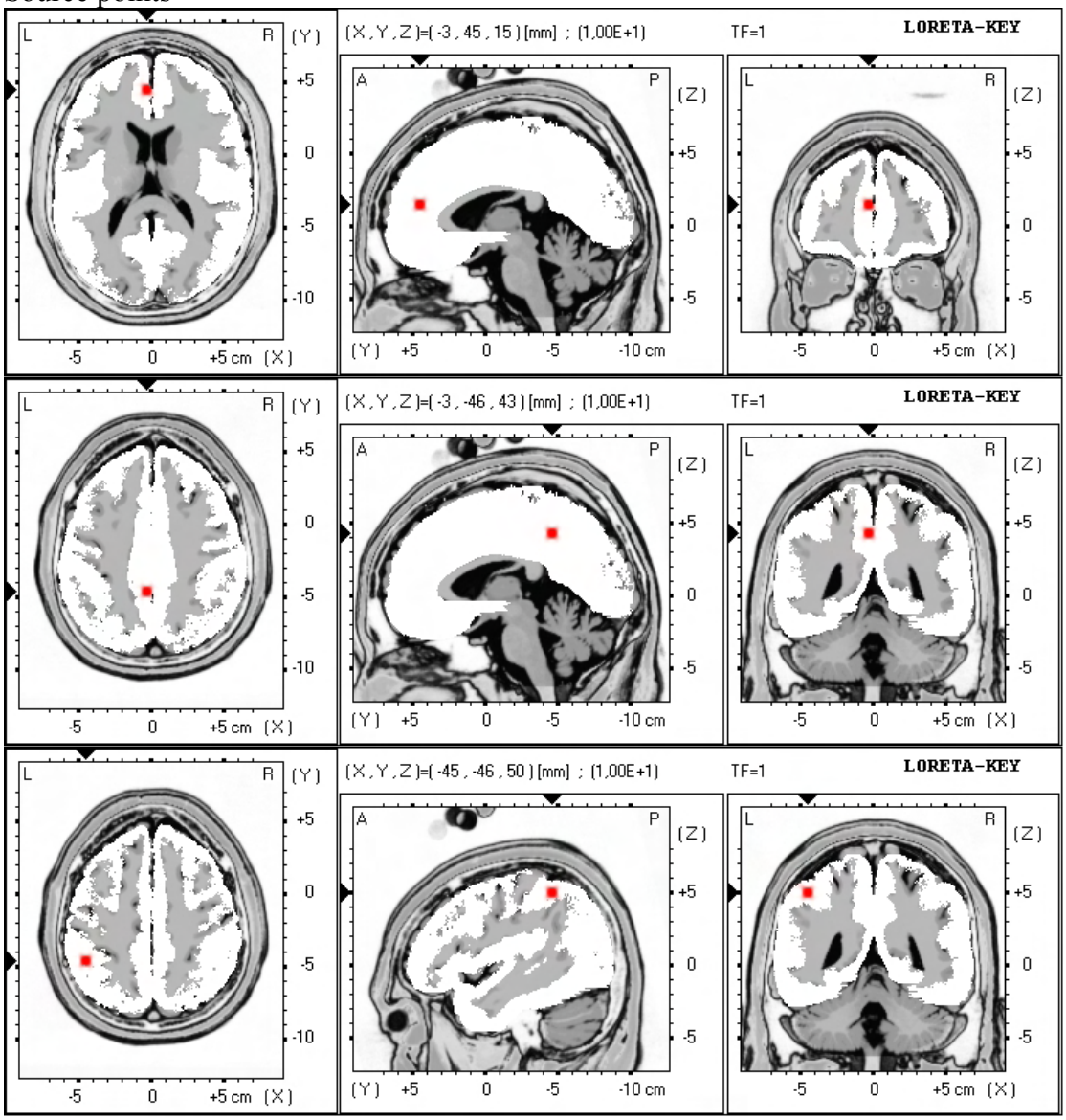


Comment: Concerning the 8-lead solution, both the left and right parietal loci of activity exists, although with a reduced Z coordinate (as in single-source solutions) but now a spurious midline locus exists, which supersedes them. The 16-lead solution overstresses this midline locus, while the best match is achieved from the 39-lead solution.

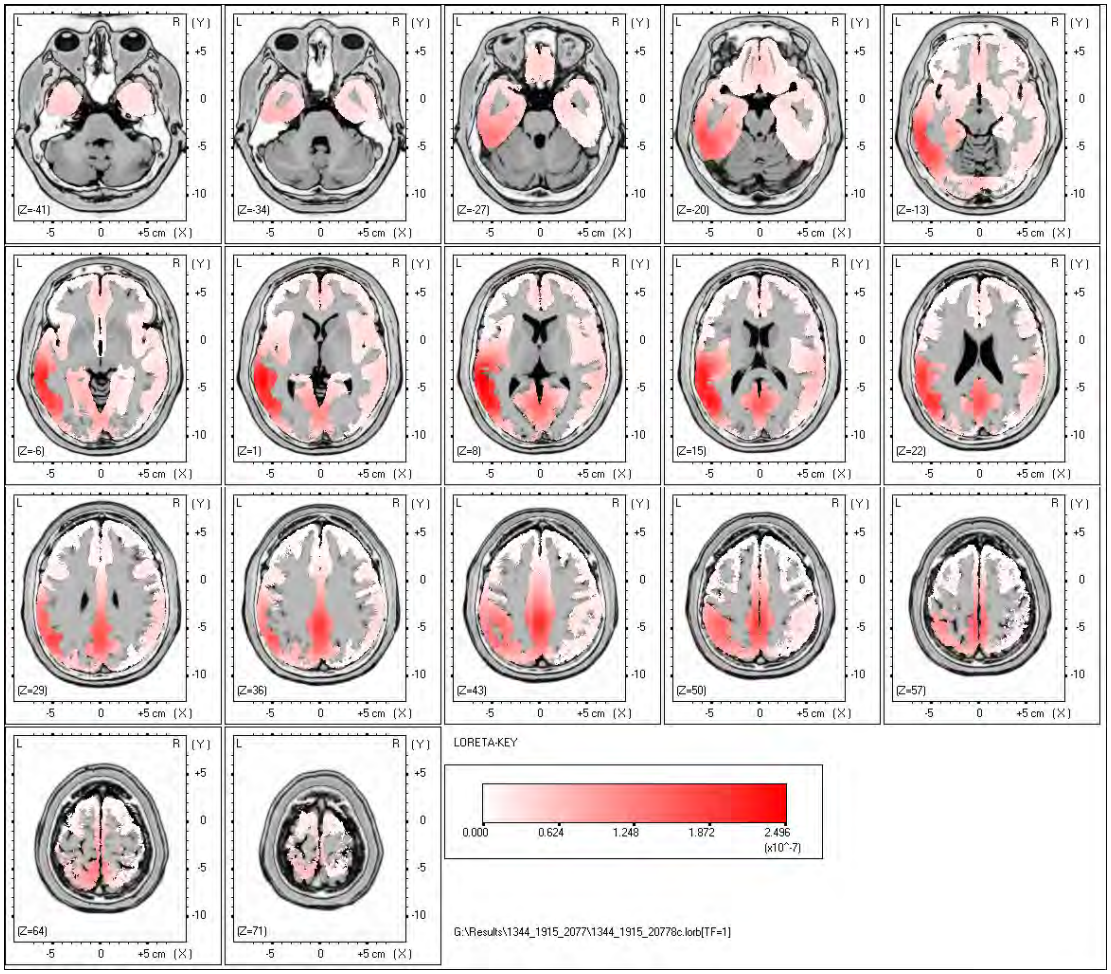
Note: In the following simulations, which involve three sources concurrently, we present, apart from the three-slice image centered on the absolute maximum, also an image which includes all the horizontal slices produced by LORETA, (this image is automatically produced by the LORETA Viewer), since due to the existence of three loci of interest, the slices centered on the maximum do not provide an overall view of the topography of the solution.

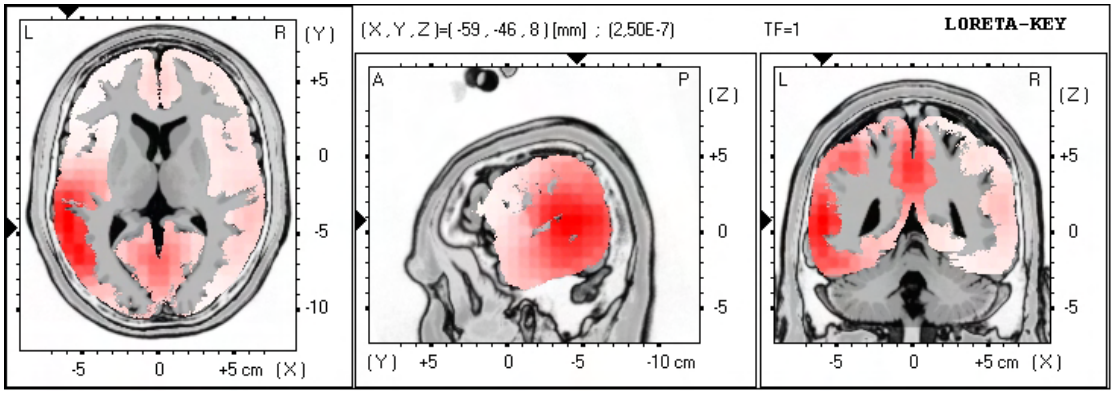
**Figures 7.2.13, Simulation 13: Sources of simulation 3,4 and 5 combined (source points 1344,1915 and 2077)**

Source points

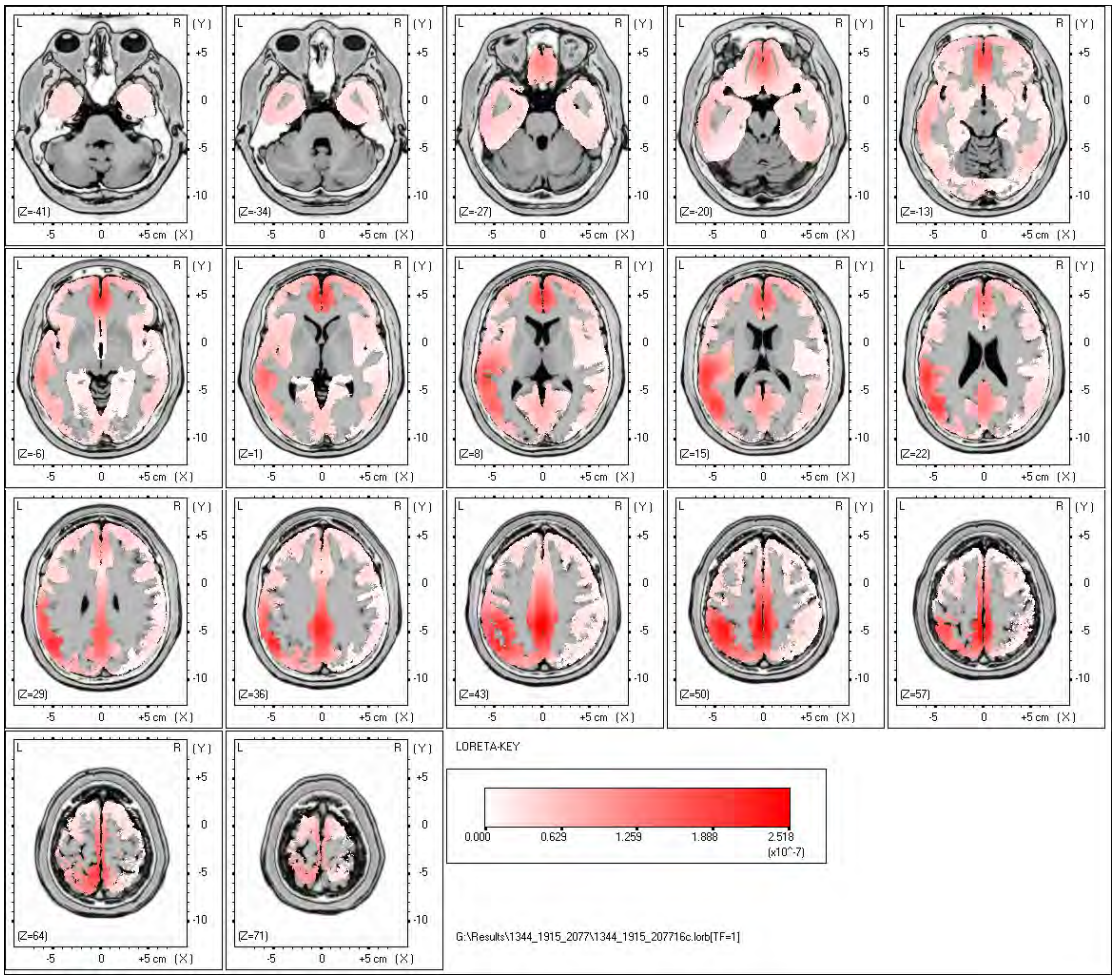


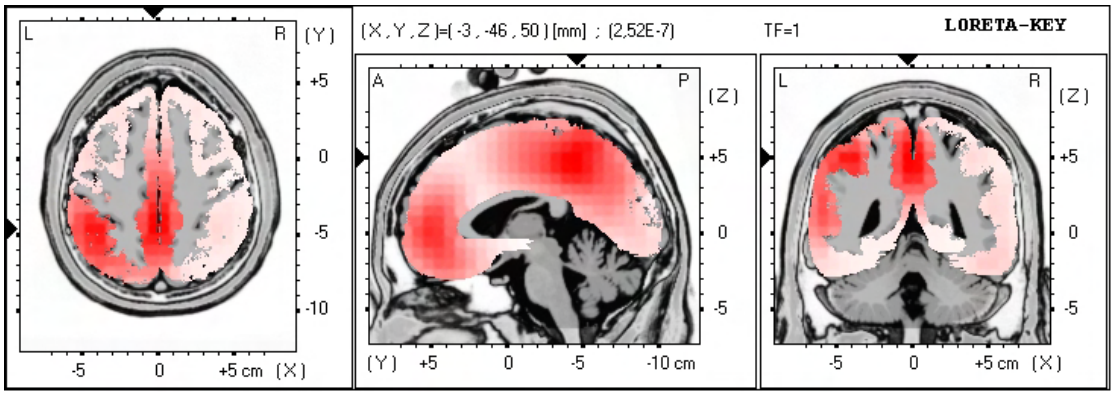
LORETA solution using 8 leads (maximum at middle temporal gyrus of the temporal lobe)



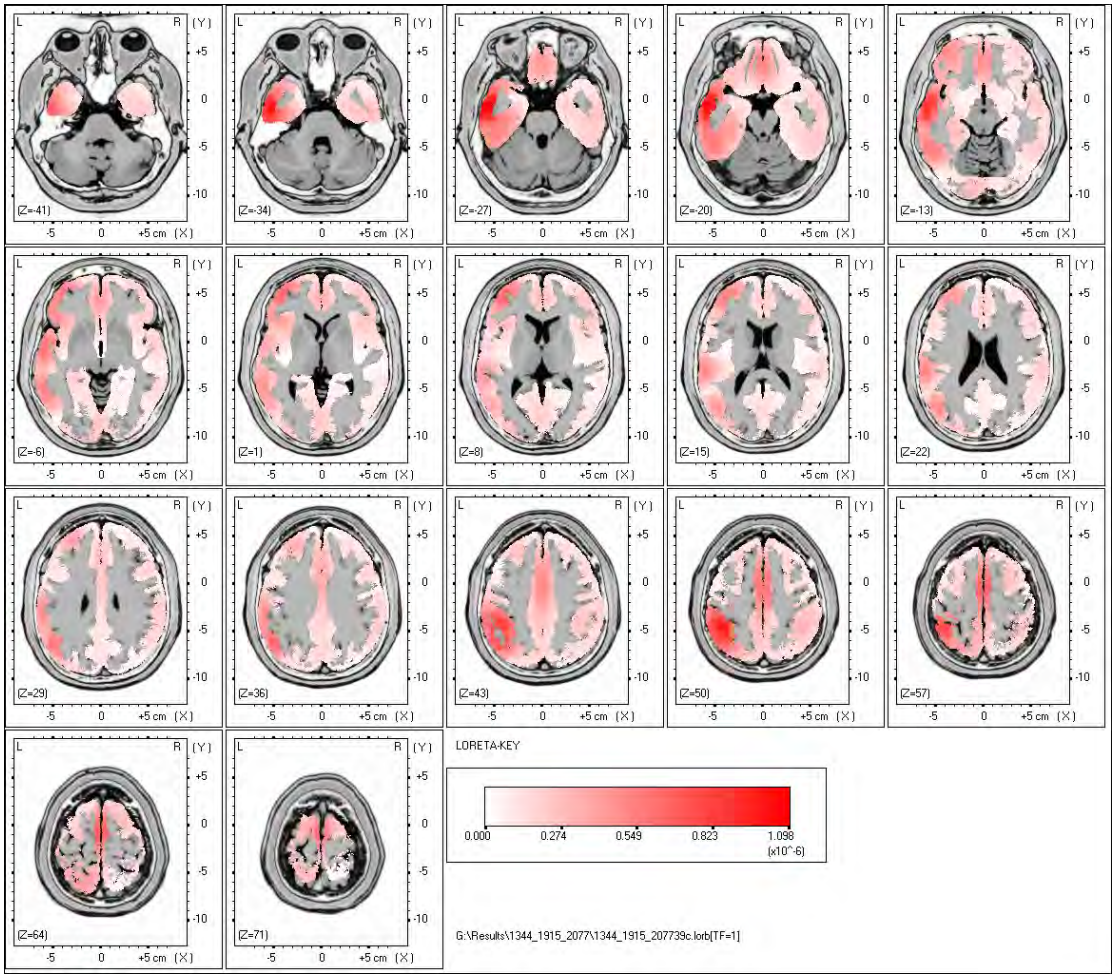



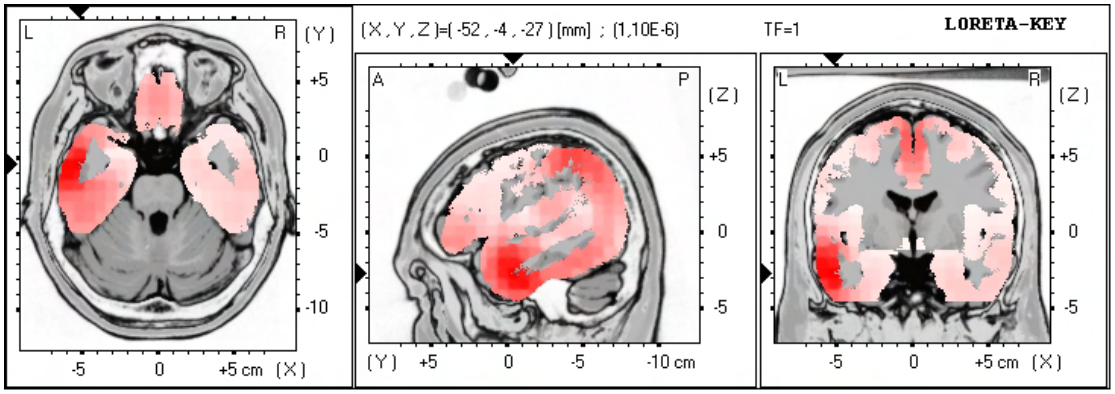
LORETA solution using 16 leads (maximum at precuneus of the parietal lobe)



LORETA solution using 39 leads (maximum at middle temporal gyrus of the temporal lobe)

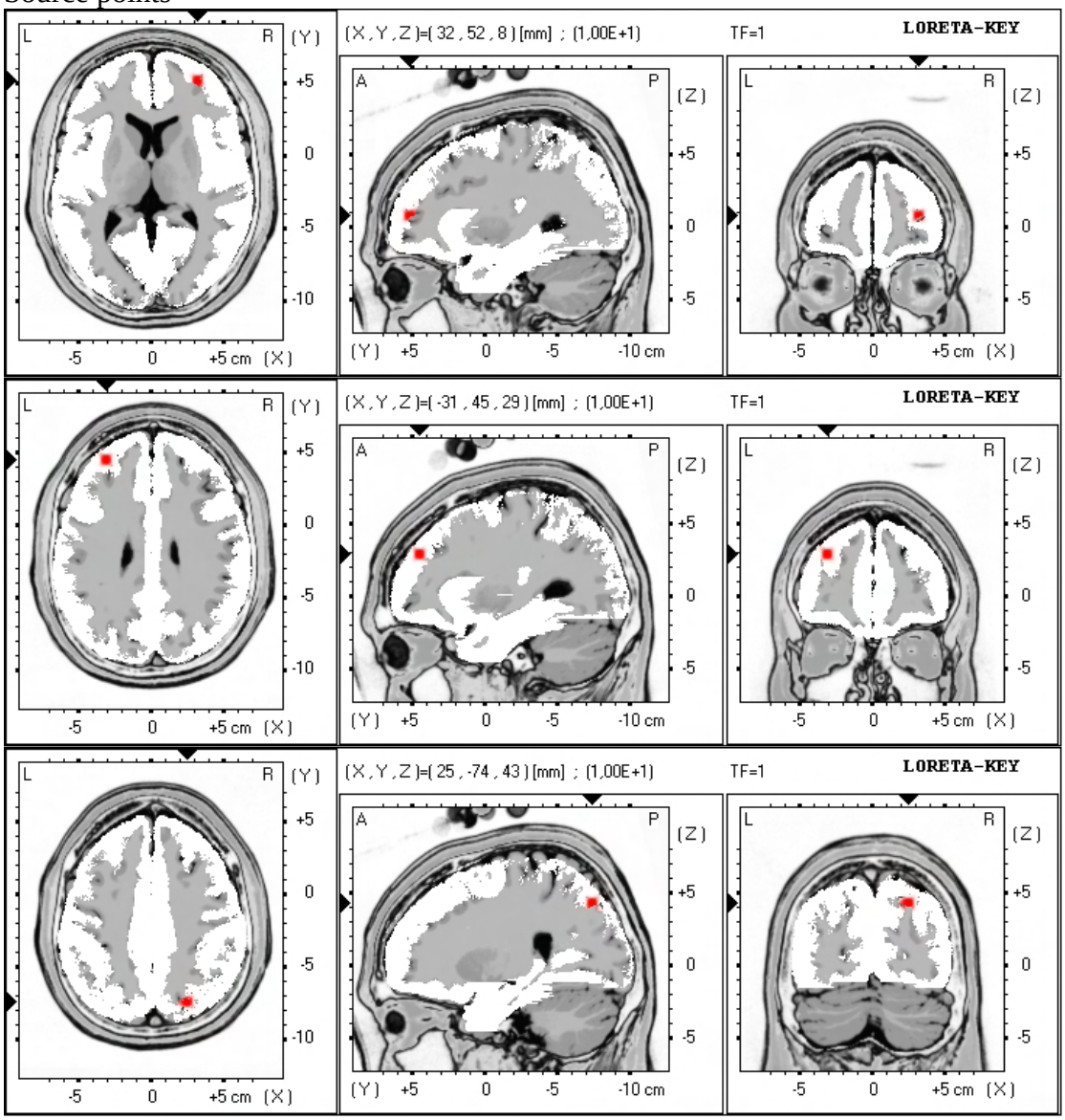


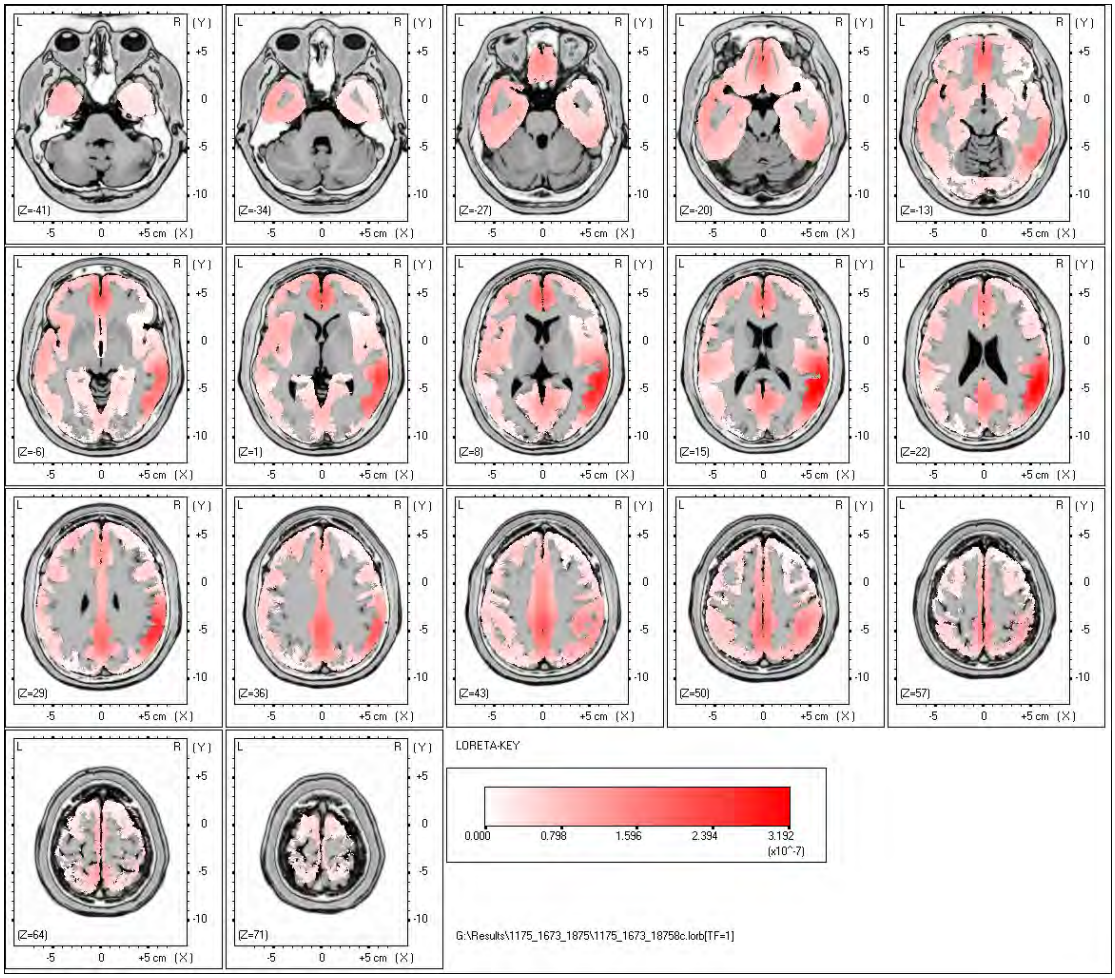

Comment: The 8-lead solution presents an image which is resembling the combination of the single-source reconstructions, i.e. the back left and the centro-posterior left midline sources keep their hemisphere positions and gross localization area but the frontal source, although detected, is much reduced, compared to the other two sources. The best reconstruction is achieved for 16-leads, which detects the frontal source on a par with the other two, while the 39-lead solution greatly mislocates the frontal source.

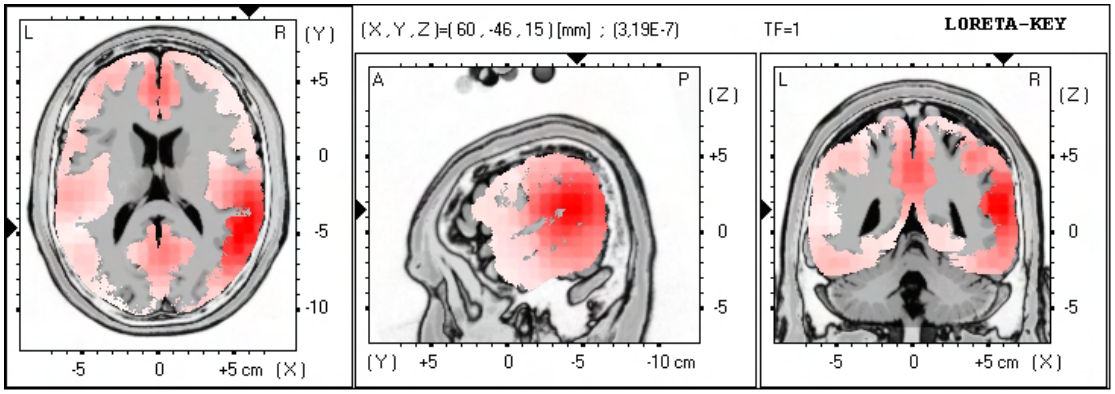
**Figures 7.2.14, Simulation 14: Sources of simulation 1,2 and 7 combined (source points 1175,1673 and 1875)**

Source points

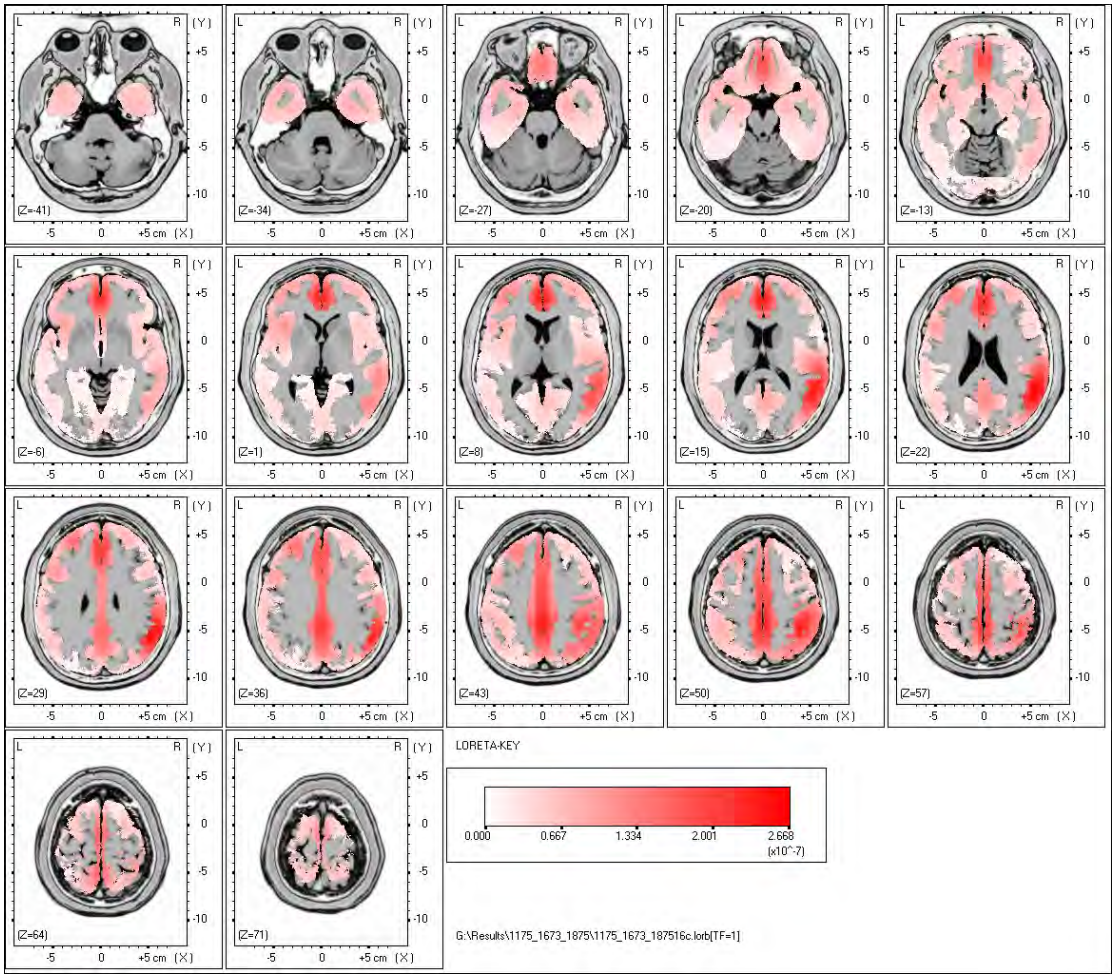


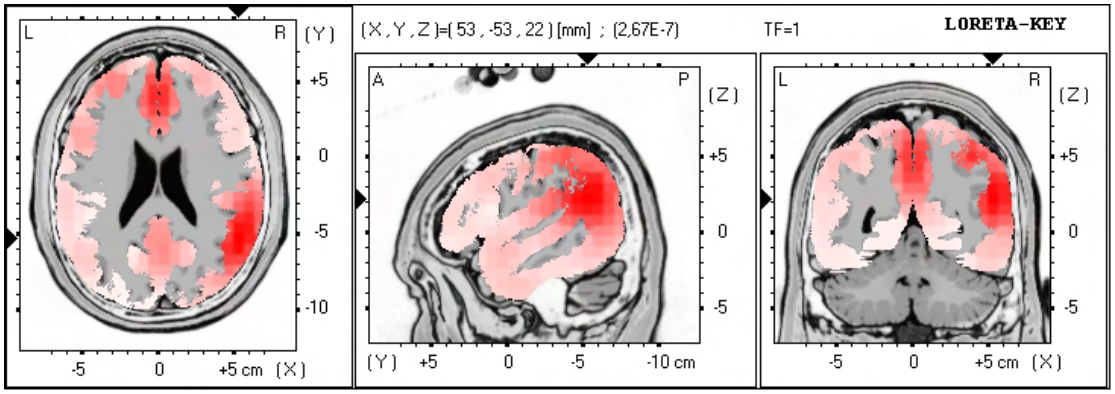
LORETA solution using 8 leads (maximum at superior temporal gyrus of the temporal lobe)



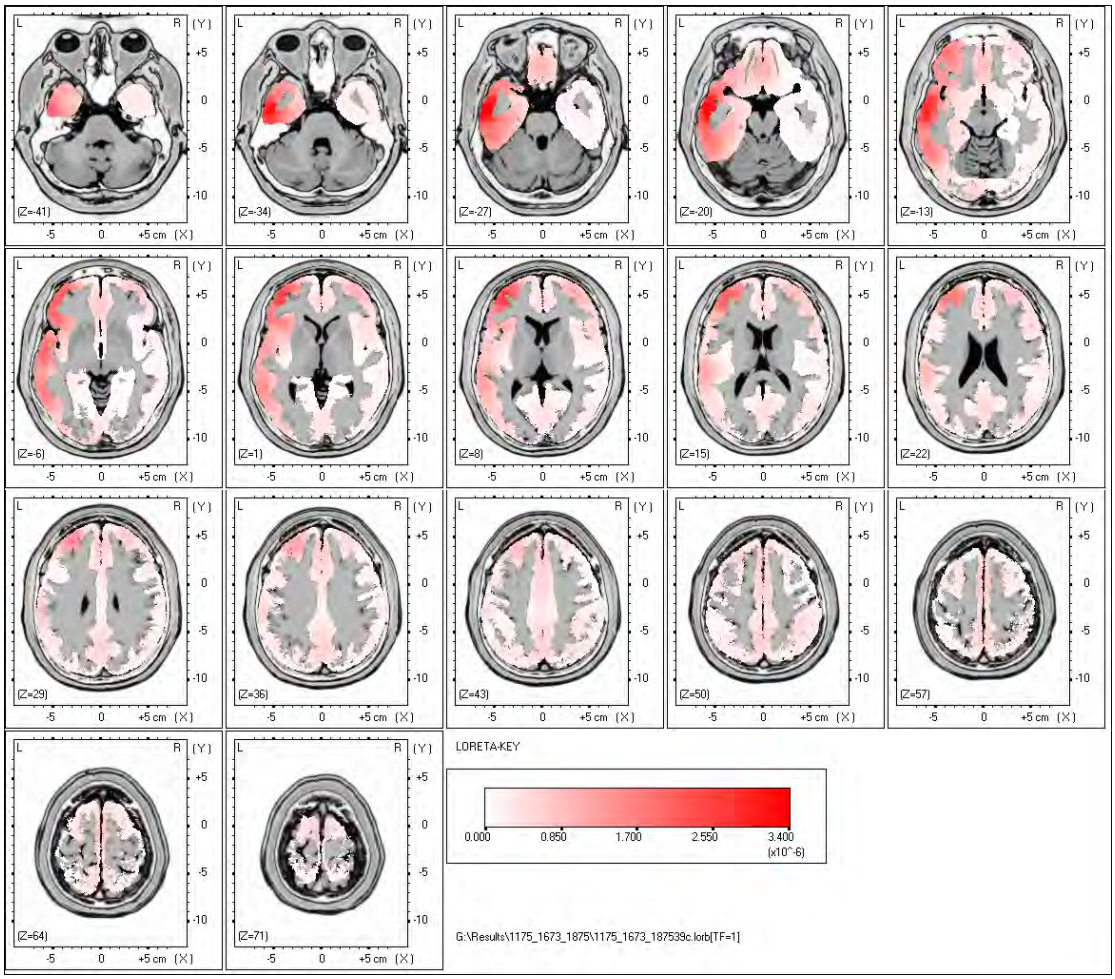



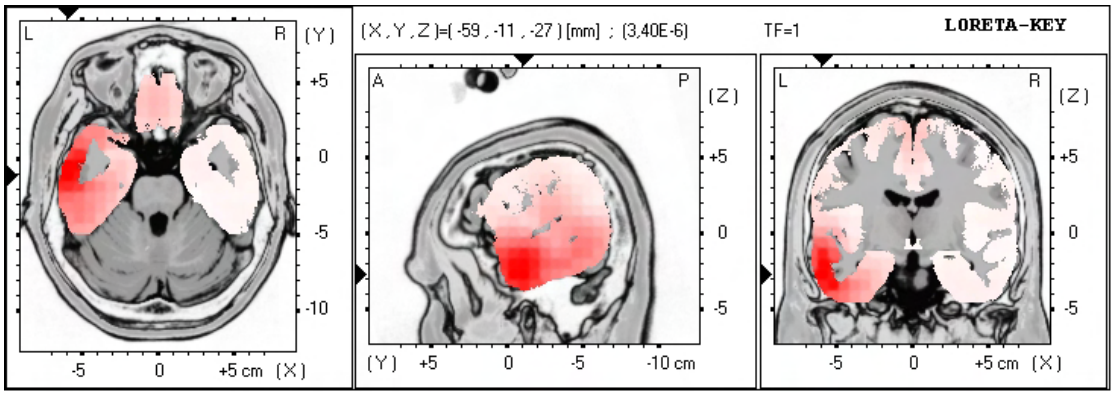
LORETA solution using 16 leads (maximum at inferior parietal lobule of the temporal lobe)



LORETA solution using 39 leads (maximum at fusiform gyrus of the temporal lobe)

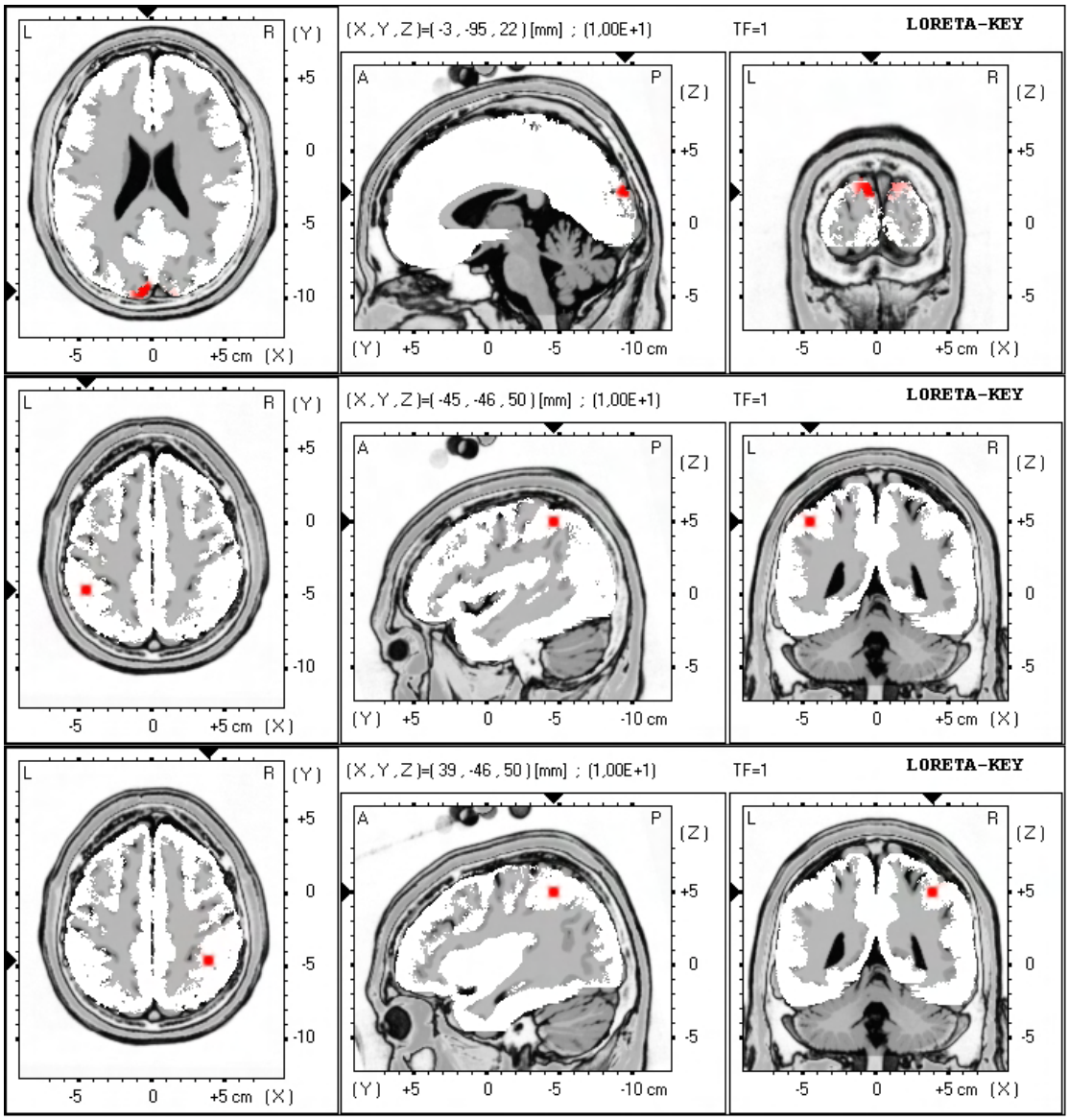


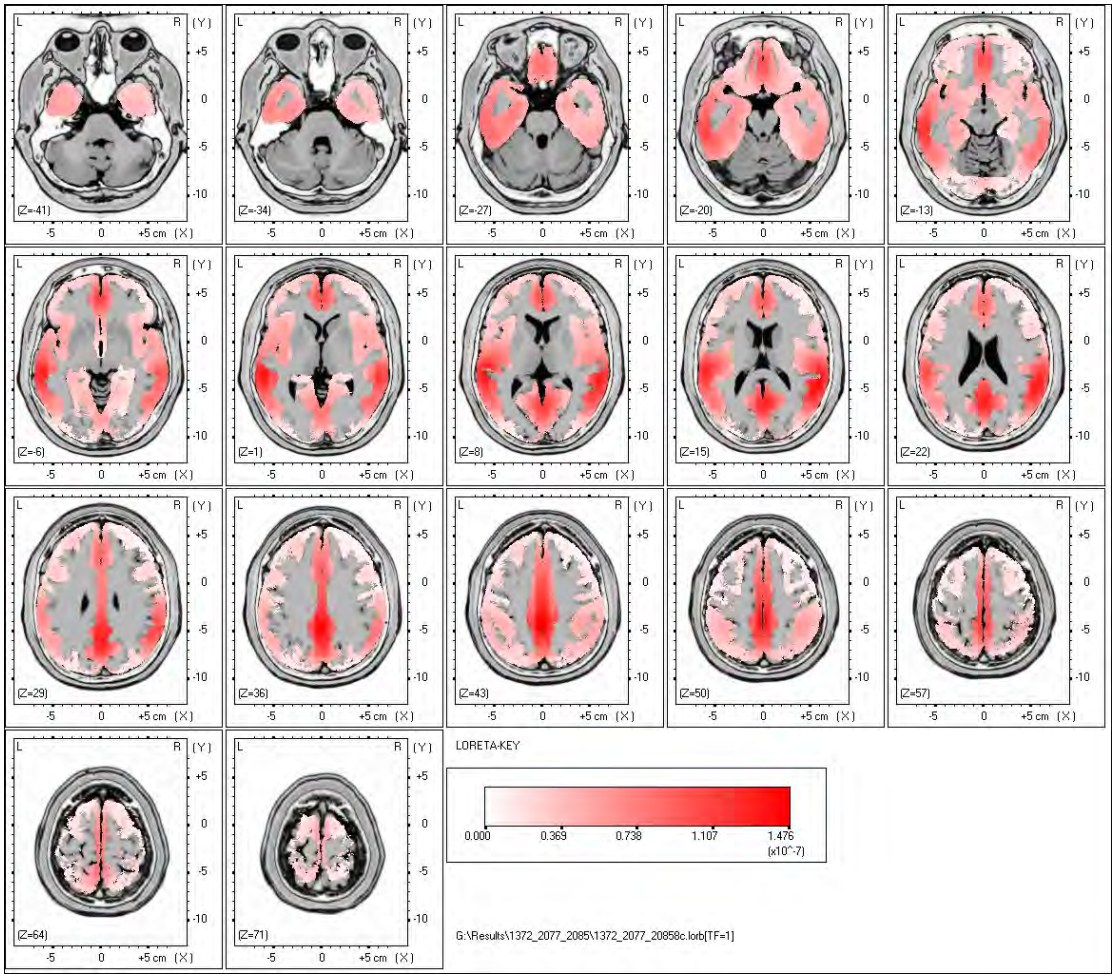

Comment: Again the 8-lead solution presents an image which resembles the combination of the single-source reconstructions, i.e. the two frontal and the back midline right sources are detected, with the same degree of mislocation as in the single-source cases. The 16-lead reconstruction resembles the 8-lead, except that it presents a spurious high amplitude centro-posterior midline locus of activity. The 39-lead solution correctly localizes the left frontal source, while mislocates the other frontal source and seems to "loose" the back source.

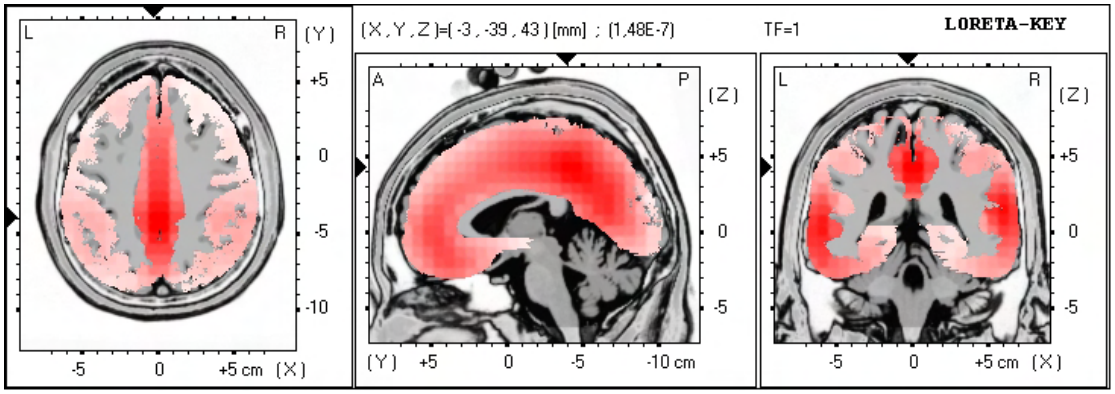
**Figures 7.2.15, Simulation 15: Sources of simulation 5,6 and 8 combined (source points 1372,2077 and 2085)**

Source Points

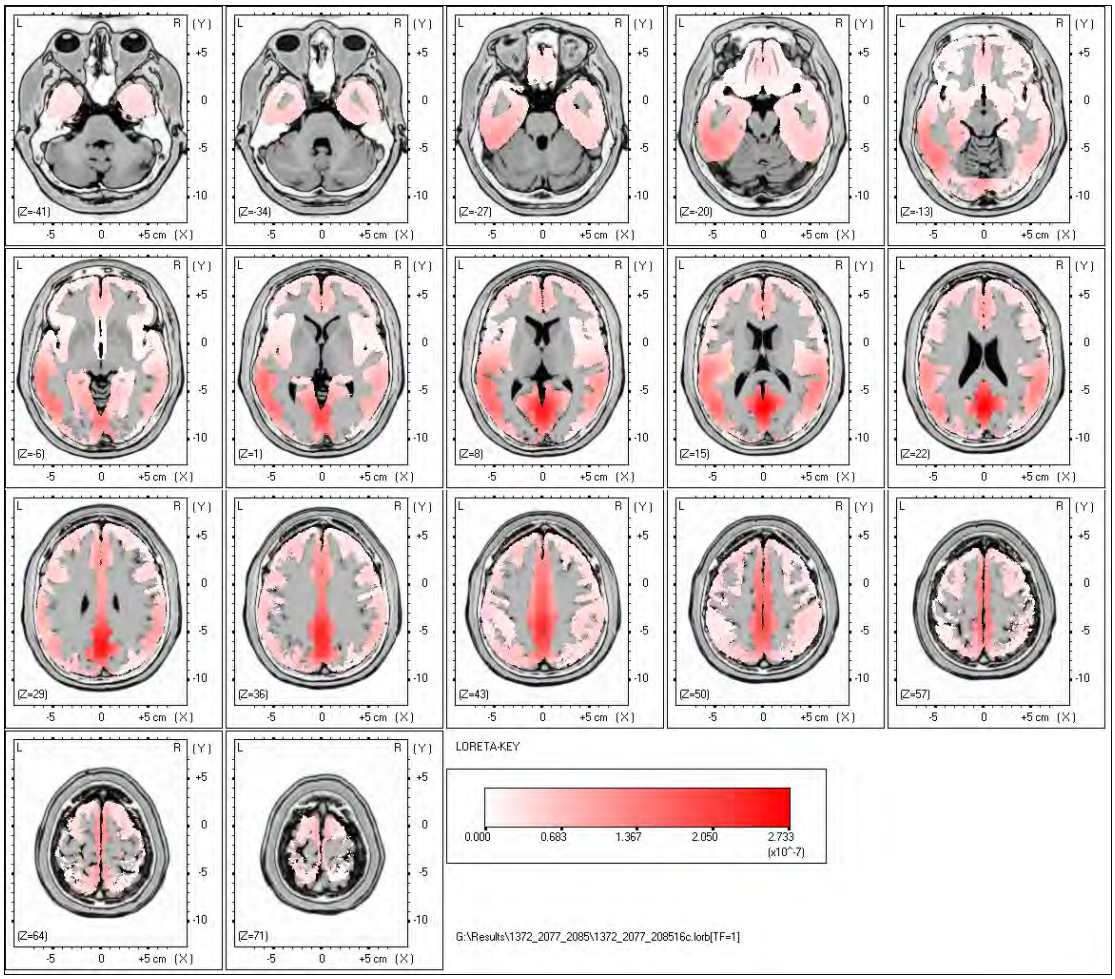


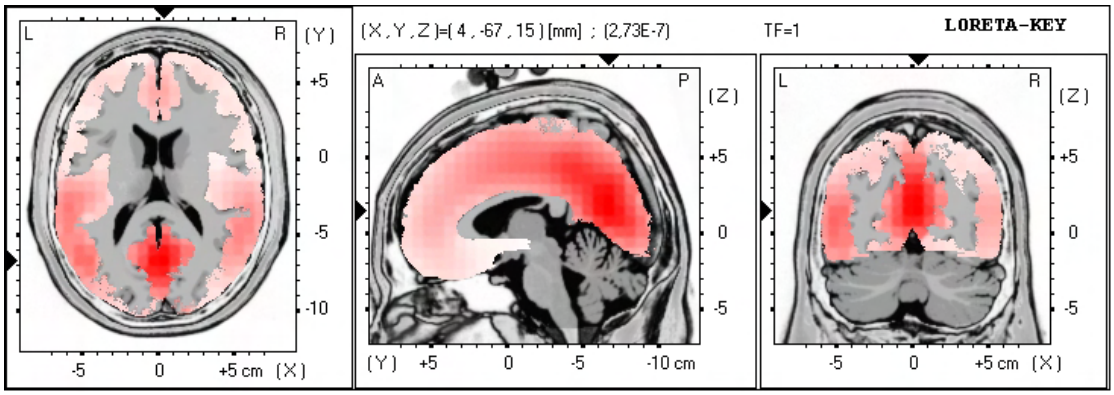
LORETA solution using 8 leads (maximum at cingulate gyrus of the limbic lobe)



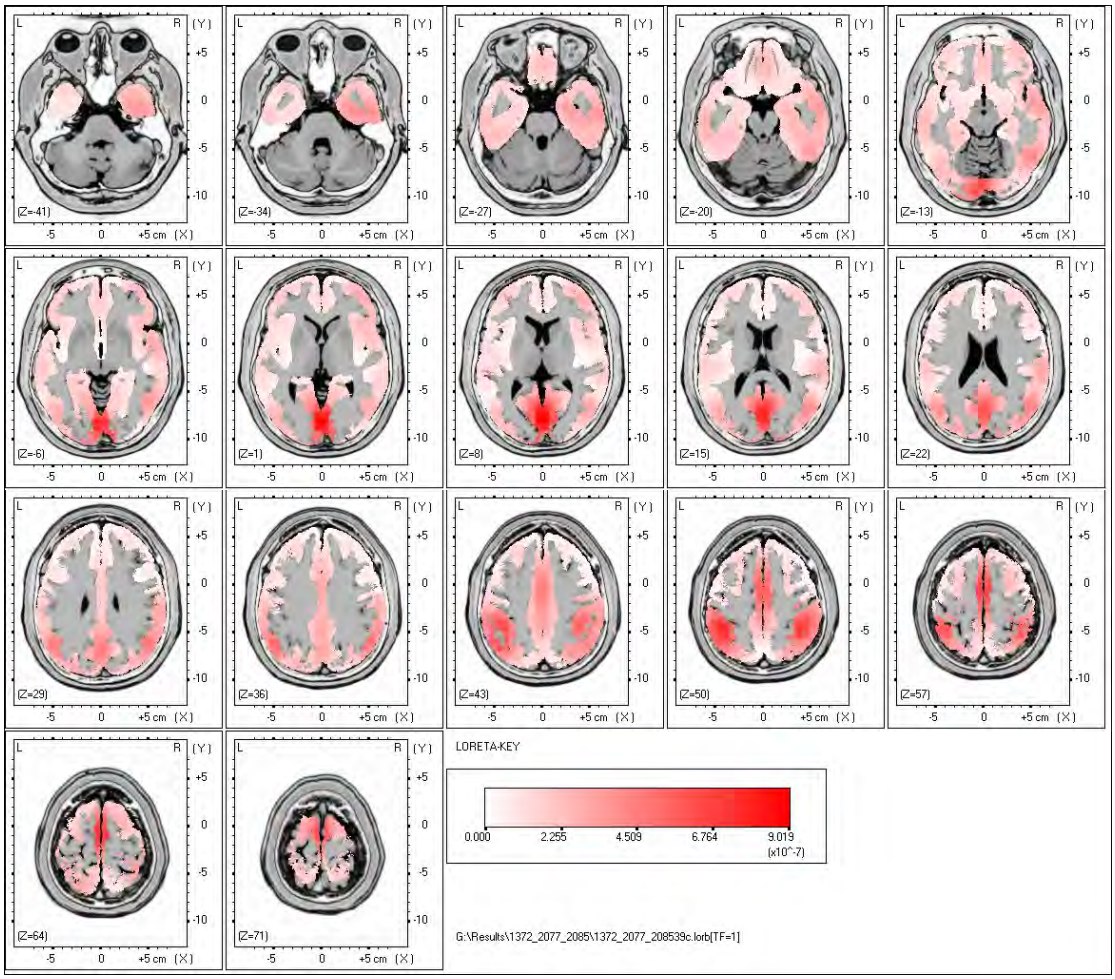



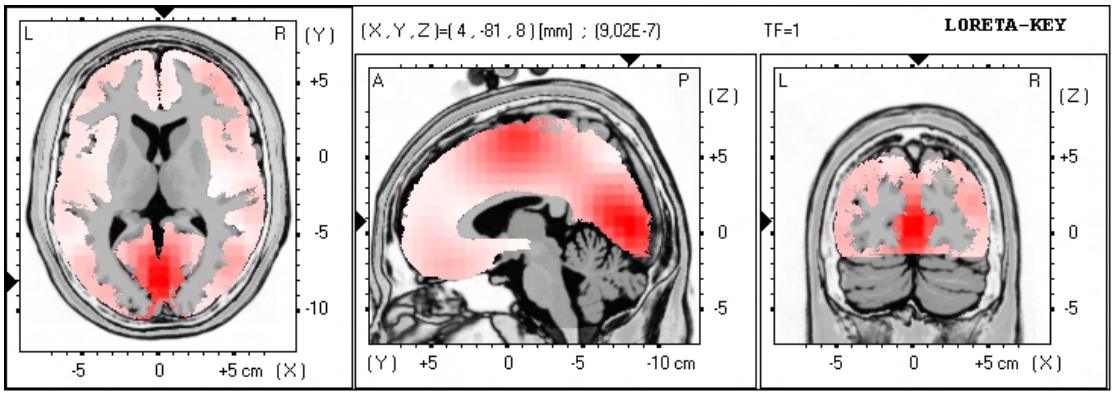
LORETA solution using 16 leads (maximum at posterior cingulate of the limbic lobe)



LORETA solution using 39 leads (maximum at cuneus of the occipital lobe)




Comment: Concerning the 8-lead solution, the two left and right parietal sources are moved to the left and right temporal position respectively, while the midline occipital source is kept to a back midline position, in part resembling the performance for single sources. The 16-lead solution detects the same three loci of activity, but reduces the amplitude of the temporal sources, while the 39-lead solution correctly locates the original parietal sources and therefore presents the best localization performance.

## 7.3) Performance evaluation

The aim of the simulation study was to determine to which level the localization information provided by LORETA solution we 8-lead data could be used in the spindle localization that was needed in the present Thesis. Based on the single-source simulations, an overall conclusion is that the reconstruction provide an indication of the gross brain area where sources may exist, i.e. whether they are anterior or posterior. This is important for our study, since the main distinction of sources for the slow and the fast spindles is between frontal and more centro-posterior areas. Lateralization information was also kept. Concerning lateralization, when the source was located at the right and left anterior brain part, the reconstructed sources was moved to the frontal midline area, in one case giving wrong hemisphere position. This may due to the reduced number of electrode available, since the simulations with 16 and 39 electrodes did not present this mislocation. On the other hand, there were cases were parietal sources were moved to temporal locations and occipital sources to more anterior position (though still clearly in posterior sites). When two or three sources were present, results did not differ significantly from single-source simulations. Another interesting insight gained from the simulation was that, although the 39-lead should, and in most single-source cases provided the best localization performance, this was not always the case when more than one sources were included in the simulation. This has to act as a reminder of the limitation of inversion techniques, especially those that use analytical instead of discrete head models.

Having the above in mind, in the LORETA results that were computed using the real 8-lead data, we concentrated our attention in whether the sources were in the anterior or posterior part of the brain, and secondarily to which hemisphere these were located. The exact brain area indicated by LORETA was not deemed to possess accurate information for making inferences about the detailed anatomical regions responsible for the spindle components. On the other hand, the locations of the local maxima of the real-data LORETA source distributions, were compared between parts of the spindle and spindle components, not from the scope of accurate localization, but from the scope of comparing whether the regions of the local maxima remained or not the same between parts of the original spindle and between spindle components. This is based on the assumption that, even if there is a mislocalization of the loci of the source activity, due to the limited number of leads, this mislocalization would be kept the same, i.e. the same regions would be indicated by the 8-lead LORETA solution, if the underlying sources are kept constant between parts of the spindle and between spindle components. In case we possessed more electrodes, the regions indicated by LORETA would additionally be the correct anatomical regions, concerning not only anterior-posterior and lateralization but also detailed brain structures, to the level provided by the Talairach atlas, on which the MNI brain is based.

# Chapter 8: Results

## 8.1) Introduction

At this chapter we will present the results of the research work carried on. We will present first the spindle characteristics, as extracted through the spectrogram analysis and ICA processing, then the activity of the sources for the parts that the original source was divided into, and finally the conclusions from the source investigation of the ICA reconstruction of the particular spindle. We present results for the division of spindles into two parts A and B, and as explained in the Chapter 6.1 "ICA-Based EEG Processing", for each part of the original spindle timeframe we possessed three 3D mean source activity maps, one for the sources of the original EEG in that part, and one map for the sources of each EEG reconstruction, i.e. each spindle component, which are presented in each spindle analyzed, together with the position and strength of the four most powerful sources.

## 8.2) Spindle 1 *(1st Third of the Night)*

**Spindle Characteristics:**

1) It starts with frequency 14(+/- 1)Hz and progressively, after about 0,5 sec we have transition to 12 Hz and after 1 sec, from the start of the spindle, to 11 Hz. The transition does not happen simultaneously at all leads.

2) EEG division and ICs grouping:

By visual observation of the spindle's morphology we locate in some of them (F4, O2, F3, C3, O1) transition to lower frequencies than at the start, slightly after 0,5 sec. The transition from 12 Hz to 11 Hz is difficult to discern. If we try to divide the spindles at two parts, then, by observing the ICs, IC 4 is the only one that presents continuous high frequency activity from the spindle start till 1 sec, without transiting to lower frequencies afterwards. IC 1 has continuous high frequency activity from the spindle start till 0,8 sec approximately, but afterwards it transits to lower frequencies (12 Hz). Also IC 7 does not possess continuous high frequency activity at the part from the start of the spindle till 1 sec, specifically the activity is interrupted in the middle of the segment and has a morphology similar to beat. IC 5 has continuous activity but also changes its frequency (from 14 Hz to11 Hz), while IC 3 presents a high frequency part and later a low frequency one. So, with regards to the first spindle part IC 4 appears to possibly represent the initial high frequency activity of the EEGs, till and after 0,75 sec. Based on the above analysis, ICs 2 and 6 are the only which do not possess high frequency spindle-like activity at the first spindle part and when they present activity, this activity is continuous and low frequency, transiting from 12 to 11 Hz. IC 2 presents low-frequency activity in the first part also. Finally IC 4 will be the main component for part A (it ends at approximately 0,55 sec) and ICs 2 and 6 for part B.

For convenience, we present in Figures 8.2.1 the original spindles and the ICs, in Figures 8.2.2 the multiplots of each original EEG lead and in Figures 8.2.3 the multiplots of the ICs, as well as in Figures 8.2.4.a and 8.2.4.b the EEGs reconstructed by the respective ICs groups.

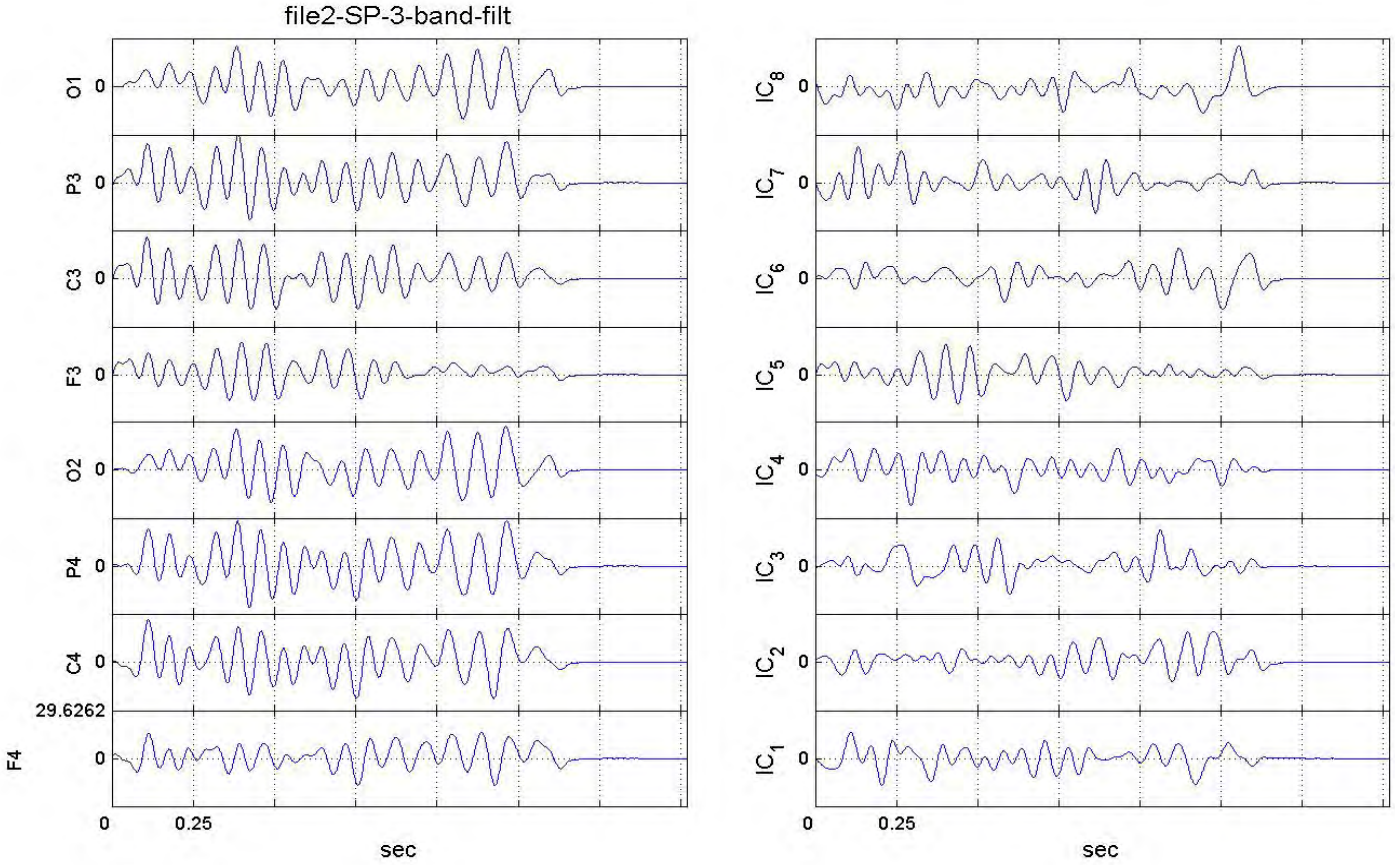
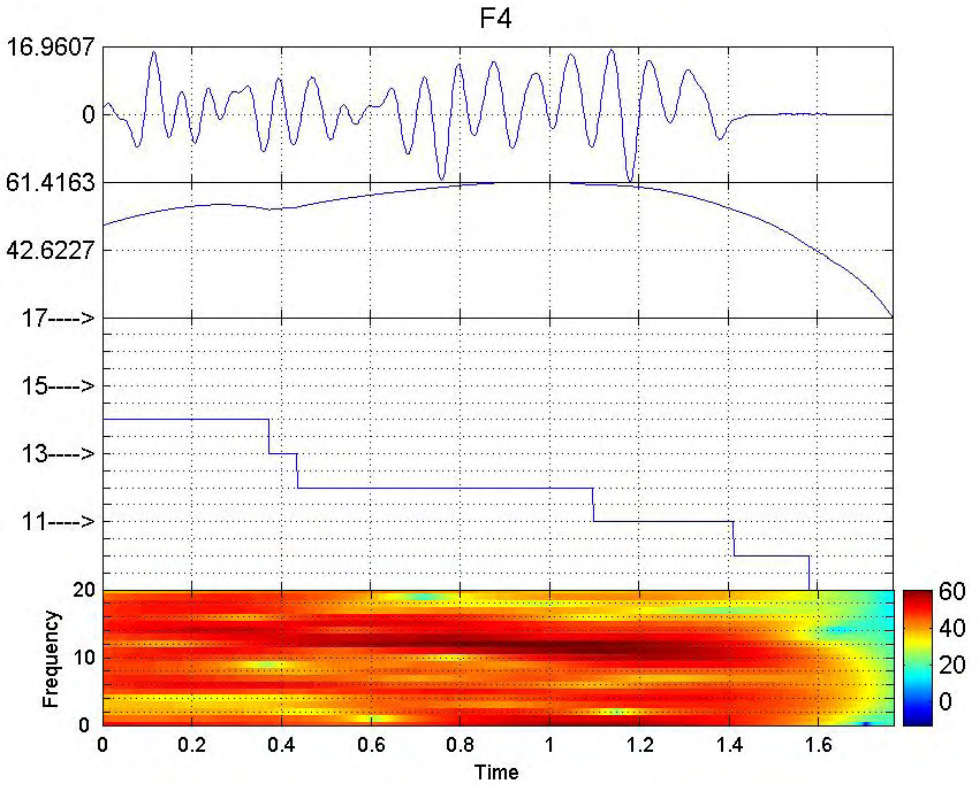
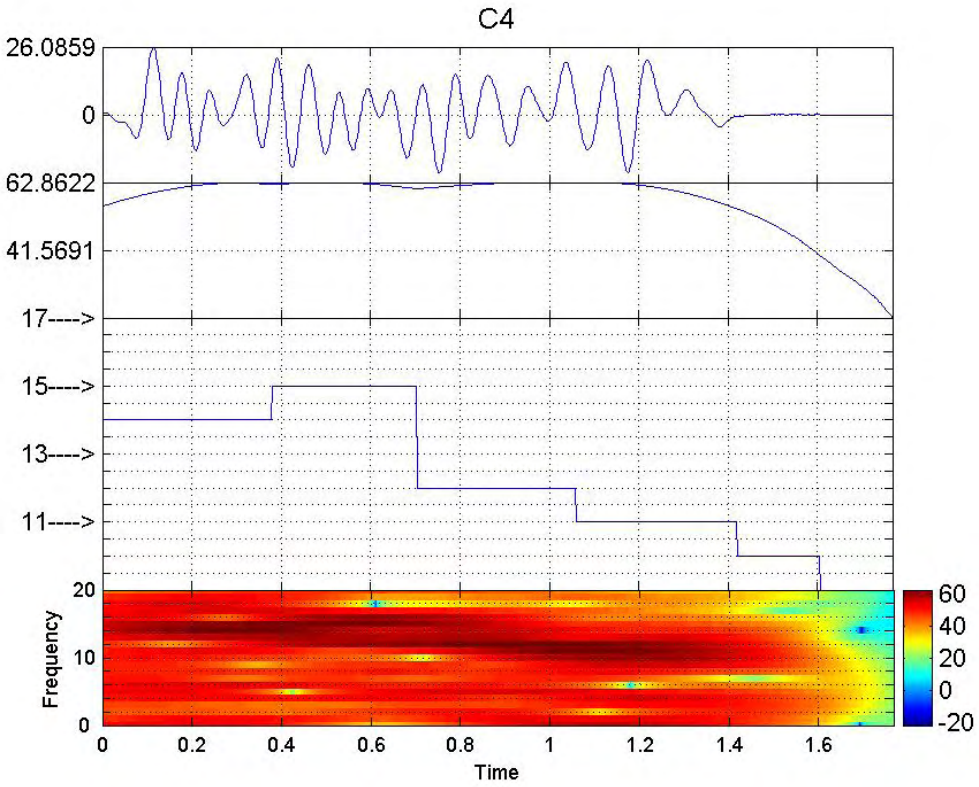
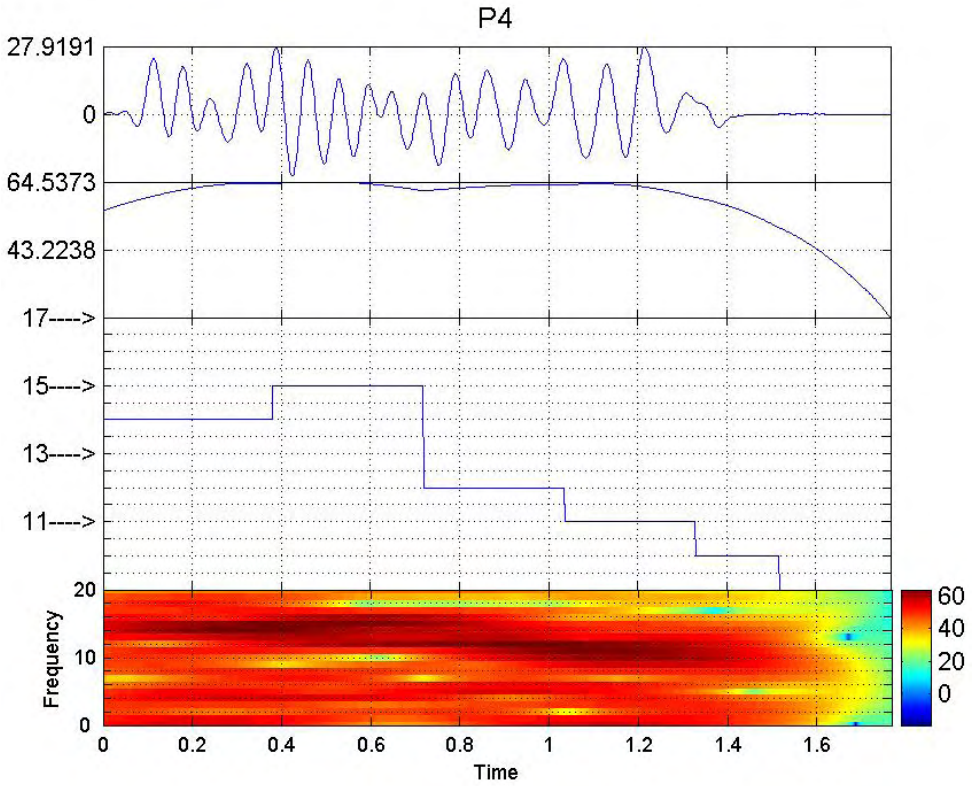


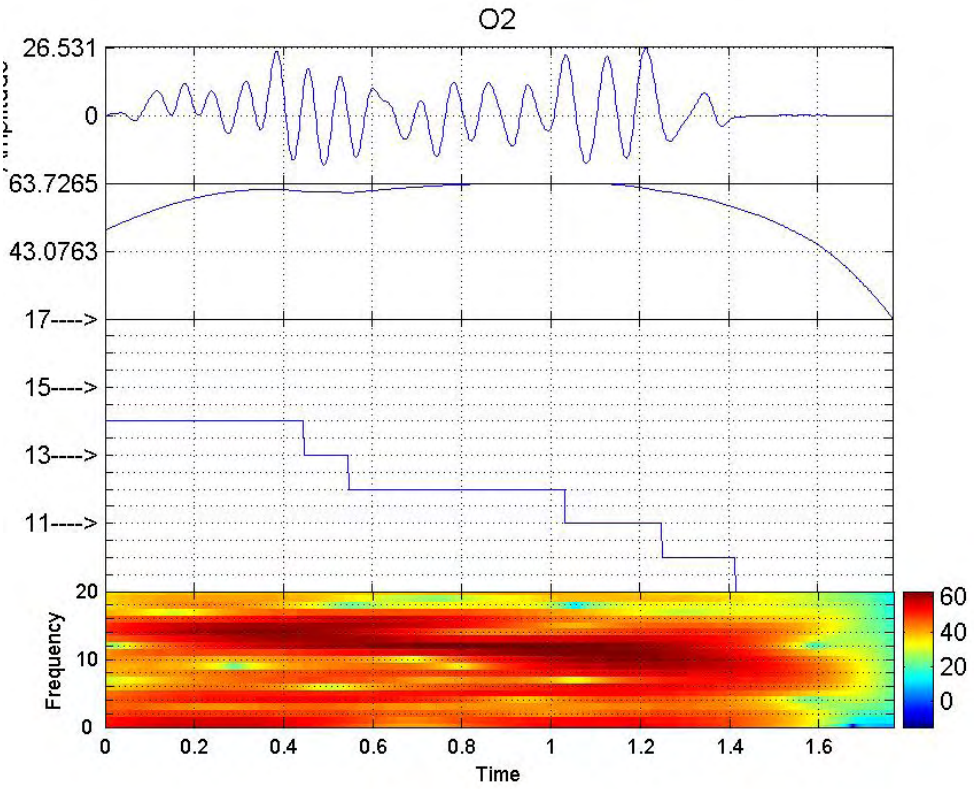

Figure 8.2.1: At left we have the original (filtered) EEGs and at right the ICs for spindle 1.

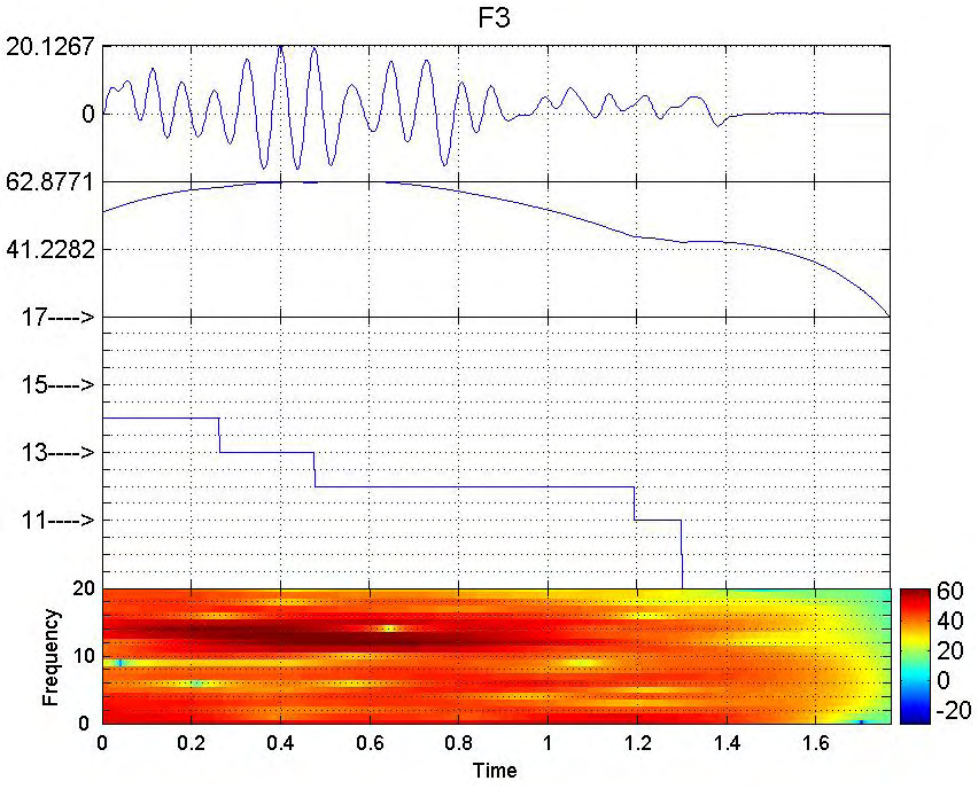
Figure 8.2.2: In the next 8 multiplots we present the spectral analysis of the original EEG channels for spindle1.

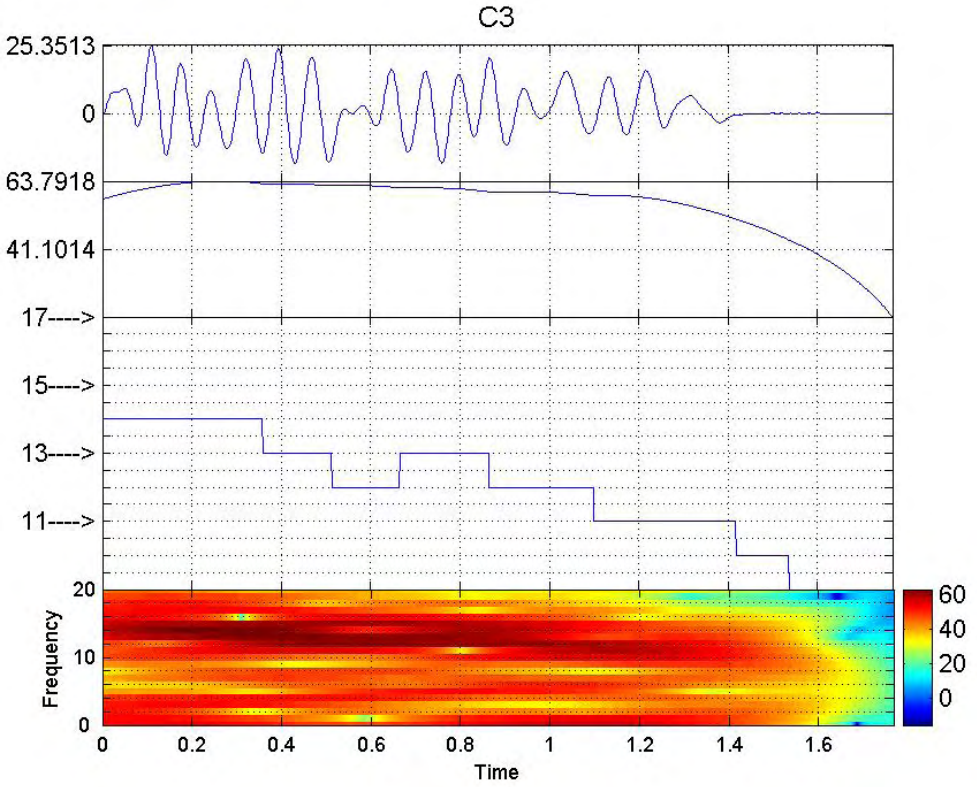


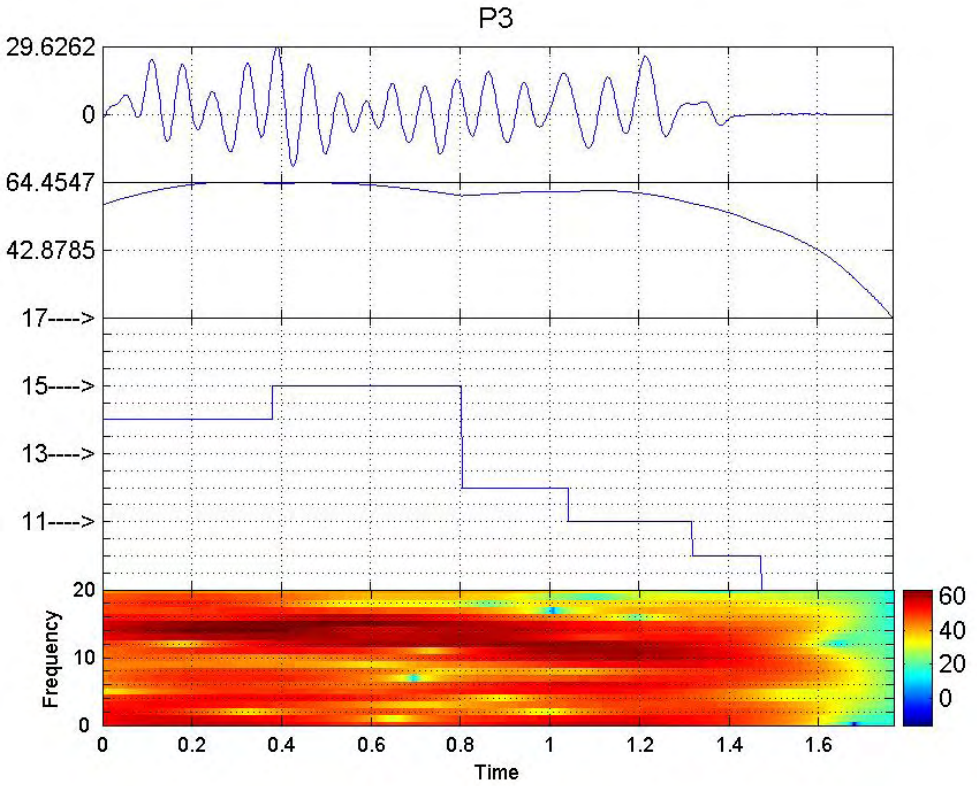




P4
27.9191
0
64.5373
43.2238
17---->
15---->
13---->
11---->
20
10
0
Frequency
0
0.2
0.4
0.6
0.8
1
1.2
1.4
1.6
Time
60
40
20
0


O2
26.531
0
63.7265
43.0763
17---->
15---->
13---->
11---->
20
10
0
Frequency
0
0.2
0.4
0.6
0.8
1
1.2
1.4
1.6
Time
60
40
20
0


F3
20.1267
0
62.8771
41.2282
17---->
15---->
13---->
11---->
Frequency
20
10
0
0
0.2
0.4
0.6
0.8
1
1.2
1.4
1.6
Time
60
40
20
0
-20


C3
25.3513
0
63.7918
41.1014
17---->
15---->
13---->
11---->
Frequency
20
10
0
0
0.2
0.4
0.6
0.8
1
1.2
1.4
1.6
Time
60
40
20
0


P3
29.6262
0
64.4547
42.8785
17---->
15---->
13---->
11---->
20
10
0
Frequency
0
0.2
0.4
0.6
0.8
1
1.2
1.4
1.6
Time
60
40
20
0

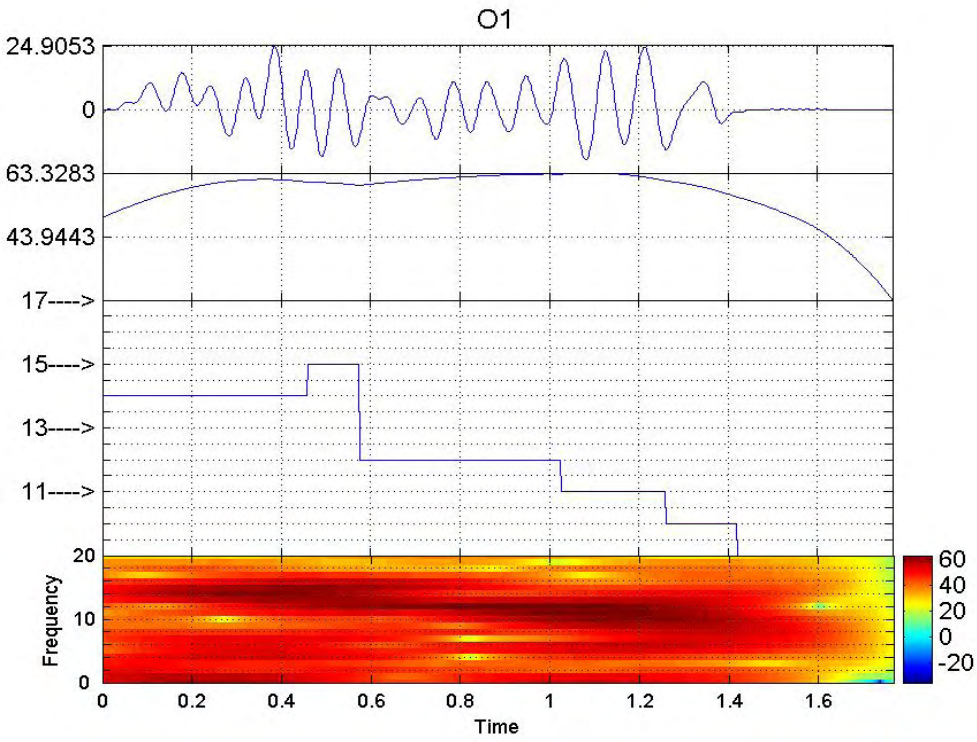
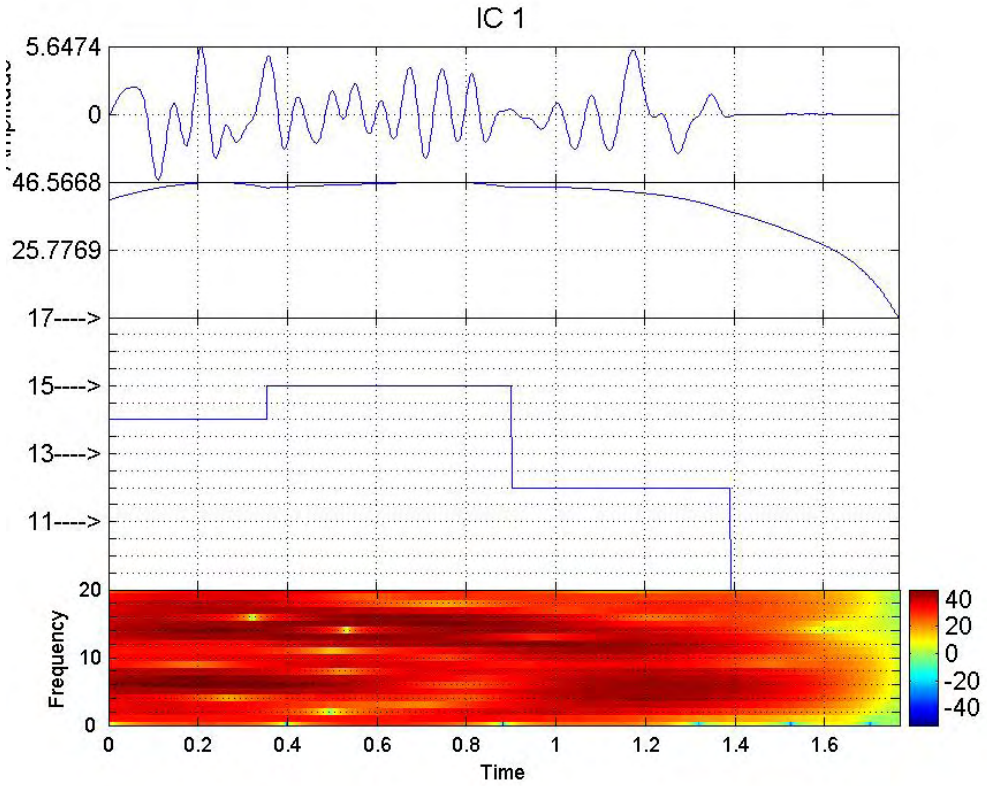
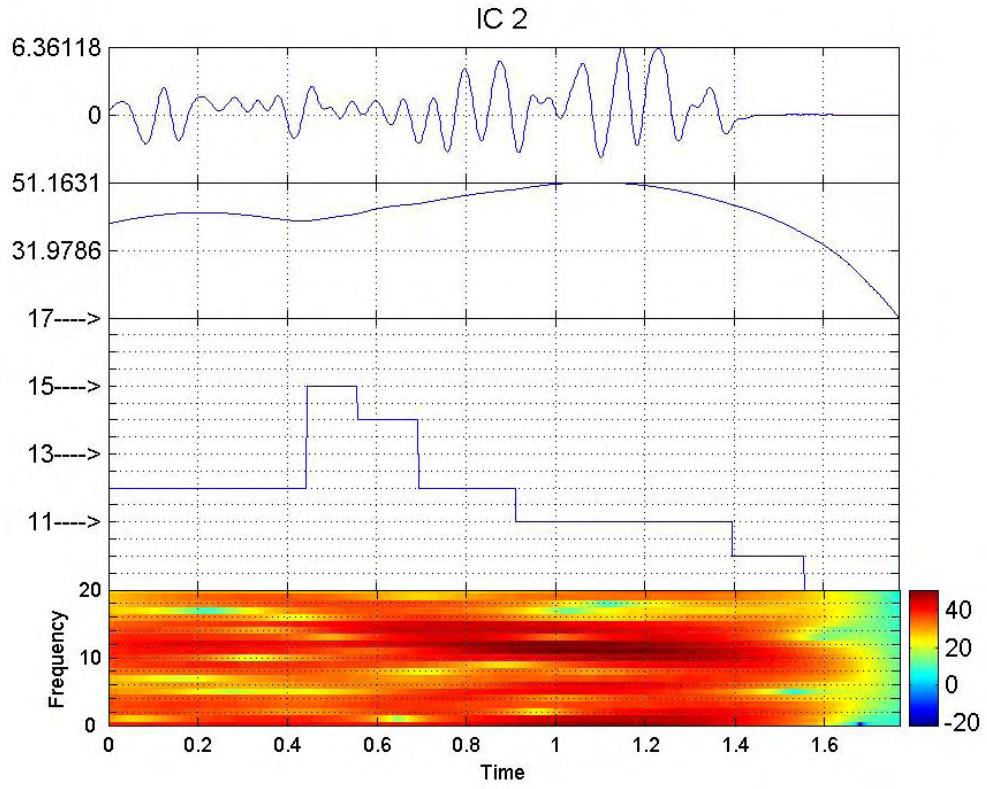
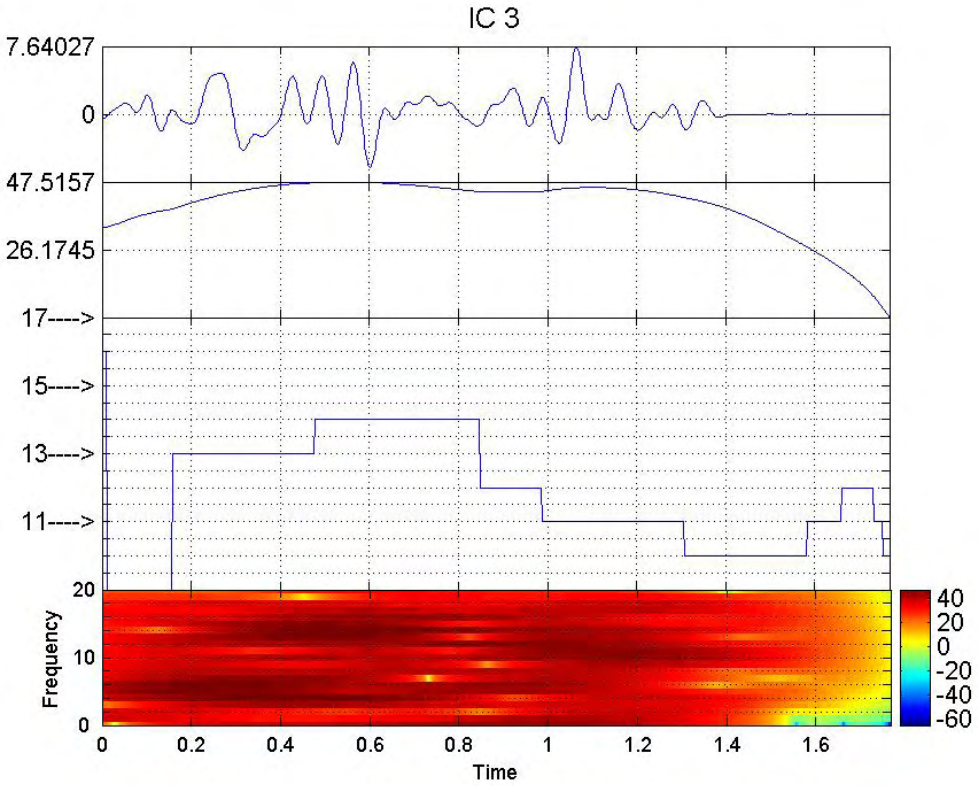
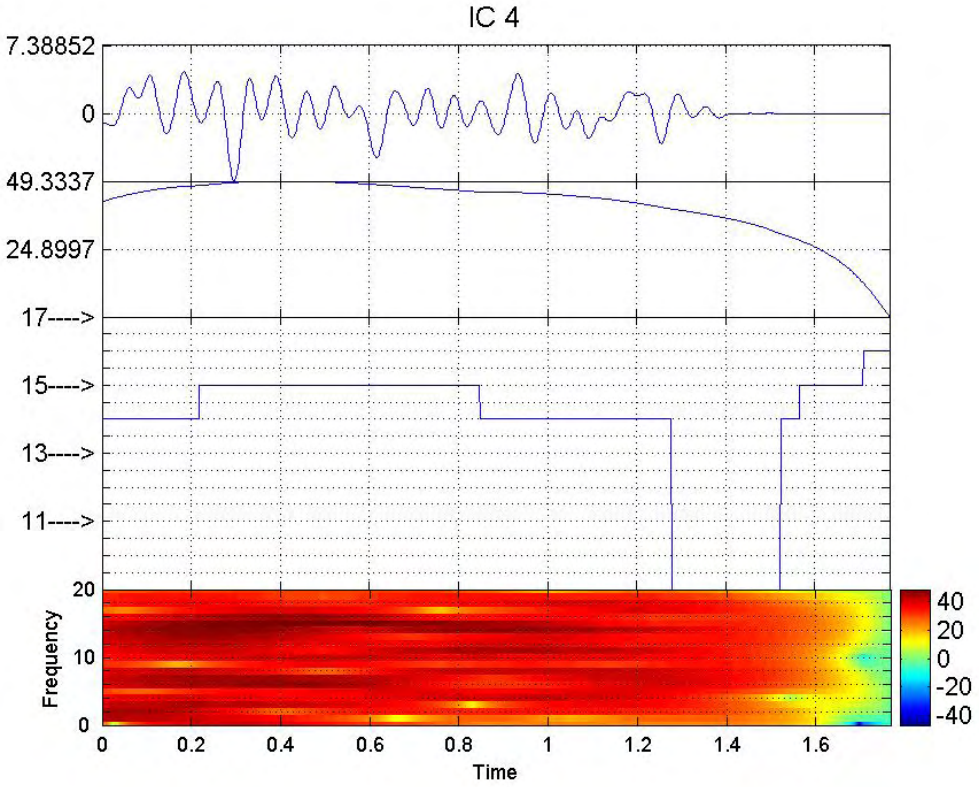

O1
24.9053
0
63.3283
43.9443
17---->
15---->
13---->
11---->
20
10
0
Frequency
0
0.2
0.4
0.6
0.8
1
1.2
1.4
1.6
Time
60
40
20
0
-20

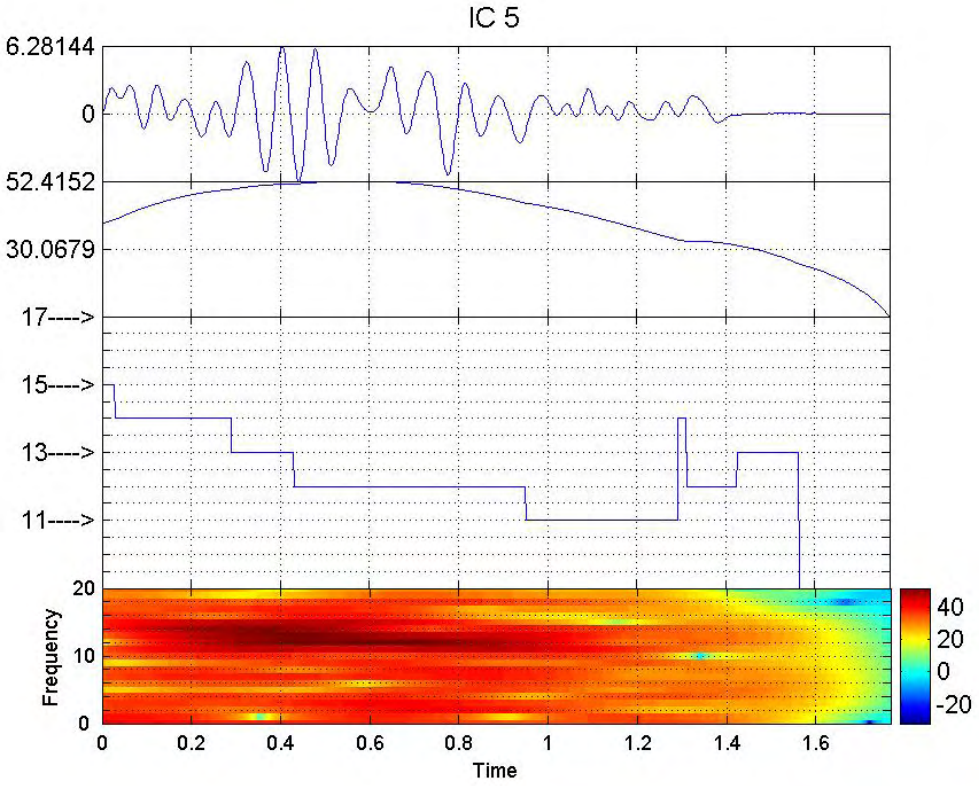
Figure 8.2.3: In the next 8 multiplots we present the spectral analysis of the ICs for spindle 1.

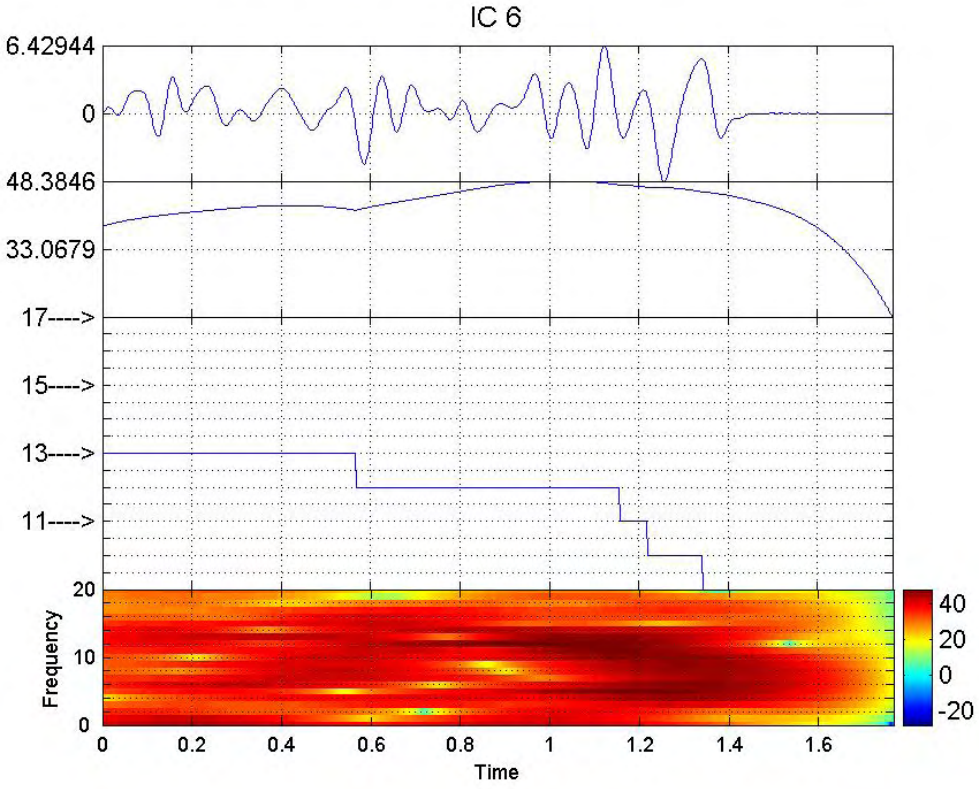


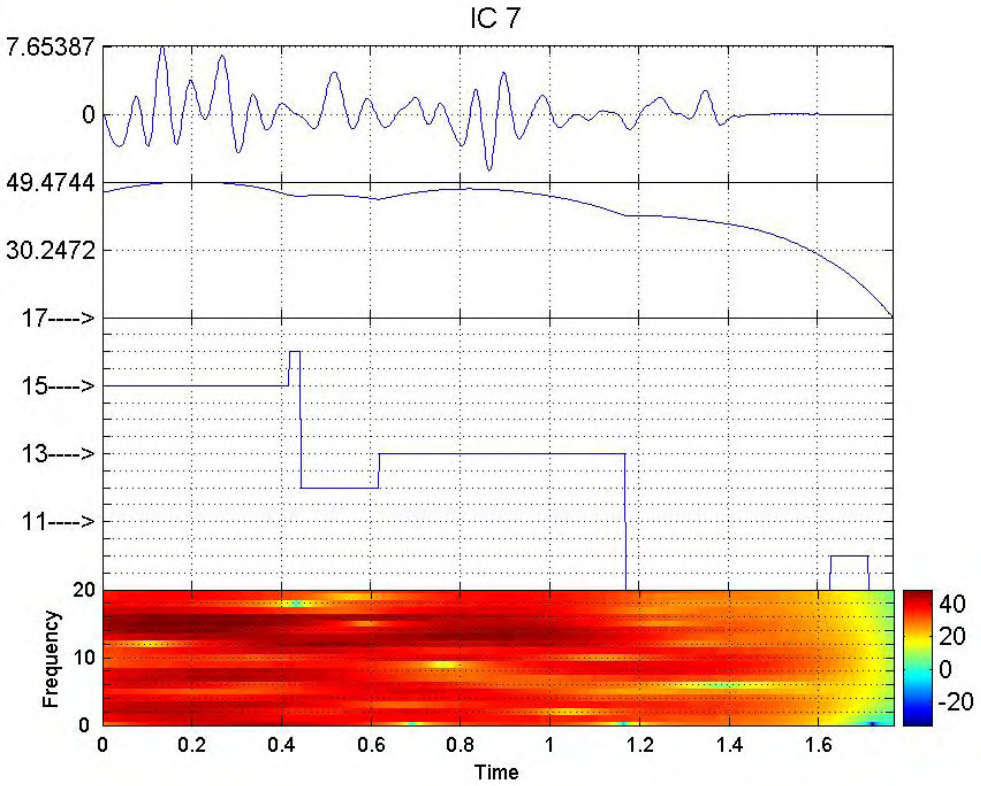



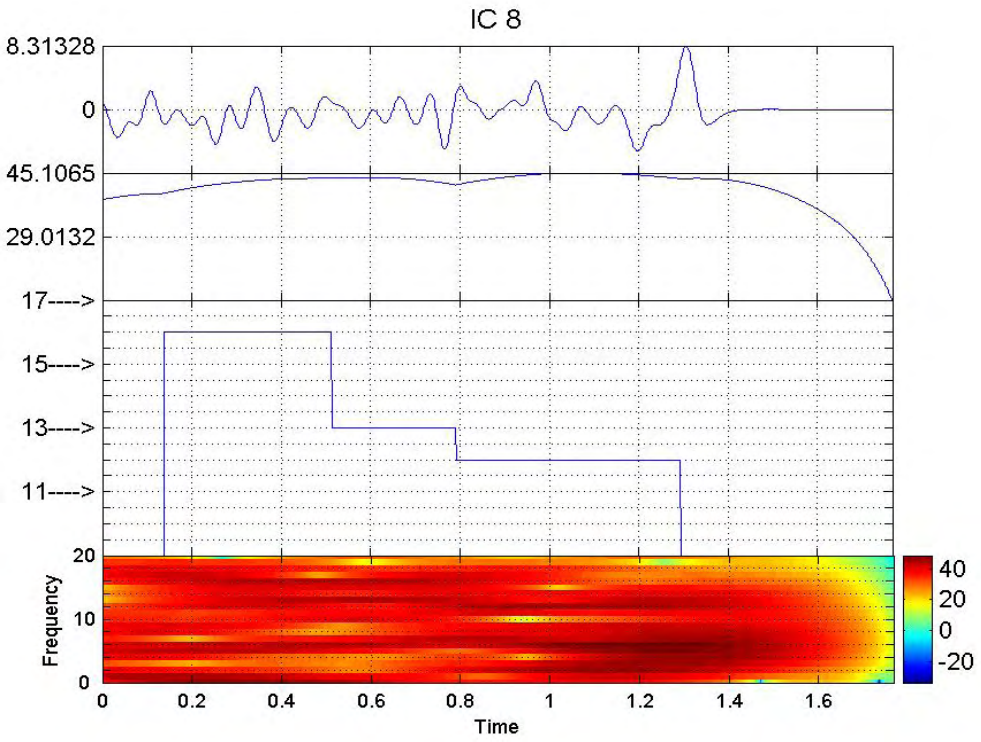

IC 3
7.64027
0
47.5157
26.1745
17---->
15---->
13---->
11---->
20
10
0
Frequency
0
0.2
0.4
0.6
0.8
1
1.2
1.4
1.6
Time
40
20
0
-20
-40
-60


IC 4
7.38852
0
49.3337
24.8997
17---->
15---->
13---->
11---->
20
10
0
Frequency
0
0.2
0.4
0.6
0.8
1
1.2
1.4
1.6
Time
40
20
0
-20
-40


IC 5
6.28144
0
52.4152
30.0679
17---->
15---->
13---->
11---->
20
10
0
Frequency
0
0.2
0.4
0.6
0.8
1
1.2
1.4
1.6
Time
40
20
0
-20


IC 6
6.42944
0
48.3846
33.0679
17---->
15---->
13---->
11---->
20
10
0
Frequency
0
0.2
0.4
0.6
0.8
1
1.2
1.4
1.6
Time
40
20
0
-20


IC 7
7.65387
0
49.4744
30.2472
17---->
15---->
13---->
11---->
20
10
0
Frequency
0
0.2
0.4
0.6
0.8
1
1.2
1.4
1.6
Time
40
20
0
-20


IC 8
8.31328
0
45.1065
29.0132
17---->
15---->
13---->
11---->
20
10
0
Frequency
0
0.2
0.4
0.6
0.8
1
1.2
1.4
1.6
Time
40
20
0
-20

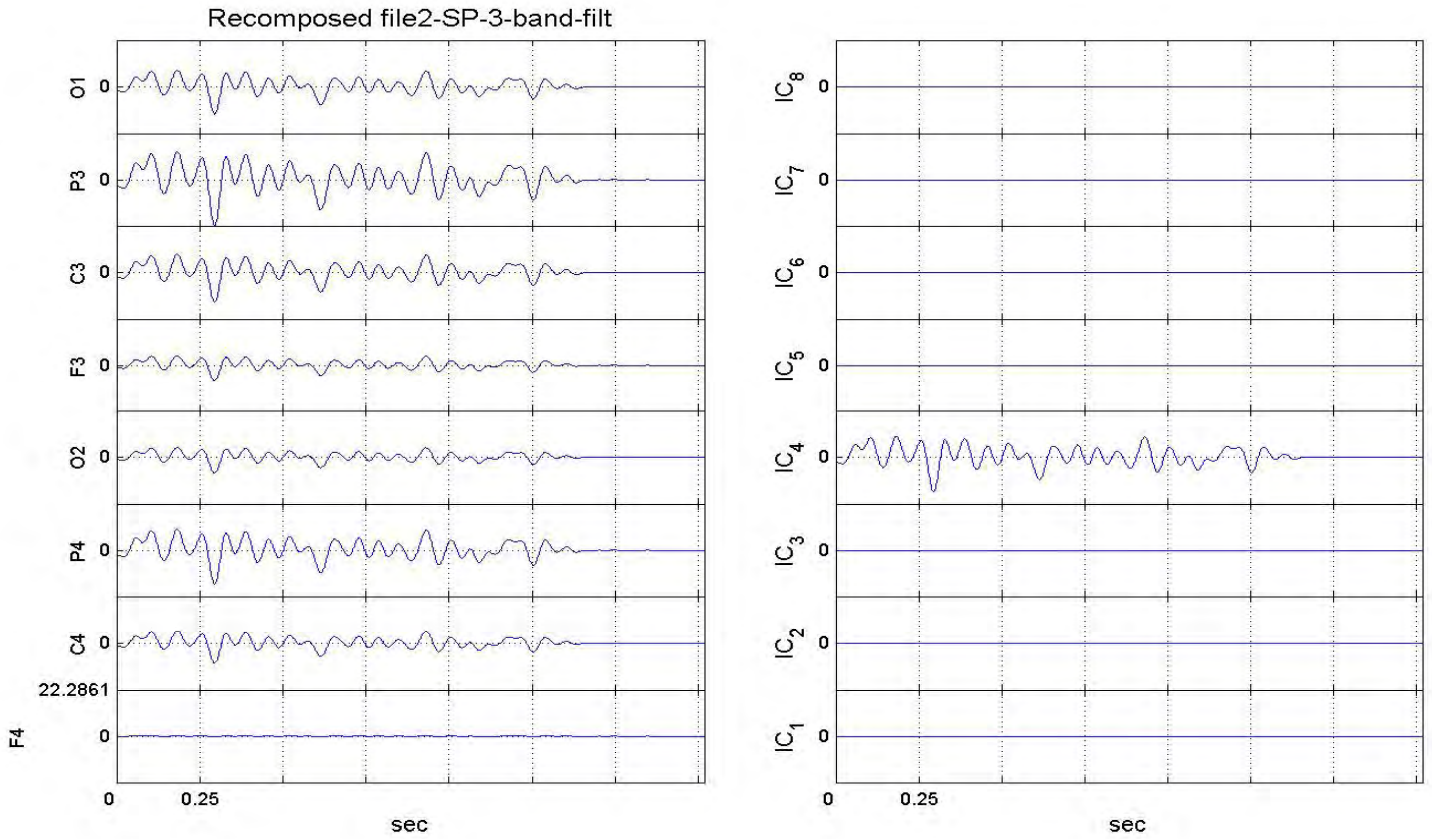



Figure 8.2.4.a: EEGs reconstructed by IC 4.

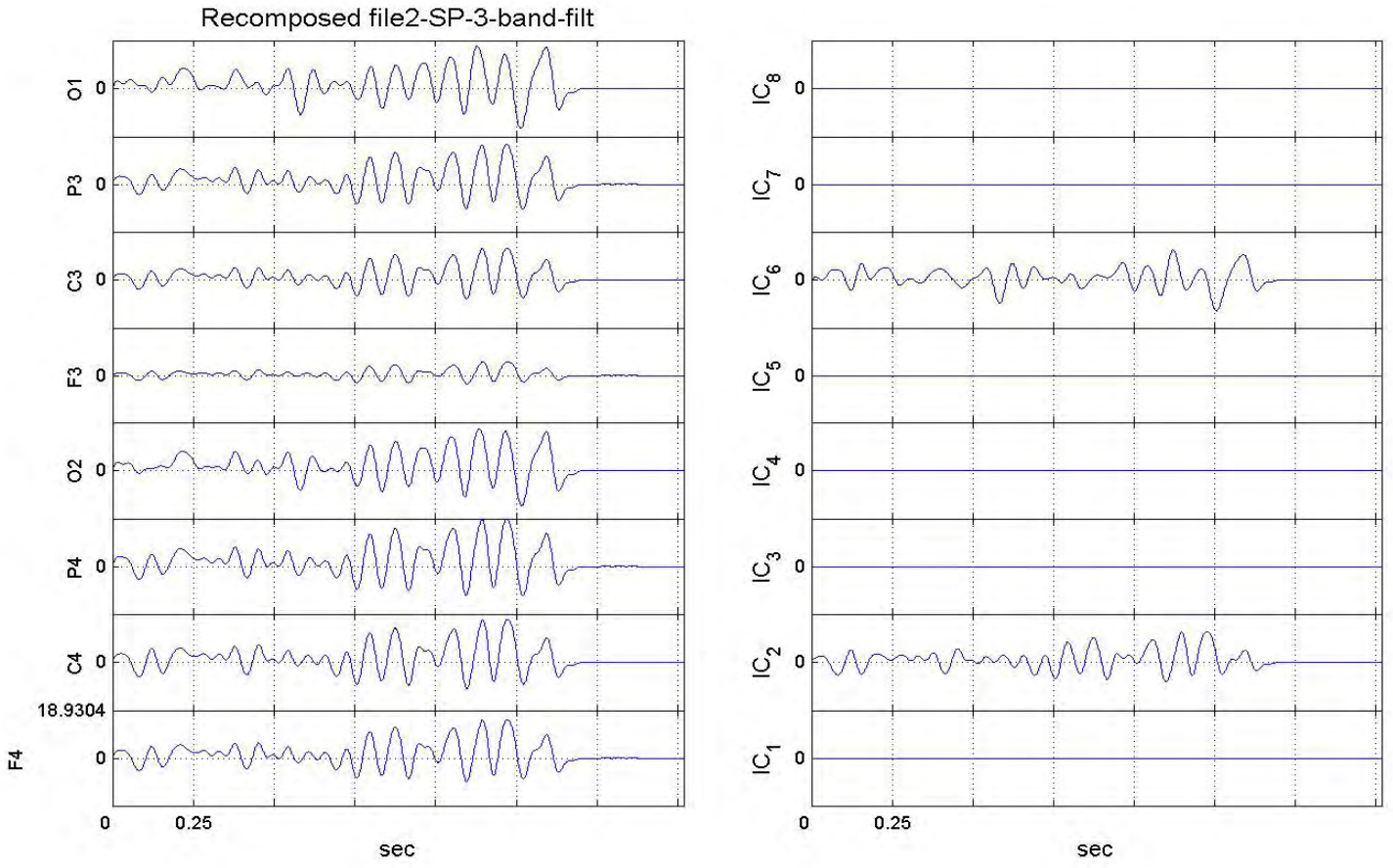



Figure 8.2.4.b: EEGs reconstructed by ICs 2,6.

**Source activity analysis (part A):**

In Fig. 8.2.5, at left we have the 3D mean source activity map image from the original data (M-L-EEG-O/A), at the center the mean source activity map image of the recomposition of the EEG based on IC 4 (M-L-EEG-A/A) and at right the mean source activity map image of the recomposition of the EEG based on ICs 2,6 (M-L-EEG-B/A).

By observing the image at left we can see that the peak of the activity is located at the anterior brain part, with the rest sources which follow in intensity order to be located at posterior brain parts. The second local maximum is located at posterior part and this activity has 14% lower intensity of the first maximum. This **does not** agree with previous research results (which form the assumption that we want to test in the present Thesis) that high frequency spindles (like these at the part A) have posterior sources. The presence of the next three local maxima at posterior parts and with intensity comparable (not lower of 70%) with the first local maximum attenuates the deviation from the expected. Also the contribution to the total EEGs which are reconstructed from the low frequency IC 2 could contribute to the presence of that local maximum.

The main IC of the spindle for this part (A) is IC 4. The recomposition of IC 4 gives us activity at posterior brain parts, as it was expected for high frequency spindles.

The recomposition of ICs 2,6 gives the peak of the activity at posterior left brain parts and also presents a source at the anterior part of the brain, which is the source with the maximum activity at the image of the original data. Only IC 2 possess (low frequency) spindle-like morphology at the first part and it is expected to have a main source at anterior parts, but the fact that the sources which are calculated are combination of two ICs, from which IC 6 does not possess spindle morphology, does not allow prediction for the spatial distribution of the total sources of the EEG which is recomposed from these two ICs

Original Data IC 4 IC's 2,6




Original Data:

| TX | TY | TZ | Value |
|---|---|---|---|
| -3 | 45 | -6 | 5.578416E-0003 |
| -59 | -32 | 8 | 4.878379E-0003 |
| 4 | -67 | 15 | 4.200219E-0003 |
| -3 | -46 | 43 | 4.068962E-0003 |

IC 4:

| TX | TY | TZ | Value |
|---|---|---|---|
| 4 | -67 | 15 | 2.551641E-0003 |
| -3 | -46 | 43 | 2.431564E-0003 |
| 53 | -53 | 15 | 2.121364E-0003 |
| 60 | -39 | 15 | 2.111358E-0003 |

IC's 2,6:

| TX | TY | TZ | Value |
|---|---|---|---|
| -52 | -60 | 8 | 1.417461E-0003 |
| -59 | -46 | 1 | 1.345198E-0003 |
| 4 | -67 | 15 | 1.334080E-0003 |
| -3 | 45 | -6 | 1.334080E-0003 |

Figure 8.2.5: Source activity analysis for part A of spindle 1

**Source activity analysis (part B):**

In Fig. 8.2.6, at left we have the 3D mean source activity map image from the original data (M-L-EEG-O/B), at the center the mean source activity map image of the recomposition of the EEG based on IC 4 (M-L-EEG-A/B) and at right the mean source activity map image of the recomposition of the EEG based on ICs 2,6 (M-L-EEG-B/B).

By observing the image at left we can see the peak of the activity at the anterior brain part. The sources which give maxima at this spindle part are the same (and by intensity order) with the sources which gave maxima at the first part (A). The EEG frequency at this part (B) is low, therefore the peak of this activity is expected at the anterior parts.

By observing the image at right, which is the image of the sources of the EEGs reconstructed from the main ICs, we can see that here also the peak of the activity is located at anterior brain part. As I have mentioned before, the ICs, but also the recomposed by them EEGs, have low frequency, therefore the peak of the activity is expected to be appeared at anterior sources. We must also mention that the other maxima are located at posterior parts of the brain, but now the second source, in intensity order, is by 48% lower than the first.

In the image at center, which is the image of sources of the EEGs recomposed by IC 4, we can observe that the activity is located at posterior brain parts. IC 4 maintains its spindle-like morphology for a big part of part B, and with high frequency, and similarly its recomposed EEGs. We can also observe the appearance of maximum activity at the same parts of the brain as at the first spindle part, keeping their order of intensity also.

**Summary of results and conclusions:**

A) We have spindle with frequency change at the two parts, from high to low. While the main source (meaning the source with the greater intensity) of the EEGs which are recomposed from high frequency ICs at the first part are posterior and from the low frequency ICs at the second part anterior, nevertheless, **the main source** which is calculated from the **total EEGs** at the **high frequency spindle part (part A)** is located **at anterior parts.** The existence of the next three local maxima at posterior brain parts and with intensity comparable (not lower than 70%) with that of the main source attenuates the deviation from the expected. The main total EEG source at the spindle part where low frequency spindles prevail (part B) is located at anterior brain parts.

B) Especially for IC 4, the sources of the EEGs, recomposed from that IC, keep their spatial distribution, with the same intensity order of the 4 first (i.e. more powerful) sources. This speaks in favour of the assumption that ICs reflect separate "local" source activities.

Original Data IC 4 IC's 2,6




Original Data:

| TX | TY | TZ | Value |
|---|---|---|---|
| -3 | 45 | -6 | 5.539882E-0003 |
| -59 | -32 | 8 | 4.540531E-0003 |
| 4 | -67 | 15 | 4.345005E-0003 |
| -3 | -46 | 43 | 4.062580E-0003 |

IC 4:

| TX | TY | TZ | Value |
|---|---|---|---|
| 4 | -67 | 15 | 8.631219E-0004 |
| -3 | -46 | 43 | 8.225044E-0004 |
| 53 | -53 | 15 | 7.175758E-0004 |
| 60 | -39 | 15 | 7.141911E-0004 |

IC's 2,6:

| TX | TY | TZ | Value |
|---|---|---|---|
| -3 | 52 | 1 | 1.660347E-0003 |
| -59 | -39 | 1 | 1.126431E-0003 |
| -52 | -60 | 8 | 1.087364E-0003 |
| -59 | -39 | -20 | 1.087364E-0003 |



Figure 8.2.6: Source activity analysis for part B of spindle 1

## 8.3) Spindle 2 *(2nd Third of the Night)*

**Spindle characteristics:**

1) It starts with frequency 13Hz and gradually pass to frequency 12 Hz. At lead F3 we have transition directly to 11 Hz. The transition does not happen simultaneously at all leads. (Figure 8.3.1).

2) EEG division and ICs grouping:

If we observe the spectral analysis of the spindles and the corresponding ICs, we can see that the end of the spindle activity of ICs 1,4 and 7 (from 1,25 till 1,5 sec) almost coincides with the time window (from 1,25 till 1,75 sec) where we the frequency transition occurs at the majority of the leads (F4, C4, P4, F3, C3, P3). From the other ICs which present spindle-like morphology (ICs 2,3,5,6), ICs 2,5,6 start the spindle almost at the finish point of ICs 1,4,7 and they present low frequency activity till the end of the lead's time window (while IC 3 presents beat). So, we have to divide the spindle in two parts, with main ICs for the first part (A), ICs 1,4,7 (we include IC 4, although it presents mixed spectral characteristics, with transition from 13 to 12 and again 13 Hz, due to its morphological similarity with the other ICs at the time duration in which the spindle-like action is active and due to the match of the finish time with the other two ICs) and for the second part (B), ICs 2,5,6.

**Source activity analysis (part A):**

In Fig. 8.3.1, at left we have the 3D mean source activity map image from the original data (M-L-EEG-O/A), at the center the mean source activity map image of the recomposition of the EEG based on ICs 2,5,6 (M-L-EEG-A/A) and at right the mean source activity map image of the recomposition of the EEG based on ICs 1,4,7 (M-L-EEG-B/A). The main ICs for this spindle part are ICs 1,4,7

By looking the source activity map of the original data we observe that the main activity of the sources is located at the central posterior and right posterior brain parts. As it is mentioned above the EEG frequency at the bigger part of part A is high, therefore the correspondence of this EEG recordings to activation of the posterior brain parts is expected.

By observing the image at right, which is the image of the sources of the EEGs reconstructed from the main ICs for this spindle part, we can see that the central posterior and right posterior brain parts are activated in this case also. More specifically, we can observe that the first three local maxima are the same with that from the original data. The ICs, as well as the EEGs recomposed from them, are mainly of (limit) high frequency so the activity of the posterior brain parts is expected.

The image at the center is of the sources of the EEGs reconstructed from ICs 2,5,6, which have no interest at this part for spindle generation because they, as well as the EEGs recomposed from these ICs, do not possess spindle-like formations.

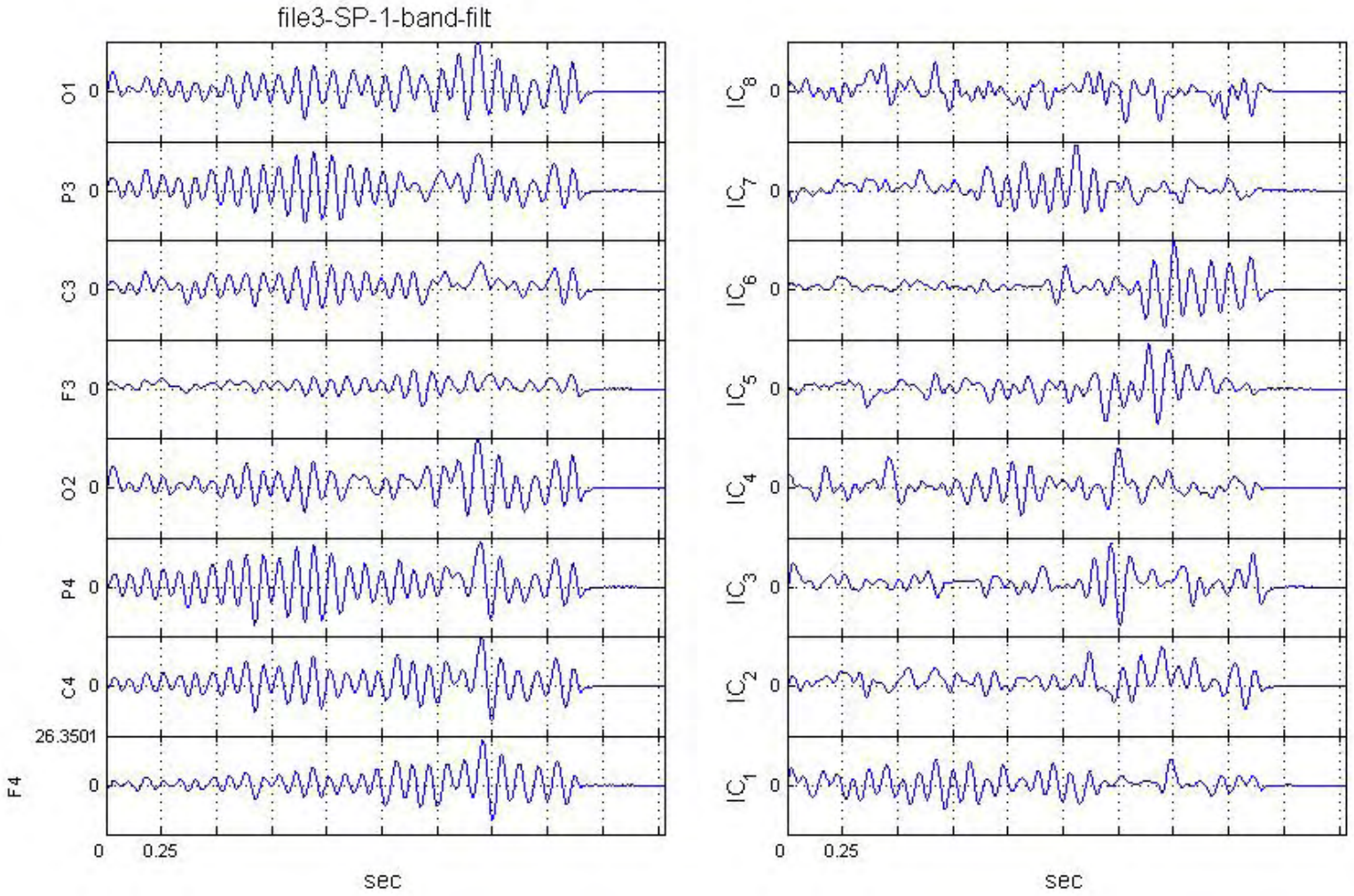
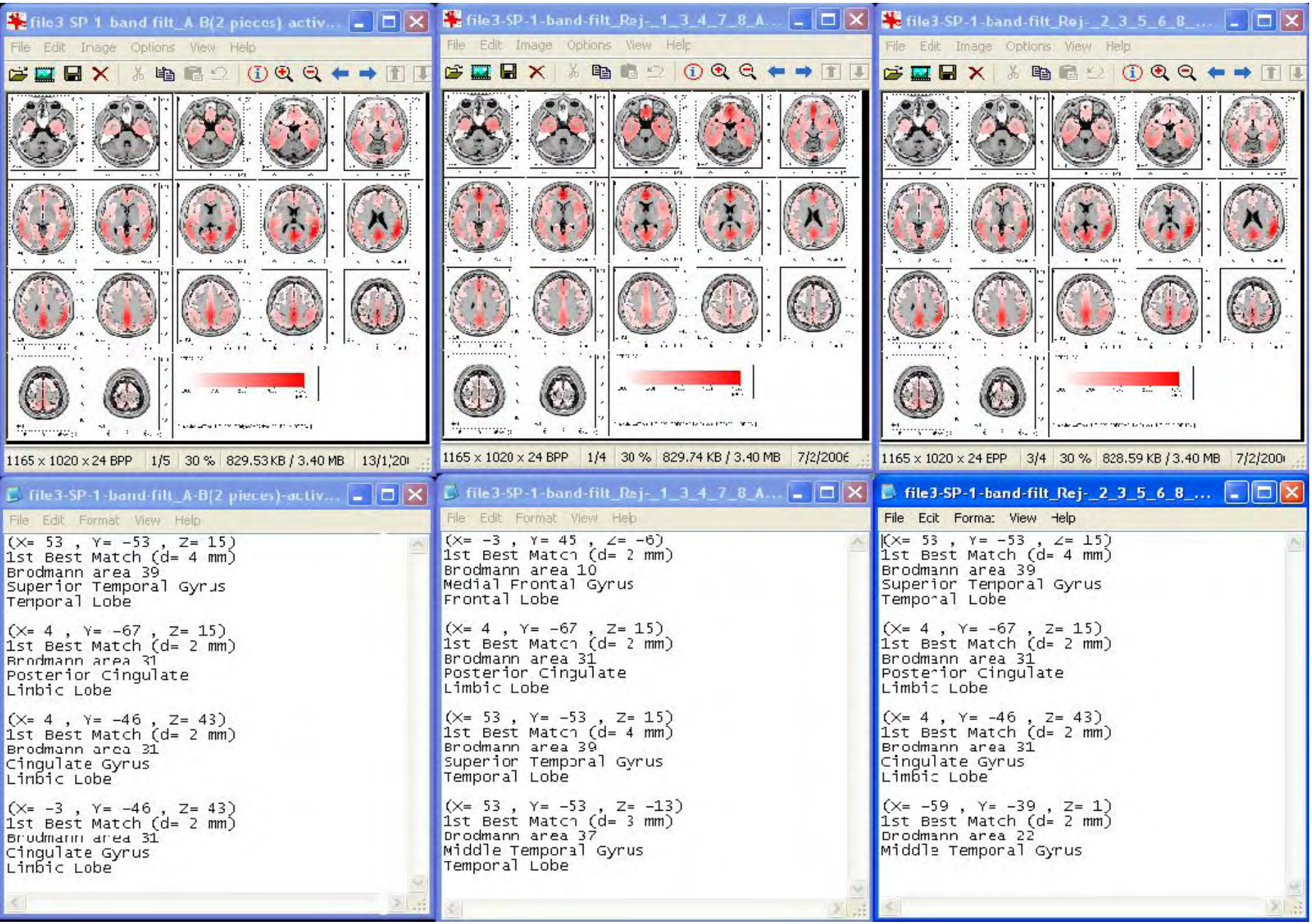



Figure 8.3.1: At left we have the original (filtered) EEGs and at right the ICs for spindle 2.

Original Data IC's 2,5,6 IC's 1,4,7




Original Data:

| TX | TY | TZ | Value |
|---|---|---|---|
| 53 | -53 | 15 | 4.674695E-0003 |
| 4 | -67 | 15 | 4.326385E-0003 |
| 4 | -46 | 43 | 3.959741E-0003 |
| -3 | -46 | 43 | 3.959741E-0003 |

IC's 2,5,6:

| TX | TY | TZ | Value |
|---|---|---|---|
| -3 | 45 | -6 | 1.725162E-0003 |
| 4 | -67 | 15 | 1.380129E-0003 |
| 53 | -53 | 15 | 1.095985E-0003 |
| 53 | -53 | -13 | 1.082454E-0003 |

IC's 1,4,7:

| TX | TY | TZ | Value |
|---|---|---|---|
| 53 | -53 | 15 | 3.946107E-0003 |
| 4 | -67 | 15 | 3.404484E-0003 |
| 4 | -46 | 43 | 3.156886E-0003 |
| -59 | -39 | 1 | 2.197440E-0003 |



Figure 8.3.2: Source activity analysis for part A of spindle 2

**Source activity analysis (part B):**

In Fig. 8.3.2, at left we have the 3D mean source activity map image from the original data (M-L-EEG-O/B), at the center the mean source activity map image of the recomposition of the EEG based on ICs 2,5,6 (M-L-EEG-A/B) and at right the mean source activity map image of the recomposition of the EEG based on ICs 1,4,7 (M-L-EEG-B/B). The main ICs for this spindle part are ICs 2,5,6.

At the source activity map of the original data we can observe that we have a clear inversion of the situation, compared to the first part. We can see that here we have active the anterior brain parts. The EEG frequency is low, therefore the appearance of activation of the anterior brain parts is expected.

At the image at center, which shows the sources of the EEGs reconstructed from the main ICs for part B (ICs 2,5,6), we can observe what was observed for the image of the original data also. We can see that the peak of the activity is located at the anterior brain parts. We can also observe that the first two local maxima sources are the same with those of the original data. It is also important to mention that these two sources are present at the first spindle part also.

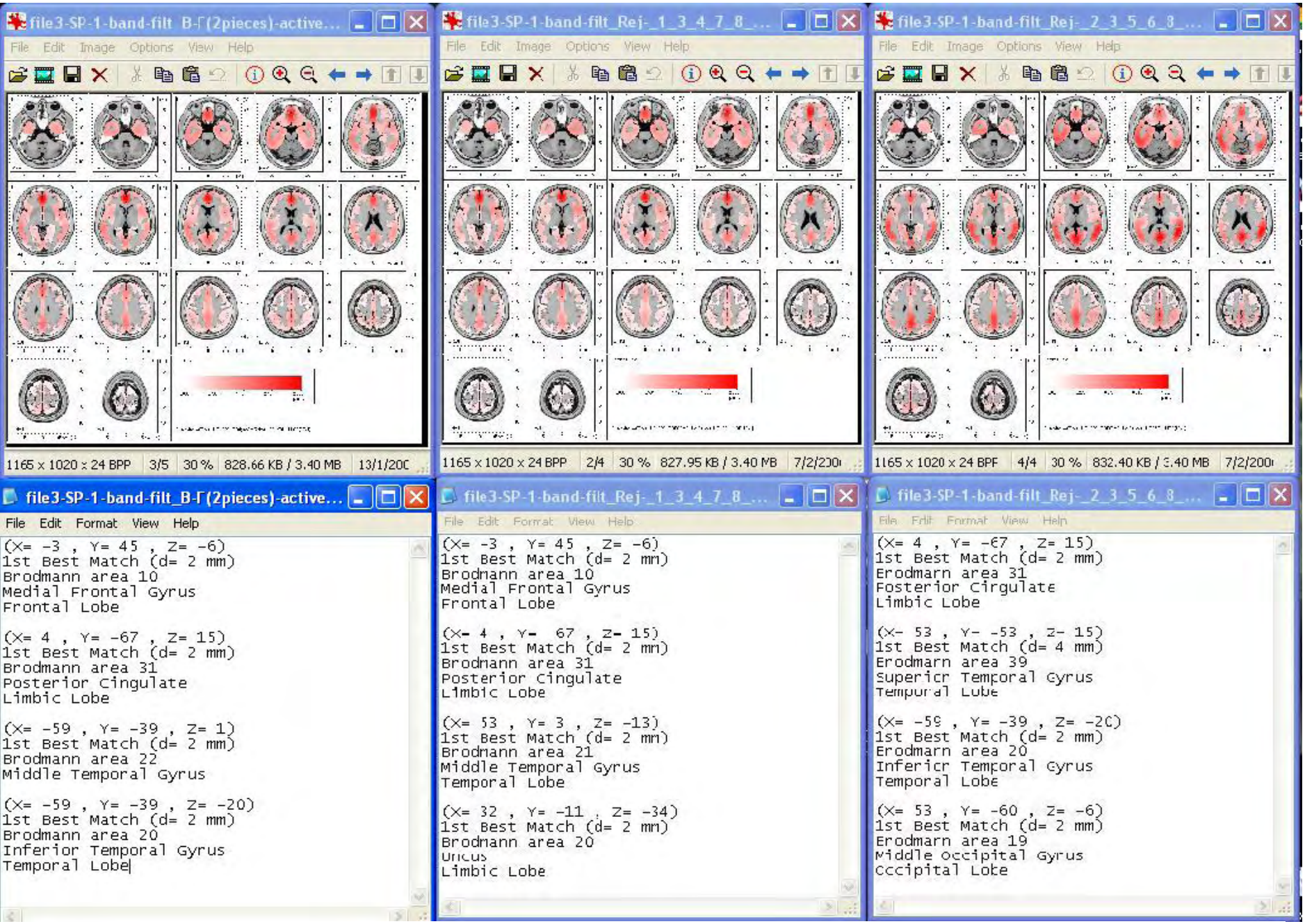
From the image of the sources of the EEGs reconstructed from ICs 1,4,7 we can observe that two of the four maximal activity sources are the same with that of the first spindle part. But, at this part, these ICs, and respectively the EEGs recomposed from these ICs, do not present interest for spindle generation because they do not possess spindle-like formations.

**Summary of results and conclusions:**

A) We have EEG with frequency change (form high to low). We have posterior sources giving the local maxima for the high frequency EEG and anterior for the low frequency EEG, which is consistent with the assumption we want to check.

B) We can observe that two main sources maintain their spatial distribution at the recompositions of both groups of ICs. This speaks in favour of the assumption that ICs reflect separate "local" source activities.

Original Data | IC's 2,5,6 | IC's 1,4,7




Original Data:

| TX | TY | TZ | Value |
|---|---|---|---|
| -3 | 45 | -6 | 2.801642E-0003 |
| 4 | -67 | 15 | 1.768880E-0003 |
| -59 | -39 | 1 | 1.494209E-0003 |
| -59 | -32 | -20 | 1.461248E-0003 |

IC's 2,5,6:

| TX | TY | TZ | Value |
|---|---|---|---|
| -3 | 45 | -6 | 2.255386E-0003 |
| 4 | -67 | 15 | 1.229406E-0003 |
| 53 | 3 | -13 | 1.140959E-0003 |
| 32 | -11 | -34 | 1.114426E-0003 |

IC's 1,4,7:

| TX | TY | TZ | Value |
|---|---|---|---|
| 4 | -67 | 15 | 1.090375E-0003 |
| 53 | -53 | 15 | 1.077547E-0003 |
| -59 | -39 | -20 | 8.851279E-0004 |
| 53 | -60 | -6 | 8.338162E-0004 |

Figure 8.3.3: Source activity analysis for part B of spindle 2

## 8.4) Spindle 3 *(2nd Third of the Night)*

**Spindle characteristics:**

1) It starts with frequency 14Hz (except O2 which starts with 13Hz) and gradually passes to 13 Hz. At leads O1, F3, C4 we have transition, near the end of the time of the spindle, again to 14Hz.

2) EEG division and ICs grouping:

By observing the morphology of the spindle we can see an initial part with low amplitude (in comparison with the amplitude of the central spindle part which follows), which contains a delta-like half-wave, at which "rides" the spindle till about 0.6 sec. Next follows a main and well formed spindle part and after about 1.25 sec the spindle-like morphology is disrupted and the spindle gradually decreases. So we divide the spindle at two parts, part A: 0-0,6sec and part B: 0,6sec – spindle end. By observing the ICs, we can see that IC 8 has an initial activity at 14 Hz and is the only one which afterwards (i.e. in part B) does not present spindle-like activity. So, IC 8 can be assumed as representative for the first part (A). ICs 1 and 2 have strong spindle-like morphology only at their central part, with frequency 13 Hz, which coincides with the frequency of the central part of all the leads, so they can be assumed as representatives for the second part (B). IC 7 is the only one that presents strong spindle-like activity only at the last part and also its activity starts when the activity of ICs 1and 2 ends, slightly after 1 sec.

**Source activity analysis (part A):**

In Fig. 8.4.1, at left we have the 3D mean source activity map image from the original data (M-L-EEG-O/A), at the center the mean source activity map image of the recomposition of the EEG based on IC8 (M-L-EEG-A/A) and at right the mean source activity map image of the recomposition of the EEG based on IC 1,2,7 (M-L-EEG-B/A). The main ICs for this spindle part is IC 8.

As we mentioned above, the EEGs are high frequency at this part of the spindle. We observe that this spindle activates the posterior brain parts, and mainly the left posterior part. The posteriority of the sources coincides with the assumption that high frequency spindles present the peak of their action at posterior brain parts.

On the other hand, from the image of the sources of the EEGs reconstructed from the main IC (8), for this part (A), we observe that the above assumption is **not** confirmed, because we see that the peak of the action is located at anterior brain areas, while the IC is clearly high frequency (14 Hz). Only one of the four local maxima is located at posterior areas.

For the sources of the EEG recomposed by ICs 1,2 and 7 we observe a strong posterior activity. This activity though, does not concern us for spindle source study because ICs 1,2,7 at part A (and respectively the recomposed EEGs from these ICs) do not possess spindle-like morphology.

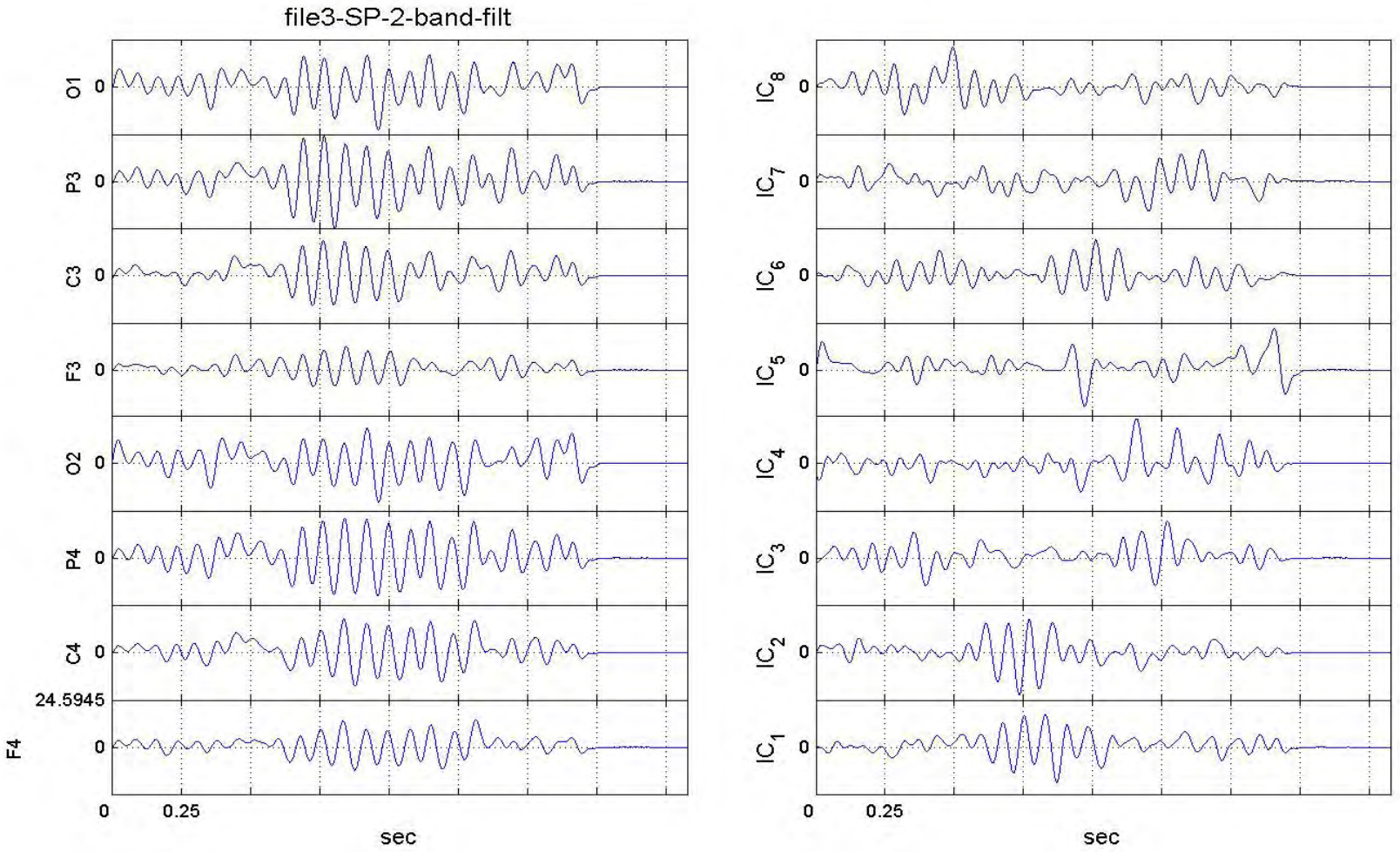



Figure 8.4.1: At left we have the original (filtered) EEGs and at right the ICs for spindle 3.

Original Data IC 8 IC 1,2,7




Original Data:

| TX | TY | TZ | Value |
|---|---|---|---|
| 60 | -39 | 15 | 2.907966E-0003 |
| 53 | -53 | 15 | 2.896562E-0003 |
| 4 | -67 | 15 | 2.417603E-0003 |
| -3 | -46 | 43 | 2.314969E-0003 |

IC 8:

| TX | TY | TZ | Value |
|---|---|---|---|
| -3 | 45 | -6 | 1.356839E-0003 |
| 60 | -39 | 22 | 1.245099E-0003 |
| 46 | 10 | 1 | 1.005657E-0003 |
| 53 | 3 | -13 | 9.843734E-0004 |

ICs 1,2,7:

| TX | TY | TZ | Value |
|---|---|---|---|
| -59 | -32 | 8 | 1.297569E-0003 |
| -3 | -46 | 43 | 1.058409E-0003 |
| 4 | -67 | 22 | 1.053320E-0003 |
| -3 | 52 | 1 | 1.022789E-0003 |

Figure 8.4.2: Source activity analysis for part A of spindle 3

**Source activity analysis (part B):**

In Fig. 8.4.2, at left we have the 3D mean source activity map image from the original data (M-L-EEG-O/B), at the center the mean source activity map image of the recomposition of the EEG based on IC8 (M-L-EEG-A/B) and at right the mean source activity map image of the recomposition of the EEG based on IC 1,2,7 (M-L-EEG-B/B). The main ICs for this spindle part are ICs 1,2,7.

From the spectral analysis of the EEGs for this part of the spindle we observe that we have a limit high frequency activity at all leads (13 Hz), which is maintained for all the part's duration, increasing to 14 Hz at three leads. From the source activity map we observe that we have activation in posterior brain areas. As was mentioned before, the EEGs are high frequency, so the activation of posterior brain parts is expected.

For the sources of the EEG recomposed by ICs 1,2,7, which are the main ICs for this spindle part (part B), we observe that there appear activation areas at the posterior brain part. This is expected because, as the spectral analysis demonstrate, we have a high frequency action. It is also important to say that three of the four local maxima are the same with that of the first spindle part (part A). So, at great percentage, the spatial distribution is maintained.

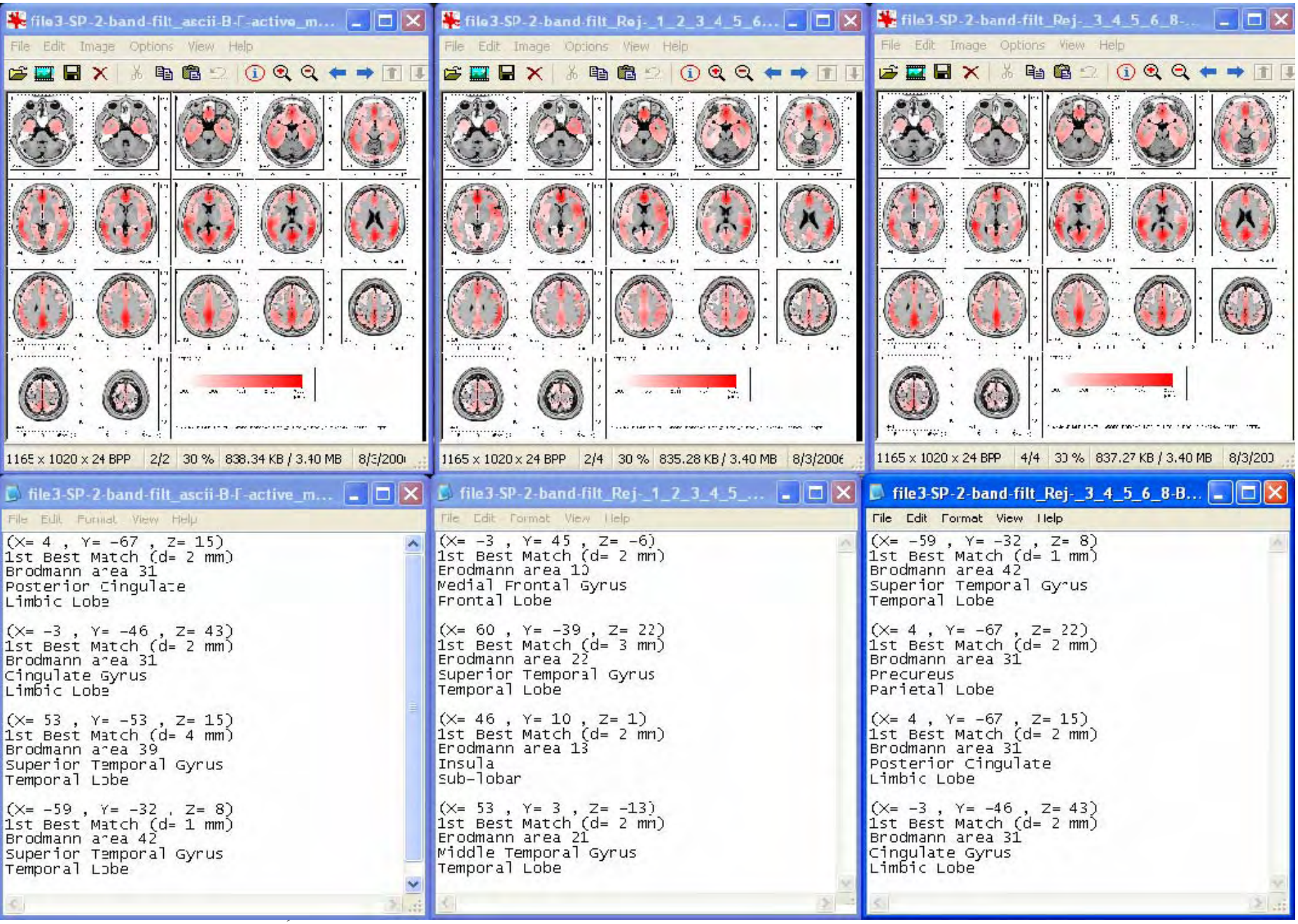
For the sources of the EEG recomposed by IC 8 at this part, we observe that we have a spread brain activity, with main maxima at anterior areas. At this part the recomposition of EEGs does not concern us for spindle creation because IC 8 does not possess spindle-like morphology. It is also important to notice that the spatial distribution of the sources is maintained, because three of the four local maxima are the same and the fourth source differentiates its sources from one part to the other marginally.

**Summary of results and conclusions:**

1) For the whole spindle duration, we have a spindle with only high or limit high frequency, but we **do not** have confirmation of the assumption that high frequency spindles activate posterior parts, because at one of the two parts at which we divide the EEG, the recomposition from the main IC activates anterior brain parts, while it has high frequency content (14 Hz). On the other hand, both for the total EEG at both parts, as well as for the recomposed EEG from the main ICs of the second part, the source analysis agree with the assumption.

2) The spatial distribution of the sources of the EEGs is maintained, for both parts of the spindle, for the EEGs which were recomposed from separate groups of ICs. This speaks in favour of the assumption that ICs reflect separate "local" source activities.

Original Data IC 8 ICs 1,2,7




Original Data:

| TX | TY | TZ | Value |
|---|---|---|---|
| 4 | -67 | 15 | 3.207927E-0003 |
| -3 | -46 | 43 | 2.981485E-0003 |
| 53 | -53 | 15 | 2.981485E-0003 |
| -59 | -32 | 8 | 2.868264E-0003 |

IC 8:

| TX | TY | TZ | Value |
|---|---|---|---|
| -3 | 45 | -6 | 5.828541E-0004 |
| 60 | -39 | 22 | 5.348544E-0004 |
| 46 | 10 | 1 | 4.319977E-0004 |
| 53 | 3 | -13 | 4.228549E-0004 |

ICs 1,2,7:

| TX | TY | TZ | Value |
|---|---|---|---|
| -59 | -32 | 8 | 2.362185E-0003 |
| 4 | -67 | 22 | 2.269550E-0003 |
| 4 | -67 | 15 | 2.269550E-0003 |
| -3 | -46 | 43 | 2.251023E-0003 |



Figure 8.4.3: Source activity analysis for part B of spindle 3

## 8.5) Spindle 4 *(2nd Third of the Night)*

**Spindle Characteristics:**

1) It starts with frequency 13Hz and gradually, after 2 sec, we have transition to lower frequencies, e.g. 12 Hz and then 11 Hz or 11 Hz and then 12 Hz. The transition does not happen simultaneously at all spindles. Also, at the left leads F3, C3, P3 the transition is only from 13 to 12 Hz.

2) EEG division and ICs grouping:

By visual observation of the spindle's morphology we can find an initial part where we have low amplitude spindle-like formations, which get stronger at about 1.75 to 2 sec. These high-amplitude spindle-like formations seem to be divided into two subdivisions. If we wanted to divide this spindle at two main parts, then, by observing the ICs, we can easily distinct ICs 5,8, which define part A (0-2 sec), while at the rest of the spindle, activity is present only for ICs 1,2,4,6,7. This grouping though has some problems, because at part B, except from the "purely" low frequency ICs (2 and 7), there are ICs with frequency transitions, from high (14 Hz) to low (IC 4), and ICs which possess limit fast frequency (13 Hz) in all of part B's duration (IC 6). Also ICs 4 and 6 present spindle-like activity in a small part at the end of part A.

**Source activity analysis (part A):**

At this part of the spindle (A) we can observe a limit high frequency activity (13Hz). In Fig. 8.5.1, at left we have the 3D mean source activity map image from the original data (M-L-EEG-O/A), at the center the mean source activity map image of the recomposition of the EEG based on ICs 5,8 (M-L-EEG-A/A) and at right the mean source activity map image of the recomposition of the EEG based on IC 1,2,4,6,7 (M-L-EEG-B/A). The main ICs for this spindle part are ICs 5 and 8.

By observing the source activity map of the original data we can see that the activity is located at the right and central posterior brain parts. As it is mentioned above, the EEG frequency is (limit) high, so the appearance of activation of the posterior brain parts is expected.

If we observe the image at center, we can see that the source with the first local maximum is the same with that from the original data image. Additionally, the third and fourth sources are at posterior brain parts. Therefore, we can see that the posterior parts of the brain are primarily activated, which, according to the assumption to be checked, are responsible for high frequency activities. The second local maximum is located at the anterior part of the brain and its activity is by 33% lower than the intensity of the first maximum.

Looking the image at right, we can observe that the activity here is more spread, since we have active left posterior, central, right and anterior brain parts. Characteristically, we see that two of the local maxima are the same with those from the original data. This activity, thought, does not concern us for spindle source study because from ICs 1,2,4,6,7 at part A (and respectively the EEGs recomposed from these ICs) only ICs 4,6 possess short-duration spindle-like morphology.

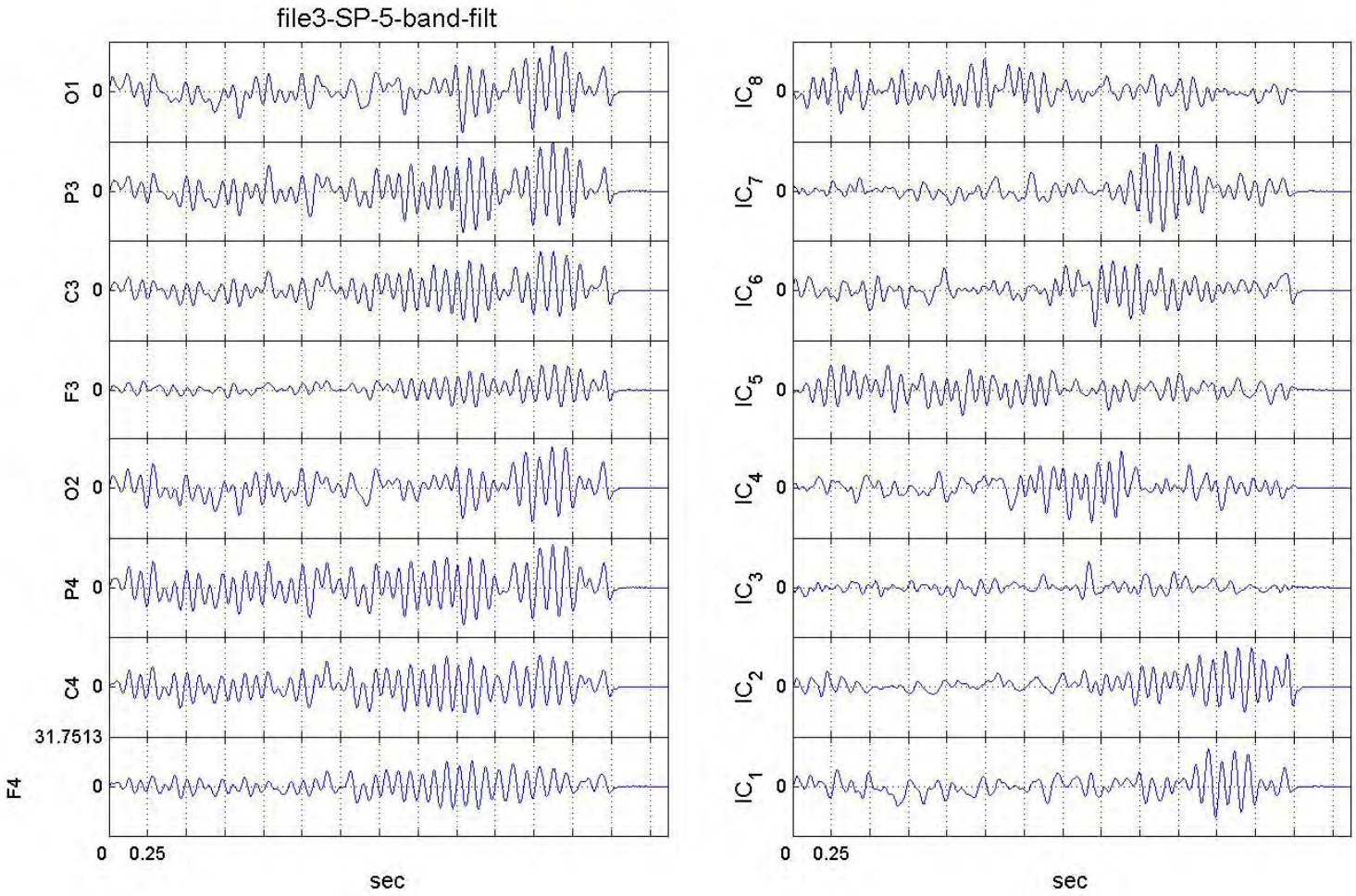
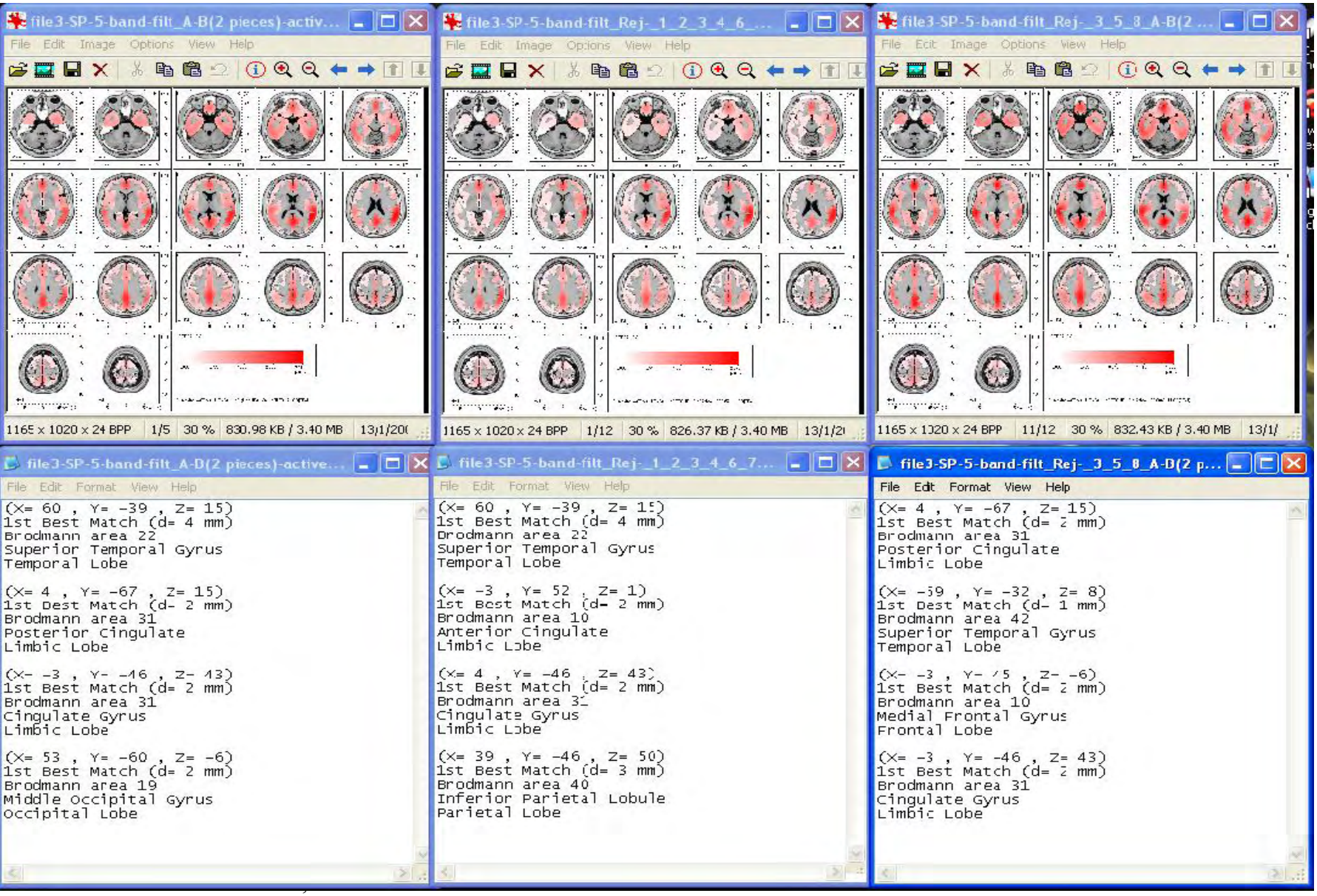



Figure 8.5.1: At left we have the original (filtered) EEGs and at right the ICs for spindle 4.

Original Data IC's 5,8 IC's 1,2,4,6,7




Original Data:

| TX | TY | TZ | Value |
|---|---|---|---|
| 60 | -39 | 15 | 3.110824E-0003 |
| 4 | -67 | 15 | 2.732645E-0003 |
| -3 | -46 | 43 | 2.537456E-0003 |
| 53 | -60 | -6 | 2.281271E-0003 |

IC's 5,8:

| TX | TY | TZ | Value |
|---|---|---|---|
| 60 | -39 | 15 | 2.073337E-0003 |
| -3 | 52 | 1 | 1.398486E-0003 |
| 4 | -46 | 43 | 1.374094E-0003 |
| 39 | -46 | 50 | 9.919495E-0004 |

IC's 1,2,4,6,7:

| TX | TY | TZ | Value |
|---|---|---|---|
| 4 | -67 | 15 | 1.891615E-0003 |
| -59 | -32 | 8 | 1.891615E-0003 |
| -3 | 45 | -6 | 1.772925E-0003 |
| -3 | -46 | 43 | 1.735835E-0003 |

Figure 8.5.2: Source activity analysis for part A of spindle 4

**Source activity analysis (part B):**

As it was mentioned above, at part B of the spindle we observe a transition from limit high frequency (13 Hz) to low frequency (12-11 Hz) activity. Specifically, while at part A all EEGs, which possessed spindles had as main frequency 13 Hz, at part B, at all right electrodes, after a time interval, there is a transition to 11-12 or 12-11 Hz and at the left electrodes, except O1, there is a transition to 12 Hz only.

In Fig. 8.5.2, at left we have the 3D mean source activity map image from the original data (M-L-EEG-O/B), at the center the 3D mean source activity map image of the recomposition of the EEG based on ICs 5,8 (M-L-EEG-A/B) and at right the 3D mean source activity map image of the recomposition of the EEG based on IC 1,2,4,6,7 (M-L-EEG-B/B). The main ICs for this spindle part are ICs 1,2,4,6,7.

At the original data image, we observe that the peak of the activity has been transferred to anterior brain parts. Having in mind that the LORETA inversion is applied to the mean value of the activity of part B, the fact that low frequencies prevail at this part is consistent to the transition of the activity to anterior parts. We also observe that there still exists a posterior activity at two sources which gave maxima at the first spindle part (A) also.

At the right image we can observe again that the same sources, as those at the first part are maintained, but the intensity order has been changed. Now we have first the source at the anterior parts, which is expected, since most ICs, which participate in the recomposition, have from the start of part B (or soon after) and for most of the duration of part B frequencies 12 and 11 Hz, which is of course also reflected at the EEGs recomposed from these ICs.

At the image at center, we can see that the both the spatial distribution is maintained as well as the intensity order of the sources. As a result, the sources which had the local maxima at the first spindle part (A) continue to give local maxima at this part. The difference is that now these ICs have no interest for spindle generation.

**Summary of results and conclusions:**

A) We have spindle with frequency transition between the two parts, from high to low, but this transition is gradual and does not happen simultaneously in all leads. Despite the problems of grouping, as they were mentioned before, which result for the second spindle part when we grouped ICs 1,2,4,6 and 7, the main sources of high frequency spindles (part A), both for the total EEG, as well as for the EEG recomposed from the main high frequency ICs, are located at posterior brain parts and the main sources of EEG where low frequency spindles prevail (part B) are located at anterior parts.

B) For both ICs groups, the sources of the EEGs which are recomposed from these ICs maintain their spatial distribution, when passing from part A to part B. This speaks in favour of the assumption that ICs reflect separate “local” source activities.

Original Data IC's 5,8 IC's 1,2,4,6,7




Original Data:

| TX | TY | TZ | Value |
|---|---|---|---|
| -3 | 45 | -6 | 3.002723E-0003 |
| 4 | -67 | 15 | 2.896745E-0003 |
| 53 | -53 | 15 | 2.602360E-0003 |
| -3 | -46 | 43 | 2.567034E-0003 |

IC's 5,8:

| TX | TY | TZ | Value |
|---|---|---|---|
| 60 | -39 | 15 | 9.102099E-0004 |
| -3 | 52 | 1 | 6.068066E-0004 |
| 4 | -46 | 43 | 5.960983E-0004 |
| 39 | -46 | 50 | 4.426119E-0004 |

IC's 1,2,4,6,7:

| TX | TY | TZ | Value |
|---|---|---|---|
| -3 | 45 | -6 | 2.876560E-0003 |
| 4 | -67 | 15 | 2.481738E-0003 |
| -3 | -46 | 43 | 2.267406E-0003 |
| -59 | -32 | 8 | 2.199722E-0003 |

Figure 8.5.3: Source activity analysis for part B of spindle 4

## 8.6) Spindle 5 *(2nd Third of the Night)*

**Spindle Characteristics:**

1) It has 13 Hz frequency and at some parts 12Hz. All right leads end with 12 Hz, while the left remain at 13 Hz . There is a spindle with 11 Hz only at lead O2.

2) EEG division and ICs grouping:

At the original EEG, we can easily distinguish the morphology of three spindle-like formations (at O1 two). The second from the third spindle-like formation are separated clearly at all leads (except O1), while the transition from the first to the second is obvious because of the decrease of the amplitude of the spindle-like formation and the increase that follows, i.e. a typical waining-waxing cycle. By observing the ICs we can see only two ICs (2,4) which are activated clearly only after 1,8 sec, with main frequency 13Hz, corresponding to the third spindle-like formation. Searching spindles related to the first two spindle-like formations, with frequency content at 12-13Hz (this rejects IC 8), without presenting activity after 1,8 sec (this rejects IC 3) and without frequency transition out of the 12-13Hz range, at the time window 0-1,8 sec (this rejects IC 1), we can choose IC 5 and 7. So, splitting the spindle window at two parts (A: 0-1,8 sec, B: 1,8 sec – spindle end), ICs 5 and 7 can be selected as main ICs for the first part and ICs 2 and 4 for the second.

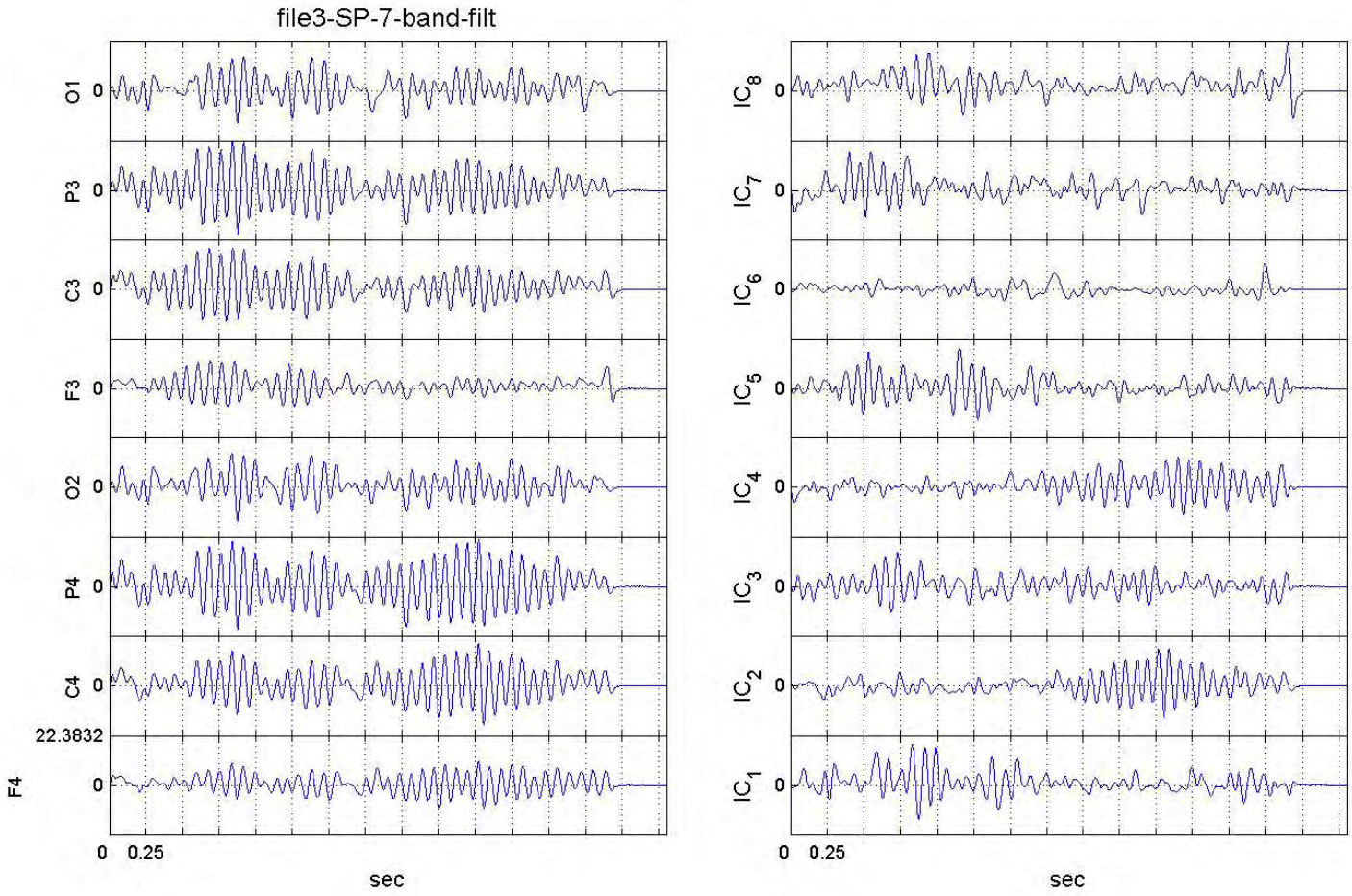
**Source activity analysis (part A):**

In Fig. 8.6.1, at left we have the 3D mean source activity map image from the original data (M-L-EEG-O/A), at the center the 3D mean source activity map image of the recomposition of the EEG based on ICs 2,4 (M-L-EEG-A/A) and at right the 3D mean source activity map image of the recomposition of the EEG based on ICs 5,7 (M-L-EEG-B/A). The main ICs for this spindle part are ICs 5,7.

If we observe the image at left we can see that the main activity is located at the posterior (central and right) brain parts. Third in intensity order, and by 12% lower amplitude than the main source, there existed an anterior source. As it is mentioned above, the EEG frequency at the majority of the leads is mainly limit high (13Hz), with only a small percentage of low (12-11Hz) waves, therefore the primary activation is expected to be in posterior brain parts, as well as the existence of a smaller intensity activity at the anterior parts.

At the image at right, which as mentioned is the image of the sources of the EEGs recomposed from the main ICs for this spindle part (5,7) we can see that three of four local maxima are the same as those present in the image of the sources of the total EEG. Therefore, we have posterior (central and right) sources, but now at the first four we have also left posterior sources and anterior sources too. The existence of primary posterior sources, but also of secondary anterior sources corresponds to the fact that the ICs which recompose the EEG (and the recomposed EEG by itself) have mainly limit high frequency spectrum, but also, at a small part of the time evolution of IC 5, low frequency spectrum.

At the image at center we have only posterior (right and central) brain parts active, but this activity does not concern us for spindle source study because ICs 2,4 at part A (and respectively the recomposed EEGs from these ICs) do not possess spindle-like morphology.


file3-SP-7-band-filt
O1
P3
C3
F3
O2
P4
C4
F4
0
22.3832
0
0.25
sec
IC8
IC7
IC6
IC5
IC4
IC3
IC2
IC1
0
0.25
sec

Original Data ICs 2,4 ICs 5,7




Original Data:

| TX | TY | TZ | Value |
|---|---|---|---|
| 4 | -67 | 15 | 3.396875E-0003 |
| 53 | -53 | 15 | 3.170417E-0003 |
| -3 | 45 | -6 | 3.037206E-0003 |
| -3 | -46 | 43 | 3.037206E-0003 |

ICs 2,4:

| TX | TY | TZ | Value |
|---|---|---|---|
| 53 | -53 | 15 | 1.236503E-0003 |
| 53 | -60 | -6 | 8.970715E-0004 |
| 4 | -67 | 22 | 8.873734E-0004 |
| 4 | -67 | 15 | 8.873734E-0004 |

ICs 5,7:

| TX | TY | TZ | Value |
|---|---|---|---|
| 4 | -67 | 15 | 2.028425E-0003 |
| -59 | -32 | 8 | 1.742059E-0003 |
| -3 | 45 | -6 | 1.638649E-0003 |
| 53 | -53 | 15 | 1.543193E-0003 |

Figure 8.6.2: Source activity analysis for part A of spindle 5

**Source activity analysis (part B):**

In Fig. 8.6.2, at left we have the 3D mean source activity map image from the original data (M-L-EEG-O/B), at the center the 3D mean source activity map image of the recomposition of the EEG based on ICs 2,4 (M-L-EEG-A/B) and at right the 3D mean source activity map image of the recomposition of the EEG based on IC 5,7 (M-L-EEG-B/B). The main ICs for this spindle part are ICs 2,4.

At the source activity map of the original data we observe that we have again posterior (right and central) sources, but now the anterior and the left posterior sources are obviously attenuated. The maintenance of the peak at posterior parts was expected because the EEG frequency remain (limit) high. Furthermore, the fact that now the time period where we have low frequency EEG is small (and only at the right leads), matches with the attenuation of the anterior sources.

At part B the main spindle-like activity of the EEG is recomposed from ICs 2,4. This is clear if we observe the sources of the EEGs which are recomposed from these ICs and compare them with the sources at the left image. All four local maxima are the same for the two images. The peak of the activity at the posterior brain parts is expected since the frequency of the EEGs recomposed by ICs 2 and 4 is purely (limit) high.

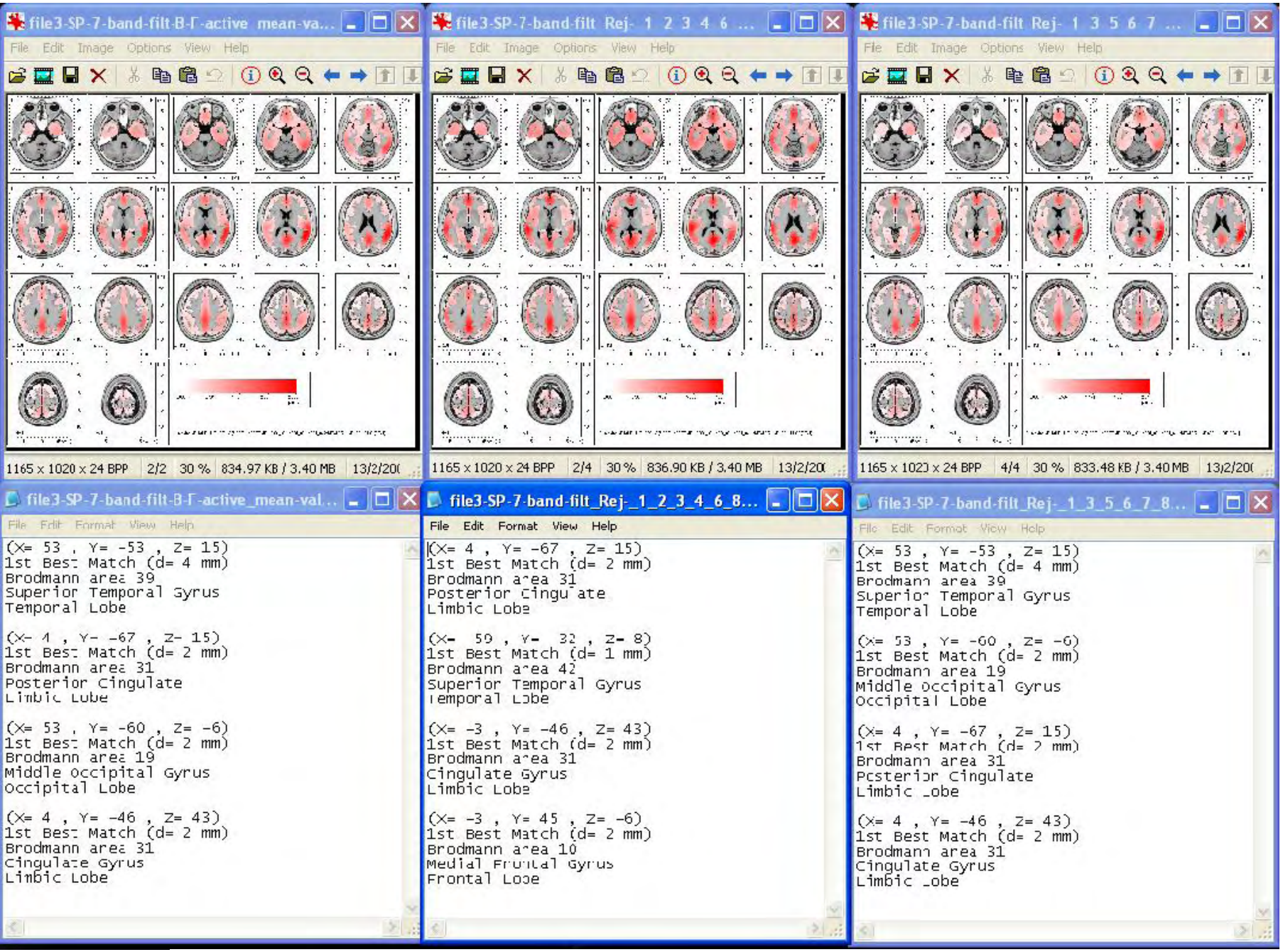
From the sources of the EEG recomposition based on ICs 5 and 7, we observe that the three of four local maxima remain the same from the first part (A). Two of them have the same intensity order. Therefore the action of these sources is maintained and at this spindle part, but with clearly smaller intensity, as it is obvious from the comparison of the morphology of ICs 5 and 7 at part A and part B. Nevertheless, this activity does not concern us for spindle source study at this part because ICs 5 and 7 (and respectively the recomposed EEGs from these ICs) do not possess spindle-like morphology.

**Summary of results and conclusions:**

A) We have mainly (limit) high frequency EEG (13 Hz) and we can see activated permanently stronger activation of sources at posterior brain parts.

B) For both groups of ICs, the sources of the EEGs recomposed from these ICs maintain their spatial distribution in the transition from part A to part B. More specifically, three of four local maxima areas appear at both parts and the two strongest remain at exactly the same Talairach point at both parts. This speaks in favour of the assumption that ICs reflect separate “local” source activities.

Original Data ICs 5,7 ICs 2,4




Original Data :

| TX | TY | TZ | Value |
|---|---|---|---|
| 53 | -53 | 15 | 2.934992E-0003 |
| 4 | -67 | 15 | 2.336484E-0003 |
| 53 | -60 | -6 | 2.221386E-0003 |
| 4 | -46 | 43 | 2.094779E-0003 |

ICs 2,4:

| TX | TY | TZ | Value |
|---|---|---|---|
| 53 | -53 | 15 | 2.347066E-0003 |
| 53 | -60 | -6 | 1.702773E-0003 |
| 4 | -67 | 15 | 1.684365E-0003 |
| 4 | -46 | 43 | 1.619936E-0003 |

ICs 5,7:

| TX | TY | TZ | Value |
|---|---|---|---|
| 4 | -67 | 15 | 7.053432E-0004 |
| -59 | -32 | 8 | 7.025772E-0004 |
| -3 | -46 | 43 | 6.057653E-0004 |
| -3 | 45 | -6 | 5.753388E-0004 |

Figure 8.6.3: Source activity analysis for part B of spindle 5

## 8.7) Spindle 6 *(2nd Third of the Night)*

**Spindle Characteristics:**

1) It starts with frequency 10-11Hz and at all leads, almost simultaneously, (from 0,75 till 1 sec from the spindle's start) there is a transition to 13 Hz that is maintained till the end of the spindle's time window. Leads F3 and F4 present a differentiation with transition from 13 to 12 and to 11 (small time duration part) and then again to 12 and 13 Hz.

2) EEG division and ICs grouping:

By observing the spindle's morphology we can distinct a well-formed low frequency part and afterwards that two well-formed limit high frequency (except leads F3, F4, see above) spindle's parts follow. Therefore, there is a possibility of dividing the spindle in two parts, with division point, as it is indicated by the spectrum of frequencies of the leads, between 0,75 and 1 sec. By observing the ICs also, the first (low frequency) spindle part A is represented by IC 2. IC 5 has intermittent low frequency activity both at the first part as well as at the second, while at the second part the spindle-like activity lasts longer, so this IC is rejected. For the second (limit high frequency) spindle's part, we cannot find ICs which morphologically represent either the first high frequency part or the second one, we do not divide further the spindle. For this second spindle part (B) we choose ICs that do not have extensive spindle-like morphology at the first part and have well formed spindle-like morphology at the second part with frequency 13 Hz (so IC's 1,3,8 are rejected). Therefore, for the second group of ICs, which is representative for the two well-formed spindle parts at the second part of the original spindle (part B) we choose ICs 4 and 7. ICs 4 and 7 have, at part B, in the spindle frequency bandwidth, spectral power peak at 13 Hz. The division of the parts is also confirmed by observing the time point at which IC 2 ends and the IC's 4 and 7 start. So, it is approximated at 1 sec.

**Source activity analysis (part A):**

At the part A we have a low frequency activity (10Hz). In Fig. 8.7.1, at left we have the 3D mean source activity map image from the original data (M-L-EEG-O/A), at the center the 3D mean source activity map image of the recomposition of the EEG based on ICs 4,7 (M-L-EEG-A/A) and at right the 3D mean source activity map image of the recomposition of the EEG based on IC 2 (M-L-EEG-B/A). The main IC for this spindle part is IC 2.

If we observe the source activity map of the original data, we can see that the activity peak is located at anterior brain parts. As it is mentioned above, the EEG frequency is low, so the appearance of activation of the anterior brain parts is expected.

If we observe the image at right we can see that we have a source at an anterior brain part, which give us the global maximum followed by sources at posterior brain parts, but with lower intensity. Therefore, the primary activity is located at the anterior brain parts, as it was expected for low frequency spindle-like EEG. We should also notice the coincidence of the four local maxima from the original data (total EEG) with the sources of EEG recomposed from IC 2 (the strongest, anterior, points are very close concerning Talairach coordinates).

If we observe the image at center we can see that the action now concerns mainly posterior brain parts. Nevertheless, this activity does not concern us for spindle source study because IC's 4 and 7 at part A (and the recomposed EEGs from these ICs) do not have spindle-like morphology.

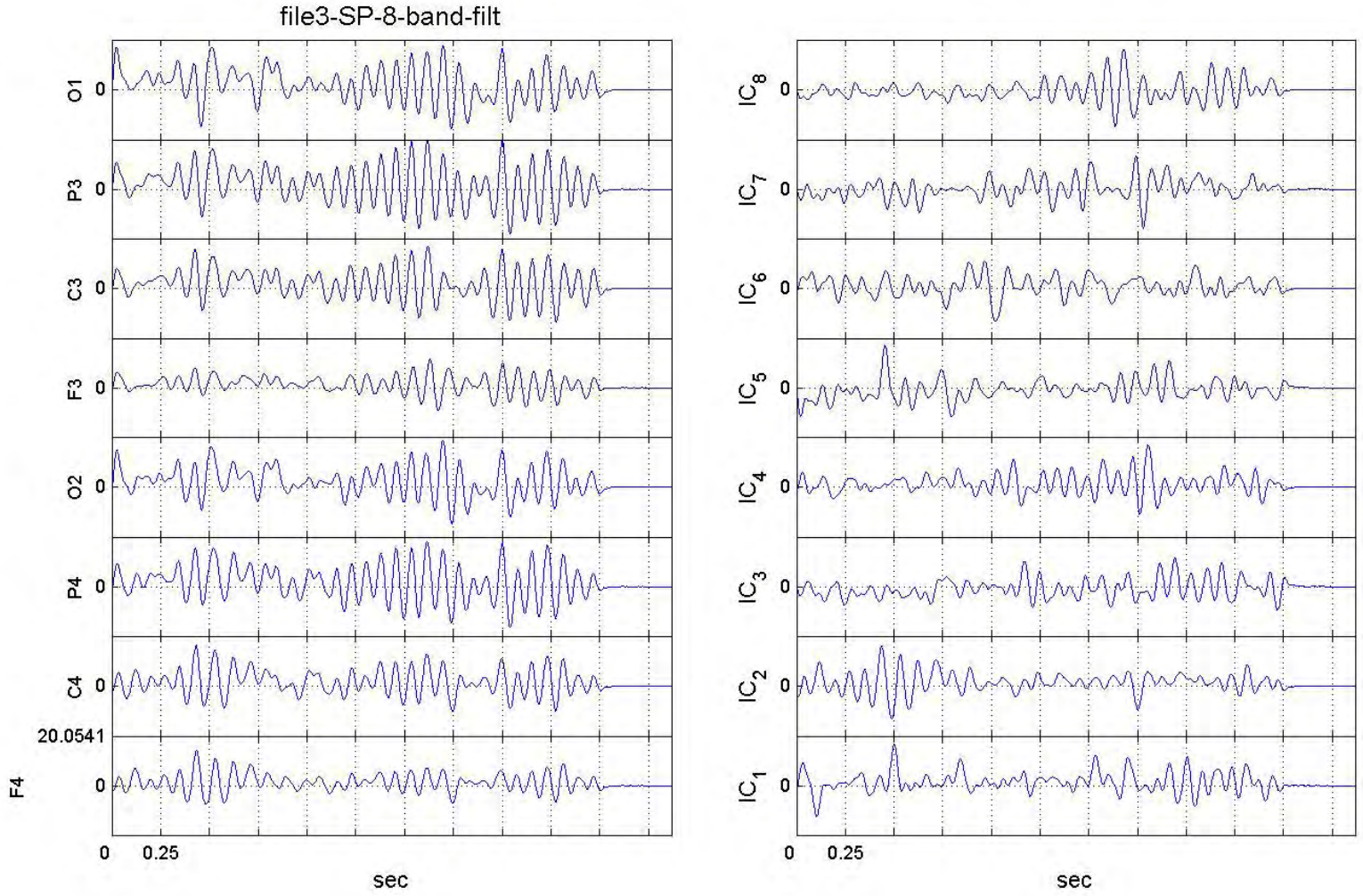



Figure 8.7.1: At left we have the original (filtered) EEGs and at right the ICs for spindle 6.

Original Data ICs 4,7 IC 2




Original Data:

| TX | TY | TZ | Value |
|---|---|---|---|
| -3 | 45 | -6 | 2.285493E-0003 |
| 4 | -67 | 15 | 2.052462E-0003 |
| 60 | -39 | 15 | 1.864245E-0003 |
| -59 | -39 | 1 | 1.765655E-0003 |

ICs 4,7:

| TX | TY | TZ | Value |
|---|---|---|---|
| -3 | -46 | 43 | 1.198625E-0003 |
| -59 | -32 | 8 | 1.123417E-0003 |
| 4 | -67 | 22 | 1.099914E-0003 |
| 53 | -53 | 15 | 1.024706E-0003 |

IC 2:

| TX | TY | TZ | Value |
|---|---|---|---|
| -3 | 52 | 1 | 1.348586E-0003 |
| 4 | -67 | 15 | 7.721316E-0004 |
| -59 | -32 | 8 | 7.351116E-0004 |
| 60 | -39 | 8 | 6.875144E-0004 |

Figure 8.7.2: Source activity analysis for part A of spindle 6

**Source activity analysis (part B):**

As it is mentioned above, at part B of the spindle we observe a limit high frequency activity (13 Hz). More specific, while at part A all EEGs that present spindle activity have main frequency 10-11 Hz, at part B we observe a transition to 13Hz, which is maintained stable at all electrodes, except the anterior ones (F4, F3, see paragraph above for spindle characteristics).

In Fig. 8.7.2, at left we have the 3D mean source activity map image from the original data (M-L-EEG-O/B), at the center the 3D mean source activity map image of the recomposition of the EEG based on ICs 4,7 (M-L-EEG-A/B) and at right the 3D mean source activity map image of the recomposition of the EEG based on IC 2 (M-L-EEG-B/B). The main ICs for this spindle part are ICs 4 and 7.

At the source activity map of the original data we can observe that the activity peak is transferred to posterior brain parts. Knowing that the EEG frequency is limit high (13Hz) at the majority of the leads, the activation of the posterior brain parts is expected.

At the image of the sources of the EEGs reconstructed by IC's 4 and 7, we can see again activated the same sources with those from the source activity map of the original data, but with different intensity order. As it is mentioned before, these are the main ICs for this part B and we can see primary activation again at posterior brain parts, which are responsible for high frequency EEGs, according to the assumption that we check.

At the image at right, we can see that the spatial distribution is maintained. As a result, the sources that gave local maxima at the first part of the spindle (A) continue giving local maxima at this part also, with the same intensity order. The anterior sources are the most powerfull and this agree with the fact that IC 2 (and the recomposed EEGs from it) maintain low amplitude and low frequency activity at part B also.

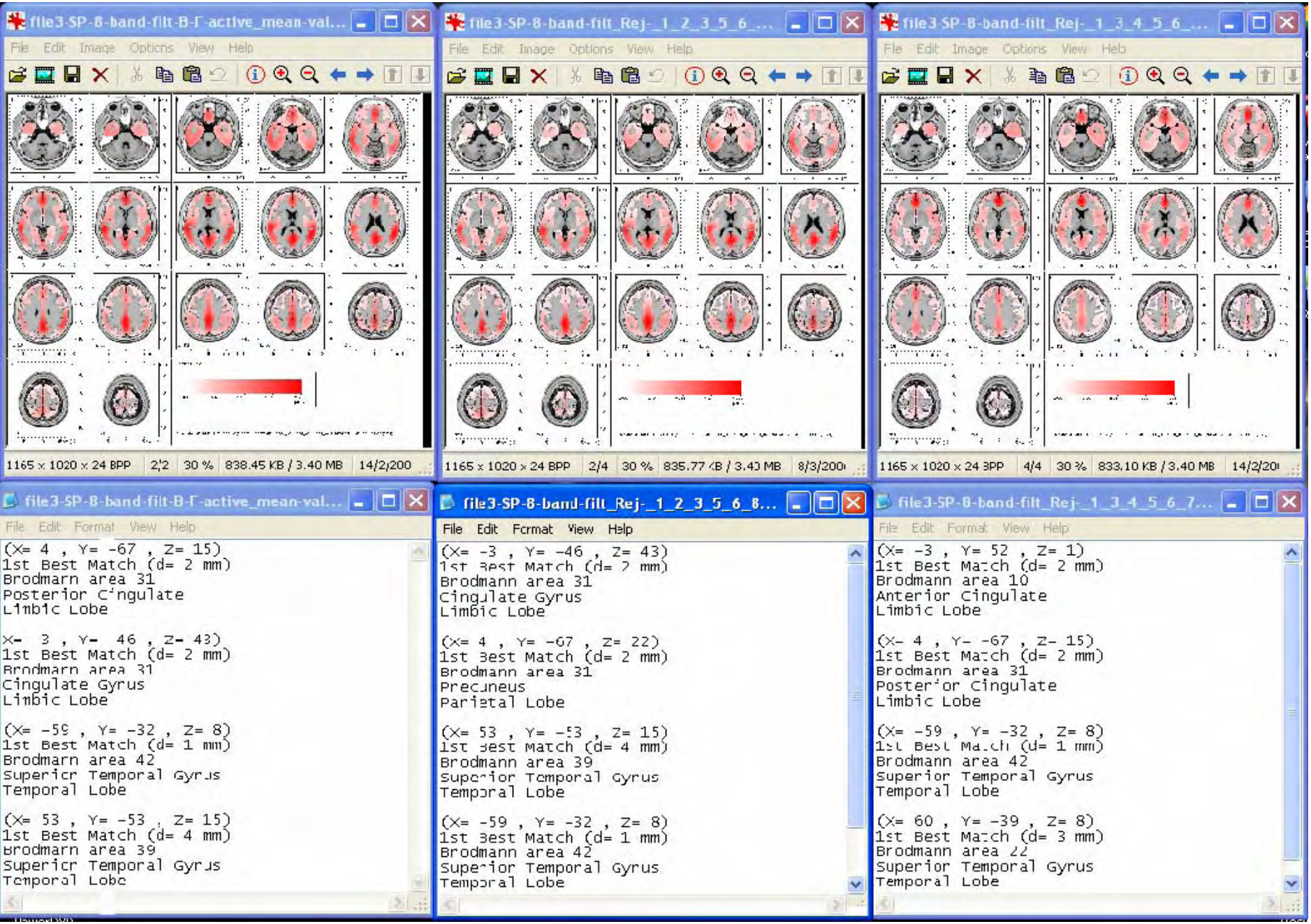
**Conclusions:**

A) We have spindle with frequency change at the two parts, from low to limit high, almost simultaneously at all recordings. We observe that the main sources of low frequency spindle parts (part A) are located at anterior brain parts and the main sources of EEGs where high frequency spindle activity prevail (part B) are located at posterior parts. The groups of ICs which where chosen based on the morphological and spectral analysis of the ICs for parts A and B recompose EEGs which have respectively anterior and posterior main sources.

B) For both groups of ICs, the sources of the recomposed EEGs from these ICs fully maintain their spatial distribution in the transition from part A to B. For IC 2 the intensity order is also maintained. This speaks in favour of the assumption that ICs reflect separate "local" source activities.

C) The sources of the original EEG changed from one part to the other and followed with great accuracy the sources of EEG which are recomposed from the main IC's of each part.

Original Data ICs 4,7 IC 2




Original Data:

| TX | TY | TZ | Value |
|---|---|---|---|
| 4 | -67 | 15 | 2.326156E-0003 |
| -3 | -46 | 43 | 2.216690E-0003 |
| -59 | -32 | 8 | 2.198445E-0003 |
| 53 | -53 | 15 | 2.180201E-0003 |

IC 2:

| TX | TY | TZ | Value |
|---|---|---|---|
| -3 | 52 | 1 | 5.634095E-0004 |
| 4 | -67 | 15 | 3.225796E-0004 |
| -59 | -32 | 8 | 3.071134E-0004 |
| 60 | -39 | 8 | 2.872284E-0004 |

ICs 4,7:

| TX | TY | TZ | Value |
|---|---|---|---|
| -3 | -46 | 43 | 1.628521E-0003 |
| 4 | -67 | 22 | 1.539112E-0003 |
| 53 | -53 | 15 | 1.449703E-0003 |
| -59 | -32 | 8 | 1.398612E-0003 |

Figure 8.7.3: Source activity analysis for part B of spindle 6

## 8.8) Spindle 7 *(2nd Third of the Night)*

**Spindle Characteristics:**

1) It has a stable frequency of 13Hz. This is an example of a very well-formed spindle.

2) EEG division and ICs grouping:

At the original EEGs, only at O1 and O2 there can be discerned a division of the spindle at two parts. At the corresponding ICs this becomes clearer, resulting in the grouping of ICs 2 and 7 for part A (because they present a continuous spindle-like activity at part A and not at part B) and ICs 1 and 8 for part B (because they present a continuous spindle-like activity at part B and not at part A). The appearance of some waves with frequency 12 Hz at ICs 2 and 7 towards the end of part B do not possess enough characteristics to be characterized as spindles (see [43], characteristics for spindle definition).

**Source activity analysis (part A):**

In Fig. 8.8.1, at left we have the 3D mean source activity map image from the original data (M-L-EEG-O/A), at the center the 3D mean source activity map image of the recomposition of the EEG based on ICs 2,7 (M-L-EEG-A/A) and at right the 3D mean source activity map image of the recomposition of the EEG based on ICs 1,8 (M-L-EEG-B/A). The main ICs for this spindle part are ICs 2,7.

By observing the left image we can see that the main activity is located at right posterior brain parts. As it is mentioned above, the EEG's frequency is limit high, so the appearance of this activation of posterior brain parts is expected.

At the image at center, which as we said before is the image of the sources of the recomposed EEGs, which result from the main ICs of this spindle part (2,7), we can see that almost the same sources as the image at the left are activated. So, we see that right posterior sources are activated again, which are responsible for high frequency EEGs, according to the assumption that is checked in the present Thesis.

At the image at right we observe that same brain sources are activated again, i.e. we have mainly right posterior sources, slight differentiation at the secondary source posterior parts (located at middle temporal gyrus) and activation of the anterior lobe also. This activity does not concern us for spindle source study because IC's 1,8 at part A (and the recomposed EEGs from these ICs) do not possess spindle-like morphology.

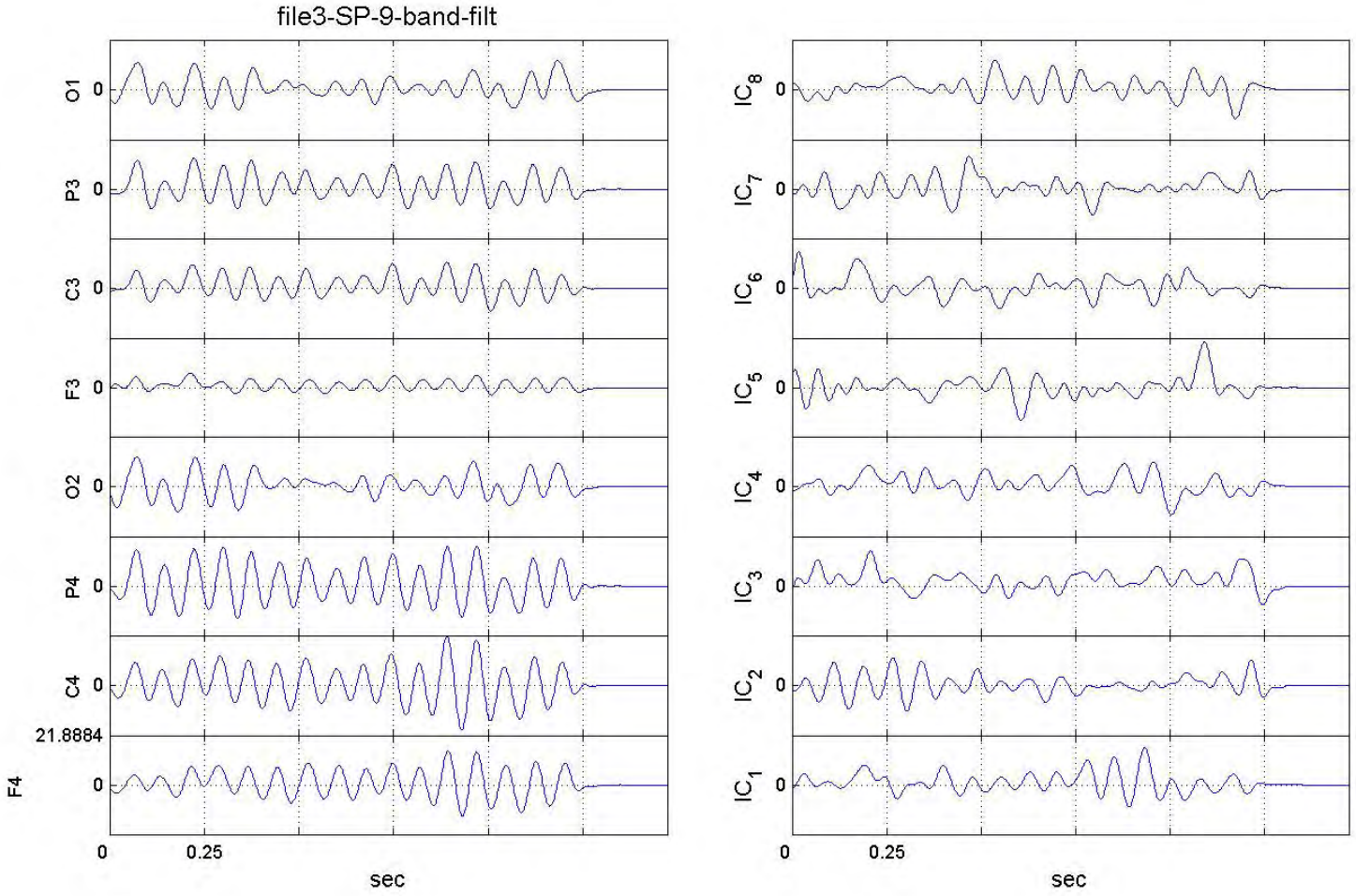



Figure 8.8.1: At left we have the original (filtered) EEGs and at right the ICs for spindle 7.

Original Data IC's 2,7 IC's 1,8




Original Data:

| TX | TY | TZ | Value |
|---|---|---|---|
| 60 | -39 | 15 | 4.859968E-0003 |
| 60 | -46 | 15 | 4.859968E-0003 |
| 4 | -46 | 43 | 3.583035E-0003 |
| -3 | -46 | 43 | 3.583035E-0003 |

IC's 2,7:

| TX | TY | TZ | Value |
|---|---|---|---|
| 60 | -46 | 15 | 3.729405E-0003 |
| 60 | -39 | 15 | 3.729405E-0003 |
| 4 | -46 | 43 | 2.866523E-0003 |
| 39 | -46 | 50 | 2.018266E-0003 |

IC's 1,8:

| TX | TY | TZ | Value |
|---|---|---|---|
| 60 | -46 | 15 | 1.820729E-0003 |
| 53 | -53 | 15 | 1.820729E-0003 |
| 4 | -67 | 15 | 1.549404E-0003 |
| -3 | 45 | -6 | 1.470863E-0003 |

Figure 8.8.2: Source activity analysis for part A of spindle 7

**Source activity analysis (part B):**

In Fig. 8.8.2, at left we have the 3D mean source activity map image from the original data (M-L-EEG-O/B), at the center the 3D mean source activity map image of the recomposition of the EEG based on ICs 2,7 (M-L-EEG-A/B) and at right the 3D mean source activity map image of the recomposition of the EEG based on ICs 1,8 (M-L-EEG-B/B). The main ICs for this spindle part are ICs 1,8.

At the source activity map of the original data we observe that the peak of the activity at the right posterior parts is maintained at this part also, as it was expected since the frequency of the EEGs is maintained at (limit) high frequency, but at slightly different points from the first part (A) of the spindle (the global maximum peak is again located at the superior temporal gyrus, but in a different Broadmann area). Additionally, the activity transits slightly to the anterior brain parts (the second local maximum is located at the medial frontal gyrus, and the third at the anterior cingulate).

At the image at right, which corresponds to sources of the EEG recomposed from the main ICs for part B (1,8), we observe what was mentioned for the original data image also. We can see that the peak of the activity remains at the right posterior parts but the activity extends now to the anterior brain parts also (the second local maximum is located at the medial frontal gyrus).

At the sources of the EEG recomposed by ICs 2 and 7 we observe that the sources which gives local maxima remain the same. So, the activity of these sources continues to exist at this spindle part also, but with smaller intensity, as it is obvious from the comparison of the morphology of ICs 2,7 at parts A and B. This speaks in favour of the assumption that ICs reflect separate "local" source activities. These sources are located mainly at the right posterior brain parts. Nevertheless, this activity does not concern us for spindle generation because the IC's 2,7 at part B (and the corresponding to these ICs recomposed EEGs) do not possess spindle-like morphology.

**Conclusions:**

A) We have only (limit) high frequency EEGs and we observe that mainly the posterior brain parts are activated.

B) For ICs 2,7 the 4 main sources of the recomposed EEGs from these ICs maintain their spatial distribution (with the same intensity order). The same happens, but less, for ICs 1,8 (3 of 4 sources are the same). This speaks, as it is mentioned before, in favour of the assumption that ICs reflect separate "local" source activities.

Original Data IC's 2,7 IC's 1,8




Figure 8.8.3: Source activity analysis for part B of spindle 7

Original Data:

| TX | TY | TZ | Value |
|---|---|---|---|
| 53 | -53 | 15 | 2.147761E-0003 |
| -3 | 45 | -6 | 1.768744E-0003 |
| -3 | 52 | 1 | 1.768744E-0003 |
| 4 | -67 | 15 | 1.701364E-0003 |

IC's 2,7:

| TX | TY | TZ | Value |
|---|---|---|---|
| 60 | -39 | 15 | 8.148348E-0004 |
| 60 | -46 | 15 | 8.148348E-0004 |
| 4 | -46 | 43 | 6.103272E-0004 |
| 39 | -46 | 50 | 4.249923E-0004 |

IC's 1,8:

| TX | TY | TZ | Value |
|---|---|---|---|
| 60 | -39 | 15 | 1.351981E-0003 |
| -3 | 45 | -6 | 1.182320E-0003 |
| 4 | -67 | 15 | 1.102792E-0003 |
| 53 | -60 | -6 | 9.649433E-0004 |

## 8.9) Spindle 8 *(3rd Third of the Night)*

**Spindle Characteristics:**

1) In all leads, except F4 and C4, the spindle is active for the whole time window and it is of high frequency (14 Hz and at F3, C3 we have 13 Hz). At F4 and C4, between 1.75 and 2 sec we have transition to 12 Hz.
2) EEG division and ICs grouping:
By observing visually the morphology of the spindles we locate a first spindle like formation at the start of the time window till almost 1 sec (see leads C4, P4, P3). Next, there is a small duration and greater (comparing to the previous formation at almost all leads) amplitude spindle-like formation (see e.g. P3) between 1 and 1.5 sec and finally one spindle like formation with great amplitude again at almost all leads (F4, O2, F3, C3, P3, O1). In order to find the way to divide the spindles, and because the morphology does not help us for that, we observe the ICs. We can see that ICs 3 and 4 have spindle-like activity only after 1,5 sec, so that leads us to two parts division: part A: 0-1,5 sec and part B: 1,5 sec – spindle end.
Afterwards, trying to group the ICs which possess spindle-like activity only at one of the two parts, for first part we chouse IC 8, which has spindle activity (14 Hz) only at the first part. This IC has smaller peak amplitude from IC 2, which has a well formed spindle (14 Hz) at the first part, even though this action extends for a small part at the second part also. Therefore, the first group, as main ICs for part A includes ICs 2 and 8. For the second part ICs 3 and 4 have clearly well formed spindle activity at the second part only. IC 4 is of high frequency (14/13 Hz) and IC 3 changes frequency from 14 to 13 and finally 12 Hz. Therefore in the second group of ICs we have only IC 4, as representative of the high frequency spindle formations which last till the end of the spindle and at the third group IC 3, as representative of the low frequency spindle formations which occur towards the end of the spindle (knowing that there are other ICs, like ICs 1,5,7 which maybe represent better the low frequency part at the end of the spindle, but they are not chosen because they present big frequency changes ( IC 1 from 14 to 12 to 13 to 10 Hz at the second part) and/or extend their action at all the time window (IC 5) or present intermittent activity (from part to part) and not well formed spindle activity (IC 7)).
Finally, we have separation at two parts, A: 0-1,5 sec, B: 1,5 sec till the end of the spindle and groups of as follows, group A: 2,8 (main ICs for part A), group B: 4 (main high frequency IC for part B), group C: 3 (main low frequency IC for part B).

**Source activity analysis (part A):**
In Fig. 8.9.1, at left we have the have the 3D mean source activity map image from the original data (M-L-EEG-O/A), at the center the 3D mean source activity map image of the recomposition of the EEG based on IC 4 (M-L-EEG-A/A), at right the 3D mean source activity map image of the recomposition of the EEG based on ICs 2,8 (M-L-EEG-B/A) and at the next page the 3D mean source activity map image of the recomposition of of the EEG based on IC 3 (M-L-EEG-C/A). The main ICs for this spindle part are ICs 2,8.
From the source activity map of the original data we observe that we have active the posterior and right posterior brain parts. This part of the spindle is of high frequency, therefore the appearance of activity of the posterior brain parts is expected.

By observing the image at right, which is the sources image of the EEGs recomposed by the main ICs, we observe a spread activity. More specifically, we observe the first local maximum at the anterior brain area, the second at the posterior and the last two at the anterior again. The activation of the anterior brain parts **is not** expected due to the fact that the ICs are high frequency.
From the sources of the recomposition of the EEG based on IC 4 and 3 separately we observe that the activity is mainly located at the posterior brain parts. This activity, though, does not concern us for spindle generation because ICs 3 and 4 (and the EEGs recomposed from these ICs) does not possess spindle morphology at this part.

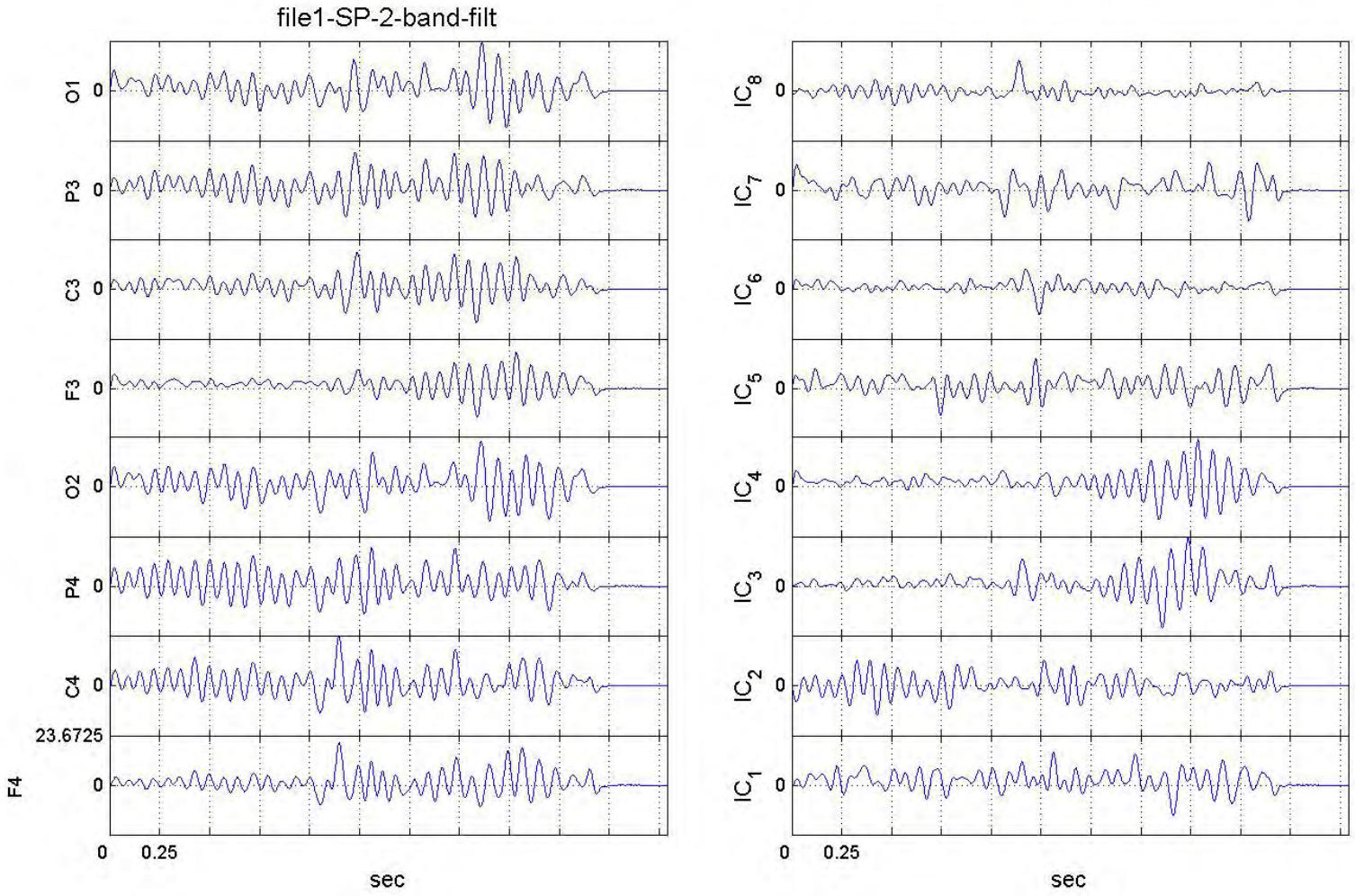
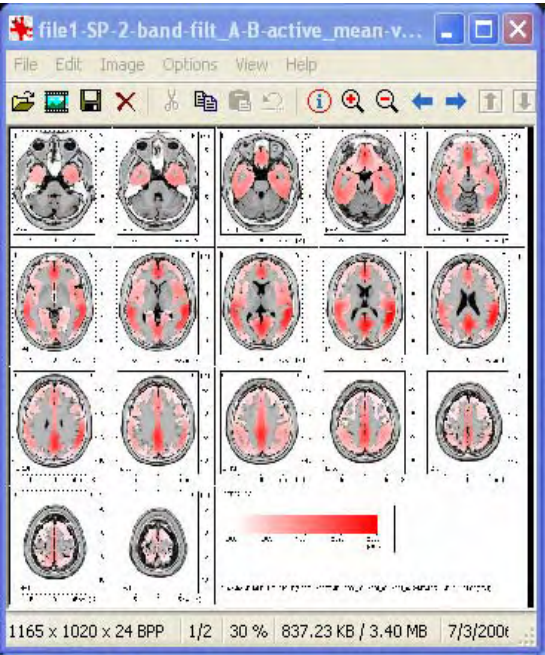
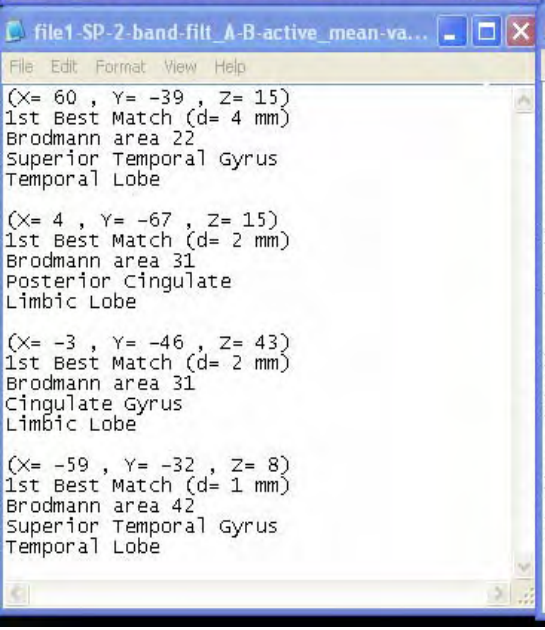


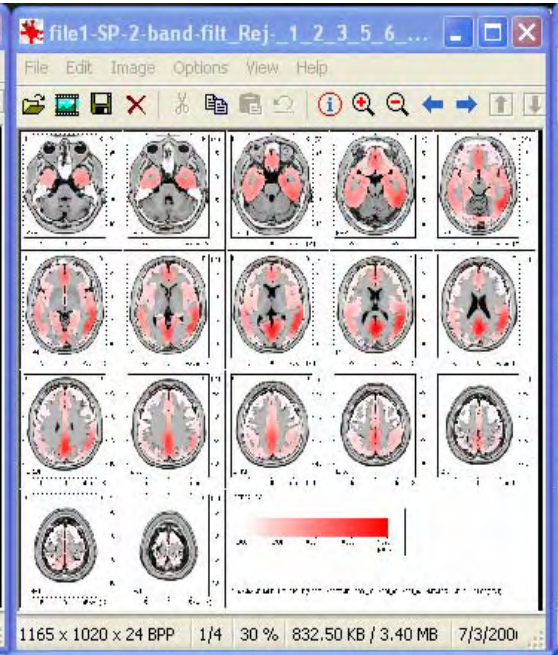

Figure 8.9.1: At left we have the original (filtered) EEGs and at right the ICs for spindle 8.

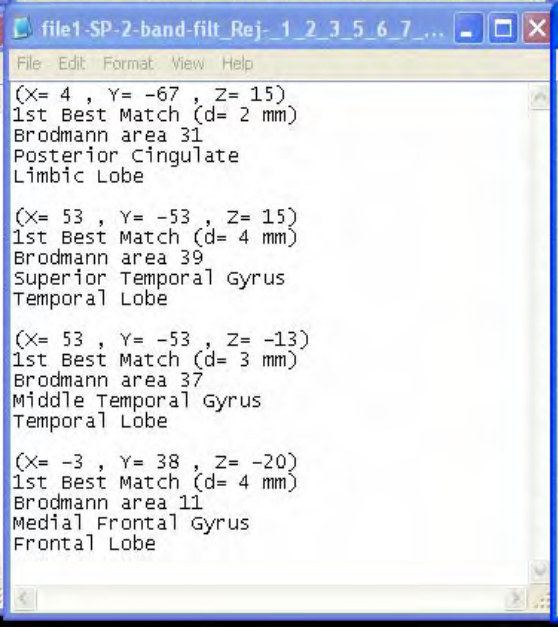
Original Data



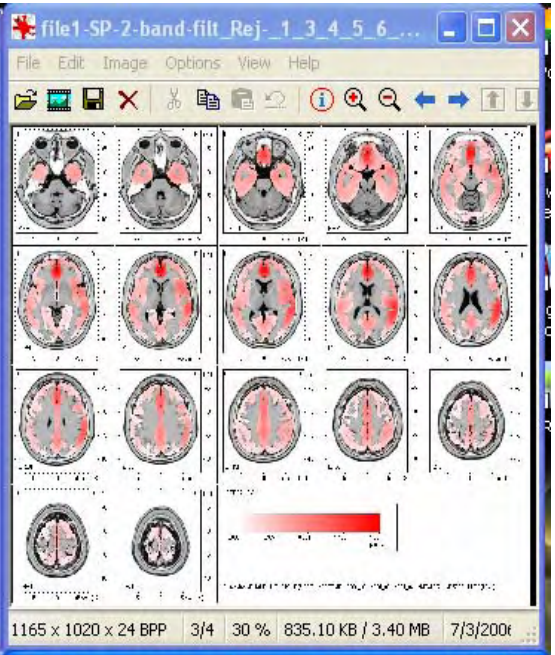



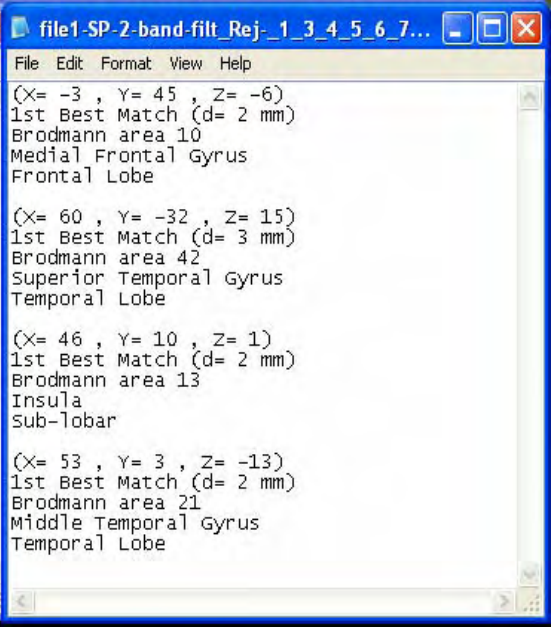

IC 4




ICs 2,8




Original Data:

| TX | TY | TZ | Value |
|---|---|---|---|
| 60 | -39 | 15 | 2.701581E-0003 |
| 4 | -67 | 15 | 2.500287E-0003 |
| -3 | -46 | 43 | 2.224831E-0003 |
| -59 | -32 | 8 | 2.108293E-0003 |

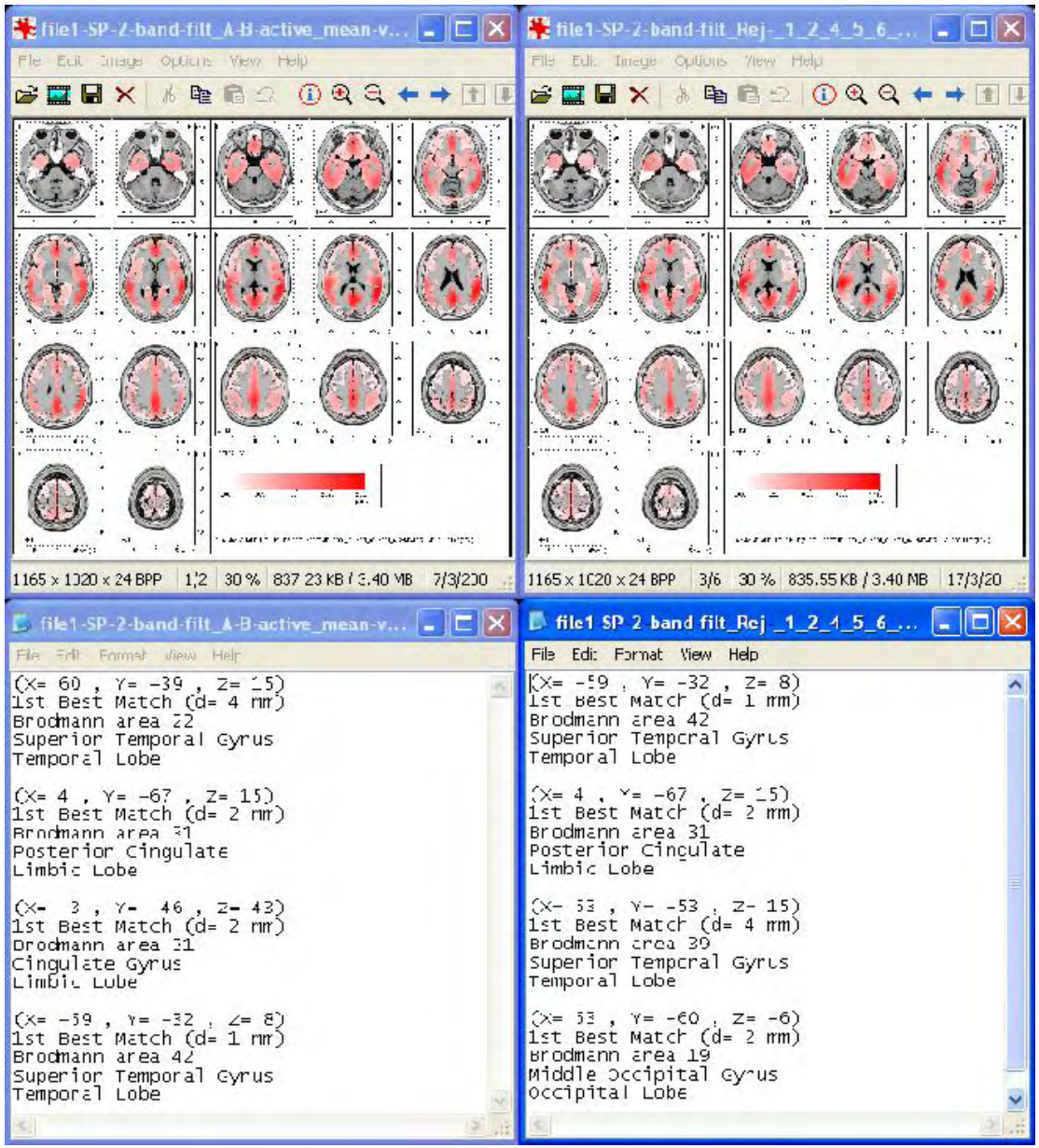
IC 4:

| TX | TY | TZ | Value |
|---|---|---|---|
| 4 | -67 | 15 | 1.322849E-0003 |
| 53 | -53 | 15 | 1.136093E-0003 |
| 53 | -53 | -13 | 1.068654E-0003 |
| -3 | 38 | -20 | 8.040846E-0004 |

ICs 2,8:

| TX | TY | TZ | Value |
|---|---|---|---|
| -3 | 45 | -6 | 1.507036E-0003 |
| 60 | -32 | 15 | 1.294278E-0003 |
| 46 | 10 | 1 | 8.805819E-0004 |
| 53 | 3 | -13 | 8.746719E-0004 |

Original Data IC 3




Original Data:

| TX | TY | TZ | Value |
|---|---|---|---|
| 60 | -39 | 15 | 2.701581E-0003 |
| 4 | -67 | 15 | 2.500287E-0003 |
| -3 | -46 | 43 | 2.224831E-0003 |
| -59 | -32 | 8 | 2.108293E-0003 |

IC 3:

| TX | TY | TZ | Value |
|---|---|---|---|
| -59 | -32 | 8 | 1.118000E-0003 |
| 4 | -67 | 15 | 9.601647E-0004 |
| 53 | -53 | 15 | 9.382432E-0004 |
| 53 | -60 | -6 | 8.067137E-0004 |

Figure 8.9.2: Source activity analysis for part A of spindle 8

**Source activity analysis (part B):**

In Fig. 8.9.2, at left we have the 3D mean source activity map image from the original data (M-L-EEG-O/A), at the center the 3D mean source activity map image of the recomposition of the EEG based on IC 4 (M-L-EEG-A/A), at right the 3D mean source activity map image of the recomposition of the EEG based on ICs 2,8 (M-L-EEG-B/A) and at the next page the 3D mean source activity map image of the recomposition of the EEG based on IC 3 (M-L-EEG-C/A). The main ICs for this spindle part are ICs 3 and 4.

From the source activity map of the original data we observe that we have an inversion of the situation which we saw at the first part, since we can see the anterior parts of the brain to be the most active and secondary the posterior. If we observe the spectral analysis of the spindle for this part we see a mixed activity, because we have low frequency parts but also high frequency parts (14 Hz) and limit high frequency (13 Hz) at the leads. So we cannot know from the beginning which will be the spatial distribution of the most powerful sources.

From the sources of the EEG recomposed by IC 4, which is the main high frequency source for this part of the spindle, we can see that we have active areas which presented local maxima also at the first part of the spindle. So, we have here again a posterior activity which it was expected due to the high frequency of the IC.

From the sources of the EEG recomposed by IC3, which is the main low frequency IC for this part of the spindle, we see that the assumption that low frequency spindles activate anterior brain parts **is not** confirmed, because we see active sources which predominated at the first part (A) to be still active. These sources are all located at posterior brain parts.

From the sources of the EEG recomposed by ICs 2 and 8 we see an activation mainly of the anterior area. This activity though does not concern us for spindle source study because IC 2 and 8 at part B (and respectively the recomposed EEGs from these ICs) do not possess spindle-like morphology.

**Conclusions:**

1) We have spindle with frequency change (from high to low) at two right leads (F4, C4). The other leads remain high. While the sources of the total activity at the high frequency first part, which presents clearly high frequency spectrum, are posterior, the recomposition from the main high frequency ICs at this part does not give as the strongest local maxima posterior sources. At the second part where we have a mixed activity, high frequency ICs gives EEGs with posterior sources but the low frequency ICs activate posterior sources also, an observation which does not confirm the assumption that low frequency spindles activate anterior brain parts.

2) With main example the IC 4 and 3, the sources from the EEG recomposed by those ICs maintain their spatial distribution passing from part A to B. This speaks in favour of the assumption that ICs reflect separate “local” source activities.

Original Data IC 4 ICs 2,8




Original Data:

| TX | TY | TZ | Value |
|---|---|---|---|
| -3 | 45 | -6 | 2.827599E-0003 |
| 4 | -67 | 15 | 2.250991E-0003 |
| 53 | -53 | 15 | 1.851800E-0003 |
| 53 | -53 | -13 | 1.774180E-0003 |

IC 4:

| TX | TY | TZ | Value |
|---|---|---|---|
| 4 | -67 | 15 | 1.323003E-0003 |
| 53 | -53 | 15 | 1.136226E-0003 |
| 53 | -53 | -13 | 1.068778E-0003 |
| -3 | 38 | -20 | 8.041783E-0004 |

ICs 2,8:

| TX | TY | TZ | Value |
|---|---|---|---|
| -3 | 45 | -6 | 1.547094E-0003 |
| 25 | -4 | -27 | 6.552398E-0004 |
| 46 | 10 | -13 | 6.491728E-0004 |
| -31 | -11 | -27 | 6.491728E-0004 |

Original Data IC 3

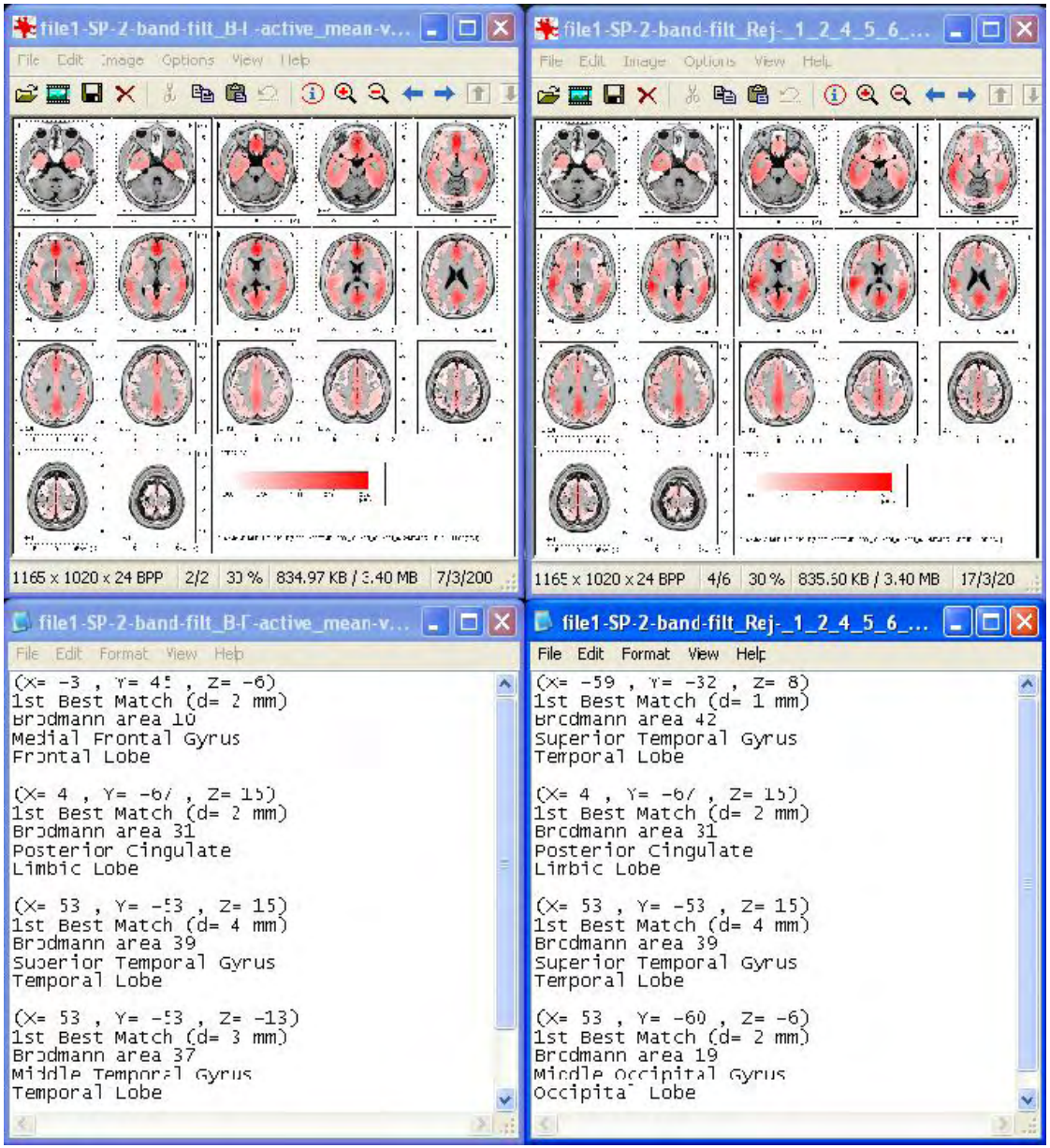



Figure 8.9.3: Source activity analysis for part B of spindle 8

Original Data:

| TX | TY | TZ | Value |
|---|---|---|---|
| -3 | 45 | -6 | 2.827599E-0003 |
| 4 | -67 | 15 | 2.250991E-0003 |
| 53 | -53 | 15 | 1.851800E-0003 |
| 53 | -53 | -13 | 1.774180E-0003 |

IC 3:

| TX | TY | TZ | Value |
|---|---|---|---|
| -59 | -32 | 8 | 5.900432E-0004 |
| 4 | -67 | 15 | 5.067430E-0004 |
| 53 | -53 | 15 | 4.951735E-0004 |
| 53 | -60 | -6 | 4.257567E-0004 |

## 8.10) Spindle 9 *(3rd Third of the Night)*

**Spindle Characteristics:**

1) It has a frequency of 14Hz (at O1 and O2 there exists a transition to 13Hz).
2) EEG division and ICs grouping:

As we can observe, at the original EEGs, there is an initial part where the spindle is well formed in all leads. At leads F3, C3, P3 the spindle ends at approximately 1,25 sec, at the others it continues until the end of the time window, but at C4, P4, O2, O1 their morphology tends to loose its initial clear spindle form, with fluctuations at the peaks amplitude of the waves and most importantly with low frequency (outside of the spindle range) single waves. Also, the amplitude of these peaks decreases progressively. Thus emerges the possibility of division in two parts. By observing the ICs we can see that ICs 1,2,3 present activity at the first part of the spindle's time window, without spindle-like activity afterwards and IC 5 presents activity at the second part, without spindle-like activity before. By looking the other ICs, IC 4 doesn't possess spindle-like activity, ICs 6,7 and 8 present activity both at the first and the second part. This would be a criterion to reject them from belonging to a group of ICs corresponding to sources of one component of the spindle, but, due to their apparent contribution to the second part, they will be studied also as a spindle component generating group. The spindle-like activity's finish time at ICs 1,2,3 and the spindle-like activity's start time at IC 5 is approximately at 1 sec. This is determined to be the division point for the two parts, while if we observed only the leads, the spindle finish time at F3, C3, P3 and the fluctuations at the spindle-like morphology and the amplitude decrease at all leads, except F4, take place slightly later, at 1,25 sec, as it was mentioned. Finally the main ICs for part A (0-1 sec) are ICs 1,2,3 (group A) and for the second part B (1sec – spindle end) are two groups, group of ICs 6,7,8 (group B) and IC 5 (group C).

**Source activity analysis (part A):**

In Fig. 8.10.1, at left we have the 3D mean source activity map image from the original data (M-L-EEG-O/A), at the center the 3D mean source activity map image of the recomposition of the EEG based on ICs 6,7,8 (M-L-EEG-A/A), at right the 3D mean source activity map image of the recomposition of the EEG based on ICs 1,2,3 (M-L-EEG-B/A) and at the next page the 3D mean source activity map image of the recomposition of the EEG based on IC 5 (M-L-EEG-C/A). The main ICs for this spindle part are ICs 2,8.

By observing the image at left, we can see that the main activity appeared at the right posterior brain parts. As it is mentioned above, the EEG frequency is high, therefore it is expected that this activity appeared as activation mainly at posterior parts.

The main ICs of the spindle for this part (A) are ICs 1,2,3. The sources of the EEG recomposition based on ICs 1,2,3 gives us activation at the posterior brain parts, as it is expected for high frequency spindles. It is also important to mention that this activation is located at symmetrical points based on the X axis.

The sources of the EEG recomposition based on ICs 6,7,8, at this part, gives the peak of the activation at posterior brain parts, as it is expected considering that the spindle activity parts from these ICs at part A are high frequency.

The sources of the EEG recomposition based on IC 5, at this part, presents the peak of the activation at anterior brain parts. At this part of the spindle, the IC 5 signal has low amplitude and doesn't possess spindle-like characteristics, so this activation does not concern us for spindle source study.

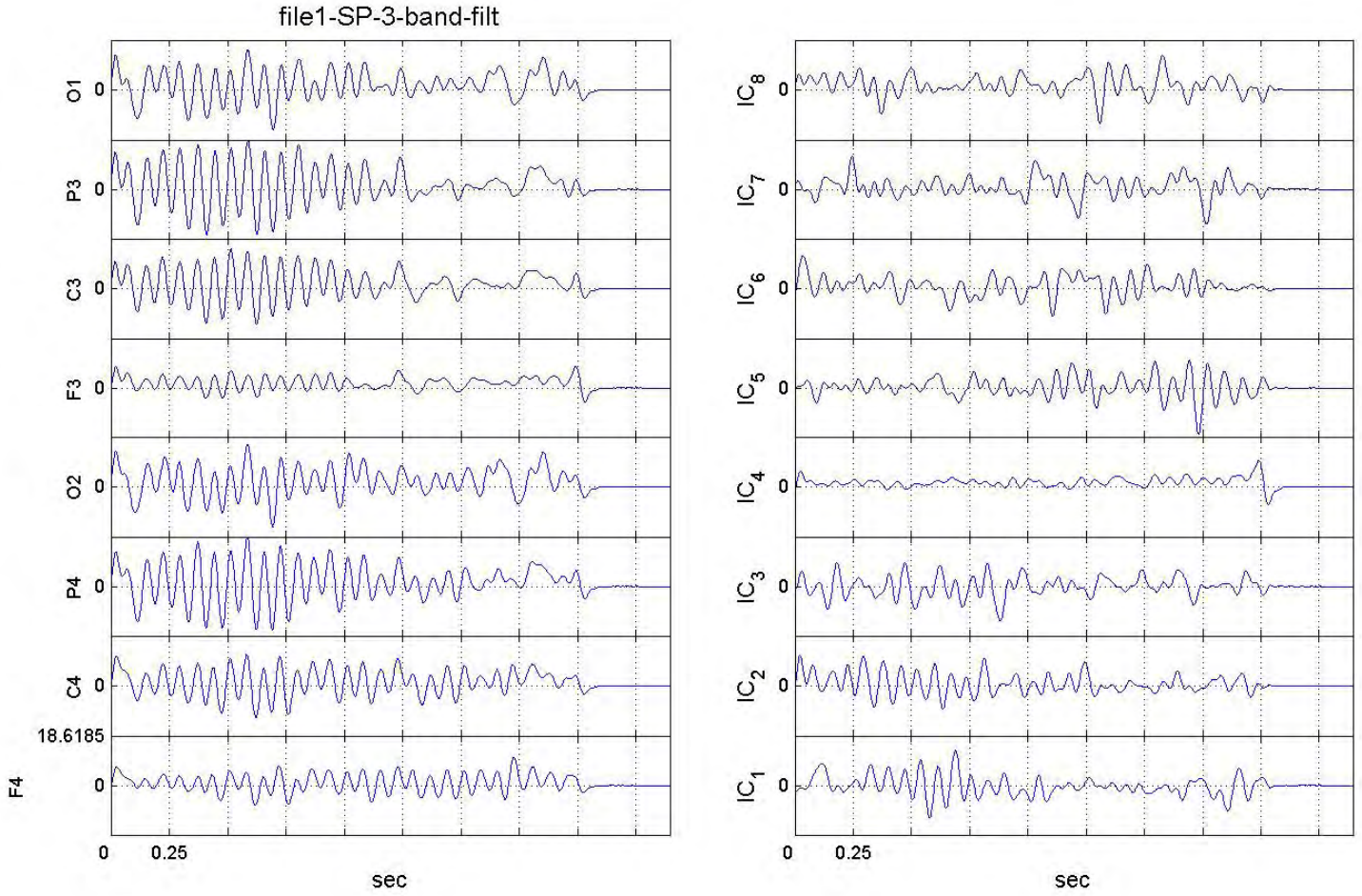



Figure 8.10.1: At left we have the original (filtered) EEGs and at right the ICs for spindle 9.

Original Data ICs 6,7,8 IC's 1,2,3




Original Data:

| TX | TY | TZ | Value |
|---|---|---|---|
| 4 | -67 | 15 | 3.465849E-0003 |
| 53 | -53 | 15 | 3.397891E-0003 |
| -3 | -46 | 43 | 3.234792E-0003 |
| -59 | -32 | 8 | 3.180426E-0003 |

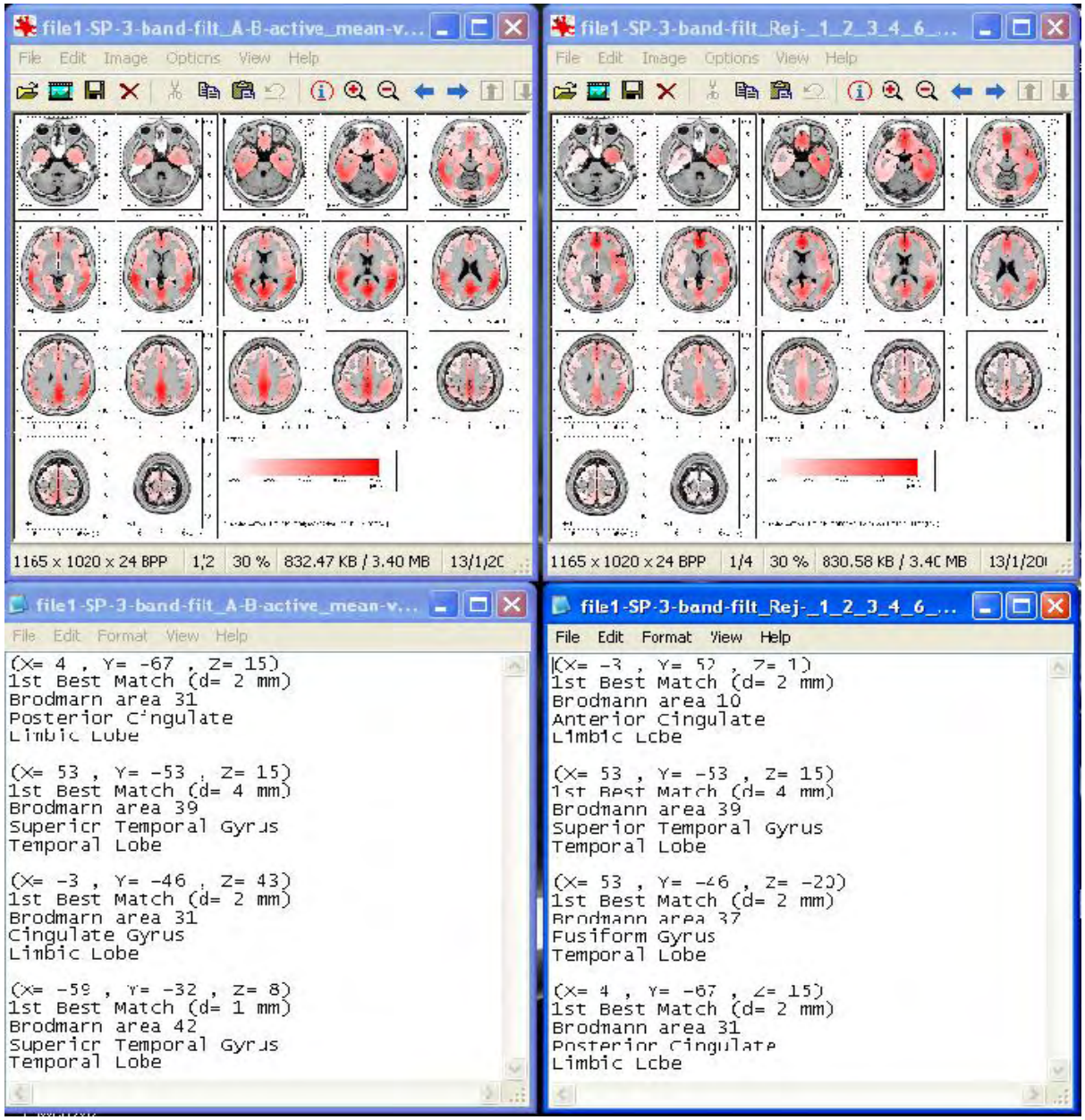
ICs 6,7,8:

| TX | TY | TZ | Value |
|---|---|---|---|
| 53 | -53 | 15 | 2.035943E-0003 |
| 4 | -67 | 15 | 1.708595E-0003 |
| 53 | -60 | -6 | 1.604802E-0003 |
| 4 | -46 | 43 | 1.397215E-0003 |

IC's 1,2,3:

| TX | TY | TZ | Value |
|---|---|---|---|
| -59 | -32 | 8 | 3.050539E-0003 |
| -3 | -46 | 43 | 2.799318E-0003 |
| 4 | -67 | 15 | 2.763429E-0003 |
| 60 | -46 | 15 | 2.380617E-0003 |

Original Data IC 5




Original Data:

| TX | TY | TZ | Value |
|---|---|---|---|
| 4 | -67 | 15 | 3.465849E-0003 |
| 53 | -53 | 15 | 3.397891E-0003 |
| -3 | -46 | 43 | 3.234792E-0003 |
| -59 | -32 | 8 | 3.180426E-0003 |

IC 5:

| TX | TY | TZ | Value |
|---|---|---|---|
| -3 | 52 | 1 | 6.071821E-0004 |
| 53 | -53 | 15 | 5.071756E-0004 |
| 53 | -46 | -20 | 4.881268E-0004 |
| 4 | -67 | 15 | 4.381236E-0004 |

Figure 8.10.2: Source activity analysis for part A of spindle 9

**Source activity analysis (part B):**

In Fig. 8.10.2, at left we have the 3D mean source activity map image from the original data (M-L-EEG-O/B), at the center the 3D mean source activity map image from the recomposition of the EEG based on ICs 6,7,8 (M-L-EEG-A/B), at right the 3D mean source activity map image from the recomposition of the EEG based on ICs 1,2,3 (M-L-EEG-B/B) and at the next page the 3D mean source activity map image from the recomposition of the EEG based on IC 5 (M-L-EEG-C/B). The main ICs for this spindle part are ICs 6,7,8 and IC 5.

By observing the image at left we ascertain a spread and almost equal source activity at various brain parts. Concretely, at decreasing order of intensity, we have sources at posterior cingulate, superior temporal gyrus, middle frontal gyrus and cingulate gyrus areas. The existence of the two main sources at posterior brain parts is consistent with the assumption that high frequency waves (which dominate at part B at the total EEG) should have mainly sources at posterior brain parts

From the sources of the EEG reconstruction based on ICs 6,7,8 we observe the activation peak to be at posterior parts. It is also important to observe that the spatial placement and the intensity order of the sources is maintained the same with the first spindle part (A). The appearance of primary anterior activity agrees with the assumption that high frequency spindles have posterior sources and low frequency spindles anterior sources.

From the sources of the EEG reconstruction based on IC 5, we can see an anterior activity and also activation in parts at the right and central posterior part of the brain. As we observe, the spatial placement of sources is maintained at great percentage (3 of 4 local maxima) from the first spindle part (A) (but at the first part this activity doesn't concern us for spindle production). The appearance of primary anterior activity does not agree with the assumption that high frequency spindles have posterior sources and low frequency spindles anterior sources.

The fact that the main source of the total activity of the brain (left image) remains at anterior parts of the brain, in agreement with the assumption that high frequency waves have mainly posterior sources but in opposition with the anterior main source of the EEG which is recomposed from the IC 5, is potentially due to the fact that at the total brain activity, at part B, predominates the activity of the brain parts that correspond to the high frequency EEGs which are recomposed from ICs 6,7,8.

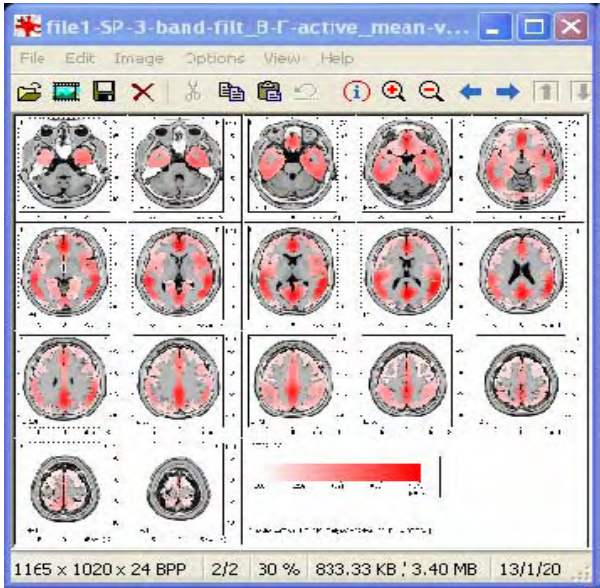
The action of the IC's 1,2,3 at this spindle part (B-C) does not possess spindle-like morphology, therefore we are not concerned about their spatial distribution, as spindle generators.

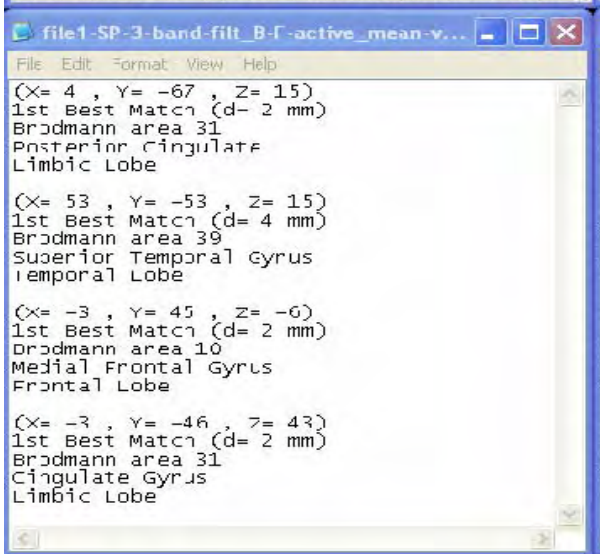
**Conclusions:**

A) The activity of the main sources of the total high frequency EEG is posterior at both spindle parts. Similarly, for part A, the action of the EEGs which is recomposed from the main high frequency ICs has posterior main sources. At part B, it is verified, for the EEGs which are recomposed from ICs 6,7,8 that the high frequency action has posterior sources.

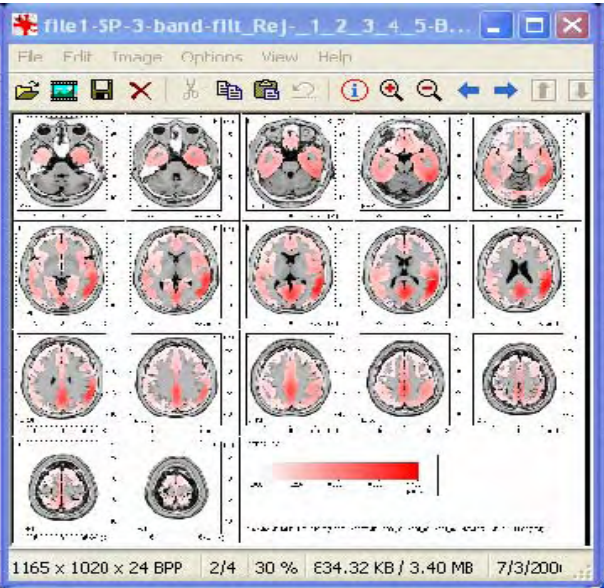
B) The sources of the recomposed EEG for each group of ICs maintain their distribution at the transition from part A to part B.

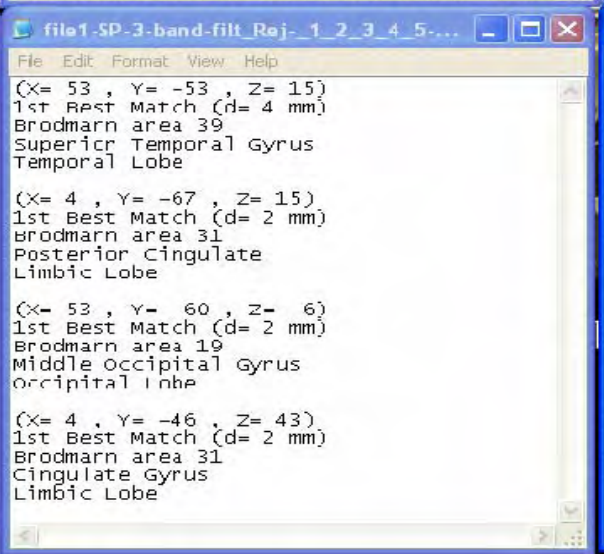
Original Data



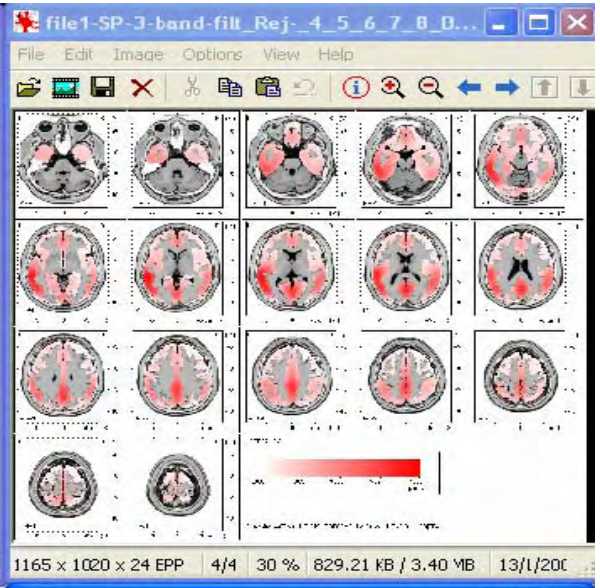



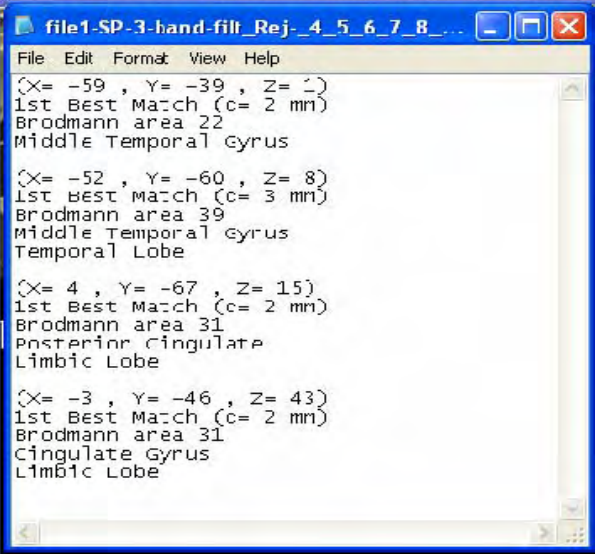

ICs 6,7,8




IC's 1,2,3




Original Data:

| TX | TY | TZ | Value |
|---|---|---|---|
| 4 | -67 | 15 | 1.048686E-0003 |
| 53 | -53 | 15 | 1.044573E-0003 |
| -3 | 45 | -6 | 9.828861E-0004 |
| -3 | -46 | 43 | 9.129737E-0004 |

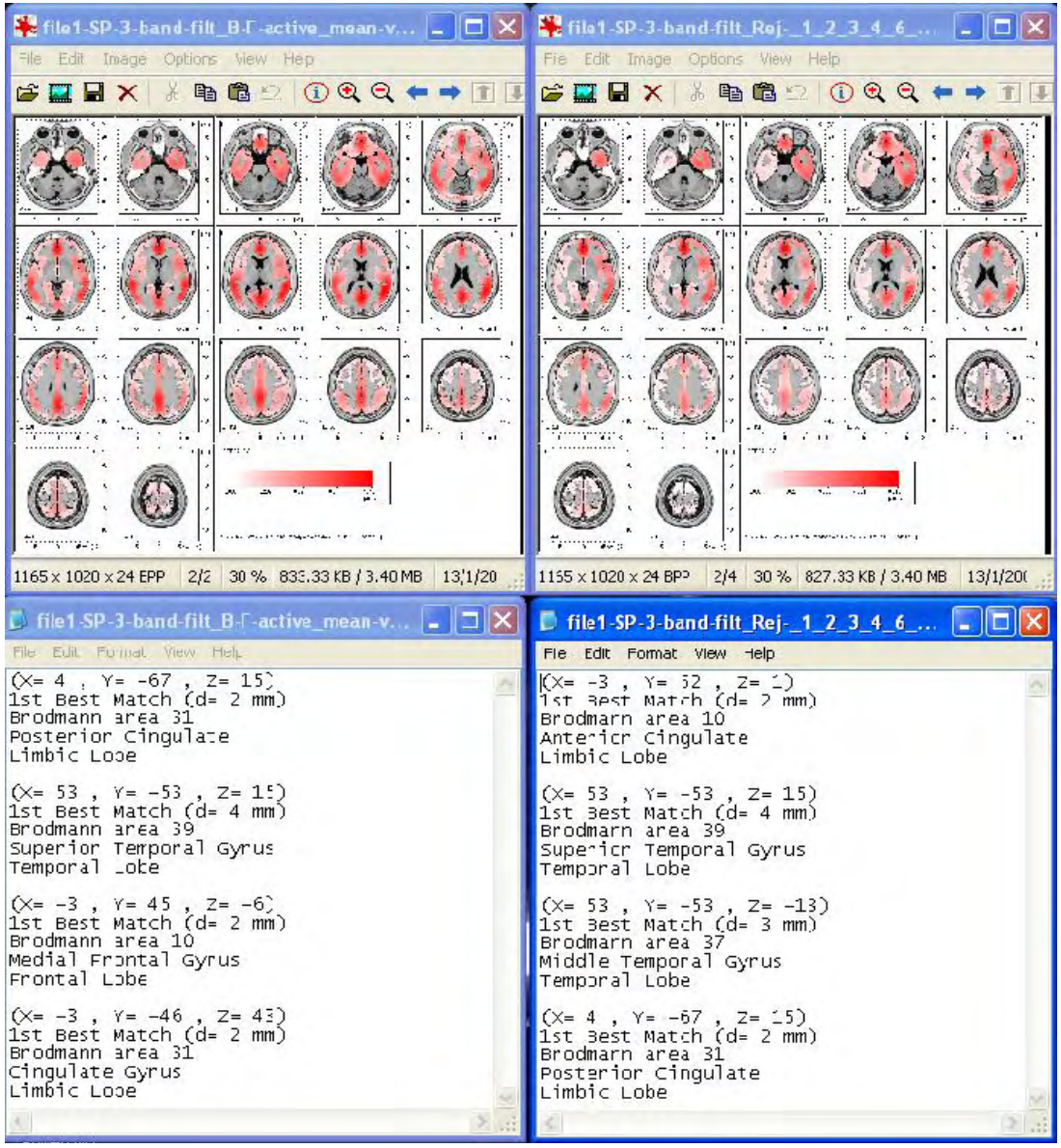
ICs 6,7,8:

| TX | TY | TZ | Value |
|---|---|---|---|
| -3 | 52 | 1 | 6.512032E-0004 |
| 53 | -53 | 15 | 5.337312E-0004 |
| 53 | -53 | -13 | 5.209626E-0004 |
| 4 | -67 | 15 | 4.545654E-0004 |

IC's 1,2,3:

| TX | TY | TZ | Value |
|---|---|---|---|
| -59 | -39 | 1 | 7.504911E-0004 |
| -52 | -60 | 8 | 6.592549E-0004 |
| 4 | -67 | 15 | 6.268808E-0004 |
| -3 | -46 | 43 | 5.945067E-0004 |

Original Data IC 5




Original Data:

| TX | TY | TZ | Value |
|---|---|---|---|
| 4 | -67 | 15 | 1.048686E-0003 |
| 53 | -53 | 15 | 1.044573E-0003 |
| -3 | 45 | -6 | 9.828861E-0004 |
| -3 | -46 | 43 | 9.129737E-0004 |

IC 5:

| TX | TY | TZ | Value |
|---|---|---|---|
| -3 | 52 | 1 | 6.512032E-0004 |
| 53 | -53 | 15 | 5.337312E-0004 |
| 53 | -53 | -13 | 5.209626E-0004 |
| 4 | -67 | 15 | 4.545654E-0004 |

Figure 8.10.3: Source activity analysis for part B of spindle 9

# Discussion

In this final chapter we shall make an overall discussion about the project. We will discuss about the problems we faced trying to implement division of spindles into parts and the corresponding source component localization and the validation of assumptions about spindles, the success or not of it, and probable reasons of failure when it occurred, and we will conclude by proposing future work.

The first methodological problem we faced concerned the division of the original single spindle into parts based on rules which are heuristic and still not totally fixed (see Chapter 6.1). We had to find the exact point at which the spindle changed frequency or passed from one cycle to another. This is not always achievable since there are cases when there exists a time lag between intra-spindle waxing-waning cycles in the various leads. Furthermore, we had to find the ICs that had the same frequency content with the original spindle at each part, but also started and finished at the same points. This was always not achievable, so we had to find the ICs that had the same frequency content and their spindle-like waveform did not extended significantly (e.g. for more than 0.5 sec) into the other part. Or, conversely, often also, the spindle-like waveform did not extend to the whole duration of the original spindle and we had to find other ICs that would "fill" the remaining time space.

These problems made imperative the visual observation of ICs and the original EEG recordings, one by one, but also the frequency analysis with the STFT, which we applied. The visual observation of the ICs helped us to find those ICs which possessed the characteristics we wanted, in order to recompose the original spindle at (at least) two parts. For parsimony reasons, related also to the simplicity of extracting conclusions on spindle components' sources we tried to find the as many ICs as possible to group together, and the contribution to that process of the frequency analysis was valuable. At this point we must state that in future work, more methods should be used concerning instantaneous frequency analysis of spindles, such as period-amplitude analysis and wavelets.

Based on the results from the spindles processed in the present study, positive indications were provided that sources related to sleep spindle components reconstructed from separate groups of ICs might be successfully extracted. As in the example presented in the Results Section, in each part of the spindle, the maximal sources of the spindle component representing the spindle activity in that part, mainly coincided with the maximal sources of the original EEG in the same part, indicating that the components' source activity was the main locus of generators for the respective parts of the EEG.

As stated in the aims of the study (see Chapter 5) one of the main goals of this project was the checking of the currently held assumption that high frequency spindles (~14 Hz) have mainly posterior and central sources and low frequency spindles (~12 Hz) have sources at anterior sites [7,8]. According to our results, we had 9 spindles, which we divided to two parts each, which gives us 18 spindle parts. From these spindle parts, 14 agreed with the previously mentioned assumption and 4 did not. By looking more closely at the cases that did not confirm the assumption, we can see that two of

them, which belong to separate spindles, had spindle-like duration smaller than 0.6 sec. This implies that we were dealing with "borderline" spindle segments, which if were not parts of a greater single spindle, might not have been initially scored as spindles by the experienced polysomnographer who visually detected the spindles. Therefore we may not be dealing with bona-fide spindles. On the other hand, the success of the results has been mitigated by the fact that in the few cases where we tried to divide a spindle into three parts, as was suggested by the observation of the original EEG waxing and waning cycles, the assumption on the location of slow and fast spindles was not confirmed. In the literature, intra-spindle multi-divisions and frequency variations, according to our knowledge, have scantily been discussed. We believe that to express sound opinion on the matter we have to check more than 8 EEG channel recordings, since this would undoubtedly provide more robustness to the source localization.

A significant finding of the present study was the provision of results contributing to the confirmation of the assumption that EEG sources generated by the same IC group remain stable across the spindle parts. The examination of the sources of each spindle component showed a remarkable stability between parts of the EEG. E.g. the maximal source regions for the reconstructed EEG that reflected the spindle activity in one part kept their primacy in the other parts, albeit with lower amplitudes, as expected since they were not the EEG component that represented the dominant spindle-like activity in the other parts. This stability of the sources was in accordance with one of the main characteristics of ICA analysis, namely that ICs, or groups of ICs, reflect functionally and topographically separate sources, if independent components are successfully separated. Therefore in conjunction with the results discussed in the previous paragraph, an indication was provided that slow and fast spindles originate in different parts of the brain and reflect distinct groups of generators, which remain active throughout the spindle duration, even if there is a frequency shift in the spindle.

Apart from the difficulties concerning the applicability of ICA assumptions in EEG data and the heuristic nature of the rules used for spindle division in parts and ICs grouping, the main limiting factor in the present study was the reduced number of electrodes available for performing the inversions to the intracranial sources. This prohibited the certainty in extracting specific regions for the sources, at the level of resolution provided by the LORETA technique, and made obligatory to use the source maps only as indicative of presence of sources in broadly defined brain areas, such as frontal, parietal, temporal, central and posterior.

Future work therefore, as stated also above, should first concentrate on using spindle data from multichannel recordings exceeding 20 channels [21]. This will enable the investigation of sources location within the voxel-per voxel accuracy provided by LORETA. Another matter of future work, as is always the case with spindle research, is the application of the proposed technique firstly to a set of healthy young adults, then to healthy subjects with ages extending to maturity and finally, if previous results would prove to be promising, to the investigation of fast and slow spindle source distributions in psychiatric patient groups.

# Appendix A: Analysis of Matlab "Specgram" function

The Matlab Signal Processing Toolbox provides a function, specgram, that returns the time-dependent Fourier transform for a sequence, or displays this information as a spectrogram. The *time-dependent Fourier transform* is the discrete-time Fourier transform for a sequence computed using a sliding window. This form of the Fourier transform is also known as the short-time Fourier transform (STFT). The *spectrogram* of a sequence is the magnitude of the time-dependent Fourier transform versus time.

Specgram calculates the spectrogram for a given signal as follows:

1.It splits the signal into overlapping sections and applies the window specified by the window parameter to each section.
2.It computes the discrete-time Fourier transform of each section with a FFT of length nfft to produce an estimate of the short-term frequency content of the signal. The quantity (length(window) - numoverlap) specifies by how many samples specgram shifts the window.
3.For real input, specgram truncates the spectrogram to the first nfft/2 + 1 points for nfft even and (nfft + 1)/2 for nfft odd.

In order to work with the specgram function we must define some parameters. First of all we must define the variable which contains our data, which we want to analyse. Next, we must define the nfft we want to apply (in our case 512). nfft specifies the FFT length that specgram uses. It is known that the smallest frequency difference (discrimination ability) that the DFT can distinguish is given by the equation:

$$(f_1 - f_2) \geq \frac{Fs}{L}$$

Where Fs= sampling frequency, L= length of the signal (in the case of specgram the nfft) and ($f_1$-$f_2$) is the smallest difference (step) between consecutive frequencies given by the FFT. The sampling frequency in our signal is 512 Hz. We defined nfft=512 in order to have smallest frequency difference equal to 1 Hz. We will examine briefly what consequences we would have if we used nfft equal to 256 or 1024. nfft=256 would be helpful, since it would analyze the signal in 0,5sec segments, in which morphological changes related to frequency shifts do occur in spindles, but it was not acceptable because it would give minimum frequency difference equal to 2 Hz, which is too coarse for our case, because we could not distinguish the low frequency (12 Hz) from the limit high frequency (13 Hz) and the limit high from the high one (14 Hz). On the other hand, nfft= 1024 was acceptable concerning frequency discriminability (it would give minimum frequency difference equal to 0.5 Hz), but it was not applied because it would it would analyze the signal in 2 sec segments, which is totally inadequate, since in many cases the spindle lasts less than 2 sec, and the benefit of STFT would disappear completely.
As it was mentioned above, the sampling frequency in our case was 512 Hz and we defined the number of overlaps (in our case 511 overlaps) also. Additionally, we must notice that we can define a window function, but if we don want to do so, the function uses the default (Hann).

As result of the function we get an image, like D in Fig.6.2. At the vertical axes we have frequency in Hz, at the horizontal time in sec and the colormap encodes the magnitude in dB of the overlapped STFTs ( 20log(abs(Y)), i.e. the quantity 20log(abs(Y)), with

$$\text{abs(Y)} = \sqrt{\{\text{real(Y)}\}^2 + \{\text{imag(Y)}\}^2} \ ,$$

where Y represents the overlapped STFTs, for the specific time point. The function calculated the spectrogram for frequencies up to fs/2=256 Hz.

# Appendix B: Reprojection of Independent Components into EEG recording electrodes

As stated in Chapter 3.1.1, "Basic principles of ICA", ICA is used for the transformation of the (bio)signals in Independent Components (IC). In the application of this method in EEG signals we try to achieve the decomposition of the recorded signals in ICs, supposing independent components, which are calculated by ICA. The re-projection of each IC onto EEG recording electrodes, gives a Projection of an Independent Component (PIC) at each recording electrode. The sum of PICs for all the ICs, per electrode, gives the original EEG signal at the electrode. The analysis of ICs seems to be able to provide ICs that represent exclusively the generators of specific components, allowing the separation of different "sources" of the components. Therefore one of the targets of sleep spindle analysis with ICA techniques is the selection of ICs, that via their PICs, recompose the "original" sleep spindle component, which is "hidden" in the original recording due to electrical noise or concurrent generators not related to the component under investigation or overlapping of two or more concurrently components' sources. Below we describe the techniques we proposed and used for the automatic selection of ICs that would recompose the sleep spindles.

For each subject we have 8 original sleep spindles recording channels with $S_{max}$=512 samples for each recording: $x_j^{ts}$, $ts=0,....,S_{max}-1$, $j=1,...,8$. In the terminology of Makeig et al.[44], each sample is considered a "mixture", because it is a combination of the effect of various intracranial sources. All of these spindle data can be written in a mixture matrix, $X=[\underline{x}^{ts}]$, $ts=0,....,S_{max}-1$, where each column $\underline{x}^{ts}$ contains the 8 samples of the original spindles at the time moment that corresponds to the sample *ts:* $\underline{x}^{ts}=(x_1^{ts},...., x_8^{ts})^T$. Each row *j* of *X*, is symbolized with $V_{\Pi\Delta,j}=(x_j^0,....,x_j^{Smax-1})$ and has the 512 samples of original spindle of channel *j*.

Also we have 8 ICs that are produced from ICA: $s_i^{ts}$, $ts=0,....,S_{max}-1$, $i=1,...,8$. Similarly with the mixture matrix we can write all the samples of the ICs in a "component activation" matrix $S=[\underline{s}^{ts}]$, $ts=0,....,S_{max}-1$, where each column $\underline{s}^{ts}$ contains the 8 ICs values at the moment that corresponds to the sample ts: $\underline{s}^{ts}=(s_1^{ts},...,s_8^{ts})^T$. Each row i of S has 512 samples of the *i*th IC: $IC_1=(s_i^0,....,s_i^{Smax-1})$. The rows of *S* are also named "component activations", i.e the time courses of relative strengths or activity levels of the respective ICs.

It is $\underline{x}^{ts}=A\underline{s}^{ts}$ and $X=AS$, where *A* is the 8x8 mixing matrix. ICA finds *A* and *S*, when we know *X*. Then, for each channel *j*, we find the re-projection of each *IC i (PICji)* at this channel:

$$\underline{p}_{ji}=\begin{pmatrix} p_{j,i}^0 \\ p_{j,i}^1 \\ : \\ p_{j,i}^{S_{\max}-1} \end{pmatrix} \quad i,j=1,...,8\,.$$

The projection of the *i*th independent component onto the original data channels is given by the outer product of the *i*th row of the component activation matrix with the *i*th column of the mixing matrix. Neither the scalp maps nor the activation time series

found by the ICA algorithm that we use are normalized. In this case, scaling information is distributed between them, and the true size of a component is given only by the size of its projection. For each sample of the original spindles we have:

$$x_j^{ts} = \sum_{i=1}^{15} p_{ji}^{ts} \text{ , } ts=0,....,S_{max}\text{-}1,\ j=1,....,8 \text{ .}$$

Our target is the "replacement" of $V_{\Pi\Delta,j}$ from a set of k new spindle components, denoted by A, B, …, K: $V_{A,Re,j}$ , $V_{B,Re,j}$ , … , $V_{K,Re,j}$ which will be produced from recomposition with a selection ICs, which we will re-project, for example if we make the assumption that there are two spindle components A and B "hidden" in the original spindle recordings $V_{\Pi\Delta,j}$ and that spindle component A is produced by ICs 1 and 3 and spindle component B by ICs 4,6 and 8 then

$$V_{A,Re,j} = \underline{p}_{j1} + \underline{p}_{j3}$$

and

$$V_{B,Re,j} = \underline{p}_{j4} + \underline{p}_{j6} + \underline{p}_{j8}$$

The calculation of ICs, and their corresponding projections (PIC), is done using the EEGLAB toolbox [45]. This toolbox is used with the Matlab software. We first had to load the data to the EEGLAB toolbox. At this point there are some parameters that we had to fill. We had to give a name to the data and also the data format. In our case the data was in Matlab format. Another parameter was the number of channels, but we could choose 0 channels and let the program find on its own what was the correct number by the data. At the same time we had to specify the number of epochs, i.e. time windows where data have been recorded under different experimental conditions, inside the data. In our data there were no epochs so we choose 0. The last two parameters was the sampling frequency (512 Hz) and the optional epoch starting time (0 sec).

Next we had to run ICA on the data. The only thing we had to choose here was the decomposition algorithm. In our case the algorithm was the "RunICA". After the ICA analysis we had to export the data and save them, using the export routine. This routine requires a name for the export data, and also requires to define some parameters. The first parameter indicated whether we wanted to export the EEG or the ICA data (in our case it was the ICA data). Also it requires an indication whether we want to transpose the output data matrix (in our case, yes) and if we want to put the names of the electrodes or the components in the export data file (in our case, no). Finally we had to define the precision of the output data (in our case we worked with 5 significant digits).

Next we studied the components and we choose those we wanted to reject. The final step of the analysis was the recomposition of the EEG data using only the remaining components. We loaded the data in the EEGLAB toolbox again and we computed the reprojections we wanted by subtracting from the computation the undesirable components. We gave a name to the export data and then we got the recomposed the EEG data.

# Appendix C: Direct problem solution code explanation

The “dir60120.exe” program is a DOS Fortran executable file, which solves the direct electric problem, for point current sources inside the inner shell of a three-shell spherical head, where the inner shell (shell 1) represents the brain tissue, the intermediate shell (shell 2) the skull and the exterior shell (shell 3) the scalp of the human head. The program solves the equation Y=A*X, where X is the vector of current sources and A the “transfer” matrix of the problem and Y the head surface potentials. The direct problem consists of knowing X and A and finding Y. The program needs as input files the spherical coordinates of the voltage measurement points at the external surface, given in file “vol.dat”. In each line of “vol.dat” the coordinates of one point are given, first the theta coordinate and the phi coordinate. Up to 120 measurement points may be included. It also needs the spherical coordinates and the current strengths of the sources, given in file “pig.dat”. In this file, in each line, one source point information is given (up to 60 source points may be included): first the current value in Amperes is given (zero if no source exists at specific point), then the radial distance of the source point and then theta and phi values for the coordinates of the source point. A final integer number gives the number of the source (from 1 to 60). The program also needs the conductivities of the three shells ($\sigma1=\sigma3=0.33$ S/m, $\sigma2=0.0042$ S/m), as well as the relative values of the three radii. The results of the program, i.e. the potential values computed by solving the direct problem are saved in file “vol.res”, where in each line the number of the measurement point is given (1 to 120) followed by the potential value in Volts.

# References


1. E. Ventouras. "*Biomedical Technology – Bioelectrical Signal Recording Systems"*. T.E.I. of Athens, Athens, 1999 [In Greek].
2. E. Kannelos and M. Limperi. "*Physiology II*". Ion, Athens, 1996 [In Greek].
3. K.R. Soldatos. "*Sleep Disorders – Treatment at the general medicine"*. Selida, Athens, 1993 [In Greek].
4. K. Susmakova. "*Human Sleep and Sleep EEG*". Institute of Measurement Science, Slovak Academy of Science, Bratislava, 2004.
5. A. Rechtschaffen, A. Kales. "*A Manual of Standardized Terminology, Techniques and Scoring System for Sleep Stages of Human Subjects*". Brain Information Service/Brain Research Institute, University of California, Los Angeles, 1968.
6. F. Dutertre. "Catalog of the main EEG-patterns". In *Handbook of Electroencephalography and Clinical Neurophysiology*, ed. A. Remond, 11A, pp.40-79. Elsevier, Amsterdam, 1977.
7. L. De Gennaro and M. Ferrara. "Sleep spindles: an overview". *Sleep Medicine Reviews*, 7:423-440, 2003.
8. DJ. Dijk. "EEG slow waves and sleep spindles: windows on the sleeping brain". Behavioral Brain Research, 69:109-116, 1995.
9. A. Destexhe, D. Contreras, M. Steriade. "Cortically induced coherence of a thalamic-generated oscillation". Neuroscience, 92:427-443, 1999.
10. S. Kohsaka, T. Sakai, M. Kohsaka, N. Fukuda, K. Kobayashi. "Dual control of the brainstem on the spindle oscillation*". Humans Brain Research*, 882:103-111, 2000.
11. M. Steriade, D. McCormick, TJ. Sejnowski. "Thalamocortical oscillations in the sleeping and aroused brain". *Science*, 262:679-685, 1993.
12. KA. Cote, TM. Epps, KB. Campbell. "The role of the spindle in human information processing of high-intensity stimuli during sleep". *Journal of Sleep Research*, 9:19-26, 2000.
13. W. Jankel, E. Niedermayer. "Sleep spindles". *Journal of Clinical Neurophysiology,* 2:1-35, 1985.
14. J. Zeitlhofer, G. Gruber, P. Anderer, S. Asenbaum, P. Schimicek, B. Saletu B. "Topographic distribution of sleep spindles in young healthy subjects". *Journal of Sleep Research,* 6:149-155, 1997.
15. E. Huupponen, A. Varri, S-L. Himanen, J. Hasan, M. Lehtokangas and J. Saarinen. "Autoassociative MLP in Sleep Spindle Detection". *Journal of Medical Systems*, 24:183-193, 2000.
16. J. Zygierewicz, K.J. Blinowska, P.J. Durka, W. Szelenberger, S. Niemcewicz, W. Androsiuk. "High resolution study of sleep spindles". *Clinical Neurophysiology,* 110:2136-2147, 1999.

17. L. McCormick, T. Nielsen, A. Nicolas, M. Pito, J. Montplaisir. “Topographical distribution of spindles and K-complexes in normal subjects”. *Sleep,* 20:939-941, 1997.

18. S. Doran. “Dynamic scalp topography of individual sleep spindles”. *Sleep Research*, 24:4, 1995.

19. H. Tanaka, M. Hayashi, T. Hori. “Topographical characteristics and principal component structure of hypnagogic EEG”. *Sleep,* 20:523-534, 1997.

20. W. Scheuler, S. Kubicki, G. Scholz, J. Marquardt. “Two different activities in the sleep spindle frequency band discrimination based on the topographic distribution of spectral power and coherence”. In *Sleep’ 90,* ed. J.Horne. Pontenagel, Bochum, 1990.

21. P. Anderer, G. Klosch, G. Gruber, E. Trenker, RD. Pascual- Marqui, J. Zeitlhofer, MJ. Barbanoj, P. Rappelsberger, B. Saletu. “Low-resolution brain electromagnetic tomography revealed simultaneously active frontal and parietal sleep spindle sources in the human cortex”. *Neuroscience,* 103:581-592, 2001.

22. A. Hyvarinen. “Survey of Independent Component Analysis”, Helsinki University of Technology, http://www.cis.hut.fi/~aapo/ (last accessed 9/06).

23. R. Vigario, E. Oja. “Independence: a new criterion for the analysis of the electromagnetic fields in the global brain?”. *Neural Networks* 13:891–907, 2000.

24. P. Comon. “Independent Component Analysis – a new concept?” *Signal Processing*, 36:287-314, 1994.

25. A. Hyvarinen, E. Oja. “Independent Component Analysis: algorithm and applications”. *Neural Networks* 13:411-430, 2000.

26. S. Makeig, A.J. Bell, T-P Jung, and T. J. Sejnowski. “Independent component analysis of electroencephalographic data”. In *Advances in Neural Information Processing Systems 8*, pp.145-151, MIT Press, Cambridge, MA, 1996.

27. R. Vigario, V. Jousmaki M. Hamalainen, R.Hari and E. Oja. “Independent component analysis for identification of artifacts in magnetoencephalographic recordings”. In *Advances in Neural Information Processing Systems 10*, pp.229-235, MIT Press, Cambridge, MA, 1998.

28. R. Vigario. “Extraction of ocular artifacts from EEG using independent component analysis”. *Electroencephalography and Clinical Neurophysioogy*, 103:395 404, 1997.

29. A.J. Bell and T.J. Sejnowski. “Learning higher-order structure of a natural sound”. *Network*, 7:261-266, 1996.

30. A.J. Bell and T.J. Sejnowski. “The independent components of natural scenes are edge filters”. *Vision Research*, 37:3327-3338, 1997.

31. J. Hurri, A. Hyvärinen, and E. Oja. “Wavelets and natural image statistics”. In *Proc. Scandinavian Conf. on Image Analysis '97*, pp.13-18, Lappenranta, 1997.

32. A. Hyvärinen, E. Oja, P. Hoyer, and J. Hurri. “Image feature extraction by sparse coding and independent component analysis”. In *Proc. Int. Conf. on Pattern Recognition (ICPR'98)*, pp.1268-1273, Brisbane, 1998.

33. J. Karhunen, A. Hyvärinen, R. Vigario, J. Hurri, and E. Oja. "Applications of neural blind separation to signal and image processing". In *Proc. IEEE Int. Conf. on Acoustics, Speech and Signal Processing (ICASSP'97)*, pp.131-134, Munich, 1997.

34. B. A. Olshausen and D. J. Field. "Emergence of simple-cell receptive field properties by learning a sparse code for natural images". *Nature*, 381:607-609, 1996.

*35.* J.F. Cardoso, "Blind signal separation: statistical principles", *Proceedings of the IEEE,* 9:2009-2005, 1998.

*36.* J.F. Cardoso and A. Souloumiac. "Blind beamforming for non Gaussian signals". *IEE-Proceedings-F*, 140:362-370,1993.

37. C. Vassios, "Brain potentials' processing and clasification techniques development", PhD Thesis, Dept. NTUA, Athens, 2004.

38. R.D. Pascual-Marqui, C.M. Michel, D. Lehmann. "Low resolution electromagnetic tomography: a new method for localizing electrical activity in the brain". *International Journal of Psychophysiology*, 18:49-65, 1994.

39. R.D. Pascual-Marqui. "Review of Methods for Solving the EEG Inverse Problem". *International Journal of Bioelectromagnetism*, 1:75-86, 1999.

40. Institute for Brain-Mind Research University Hospital of Psychiatry, Zurich, (http://www.keyinst.unizh.ch/loreta.htm) (last accessed 5/06).

41. Brain Imaging Centre, Montreal Neurologic Institute, http://www.bic.mni.mcgill.ca (last accessed 7/06).

42. E.Ventouras, "Development of a Tomographic Imagine Technique and Simulation with use of Artificial Neural Networks of the Intracranial Sources of Electrical Event-Related Activity", PhD Thesis, Dept. of Electrical and Computer Engineering, NTUA, Athens, 1994.

43. E.Ventouras, E.Monoyiou, P.Ktonas, T.Paparrigopoulos, D.Dikeos, N.Uzunoglu, and C.Soldatos. "Sleep Spindle Detection Using Artificial Neural Networks Trained with Filtered Time-Domain EEG: A Feasibility Study", *Computer Methods and Programs in Biomedicine,* 78:191-207, 2005.

44. S. Makeig, M. Westerfield, T.P. Jung, J. Covington, J. Townsend, T.J. Sejnowski, and E. Courchesne, "Functionally Independent Components of the Late Positive Event-Related Potential during Visual Spatial Attention". *The Journal of Neuroscience*, 19:2665–2680, 1999.

45. EEGLab Matlab Toolbox, Swartz Center for Computational Neuroscience, (http://www.sccn.ucsd.edu/eeglab) (last accessed 9/06).